STUDY REPORT

Mitigation Strategies for the Urban Microclimate of Dhaka Megacity to Reduce Adverse Climatic Change Impacts

Submitted to

The World Bank

Washington, DC

Prepared by

Curtin University

Collaborating Institutes

Bangladesh

SDGs

April 2020

STUDY TEAM

Ashraf Dewan, PhD
Principal Investigator (PI)
School of Earth and Planetary Sciences (EPS)
Curtin University, Western Australia
Email: a.dewan@curtin.edu.au

Ruhul Salim, PhD
Co–Investigator (CI)
School of Economics and Finance
Curtin University, Western Australia
Email: Ruhul.Salim@cbs.curtin.edu.au

Towhida Rashid, PhD
Co–Investigator (CI)
Department of Meteorology
University of Dhaka, Bangladesh
Email: towhida_rashid@du.ac.bd

Mahfuz Kabir, PhD
Co–Investigator (CI)
Bangladesh Institute of International and Strategic Studies (BIISS)
Dhaka, Bangladesh
Email: mahfuz@biiss.org

ACKNOWLEDGEMENTS

This study on Mitigation Strategies for the Urban Microclimate of Dhaka Megacity to Reduce Adverse Climatic Change Impacts has become possible due to funding by the World Bank's Development Data Group (DECDG) and the Global Partnership for Sustainable Development Data (GPSDD), and is supported by the World Bank's Trust Fund for Statistical Capacity Building (TFSCB) with financing from the United Kingdom's Department for International Development (DFID), the Government of Korea, and the Department of Foreign Affairs and Trade of Ireland. The project team expresses their gratitude to the funder as well as organisations noted above.

We would like to sincerely acknowledge the following institutions who have supported this work, consisting of the lead organisation (Curtin University) and collaborating institutes (University of Dhaka, and Bangladesh Institute of International and Strategic Studies, BIISS).

Special thanks and gratitude also to the people who have supported the production of this report, especially Dirk Botje of Curtin University. Also, the help of Grigory Kiselev, Dr Emmanuel Ongee and Rupa Rai of the same institute are gratefully acknowledged.

The team wishes to extend heartiest thanks to AYM Abdullah of University of Waterloo, Canada for his help. Md Masudur Rahman, Ahamed Sakib Antor, Tonim Shawon and Monojit Saha of University of Dhaka were highly supportive in the collection of field data and the study team expresses profound indebtedness to them. Ahsan Rony of Green Savers was very cooperative during this work and the team is grateful for his cooperation and logistic support.

The comments and suggestions received from the inception workshop by various experts and professionals also contributed a great deal to this work. The study team is thankful for their advice.

Finally, the input and help received from the Innovation Fund Team, particularly Leslie Ricketts, Siddesh Vishwanath Kaushik and Sun Hwa Song, was much appreciated and we gratefully acknowledge their support.

TABLE OF CONTENTS

APPENDICES

LIST OF FIGURES

LIST OF TABLES

ABBREVIATIONS AND ACRONYMS

AAT	Area average temperature
AIC	Akaike Information Criterion
AOD	Aerosol optical depth
ASTER	Advance Spaceborne Thermal Emission and Reflection Radiometer
AUHI	Atmospheric urban heat island
BBS	Bangladesh Bureau of Statistics
BCI	Biophysical composition index
BCR	Benefit–cost ratio
BCR	Building coverage ratio
BDP	Bangladesh Delta Plan
BMD	Bangladesh Meteorological Department
BRDF	Bi–directional reflectance distribution function
BSA	Black–sky albedo
BVD	Building volume density
CBA	Cost–benefit analysis
CBD	Central business district
CEGIS	Center for Environmental and Geographic Information Services
CR	Cooling rate
CUHI	Canopy layer heat island
DAP	Detailed Area Plan
DMA	Dhaka Metropolitan Area
DMDP	Dhaka Metropolitan Development Plan
DNCC	Dhaka North City Corporation
DSCC	Dhaka South City Corporation
ETM+	Enhanced Thematic Mapper Plus
EVI	Enhanced vegetation index
GCR	Green cover ratio
GED	General economic division
GIS	Geographic information systems
GoB	Government of Bangladesh
GWR	Geographically weighted regression
IFOV	Instantaneous field–of–view
IGBP	International Geosphere–Biosphere Programme
IPCC	Intergovernmental Panel on Climate Change
ISA	Impervious surface area
KII	Key information interview
LAI	Leaf area index
LaSRC	Landsat 8 Surface Reflectance Code
LEDAPS	Landsat Ecosystem Disturbance Adaptive Processing System
LPDAAC	Land Processes Distributed Active Archive Center

LST	Land surface temperature
LULC	Land use/land cover
MNDWI	Modified normalised difference water index
MODIS	Moderate Resolution Imaging Spectroradiometer
MSAVI	Modified soil–adjusted vegetation index
NBAR	Nadir BRDF–adjusted reflectance
NDBI	Normalised difference built–up index
NDMI	Normalised difference moisture index
NDVI	Normalised difference vegetation index
NDWI	Normalised difference water index
NGO	Non–governmental organisation
NPV	Net present value
OLS	Ordinary least–square
OLS/TIRS	Operational Land Imager/Thermal Infrared Sensor
RAJUK	Rajdhani Unnayan Kartripakkha
REHAB	Real Estate and Housing Association of Bangladesh
SAVI	Soil–adjusted vegetation index
SCR	Street coverage ratio
SDGs	Sustainable Development Goals
SEDAC	Socioeconomic Applications and Data Centre
SLC	Scan–line corrector
SUHI	Surface urban heat island
SUHIM	Surface urban heat island magnitude
SVF	Sky view factor
TM	Thematic Mapper
UBL	Urban boundary layer
UCI	Urban cool island
UCMap	Urban climate map
UC–ReMap	Urban climate planning recommendation map
UGI	Urban green infrastructure
UHI	Urban heat island
UI	Urban index
UN	United Nations
UPI	Urban planning indicators
VCF	Vegetation continuous function
VIF	Variance inflation factor
WCR	Water cover ratio
WSA	White–sky albedo

EXECUTIVE SUMMARY

The population increase evident in many cities across the world has resulted in a rapid expansion of the global urban footprint and has contributed to an observed temperature differential between city areas and the rural periphery. This increase in temperature in the urban areas is popularly known as the Urban Heat Island (UHI) effect and is being increasingly recognised as a significant impact by mankind on the environment; an effect with both local and global implications. Measurements can be taken at the earth's surface (surface urban heat island or SUHI), or at canopy level (canopy layer heat island or CUHI). It is expected that the rapidly–expanding populations residing in Asian cities will be very susceptible to these impacts.

In 2017, World Bank's Development Data group and the Global Partnership for Sustainable Development Data requested expressions of interest from researchers on ways to improve the production, management and use of data. This study is an outcome of that call. Although the UHI effect is a widely studied phenomenon across both large and medium–sized cities of the world, very few studies have been undertaken on Dhaka, the rapidly developing capital of Bangladesh. Furthermore, the majority of existing research has used either satellite data, or in–situ data, rather than both simultaneously, to characterise and quantify urban microclimate. Studies utilising both data are few and far between. The current research focus was specifically on UHI intensity and magnitude, at various spatial and temporal scales, and in both urban area rural areas, to determine any possible influencing factors. The innovative nature of this study lies in the use of both remotely sensed data and in–situ measurements together to quantify the spatiotemporal variability of microclimate of Dhaka, as well as to evaluate the efficacy of green spaces (parks, rooftop gardens, vertical green wall) and blue spaces (ponds and lakes) in mitigating the effects of urban warming. This information, in association with a provided cost/benefit analysis, could prove useful in determining the value of using these techniques in areas of rapid urbanisation.

The following research questions were posed for this study:

- How is land use change and population (both growth and shift) associated with urban warming of the Dhaka megacity, and what are the factors influencing the UHI, particularly SUHI?
- How, and to what extent, has past and current urban morphology, material surface type, land use and green/blue spaces affected Dhaka's microclimate?
- What are the costs and benefits of introducing potential heat mitigating measures (such as greenspaces, green walls and green roofs) into the urban environment?
- What specific policies are required for the city to adapt to a changing climate?

The current study attempted to address these questions by:

- Identifying spatiotemporal variability of UHI within the Dhaka development plan region, at monthly, seasonal and annual intervals, during the period 2000 to 2018, using both remotely–sensed (MODIS, Landsat and ASTER), population and climatological data.
- Determining possible driving factors for these observations.
- Proposing management strategies to mitigate the observed effects.

Two spatial scales were undertaken. They were:

- The "mesoscale". This area consisted of the larger Dhaka Metropolitan Development Plan (DMDP) area, and utilised MODIS (1 km resolution), Landsat (30 m resolutions) and population data.
- The "microscale". This area comprised the smaller Dhaka Metropolitan Area (DMA) within the DMDP and utilised Landsat and ASTER data. Various "on-the-ground" data collection techniques were also used to further evaluate the DMA microclimate, including fixed station data recording, traverse surveys and thermographic analysis.

The mesoscale satellite–derived results revealed that:

- SUHI varies substantially in the DMDP, both in space and time.
- Demographic shift and percent increase in built–up covers have significantly affected SUHI variability.
- April is the hottest month and the SUHI can be as high as 3.4 °C, compared with the rural surface, during daytime.
- A nocturnal heat island is highly pronounced in December–February, with January showing the greatest intensity (2.23 °C).
- On an annual basis, the daytime SUHI exhibited a higher temperature than during nighttime and it appears that areas recording a temperature >=2 °C are increasing over time.
- Anthropogenic and physical factors both appeared to be drivers for SUHI generation.
- Geographically weighted regression (GWR) models indicated that imperviousness and sparse vegetation cover significantly affects SUHI variability over the DMDP area.

At the micro–scale, the satellite–derived results indicated that:

- The daytime DMA's urban core has a 1.2 °C higher temperature than the surrounding vegetative cover.
- At night, the temperature appears to be 0.28 °C higher than the natural land cover.
- The difference between the day and nighttime SUHI is 2.48 °C, and indicates a notable degree of local warming.

- Regression analysis conducted on a number of indices derived from satellite data suggested that the built–up index (NDBI), moisture index (NDMI) and vegetation index (EVI) all have a significant influence on urban warming.

The data collection techniques used in the DMA microclimate study included the use of fixed station and traverse surveys, as well as the thermographic analysis of both biotic and abiotic elements. The results indicated:

- The urban core is experiencing consistently elevated temperatures across the diurnal cycle, albeit with marked temporal variability.
- At the monthly scale, February showed the highest SUHI (2.04 °C) whilst January exhibited the greatest CUHI intensity (1.96 °C). In contrast, November had the lowest SUHI (–0.14 °C) and August indicated the lowest CUHI intensity (0.39 °C).
- Seasonal data for SUHI and CUHI revealed that both phenomena are highly pronounced during winter. CUHI was also higher during post–monsoon months when SUHI is lowest in its intensity (0.09 °C).
- Traverse surveys indicated significant variations in both air and surface temperatures between planned, unplanned and mixed zones. This was driven by relative humidity, solar radiation and anthropogenic activities.
- The intensity of SUHI was higher in the planned locations, whilst both planned and unplanned locations experienced elevated temperatures during the pre–monsoon and monsoon seasons.
- The correlation between urban planning indicators and surface/air temperatures (obtained from traversing), was generally inconsistent, possibly related to other factors which were not quantified, such as sky view, amount of waste heat released to the environment, and land use of the respective traverse zones.

The thermo–physical analysis indicated a wide cooling potential range.

- Buildings with a high glass surface area appeared to both warm and cool faster than other features analysed.
- Solid brick tended to store more heat than both hollow bricks and concrete.
- Neon sign and plastic billboards appeared to affect nighttime temperatures significantly.
- Rooftops with an associated garden appear to be very effective in reducing the temperature of the immediate environment although the effectiveness to diminished during pre–monsoon months.
- Among dominant rooftop plant species, *Combretum indicum* exhibited the greatest plant cooling potential.
- The cooling potential of open space species varied between seasons. *Barringtonia* (a mangrove plant) exhibited the greatest cooling potential during winter, while *Earleaf Acasia* performed better in the pre–monsoon period.

- A green hanging wall appeared to provide day–long cooling benefits.
- The results of an analysis of park and lake effectiveness in reducing heat were generally inconclusive.

A greenspace database was developed using high–resolution imagery with subsequent field verification. A general assessment of green roof retrofitting revealed that assumptions made on the degree of overshadowing by tall buildings substantially impacts the number of buildings available for retrofitting.

- The DMA currently contains a total of 321 greenspaces of different types and sizes, making up about 2.41% of the total area.
- The study indicated that potential buildings make up 1 to 4% of the total buildings in the DMA suitable for green retrofitting.
- A study of suitability of greenspace locations and selected variables defined an area of approximately 800 ha which was potentially available within the DMDP.

A survey conducted on attitudes to green/blue spaces indicated that:

- Perceived benefits of a home/office greenspace included beautification, biophilia, aesthetic, psychological, health benefits and reduction of environmental temperature.
- Defined costs were mainly related to the installation and maintenance of building greenspaces and the annual life–cycle cost of plants.
- An analysis of the cumulative net present value (NPV) of benefits and costs revealed that all building greenspaces were financially viable.
- The most important social benefits provided by using public green/blue spaces appeared to be related to improved public health, positive psychological effects and the higher productivity of regular users.

Based on this study and on an extensive literature review, a range of mitigation measures were suggested including the generation of urban (local) climate maps.

- Location–specific measures are regarded as essential in curbing heat increase, as a ‘one–size–fits–all’ is not always appropriate for improving the microclimate of urban areas.
- Integrating local climate information into urban planning and city design, and the promotion of green infrastructures, are regarded as two of the most effective methods planners can use to ensure the development of healthier cities.
- A review of public policies and key informant interviews demonstrated that existing policies should be revised to meet the current and future needs of the cities. Failure to do so may seriously jeopardise the achievement of any of the defined Sustainable Development Goals (SDGs).

1 INTRODUCTION

1.1 The context

The global urban population, which is undergoing a process of demographic shift from rural to urban areas, increased in size by 30% in 1950 to 55% in 2018, and is expected to be 68% by 2050 (UN, 2018). Despite urban areas constituting a small amount (about 4–5%) of the earth's surface area, current estimates reveal that the rate of urban growth is higher than the growth rate of urban population (Seto et al. 2010), underlining the degree of anthropogenic activities (He, 2018). A very recent estimate reveals that global urban growth may remove significant amounts of existing cropland, which will seriously affect future food security (Chen et al. 2020). On the one hand, urbanization drives increased economic growth (Cole and Neumayer, 2004), while on the other hand, cities and their inhabitants are key drivers of global climate change (Maheshwari et al. 2020; Grimmond et al. 2010; Jin et al. 2005; Kalnay and Cai, 2003). Studies show that urbanisation contributes to increased greenhouse gas emissions (Hopkins et al. 2016), loss of natural habitat at the local level (Ke et al. 2018), deterioration in greenspace areas (Xu et al. 2019; Bowler et al. 2010), and above all, a general reduction in general human health and well–being (Christidis et al. 2019; Liao et al. 2018; Park et al. 2014; Tan et al. 2010; Tzoulas et al. 2007). Furthermore, urbanisation has the potential to amplify the effects of global warming (Alexander, 2020), so the achievement of sustainable development goals (SDG) (Halisçelik and Soytas, 2019) requires the construction of sustainable cities.

One remarkable effect of urban expansion is the generation of excess heat (Chapman et al. 2017; Anguelovski et al. 2014; Buyadi et al. 2013; Stone, 2007; Bosilovich, 2006), caused by human–dominated land use/cover changes at varying scales (Alexander, 2020; Zhang and Sun, 2019; Yoo, 2018; Golden, 2004). As urbanisation modifies the local environment, cities respond by developing their own microclimate (Roth, 2007). Consequently, urban areas tend to exhibit elevated temperatures when compared to the rural periphery, an effect predominantly due to the replacement of natural surfaces by impervious materials. This phenomenon is known as the urban heat island (UHI) effect (Oke, 1988), and is linked with modifications to the surface energy balance (Weng, 2009). The UHI phenomenon can nominally be sub–divided into two general types based on the height above the ground at which it is observed and measured (Oke, 1995). These consist of: i) the atmospheric urban heat island (AUHI); and ii) the surface urban heat island (SUHI) (Deilami et al. 2018; Oke, 1995). The AUHI phenomenon can further be divided into the canopy layer heat island (CUHI) and the urban boundary layer (UBL) heat island, though it should be noted that the UBL heat island phenomenon has not been examined in any great detail.

1.2 Approaches to measuring UHI, its causal factors and effects

Howard (1833) first documented the UHI issue nearly a century ago. Since that time there has been a lot of work conducted on this issue (regardless of city size and geographical location), emphasising the magnitude and role of the phenomenon on both the global and regional climate (Li et al. 2019; Giridharan and Emmanuel, 2018; Levermore et al. 2018; Peng et al. 2018). The Intergovernmental Panel on Climate Change (IPCC), estimated that heat island intensities in cities range from 1.1 to 6.5 °C (Celsius) (Pachauri et al. 2014), primarily driven by increased human activities (Parsaee et al. 2019; Akbari et al. 2016; Roth, 2007). Stewart (2011) demonstrated that more than 1100 cities around the world experience various degrees of UHI intensity, irrespective of their geographical position, city size or climatic zone. Chakraborty and Lee (2019), using 15 years of satellite data, showed that daytime UHI intensities have increased globally over the last decade. Major determinants of summertime UHI across the world appear to be related to population size and mean annual precipitation (Manoli et al. 2019), though cities in humid regions tend to have higher daytime UHI intensities than cities in the arid regions (Zhao et al. 2014). Some research suggests that nocturnal UHI will intensify under warmer climate conditions (Arsiso et al. 2018), though this is contradicted by other research which suggests the intensity would decrease under warming scenario (Scott et al. 2018). As a result of these observations, there is now considerable effort being undertaken to develop mitigation strategies and tools to assist in reducing the heating of urban environments.

A range of methods have been employed to characterise and quantify the UHI effect across various cities. These can be divided into two major categories; those using in–situ measurements, and those using satellite data estimation methods (Parsaee et al. 2019). In most studies, land surface temperature (also known as land surface skin temperature), appears to be greatest during the daytime. In contrast, air temperature tends to be elevated during the nighttime period due to the interaction between various 2D (e.g. land use/cover, vegetation) and 3D (e.g. building height, sky view, solar radiation) features (Chun and Guldmann, 2018; Lin et al. 2017). The impact of each feature differs, however, and there tends to be a sharp seasonal variation as a result of climatic zone differences (Kotharkar et al. 2018; Peng et al. 2011). An overview of the mechanisms of the UHI effect can be found in Deilami et al. (2018), Giridharan and Emmanuel (2018), Weng (2009), Rizwan et al. (2008) and Arnfield (2003).

Air temperature recordings from fixed stations and/or mobile stations across urban canyons constitute the major data source for studying the CUHI in cities (Kotharkar and Bagade, 2018; Drach et al. 2018; Chakraborty et al. 2017; Sheng et al. 2017; Wang et al. 2017; Clay et al. 2016; Mohan et al. 2013; Kantzioura et al. 2012; Basara et al. 2008; Jusuf et al. 2007; Kim and Baik, 2005). A study in Nagpur, India, indicates that CUHI intensity can range from 1.76 to 4.09 °C during winter (Kotharkar and Bagade, 2018). The diurnality of urban–rural surface and air temperature differences appear to be dependent on the seasons (Chakraborty et al. 2017).

The study also shows that the diurnality of nighttime UHI (canopy layer) dominates both in the pre–monsoon and monsoon seasons, whereas daytime SUHI is greater during the pre–monsoon period than during the monsoon. Using mobile transects and fixed weather stations, Rodríguez et al. (2020) show that the maximum observed UHI ranged from 3.1 to 7 °C in the city of Seville, Spain. In New York City four areas studied in detail showed an average 2 °C difference between the most and least vegetated surfaces (Susca et al. 2011). A study by Scott et al. (2017) in Baltimore, USA revealed that in–situ temperature measurements of intra–urban areas recorded values much smaller than surface temperatures obtained from satellite data. Drach et al. (2018) noted that the maximum daytime intra–urban temperature differences in Glasgow, UK, were predominantly related to urban form and atmospheric stability. Using temperature data from 289 in–situ stations in the contiguous USA, Peterson (2003) demonstrates that there appeared to be no statistically significant impact of urbanisation on the UHI, an affect probably related to micro and local–scale influences dominating over the mesoscale UHI.

Remotely–sensed data has typically been used to reveal spatial patterns of SUHI in cities, at both the meso and microscale (Zullo et al. 2019; Liu et al. 2019; Yao et al. 2018a,b; Zhou et al. 2018; Peng et al. 2018; de Faria Peres et al. 2018; Li et al. 2018; Lai et al. 2018a,b; Wang et al. 2017; Shastri et al. 2017; Estoque et al. 2017; Li et al. 2016; Coutts et al. 2016; Coseo and Larsen, 2014; Sobrino et al. 2013; Lazzarini et al. 2013; Clinton and Peng, 2013; Tomlinson et al. 2012; Schwarz et al. 2011; Bottyán et al. 2005; Golden, 2004; Gallo et al. 2002). The widespread use of this type of data is due to the fact that weather stations are not uniformly distributed within many city areas, and therefore, the spatial coverage of any weather data available for research is not ideal. Thermal infrared data from earth–orbiting satellites has been used extensively in many cities to overcome this lack of optimal ground coverage. Most satellites have wide areal coverage and the data is relatively easy to access. Using satellite data, Alexander (2020), demonstrates that the mean temperature difference between urban and rural locations in Aarhus, Denmark was 3.96 °C. Silva et al. (2018) examines the impact of land use/ cover change on daytime maximum intensity of SUHI in Paco do Lumiar in Brazil. A study by Peng et al. (2018) reveal a sharp increase in nighttime temperature between 2001 and 2010 in a number of major Chinese cities, with 98.9% of the 285 cities studied exhibiting a high UHI during summer nights. Sobrino et al. (2013) undertake SUHI research in Madrid City using remote sensing which shows that while SUHI is highest during the night, during the daytime this actually reverses. Peng et al. (2011) use time–series MODIS (Moderate Resolution Imaging Spectroradiometer) to examine diurnal and seasonal variations of SUHI across 419 global cities. This study indicates that the average annual daytime SUHI intensity is generally higher than the nighttime intensity, and that the driving mechanisms vary according to latitude and the particular climatic zone. Li et al. (2016) show that physical, ecological and socioeconomic drivers within cities could also have a significant influence on the occurrence of SUHI. Although the majority of the SUHI studies are based on satellite data, the use of thermography/infrared cameras, has recently been shown to have great potential in providing

insights into urban microclimate features (Dwivedi and Mohan, 2018; Hartz et al. 2006). Apart from in–situ and remote sensing measurements of the SUHI and AUHI, a number of studies use simulation techniques to evaluate the UHI phenomenon (Li et al. 2019; Zolch et al. 2016; Lin and Lin, 2016; Sharmin et al. 2015; Kakon et al. 2009).

The effects of UHI have also been shown to vary significantly with city size and latitude. As cities account for 60–80% of the world's energy consumption and 75% of carbon emission (Akbari et al. 2016), an increase in energy demand is one of the first and most noticeable effects of any general temperature increase (Yang et al. 2020; Santamouris et al. 2015; Akbari et al. 2001) and UHI is regarded as one of the major drivers of local climate change (Luber and McGeehin, 2008). This is closely followed by high mortality and morbidity rates resulting from periodic heat waves (Pyrgou et al. 2020; Scherer et al. 2014) and air pollution issues (Li et al. 2019; Pandey et al. 2014). In addition, higher ambient urban temperatures have the potential to increase the global ecological footprint of the cities (Santamouris et al. 2007), and any modifications to city microclimate can greatly influence the macro–climatic environment (Akbari et al. 2016; Golden, 2004). Other adverse impacts include a decrease in the diurnal temperature range (Yang et al. 2019), an increase in disease vector development rates (Connolly et al. 2020; LaDeau et al. 2015), elevated water demand (Guhathakurta, and Gober, 2007) and a deterioration in general thermal comfort levels (Muniz-Gäal et al. 2020; Salata et al. 2017; Santamouris et al. 2015).

The causative factors and influences driving UHI development include such factors as the background climate, urban form and structure, street orientation, urban functions, geographic location, timing and season, population density, lack of greenspace and air quality (Manoli et al. 2019; Ferreira and Duarte, 2019; Zhang and Sun, 2019; Giridharan and Emmanuel, 2018; Zhou et al. 2018; Yao et al. 2018a; Deilami et al. 2018, Drach et al. 2018; Cao et al. 2016; Phelan et al. 2015; Ruiz et al. 2015; Petralli et al. 2014; Zhao et al. 2011; Roth, 2007). An increase in impervious surface area (resulting from land use change and population shift), also significantly influences the urban area temperature (Li et al. 2019; Coseo and Larsen, 2014; Lazzarini et al. 2013). Waste heat generation from anthropogenic activities is always higher in the urban environment than in rural areas so any additional heat can further aggravate the urban microclimate (Rodríguez et al. 2020; Li et al. 2019; Rouhollahi and Masouleh, 2016). The cooling effect of different surface materials can vary widely due to an inverse relationship between albedo and surface temperature (Aflaki et al. 2017). Morphological changes due to land cover change in urban areas are also shown to influence the UHI (Zheng et al. 2014). Urban planning indicators such as green cover ratio, tree cover ratio, aspect (height/width ratio), floor area ratio, building volume density etc. are all associated with urban heat and intra–urban temperature variability (Shiflett et al. 2017; Petralli et al. 2014; Zhao et al. 2011).

1.3 Relevance to Dhaka megacity

Dhaka, the capital of Bangladesh, is one of the largest megacities in the world. It is also a hub of major socioeconomic, administrative and cultural activities. Dhaka experienced phenomenal growth since the granting of independence in 1971, and the population has grown dramatically from 2.06 million (M) people in 1974, to 14 M in 2011 (http://www.bbs.gov.bd/). If current trends continue, it is estimated that the megacity will have a population of 27.3 M by 2025 (UN, 2018). The mean population density also increased from 4,513 persons per km^2 (p/km^2) in 1991 to 9,555 p/km^2 in 2011 (Corner et al. 2014). As far as land use change is concerned, study reveals that built–up surfaces (collectively referred to as 'urban') increased from 11,696 hectares (ha) in 1990 to about 19,556 ha in 2011, indicating an overall increase in area of 7,860 ha between the years 1990 and 2011 (Corner et al. 2014). In contrast, natural land covers such as vegetation and cultivated categories decreased substantially. To accommodate the ever–increasing population (an increase primarily driven by the rural to urban migration), natural, usually pervious, surfaces are being rapidly transformed into generally impervious covers by ongoing development, and these activities modified the thermal characteristics of the megacity (Rana, 2011). A number of studies employed satellite data to examine the effect of land use/cover change on land surface temperature (Trotter et al. 2017; Itzhak–Ben–Shalom et al. 2017; Dewan and Corner, 2014a, b; Ahmed et al. 2013). A couple of works examined the canopy layer heat island with in–situ measurements (Sharmin et al. 2015; Kakon et al. 2009). These studies, albeit with limited scope and data, indicate that the microclimate of Dhaka changed significantly in response to the widespread replacement of natural covers (specifically vegetation and waterbodies) with concrete structures. Recently developed building rules are also not conducive to improving outdoor thermal conditions (Kakon et al. 2009). Kotharkar et al. (2018) undertake a critical review and conclude that UHI studies, and possible mitigation measures to combat this phenomenon, are seriously lacking in South Asia, and particularly for the Dhaka. It should be noted that the urban populations of developing countries are directly exposed to the impacts of UHI (Rizwan et al. 2008), and typically lack the resources to deal with the consequences related to rapid urban growth (Moretti, 2014). For these reasons, Dhaka (an area which undergone rapid land use/cover change and ongoing demographic shift), is regarded as an ideal location for a detailed study of local climatic conditions.

Numerous studies have been conducted on the UHI phenomenon and this number has been steadily increasing, particularly in recent years (Giridharan and Emmanuel, 2018). This clearly shows the considerable interest in this area of research and the ongoing focus on issues regarding urban vitality and sustainability. It should be noted, however, that the majority of existing works focus primarily on temperate climate areas (Giridharan and Emmanuel, 2018), or the findings predominantly deal with a particular season when depicting spatiotemporal variations in urban temperature (with a general focus on the summer season). It is very likely that mitigation measures based on a single season may not be appropriate given that seasonal

variations in climatic parameters could potentially hinder the development of relevant indicators for sustainable urban development (Chun and Guldmann, 2018). This study points out that the seasonality of the UHI problem has largely been overlooked in existing research and flags that seasonality should actually be regarded as a crucial element to be included when developing mitigation strategies. The strong diurnality and inter–seasonality of UHI at different latitudes means that influencing factors can also be different (Peng et al. 2011), which underlines the requirements for an area–specific study before reaching any generalised conclusions (Chakraborty et al. 2017). Mitigation measures developed for a particular area should be based on the particular geographic and climatic influences in that area in order to maximise the effectiveness of any urban planning activities (Martilli et al. 2020). It appears that studies that utilised both remote sensing and in–situ measurements, across different seasons, are rare. This particular approach has the potential to add significant value to the description of the urban microclimate (Wang et al. 2017; Rouhollahi and Masouleh, 2016; Schwarz et al. 2012), and may overcome shortcomings associated with using either of the techniques in isolation when conducting urban thermal environment studies.

1.4 Strategies to mitigate urban warming

An increase in the local warming effects associated with urban development is almost certain to increase in future and is currently becoming a matter of serious global concern. Various strategies to curb this phenomenon have been suggested in the literature, and can broadly be divided into three main categories. They are: (i) development and implementation of green infrastructures; (ii) use of highly reflective and cool materials; and (iii) integration of climate knowledge into local planning practices. Even through the basic aim of these measures is essentially to modify the surface energy balance over the built environment (see Aflaki et al. 2017; Akbari and Kolokotsa, 2016), many researchers point out that there is no 'one–solution–fits–all' approach to addressing the UHI issue. This is due to its multi–scale nature and complicating factors including local climate, the urban environment, building characteristics, public policies and geographical location (Baklanov et al. 2018; Yang et al. 2015; Saneinejad et al. 2014; Kleerekoper et al. 2012). Manoli et al. (2019) note that while increasing the green cover and albedo are effective measures for cities in dry regions, these measures appear to be generally ineffective for tropical cities, and therefore, cities in tropical climate require more innovative solutions. It should be noted that the prerequisite for developing effective solutions depends, in large part, on good baseline data about the issue, data which are generally unavailable for South Asian cities, a situation which is very true for Dhaka (Kotharkar et al. 2018).

The importance of urban forest, parks, street trees, greening systems (living walls, green façades etc.) and blue space (such as waterbodies) in alleviating human–induced temperature increase in urban areas, has been extensively studied (Saaroni et al. 2018; Gunawardena et al.

2017; Zhang et al. 2017; Tan et al. 2016; Akbari and Kolokotsa, 2016; Jim, 2015; Santamouris, 2014; Wong and Lau, 2013; Perini et al. 2011; Onishi et al. 2010; Wong et al. 2003). Although vegetation reduces temperature during the summer, its role appears to be reversed during the winter, suggesting that any green strategies developed must account for seasonal effects (Chun and Guldmann, 2018). Others show a range of economic and environmental benefits associated with the use of green infrastructures (Netusil et al. 2014; Soares et al. 2011; Carter and Keeler, 2008; Tyrvaiinen and Vaananen, 1998). Zhang et al. (2017) demonstrate that the use of cool and green roofs are two important methods that can lead to lower surface and near–surface air temperature. Wong et al. (2003) indicate that rooftop gardens could produce thermal benefits to the building, as well as the surrounding environment. Perini et al. (2011) show that vertical greening systems can be effective natural sunscreens and assist in reducing surface temperatures in the urban environment. Jim (2015) examines the thermal benefits of green roof plots (using in–situ measurements) and concludes that this could be an effective mitigation measure. Tan et al. (2016) observe that the cooling effect of trees in the urban landscape was closely associated with the sky view factor (SVF). Cameron et al. (2014) report that the cooling effect varies according to plant types, leaf area/morphology and physiology. Feyisa et al. (2014) also obtain similar results when measuring plant types with a propensity to lower temperature in an urban microclimate in Ethiopia. In a comprehensive review of this topic, Getter and Rowe (2006) show that green roofs could provide economic benefits and contribute to sustainable development. Although the range of benefits resulting from using green infrastructures has been well documented, such strategies have not attracted much attention in developing countries. Reasons for the lack of this type of infrastructure uptake include the perceived life cycle cost and doubts about the economic and environmental returns of green infrastructure use. Due to the fact that benefits can be difficult to measure and economically quantify, these inherent uncertainties are probably the main barriers to the introduction of green infrastructures in the urban areas in developing countries (Perini and Rosasco, 2013).

The UHI effect and global warming generally increase the ambient air temperature (Santamouris et al. 2015), and so a number of studies have focused on the role that highly reflective and cool materials can have in reducing heat generation (Akbari and Kolokotsa, 2016; Yang et al. 2015; Santamouris, 2014; Li and Kendall, 2013; Shahidan et al. 2012; Synnefa et al. 2008). The effectiveness of these materials in lowering the temperature of urban areas is largely based on simulation and numerical modelling as definitive field–based research on this is lacking (Li and Kendall, 2013). Rooftops, pavement, driveways, parking lots and sidewalks constitute a large portion of an urban surface, so increasing albedo or high solar reflectivity could potentially lower daytime urban temperature by increasing sensible heat flux to the atmosphere (Santamouris, 2014), though its effectiveness is limited during the nighttime due to the absence of solar radiation (Shahidan et al. 2012). The magnitude of the reduction, however, varies according to latitude and climatic zone (Saneinejad et al. 2014). A point of major concern is also the fact that widespread use of albedo in buildings and pavements could

actually enhance global warming (Jacobson and Ten, 2012). Little research has been undertaken to test these techniques for curbing the UHI effect. Shahidan et al. (2012) demonstrate that a combination of larger tree quantities, high tree canopy and cool materials can significantly reduce temperatures in the urban outdoor landscape. Shading provided by tall buildings, or trees, in high–density environments appears to be another method of reducing daytime heat stress (Lau et al. 2016; Emmanuel et al. 2007). Coating type, painted metals and glasses are other materials commonly utilised in the urban environments, however their role in either enhancing or reducing local temperatures has not attracted much attention. The widespread use of glass in newer buildings, for example, and any impacts on urban warming, has seen little research activity (Giridharan and Emmanuel, 2018).

A relatively new avenue of research associated with the development of mitigation strategies proposes the inclusion of microclimate information into the urban planning and design process (Parsaee et al. 2019; He et al. 2015; Stewart and Oke, 2012; Houet and Pigeon, 2011; Ren et al. 2011; Wong et al. 2010; Alcoforado et al. 2009; Oke, 2004; Erell et al. 2003; Eliasson, 2000; Scherer et al. 1999; Evans and Schiller, 1990). The logic behind these initiatives is the integration of local climate knowledge into local planning practices so that climate–sensitive areas can be mapped, and used to more effectively control microclimatic and environmental conditions (Parsaee et al. 2019; Ren et al. 2011; Evans and Schiller, 1990). As noted previously, there is no 'one–size–fits–all' approach to curbing a changing climate, so the generation and use of an urban climatic map (UCMap), together with an urban climatic recommendation map (UC–ReMap), appears to offer planners a useful tool in the development of urban warming mitigation strategies, particularly in high–density cities (He et al. 2015; Ren et al. 2011). A recent review of mitigation measures proposed for the UHI phenomenon (regardless of SUHI or CUHI), indicates that, overall, the use of urban development polices and action plans has been overlooked (Parsaee et al. 2019). The review further suggests that mitigation strategies and urban climate maps should be integrated into the decision–making processes.

1.5 Significance of this work

In 2017, an international call was made for proposals for sustainable development–focused research projects (https://wb-gpsdd-datainnovation.forms.fm/call-for-proposals-collaborative-data-innovations-for-sustainable-development/forms/3431). Research projects deemed to align with the aims of this sustainable development initiative were to be provided funding by the World Bank's Development Data group and the Global Partnership for Sustainable Development Data. These groups requested expressions of interest from researchers in developing ideas to improve the production, management, and use of data. A research project titled "Mitigation Strategies for the Urban Microclimate of Dhaka Megacity to Reduce Adverse Climatic Change Impacts" was accepted for funding (https://blogs.worldbank.org/opendata/announcing-funding-12-development-data-innovation-

projects). Following a formal award/agreement, an inception workshop was held on the 28th November 2018 with multi–stakeholders from a range of government, non–government and academic institutions (Appendix I). The research was to be jointly undertaken by Curtin University in Australia, the Bangladesh Institute of International and Strategic Studies (BIISS), and the Department of Meteorology, University of Dhaka with funding to be provided as part of the World Bank's "Innovation Funding and Global Partnership for Sustainable Development Data" initiative. The workshop highlighted the fact that the Dhaka megacity was clearly witnessing an Urban Heat Island (UHI) effect, a unique feature arising from climate change and intense human activities, and that the city dwellers were being adversely impacted by this phenomenon.

Dhaka is a fast–growing megacity where land use change and demographic shift is occurring at an unprecedented rate. The observed UHI results from a range of factors including human activities, however detailed knowledge regarding the microclimate of Dhaka is very limited. A few studies attempted to examine both surface and canopy layer heat islands (see Trotter et al. 2017; Sharmin et al. 2015), however these studies have been based on a single season or on limited data. Neither of the studies considered using a combination of satellite data and in–situ measurements to quantify the urban microclimate (specifically the surface and canopy layer). With only one weather station in place (operated by the Bangladesh Meteorological Department (BMD)), it is impossible for researchers to determine the spatiotemporal variability of the UHI effect. Since the UHI is a multi–scale issue, an integrated study that utilises both remote sensing and field–based data, across different seasons, is needed. This can provide opportunities for the development of climate change mitigation and adaptation strategies by making efficient use of all available resources (Seto et al. 2011). Accurate microclimate information is deemed essential in providing for the development of comprehensive adaptation plans and policies, planning documents and processes which can be used to enhance the resilience of urban areas and the comfort of residents inhabiting those areas (Urge–Vorsatz et al. 2018; Rouhollahi and Masouleh, 2016; Anguelovski et al. 2014).

The overarching goal of the study was to examine the UHI effect in the megacity of Dhaka. The research focus was specifically on UHI intensity and magnitude, at various spatial and temporal scales, and in both urban and rural areas, to determine any possible influencing factors. Information obtained regarding the predictive ability of the various variables could prove useful for further research into the UHI effects. The study was also designed to assess the benefits of using remotely sensed data and in–situ measurements in specific microclimate investigations, as well as to evaluate the efficacy of green spaces (parks, roof gardens and vertical green walls) and blue spaces (ponds and lakes) in mitigating the effects of urban warming. This information, in association with a provided cost/benefit analysis, could prove useful in determining the value of using these techniques in areas of rapid urbanisation. A general assessment of public attitude, which was included, also provides information on the

perceptions of the public regarding urban climate change issues and willingness to change current practices.

Specifically, this study aims to answer the following research questions:

- How land use change, changes in surface layers, and demographic shifts (e.g. population growth) are associated with urban warming of Dhaka megacity? What are the factors influencing the UHI effect?

- How, and to what extent, urban morphology, material surface type, land use and green/blue spaces affect Dhaka's microclimate?

- What are the costs and possible benefits of introducing self–sustaining greenspace and green roofs into the urban environment, which can mitigate the adverse effects of climate change?

- What are the implications for government policies on possible changes to land use zoning and the development of practical, effective strategies for mitigating excessive urban warming?

- What specific policies are required for Dhaka megacity to adapt to a changing climate?

1.6 Report structure

This report details the results of research activities undertaken between August 2018 and December 2019. The final report structure reflects the spatial scale of each facet of the analysis conducted, from the 'mesoscale' to the 'microscale', and details the various in–field microclimate assessments conducted within the Dhaka Metropolitan Development Plan (DMDP) area of Bangladesh. The report has seven chapters, each of which elaborates data sources, pre– and post–processing, analytical techniques and major findings. Figure 1-1 provides a summary of the overall study process.

Chapter one describes the concept of the urban heat island (UHI) effect, methods of characterisation, influencing factors and various mitigation strategies adopted globally. It also explains the significance of this work, together with some specific research questions.

Chapter two explains the UHI intensity and its driving factors over the DMDP area. Time–series MODIS satellite data was used at the mesoscale, using data recorded at a low spatial but high temporal scale. This data was used to calculate the intensity of surface urban heat island (SUHI), during both daytime and nighttime, and across monthly, seasonal and annual scales.

This chapter also discusses land use/cover changes between 2000 and 2017 using multi–date Landsat data. Population data from two decennial census (e.g. 2001 and 2011) are used to understand the effect of land use/cover change and demographic shift on the SUHI. Finally, factors influencing the phenomenon at the mesoscale are analysed using spatial and statistical techniques.

Chapter three focuses on the SUHI feature and associated factors on a much smaller scale within the DMDP, an area known as the Dhaka Metropolitan Area (DMA). The analysis is based on 30 metre (m) resolution Landsat data to characterise daytime SUHI, and 90 m ASTER (Advanced Spaceborne Thermal Emission and Reflection Radiometer) data to map the nighttime SUHI. Landsat–based biophysical indices are also calculated to isolate factors associated with SUHI at the microscale.

Chapter four deals solely with the microclimate of the DMA across the four different seasons. In–situ measurements, comprising fixed weather stations and mobile traversing, are employed to determine variations in surface and canopy layer heat islands. In addition, data loggers were employed to understand thermal response of green/blue space over time. Using high resolution hand–held infrared camera, the thermo–physical behaviour of various urban features are investigated in detail. The effect of a vertical greening system in reducing temperature is measured and discussed. Finally, the effectiveness of rooftop plants and open space vegetation in reducing the effects of heating is explained.

Chapter five details the techniques used to develop a database on existing greenspaces in the Dhaka Metropolitan Area (DMA). An analysis of green roof retrofitting potential and suitable locations for greenspaces is also included.

Chapter six provides a cost–benefit assessment of green/blue space in the DMA based on data collected through households and corporate survey. In addition, users of public green and blue spaces were interviewed to determine willingness to pay for using any improved services.

Chapter seven details a range of mitigation measures, which have the potential to reduce urban heat in the megacity. The identification of these possible measures is based on an extensive literature review and findings from the current research. This chapter sheds light on policies, which should be considered in reducing the increasing temperature in the megacity. It includes a review of existing public polices in association with interviews conducted with key stakeholders.

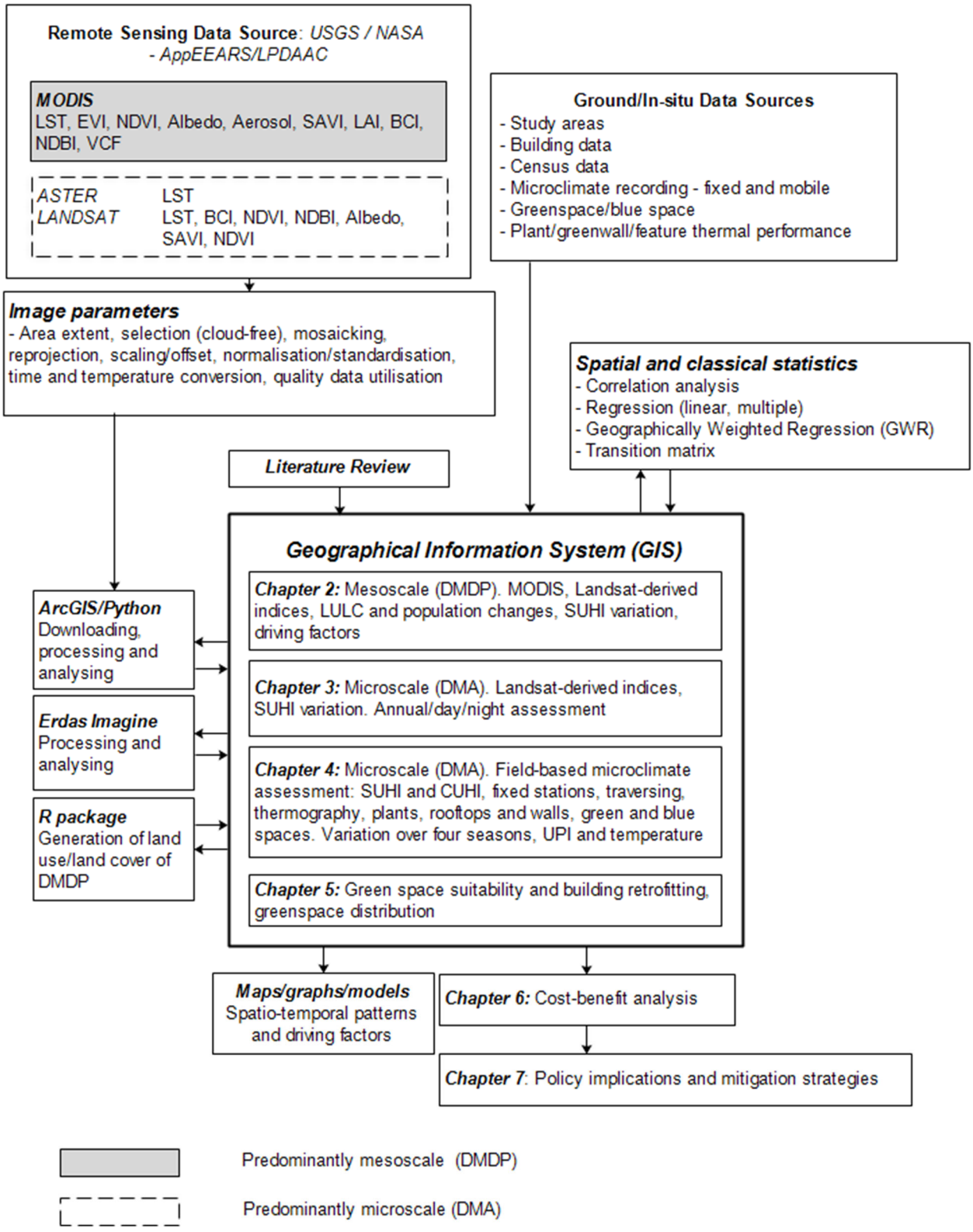

Figure 1–1 Flowchart of overall project

2 MESOSCALE ANALYSIS – DHAKA METROPOLITAN DEVELOPMENT PLAN (DMDP)

2.1 Introduction

This chapter describes the surface urban heat island (SUHI) phenomenon (including intensity and magnitude) at the mesoscale in the Dhaka Metropolitan Development Plan (DMDP) area, for the period 2003 to 2018. It examines land use/cover (LULC) change, based on multi–temporal Landsat data. Population data from two recent censuses and percent built–up area was used to establish the relationship between demographic shift, land use/cover change and SUHI. Biophysical indices obtained from MODIS products were used to determine possible factors influencing the SUHI at the mesoscale.

2.2 Description of the study area

This chapter is focused on the DMDP area in Bangladesh (centred on latitude 23.50°, longitude 90.25°) (Figure 2–1), an area delineated in the early nineties by RAJUK, the capital development authority (SENES Consultants Limited, 2007). The study area defines the limits of the fifty *upazila* (sub–district), otherwise known as *thana* (administrative boundaries), which make up the DMDP. The area is located within a deltaic system, resulting from the confluence of three major river systems in Bangladesh, and covers an area of approximately 1,528 km^2. According to 2011 population and housing census, total population of DMDP area is 163,38,208 (http://www.bbs.gov.bd/), with a mean density of 1719 persons/ha. The urbanized parts of Dhaka occupy a floodplain area composed of an intricate system of rivers and natural drainage channels. As a result, most of the land within the delta lies about 2–6 m above MSL (mean sea level) except for the Mirpur highlands located along the central axis, where the elevations rise to about 13 m (SENES Consultants Limited, 2007). The population of Bangladesh was estimated at approximately 165 M people in 2017, of which >10 M are located within Dhaka itself (http://www.bbs.gov.bd/). It has a tropical monsoon climate characterised by wide seasonal variations in rainfall, high temperatures, and high humidity. The seasons of Bangladesh have been divided into four distinct periods – winter, pre–monsoon, monsoon and post–monsoon (Table 2–1). In general, the maximum summer temperatures range between 38 and 41 °C (100.4 and 105.8 degrees Fahrenheit (°F)). April is the hottest month in most parts of the country. January is the coolest month, when the average temperature for most of the country is 16–20 °C (61–68 °F) during the day and around 10 °C (50 °F) at night. Table 2–1 provides information on the definition of the four seasons used in this study.

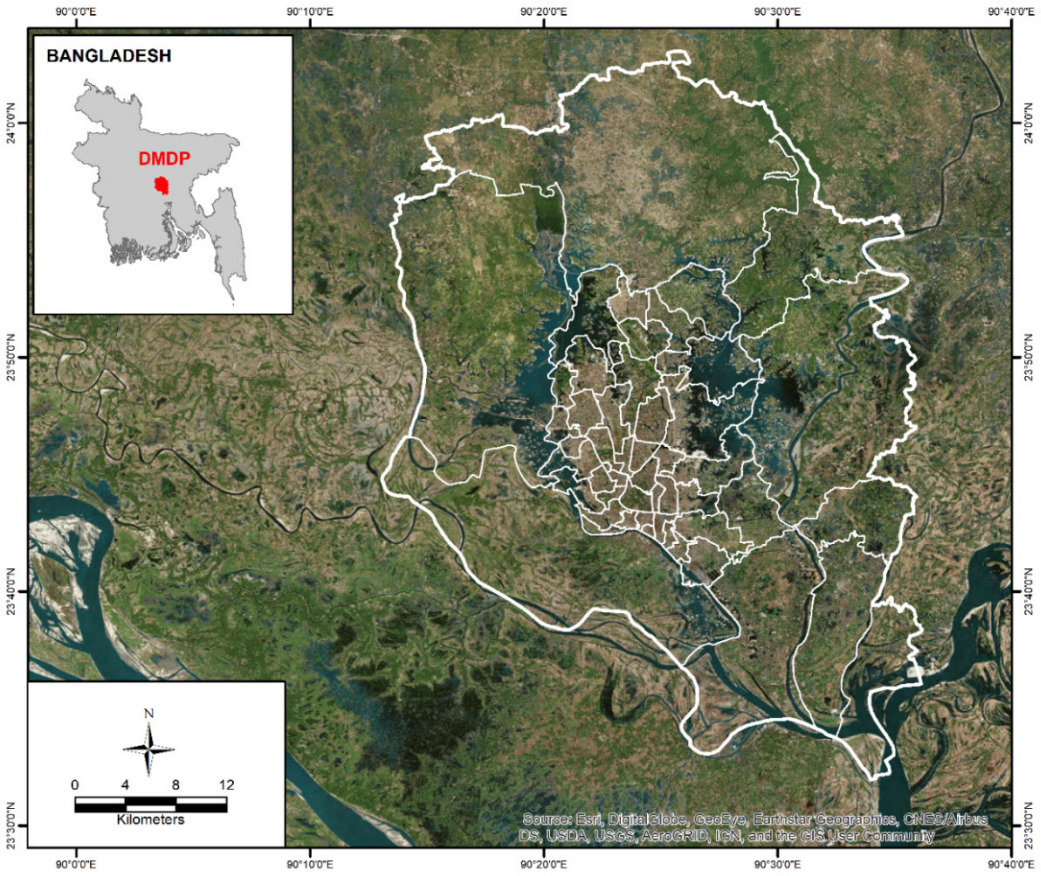

Figure 2–1 Location of the study area and boundary of administrative units (*Thana* or sub–district boundary is in white) of the Dhaka Metropolitan Development Plan (DMDP) area (image source: *ESRI, DigitalGlobe, Geoeye, EarthStar Geographics, CNES/Airbus DS, USDA, USGS, AeroGrid, IGN and the GIS User Community*)

Table 2–1 Definition of seasons

Months	Season
December–February	Winter
March–May	Pre–monsoon
June–September	Monsoon
October–November	Post–monsoon

2.3 Materials and methods

2.3.1 Satellite data preparation

Cloud–free Landsat Thematic Mapper/Enhanced Thematic Mapper Plus (TM/ETM+) and Landsat 8 (L8), the Operational Land Imager/Thermal Infrared Sensor (OLI/TIRS) imagery for

the years 2000 (December 20), 2004 (December 31), 2010 (December 16) and 2017 (December 03) was downloaded from the EarthExplorer website (https://earthexplorer.usgs.gov/). To minimize atmospheric disturbances in the datasets, only dry season images with <10% cloud cover were selected. Radiometric corrections were performed by converting raw digital numbers to top–of–atmosphere (TOA) reflectance (https://www.usgs.gov/land-resources/nli/landsat). Atmospheric corrections were also performed to remove any remaining atmospheric disturbances (e.g. haze) through identification of the darkest pixel value in each band and subtraction of this value from every image pixel (Song et al. 2001; Chavez, 1988). All thermal bands were excluded and only the reflective bands were used for LULC classification.

Moderate Resolution Imaging Spectroradiometer (MODIS) Version 6 data from 2000 to 2018 is available from both the Terra–MOD (10.30 am and 10.30 pm overpass) and Aqua–MYD (1.30 am and 1.30 pm overpass) satellites, providing both day and night recording ability and allowing the capture and use of thermal information (land surface temperature (LST)) over these intervals. The data is captured at a nominal spatial resolution of 1 km x 1 km. The Terra satellite commenced data collection on the 24th April, 2000 and Aqua on the 12th July, 2002. Raw, 8–day MOD11A2 and MYD11A2 LST day/night products for the period 2003 to 2018 was obtained with only clear sky pixels with an LST error of ≤ 2° K, emissivity error <= 0.02 and data quality/mandatory QA flags of 00 and 01 being selected for analysis. The images were rescaled and clipped to the DMDP boundary. The data was subsequently processed to provide annual, seasonal and monthly average datasets. The accuracy of the Version 6 LST data has been validated in a wide range of climatic regions and over different land cover types (Wan, 2014). In this study, a combined LST product (combining Terra and Aqua data for the 2003 to 2018 period) was used. A summary of all datasets is provided in Table 2–2.

A *thana* (sub–district) administrative boundary shape file was obtained from the Centre for Environmental and Geographic Information Services (http://cegisbd.com). This data consisted of the DMDP boundary, and included a major part of Dhaka megacity defined by the Bangladesh Bureau of Statistics (BBS) in 2008 (Dewan and Corner, 2014a). Sub–district level population data for the DMDP area for the years 2001 and 2011 was also obtained from BBS (http://www.bbs.gov.bd/). Separate Gridded Population of the World (GPW) data for 2000, 2005, 2010 and 2015, at a nominal resolution of 1 km (30 arc–second), was obtained from Socioeconomic Applications and Data Centre (SEDAC) hosted by CIESIN at Columbia University, providing estimates of population density based on counts consistent with national censuses and population registers (SEDAC, 2019).

Table 2–2 Summary of datasets used in the mesoscale analysis

Data	Further detail	Descriptor	Spatial resolution	Temporal resolution	Reference/Source
LST (Terra satellite) *LST (Aqua satellite)*	*Land Surface Temperature*	MOD11A2 MYD11A2	1 km 1 km	8 day (day/night) 8 day (day/night)	*DOI: 10.5067/MODIS/MOD11A2.006* *DOI: 10.5067/MODIS/MYD11A2.006*
NDVI/EVI	*Normalised Difference Vegetation Index /Enhanced Vegetation Index*	MOD13A2	1 km	16 day	*DOI: 10.5067/MODIS/MOD13A2.006*
BRDF/Albedo (Shortwave)	*BRDF (Bidirectional Reflectance Distribution Function) /Albedo – WSA/BSA – White/Black Sky Albedo*	MCD43A3	500 m	daily	*DOI: 10.5067/MODIS/MCD43A3.006*
AOD	*Aerosol Optical Depth*	MCD19A4	1 km	daily	*DOI: 10.5067/MODIS/MCD19A4.006*
LAI	*Leaf Area Index*	MCD15A2H	500 m	8 day	*DOI:10.5067/MODIS/MCD15A2H.006*
VCF (ptc, pntc, pnv)	*Vegetation Continuous Fields*	MOD44B	250 m	Annual	*DOI: 10.5067/MODIS/MOD44B.006*
Land cover	–	MCD12Q1	500 m	Annual	*DOI: 10.5067/MODIS/MCD12Q1.006*
BCI	*Biophysical Composition Index*	MODIS NBAR	500 m	NA	*Derived from NBAR Reflectance*
SAVI	*Soil–Adjusted Vegetation Index*	MODIS NBAR	1 km	NA	*Derived from NBAR Reflectance*
NDBI	*Normalised Difference Built-up Index*	MODIS NBAR	500 m	NA	*Derived from NBAR Reflectance*
ISA Vr–NIR–BI	*Impervious Surface Abundance* *Spectral Built–up Index*	Landsat	30 m	2000, 2004, 2010, 2017	*Derived from Landsat images*
Land use/cover	–	Landsat	30 m	2000, 2004, 2010, 2017	*Derived from Landsat images*
Gridded population density	*NA*	GPW4	1 km	2000, 2005, 2010, 2015	*http://sedac.ciesin.columbia.edu/data/collection/gpw-v4*
Population	*NA*	Sub–district level	Tabular	2001, 2011	*http://www.bbs.gov.bd.*
Administrative unit	*NA*	*Thana*/Sub–district	vector	2017	*http://cegisbd.com*

2.3.2 Extracting indices from MODIS and Landsat sensors

Although normalised difference vegetation index (NDVI), enhanced vegetation index (EVI), albedo products (WSA and BSA), vegetation continuous function (VCF), and leaf area index (LAI) are readily available (with associated quality flag) from the Land Processes Distributed Active Archive Center (LPDAAC) (https://lpdaac.usgs.gov/), a number of other indices needed to be generated from the MODIS NBAR (Nadir BRDF–Adjusted Reflectance) data to aid the analysis. The Aerosol Optical Depth (AOD) was retrieved from the MCD19A4 product and only green band (0.55 μm) over land was extracted to derive multi–temporal AOD data. The methods associated with other indices are:

a) Biophysical composition index (BCI): The biophysical composition index is believed to assist in estimating impervious surface abundance from remotely sensed data (Deng and Wu, 2012). The MCD43A4 NBAR was used to compute BCI over the study area from 2003 to 2018. The coefficients to use for estimating tasselled cap transformation (a requirement for the BCI computation) from the MODIS NBAR data was obtained from Wu et al. (2013). Details regarding this method can be found in Deng and Wu (2012). Monthly, seasonal and annual scale BCI datasets were produced.

b) Normalised difference built–up index (NDBI): This index was designed to aid the mapping of land cover classes – most notably built–up land (Zha et al. 2003). Reflectance in the SWIR against NIR regions of the electromagnetic spectrum are normally greater for built–up area than for vegetated area, allowing for the standardised differentiation of these bands to form the index (Zha et al. 2003). NDBI ranges from –1.0 to 1.0, where values close to 0 refer to vegetation, negative values refer to waterbodies and positive values refer to built–up surface.

c) Soil–adjusted vegetation index (SAVI) is calculated as:

   SAVI = (NIR–RED)/(NIR+ RED+L) * (1+L)

   where, L = scale factor ranging from 0 (for highly vegetated areas) to 1 (for no vegetation cover). For this study, L = 0.5 is used. This index was first established to distinguish and minimise soil brightness from canopy spectra (Huete, 1988), in areas with low vegetation coverage (generally <40 %) and where the soil surface is exposed, soil may reflect different amounts of light to the sensor which may result in incorrect measurements (Huete, 1988). The scale factor, L, controls the normalised difference vegetation index component of the equation to mitigate reflectance from soil (Huete, 1988). SAVI has a range of –1 to 1, where higher values indicate greater amounts of vegetation.

Information and further details on the particular algorithms used to generate the different products and any associated processing requirements can be found at: https://lpdaac.usgs.gov/dataset_discovery/modis/modis_products_table

Apart from the MODIS–derived indices, this study also computed two indices based on multi–date Landsat images. They were:

a) Impervious surface abundance (ISA): Wu and Murray (2003) proposed a method to estimate ISA from remotely sensed data. The same method was used to extract ISA over the DMDP from Landsat data. As the ISA algorithm requires waterbodies to be masked out, a modified normalised difference water index (MNDWI) (Xu, 2006) from Landsat images was first extracted and the spectral profile tool of an image processing software was used to obtain endmember pixels. Four types of endmembers were selected for vegetation, high albedo, low albedo and soil, and used in the linear unmixing model. The fraction of impervious surface for each pixel was then estimated from the sum of fractions of high albedo and low albedo (Wu and Murray, 2003).

b) Vr–NIR–BI: Landsat red and near–infrared bands were utilised to derive spectral–based built–up index over the DMDP for four years. This index is useful in estimating impervious surfaces of an urban area (Estoque and Murayama, 2015).

Upon deriving the required satellite–based products, all datasets, excluding vector–based data such as census population and Landsat derived LULC, were resampled to 1 km to align with the MODIS products. A summary of the study workflow is shown in Figure 2–2.

2.4 Analytical techniques

2.4.1 Land use/land cover (LULC) classification

Cloud–free Landsat data for the 2000, 2004, 2010 and 2017 years were processed to develop land use/land cover (LULC) datasets for determining changes over time. Dewan and Yamaguchi (2009) demonstrated that six land cover types can be effectively mapped from medium–resolution Landsat data over the greater Dhaka area, and the same classification scheme was adopted here. The training data for the six LULC types (Table 2–3) was generated using a visual interpretation of the land cover patches in Google Earth images (Google Earth, 2018). Between 800 and 900 training samples were defined for each of the years (comprising about 150 training samples for each of the land cover classes). These were used to train each of the Random Forest (RF) classifier models, which provided the final datasets. The training samples were selected at random from throughout the study area.

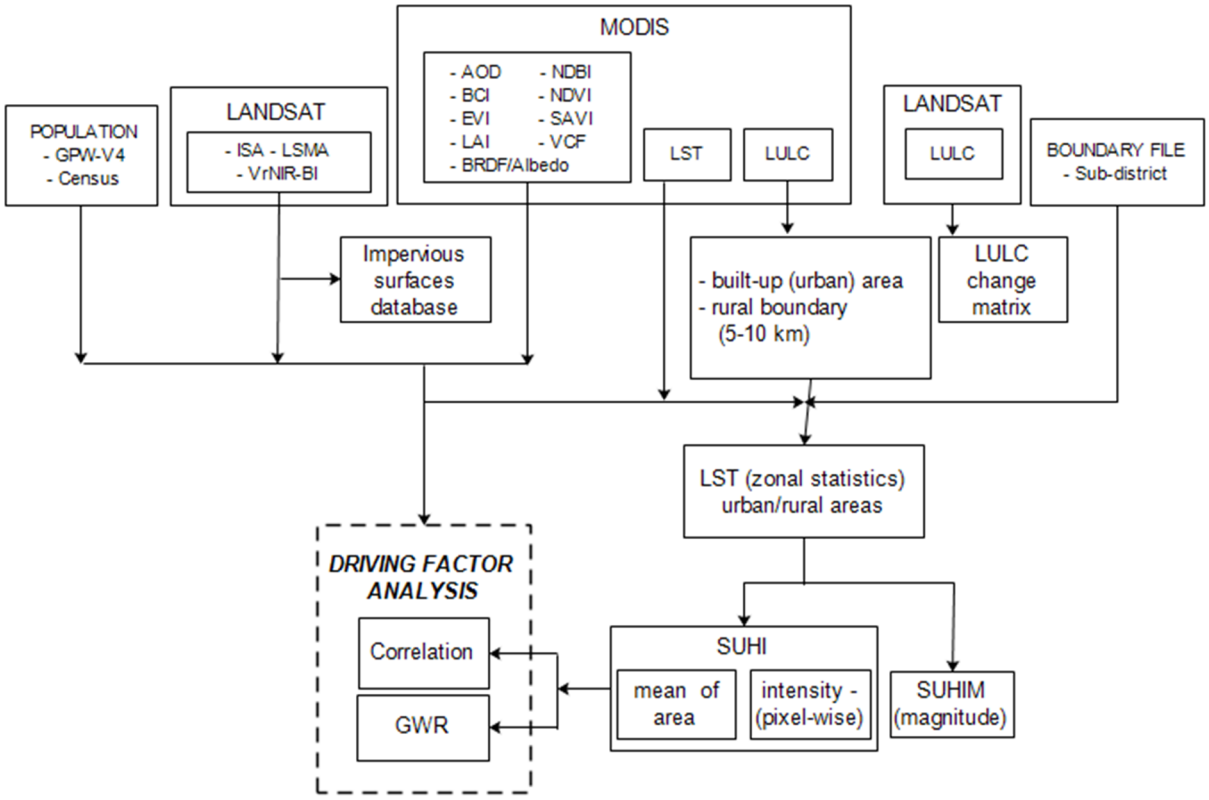

Figure 2–2 Flowchart, showing methods used for mesoscale analysis

Table 2–3 LULC classification scheme

LULC types	Description
Built–up	Residential, commercial and services, industrial, transportation, roads, mixed urban, and other urban
Bare soil	Exposed soils, landfill sites, and area of active excavation
Cultivated land	Agricultural lands, crop fields, fallow lands and vegetable lands
Vegetation	Deciduous forest, mixed forest lands, palms, conifer, scrub and others
Wetland/lowlands	Permanent and seasonal wetlands, low–lying areas, marshy land, rills and gully, swamps
Waterbodies	River systems, permanent open water, lakes, ponds

Adapted from Dewan and Yamaguchi (2009)

To assist in the identification of LULC classes and the training data sample generation process, for each of the years a normalized differential vegetation index (NDVI) (Rouse et al. 1974), normalized difference water index (NDWI) (McFeeters, 1996), and normalized difference built–up index (NDBI) (Zha et al. 2003) were produced. Areas of land were assigned to a particular class using the Google Earth images, and then validated using the NDVI, NDWI and NDBI data. Only the training samples that were consistent across all three indices were retained in the dataset.

The random forest classification was carried out using the 'randomForest' package in R (https://www.r-project.org). The training samples produced from the Google Earth images were further randomly split into a training dataset (75%) and a test dataset (25%). The number of decision trees (ntree) was set to 500 and the number of input predictors (mtry) was obtained based on the lowest inspect out–of–bag (OOB) error rates. In general, the models comprising an mtry value of three were found to yield the lowest OOB error rates. The final model, trained using the aforementioned parameter settings, was used to classify the satellite images. Although a feature selection process contributes to an increased accuracy, it is only necessary when the number of variables predicting LULC is large (Hapfelmeir and Ulm, 2014). As the total number of variables (the reflected bands) ranged from six to seven (six for TM/ETM+ and seven for L8), no feature selection process was required to remove the least important variables. Hence, all the available bands of Landsat images were used during the training of the final model. Finally, the user's accuracy and kappa coefficient was estimated using the test dataset. As the test dataset already contained information pertaining to the LULC classes, accuracy assessments were then carried out by the 'randomForest' package to evaluate how many of the pixels in the classified images were in agreement with the class–related information stored in the testing dataset LULC conversions, 2000–2017.

The classified LULC images were used to generate conversion maps as well as associated statistical tables for the 2000–2017 period. A LULC conversion matrix was used to obtain spatial and temporal changes in LULC during three intervals, 2000–2004, 2004–2010 and 2010–2017. A pixel–by–pixel cross tabulation assessment was performed to determine land cover conversions from one category to another, and the corresponding area was calculated. To understand homogeneity/dispersion of any spatial phenomenon (such as urbanisation), a map density matrix was used. The density was calculated by dividing the number of built–up pixels by the total number of pixels in a 3 x 3 kernel (Sudhira et al. 2004). Nine density classes were initially produced, which were subsequently reclassified into three density groups (low, medium and high). Area statistics were then computed for the defined groups.

2.4.2 Analysis of population change and built–up land dynamics

Population census data for 2001 and 2011 was encoded to each sub–district boundary. As the 2004 and 2017 census data was missing, a mean of 1.05 annual population growth rate was employed to estimate the total population of each sub–district. Multi–temporal LULC data, obtained from Landsat images, was used to calculate the built–up surface for each *thana* or sub–district. A regression analysis incorporating population density and percent built–up land for each year (i.e. 2000, 2004, 2010 and 2017) was conducted to determine the effect of demographic shift on built–up surface. As the census years are 2001 and 2011, it was decided that it would be suitable to use the population of 2001 and 2011 in the regression model for the 2000 and 2010 built–up cover.

A series of regression models were also constructed to examine the effect of population density and percent built–up land on surface urban heat island (SUHI) in the DMDP area. Population density and percent built–up land in 2004, 2010 and 2017 were extracted for each sub–district of DMDP. No attempt was made to regress against 2000 SUHI as this data was not available. The mean SUHI intensity, in degree Celsius, was calculated using MODIS LST data for each of the sub–districts (see sub–section 2.4.4). The SUHI was used as the dependent variable with percent built–up and population density as the independent variables.

2.4.3 Land surface temperature (LST) by LULC

Initially, Landsat–derived LULC was used to compute the thermal response of each land use/cover category over seasonal and annual time scales. Due to the leapfrog type of urban development in the DMDP area, particularly in recent times, this was not possible. Additionally, the rural boundary to be used for SUHI estimation was difficult to obtain with Landsat–derived LULC data because the images contained only the DMDP area. Furthermore, concurrency of LULC data in accurately estimating SUHI was suggested (Zhao et al. 2016). Therefore, the MODIS MCD12Q1 annual Combined Land Cover 500 m dataset (containing Land Cover Type 1: Annual International Geosphere–Biosphere Programme (IGBP) classification) (Sulla–Menashe and Friedl, 2018) was employed in this work to determine the thermal response of the LULC categories. The original IGBP system consisted of 17 classes, of which Class 13 (urban and built–up) was used as the identified urban core area for subsequent SUHI calculations. The original 2003 to 2017 MCD12Q1 rasters were reclassified from the original 17 class IGBP to one consisting of eight classes (Table 2–4). The original MCD12Q1 data were resampled to 1 km to match with multi–temporal LST and to aid in the analysis of SUHI. Two subsets were created: i) an urban/built–up area (denoted by a pixel value of 13); and ii) a rural area, defined by a 5–10 km buffer from the existing built–up or urban boundary. The rural buffer layer was dynamically constructed using yearly MODIS LULC data as a fixed urban boundary had the potential to produce erroneous results at the various temporal scales used. An example of the dynamic buffering for years 2003 and 2017 is shown in Figure 2–3. Water and built–up/urban pixels have been removed from the rural buffer area to negate any impacts on the SUHI calculations (Chakraborty and Li, 2019). The initial requirement was to define LST for each of the land cover classes, principally urban and rural.

Table 2–4 Reclassified LULC data based on MODIS IGBP classification

Name	Original	New	Name	Original	New
Forest	1–5	1	Urban/Built–up	13	5
Grassland, shrub land	6–10	2	Snow and Ice	15	6
Permanent wetlands	11	3	Barren	16	7
Croplands	12, 14	4	Water Bodies	17	8

(https://lpdaac.usgs.gov/sites/default/files/public/product_documentation/mcd12_user_guide_v6.pdf)

2.4.4 Surface urban heat island (SUHI) computation

The SUHI calculation requires a clear definition of the urban and sub–urban/rural area to be used for intensity comparisons. The SUHII (intensity) has been defined as the difference in temperature between an urban centre and the less urbanised city outskirts (Peng et al. 2011). The current study defines and evaluates the intensity in two distinct ways: (i) the area–wise difference in LST between urban and rural locations, and (i) the pixel–wise difference in LST between urban and rural settings. The first case is commonly used in studies of several cities (Sun et al. 2019; Peng et al. 2011), while the second case is mostly applicable to a single city scenario (Guo et al. 2015). The literature provides a number of different techniques for generating the ex–urban area, including using a percentage of the calculated urban area (Zhou et al. 2014; Peng et al. 2011), as well as using defined distances from the urban core (Clinton and Gong, 2013). As noted above, 8 day Aqua–Terra (MYD11A2 and MOD11A2) composites were combined to produce separate day and nighttime LST data. The rationale for doing this was that using the combined data would provide a more accurate LST estimate given that the data would average all four data capture times (Lai et al. 2018a, b; Yao et al. 2018b). The data was further processed to produce average monthly, seasonal and yearly datasets for the period 2003 to 2018 (the period when both the Terra and Aqua sensors were operational and a complete annual data interval was captured). The definition of seasons has been shown previously in Table 2–1.

Intensity has been defined in this report as the difference in observed LST between an urban core and the less urbanised city outskirts, i.e. in areas less affected by the UHI effects. Imhoff et al. (2010) in the USA, define an unaffected rural area 45–50 kilometres from the urban area. Yao et al. (2018b), in an analysis of 31 cities in China, consider a 20–25 km buffer around the urban area of Beijing to use as a rural reference. The current study uses a buffer, however since the DMDP's areal extent is substantially smaller than that of other cities such as Beijing, a 5–10 km buffer from the existing urban boundary was used to define the "rural" area (Figure 2–3). Sixteen buffer polygons (2003–2018) were derived due to the fact that the urban pixels change every year. The rural area LST, averaged separately for day and nighttime, was used to reflect background variability with the assumption that this area was not impacted by any

possible UHI effects. The urban area was extracted from the MODIS land cover, and was then used to extract the temperature of the urban surface. The mean LST between urban and rural pixels was obtained and SUHI intensity/magnitude was estimated over the monthly, seasonal and annual periods. Note that many studies use surface urban heat island intensity (SUHII) to characterise the effect, but this study uses the term SUHI to represent the same phenomenon. Therefore, SUHII/SUHI is used interchangeably in this report.

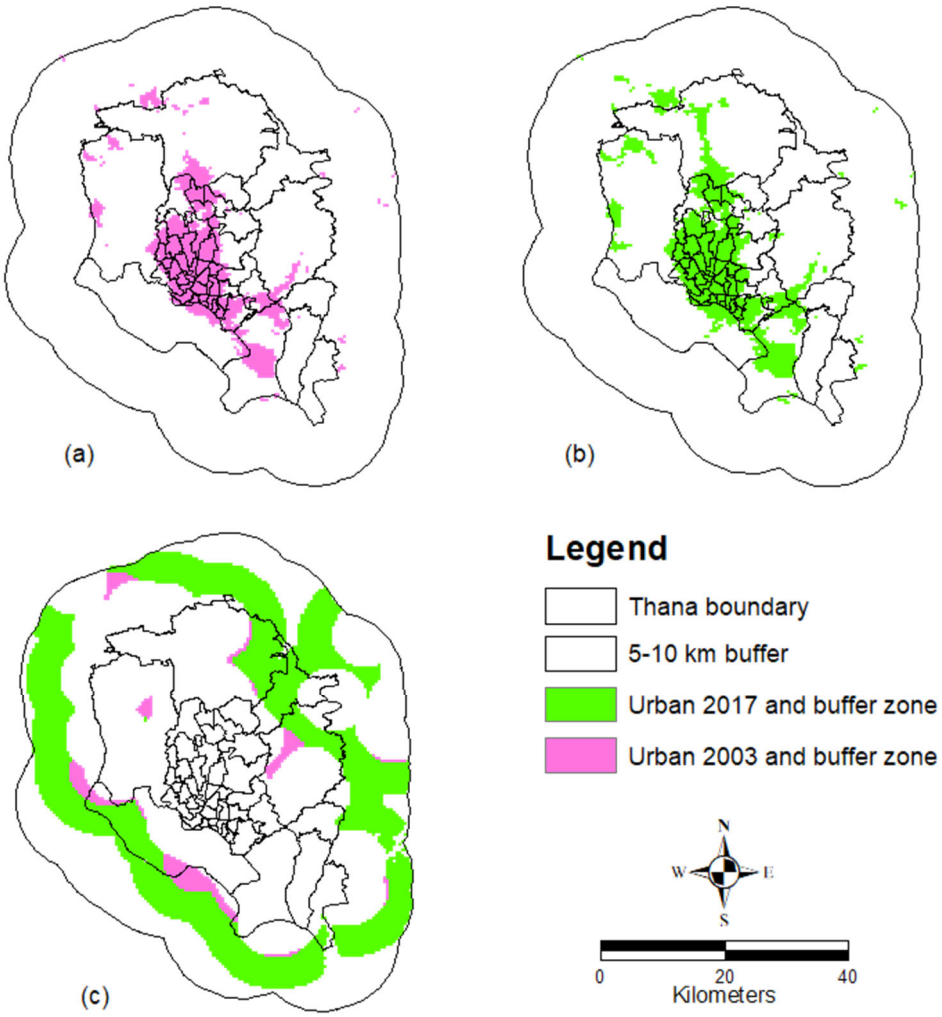

Figure 2–3 Rural boundary defined by 5–10 km buffer from existing built–up locations: a) Urban area in 2003 with 5–10 km buffer; b) Urban area in 2017 with 5–10 km buffer; and c) combined buffers for 2003 and 2017

2.4.5 SUHI magnitude (SUHIM)

The SUHIM can be defined as the difference between the average LST of the warmest quarter of the year and annual average LST over a defined period (Rajasekar and Weng, 2009; Metz et al. 2014; Nastran et al. 2019). Yao et al. (2018a) defined the heat magnitude as the changes in LST and SUHI in hot summers: LST in hot summer minus the LST in other summers. Hot

summers were defined as the average LST in the hottest three summers and the LST of other summers was the average of the remaining summers over the period of study. Due to the volume of data acquired, this calculation was difficult to use successfully. Moreover, coldness (used in other studies) is not relevant in the study area. This work utilises the methodology detailed in Nastran et al. (2019), and defines the magnitude as the difference between the average LST of the hottest quarter of the year (pre–monsoon was regarded as the hottest quarter) and annual average LST over the 2003–2018 period. Pixel–wise aggregation was carried out to extract the spatial distribution of the UHI magnitude over the entire period.

2.4.6 Space–time variation of SUHI

To determine the degree of SUHI clustering or dispersion, annual SUHI data was utilised to retrieve pixels with various values (e.g. >= 0.5 °C, <=2 °C etc.) from separate day and night data. These were mapped to give an indication of the spatial changes of SUHI within the DMDP area. The individual pixel area was then converted to km^2.

2.4.7 Driving factor analysis

SUHI has been shown to be influenced by many factors, including physical (e.g. albedo) and anthropogenic (e.g. urbanisation) (Rizwan et al. 2008), however these factors seem to vary according to locations, timing and season (Giridharan and Emmanuel, 2018; Deilami et al. 2018). Various factors, derived from both satellite images and other sources, were used to examine those most affecting SUHI in the DMDP area. The following sections describe the statistical methods used to isolate the most influential factors.

2.4.7.1 Correlation analysis

Sixteen variables, comprising five groups of covariates, were used (Table 2–5). The most important variable from each of these groups was chosen based on the strength of correlation with SUHI. Two pair–wise Pearsons's correlation coefficients were separately produced for day and night using the mean annual values of the covariates. This process allowed a detailed examination of the interrelationship between the potential predictor variables. Two correlation matrices (between the dependent and independent variables) were constructed to isolate the variables to be used in the global and local regression analyses.

2.4.7.2 Grid–based correlation analysis

To assist in understanding the factors influencing SUHI, r values for individual grids were obtained using the Pearson's product–moment correlation coefficient (r). Tests for significance of r were performed at the 95 and 99% significance level. This analysis was restricted to the seasonal scale.

Table 2–5 Variable groups used in this analysis

Groups	Variables
Vegetation indices	Normalised difference vegetation index (ndvi); Enhanced vegetation index (evi); Leaf area index (lai); Soil–adjusted vegetation index (savi); Vegetation Continuous Field (vcf) – Percent_tree_cover (ptc), Percent_non_vegetated (nv), Percent_nonTree_Vegetation (ntv)
Aerosol	Aerosol optical depth (aod)
Albedo (shortwave)	Black–Sky Albedo (bsa); White–Sky Albedo (wsa)
Demographic	Total population (poptot); population density (popden)
Imperviousness	Biophysical composition index (bci); Normalised difference built–up index (ndbi); Vr–NIR–BI (isabi); ISA

2.4.7.3 Global and local regressions

Spatial statistics were used to determine the spatial relationships between SUHI and the defined environmental variables. Ordinary Least Square (OLS) is a global regression model that can be used to examine predictors which are free from multi–collinearity, where coefficients are statistically significant, and where the residuals are not spatially correlated (ESRI, 2011). However, the OLS examines variables globally and can give misleading results when applied to phenomena that vary over space (Clement et al. 2009) or variables which are spatially autocorrelated. Based on the variance inflation factor (VIF), variables with values >=8 were removed (ESRI, 2012). The residuals from OLS were then tested. The results indicated that the data were not normally distributed. Further modelling was then used to investigate the spatial relationships at the local level.

A geographically weighted regression (GWR) technique examines spatial dependency and local variability. This technique is particularly suitable for identifying local factors that affect geographical phenomenon such as SUHI (Fotheringham et al. 2001). A user–defined bandwidth (in terms of an adaptive kernel) was used, and the outputs of two models (e.g. OLS and GWR) were tested using the Akaike Information Criterion (AIC). Both annualised day and night SUHI were included as dependent variables while the annual average of factors (e.g. ndvi, evi, aod etc.) was used as independent variables in the local and global regression models. Separate day and night models were executed.

2.5 Results

2.5.1 LULC changes

Changes in the spatial patterns of LULC in the DMDP area are evident for the period from 2000 to 2017 (Figure 2–4). The predominant expansion direction of the built–up areas has been

essentially along a north–south axis. An analysis of the area statistics indicates that built–up areas increased from 11,122 ha to 58,310 ha during the study period, an increase from 6.5% to 34% of the available land area. Only cultivated land makes up a greater proportion (44%), however this figure also experienced a decrease from 2000, when 53% of the area was under cultivation (Table 2–6). Similarly, vegetation and wetland/lowland areas decreased. The waterbody statistics show an anomalous low value (4.9%) in 2000, with the 2004 value being almost 300 percent higher before trending back to a value of 5.8% in 2017, probably due to climatic–related factors such as flooding that may have resulted in pixels misclassification.

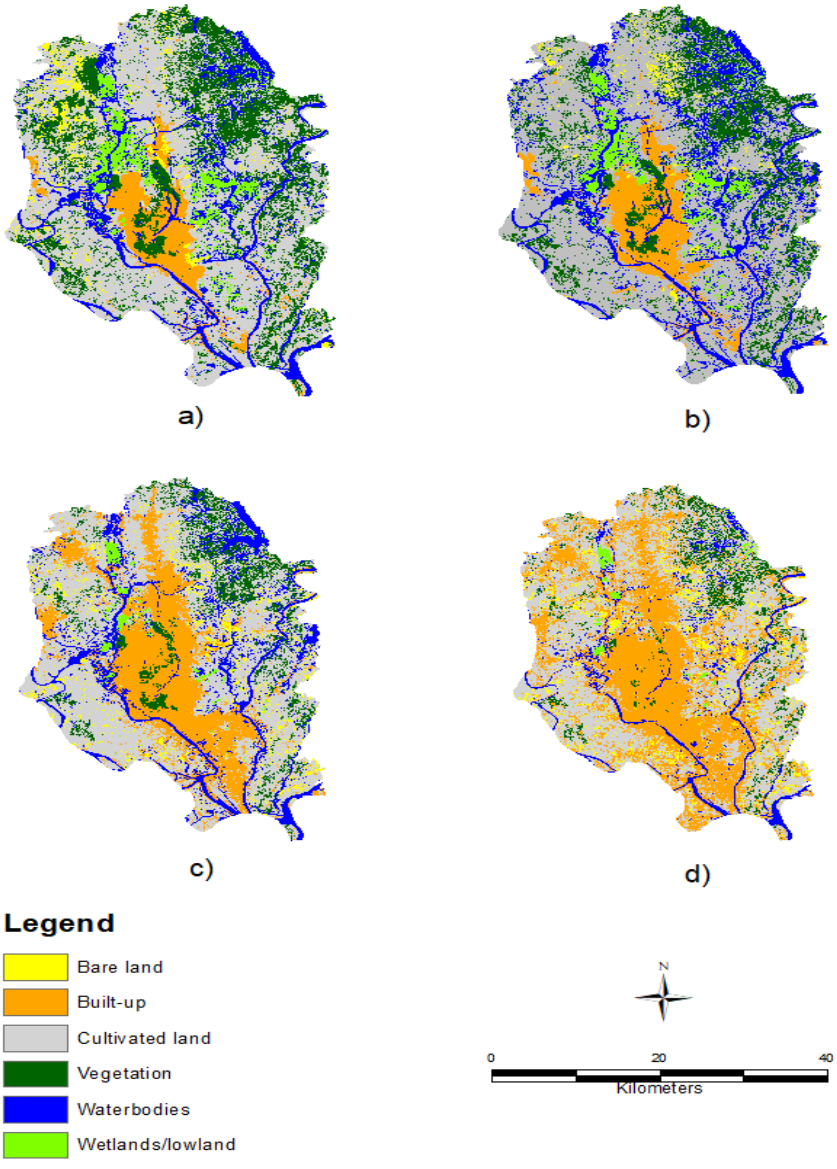

Figure 2–4 Classified LULC maps of the DMDP: a) 2000; b) 2004; c) 2010; and d) 2017

The "from–to" statistics show that the amount of cultivated land transformed to built–up increased by 400% in 2000 to 2010 (from 2.5% to 11% of the area) but increased only slightly

from 2010 to 2017 to 12% (Table 2–7). The vegetation category has been a major source for agriculture and built–up category over the study area. Figure 2–5 provides details on the major LULC conversions during the three periods.

Table 2–6 LULC classification for the period 2000–2017

Class	2000		2004		2010		2017	
	Area (ha)	%	Area (ha)	%	Area (ha)	%	Area (ha)	%
1 Cultivated Land	91720.6	53.8	85801.1	50.3	82837.4	48.5	76124.9	44.6
2 Built–up	11122.4	6.5	13453.6	7.9	35628.0	20.9	58310.2	34.2
3 Bare Land	6393.5	3.7	2880.9	1.7	7212.0	4.2	8829.5	5.2
4 Waterbodies	8322.4	4.9	27426.3	16.1	21567.0	12.6	9962.73	5.8
5 Vegetation	45407.6	26.6	33955.5	19.9	20888.2	12.2	15508.2	9.1
6 Wet/Lowlands	7674.4	4.5	7123.59	4.2	2508.3	1.5	1905.4	1.1

Table 2–7 LULC conversions for the 2000 to 2017 period

'From Class'	'To Class'	2000–2004		2004–2010		2010–2017	
		Area (ha)	%	Area (ha)	%	Area (ha)	%
Cultivated land	Built–up	3729.4	2.5	16294.0	11	17800.6	12
	Bare land	1402.4	0.9	359.1	0.2	798.8	0.5
Bare land	Cultivated	4197.1	2.8	909.4	0.6	3664.0	2.5
	Built–up	611.8	0.4	506.5	0.3	394.2	0.3
Vegetation	Cultivated	6017.4	4.1	3571.3	2.4	2677.8	1.8
	Built–up	610.3	0.4	697.4	0.5	1714.5	1.2
	Bare land	94.5	0.1	5723.5	3.9	98.7	0.1
Wet/Lowland	Cultivated	434.5	0.3	2398.9	1.6	612.99	0.4
	Built–up	87.4	0.1	1577.9	1.1	307.8	0.2
	Bare land	7.1	0.0	327.2	0.2	213.2	0.1
Waterbodies	Cultivated	599.9	0.4	4913.4	4.3	5974.6	4.0
	Built–up	185.0	0.1	1996.2	1.4	3496.7	2.4
	Bare and	44.3	0.0	313.2	0.2	640.4	0.4

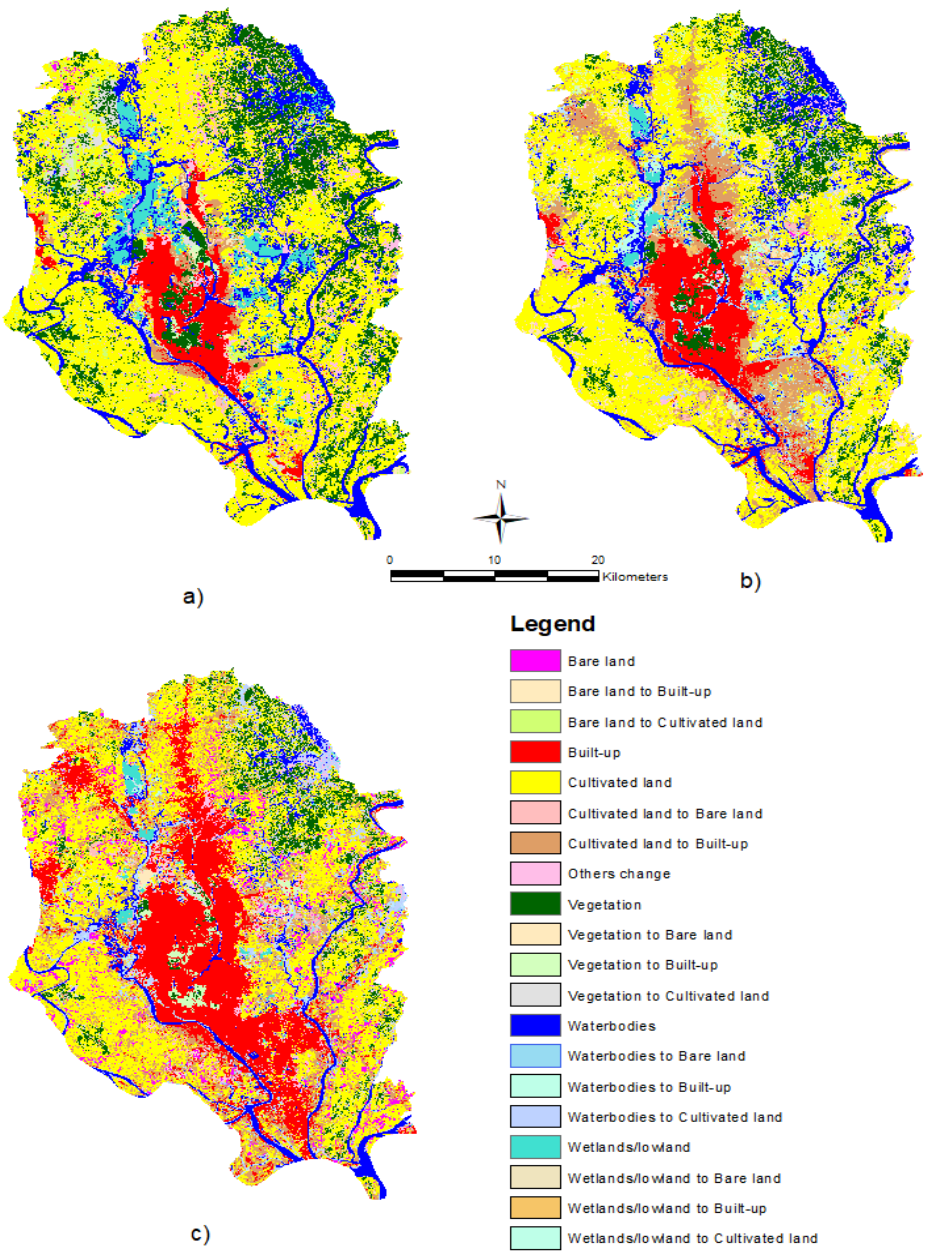

Figure 2–5 Major LULC conversions: a) 2000–2004; b) 2004–2010; and c) 2010–2017

The statistics produced from the map density estimation are shown in Table 2–8. The results indicate that the percentage of low–density areas initially decreased from 2000 to 2010, but then increased in the years to 2017 when it reached 30.2%. Medium density shows a general increase from 13.7% in 2000 to 19.0% in 2017. The percentage of high density increased from 58.9% in 2000 to 61.8% in 2010 before declining to 50.7% in 2017. An inspection of Figure 2–6 suggests that most of the high–density expansion is associated with the established urban areas, with low and medium density development occurring around the city periphery and along the road networks.

Table 2–8 Density of built–up surface between 2000 and 2017

	2000		2004		2010		2017	
	Area (ha)	%	Area (ha)	%	Area (ha)	%	Area (ha)	%
Low	4215.24	27.38	4777.38	25.04	8846.01	19.94	24632.91	30.26
Med	2112.48	13.72	2497.23	13.09	6293.7	14.18	15480.72	19.01
High	9070.38	58.91	11804.94	61.87	29232.9	65.88	41301.09	50.73

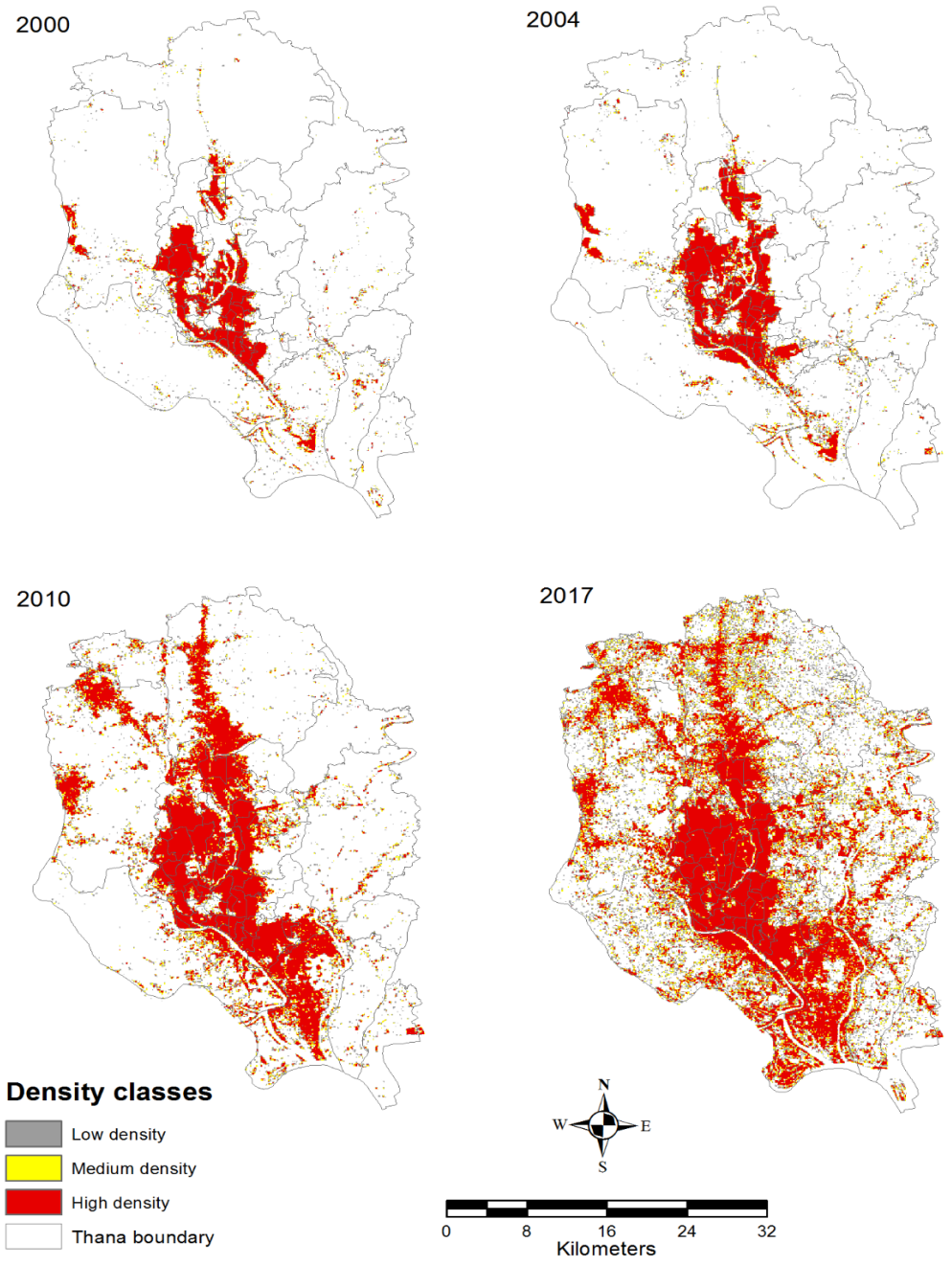

Figure 2–6 Density of built–up surface between 2000 and 2017

Population change in each sub–district for the years 2001 and 2011 was examined. The 2001 population in each sub–district was subtracted from the 2011 population and then the derived value was divided by 10 to get the population change in the DMDP. Figure 2–7 shows the average population change (increase/decrease) over the 10–year period and is particularly useful in identifying which areas grew rapidly and which grew slowly. Except for a few sub–districts in the already developed urban core, many sub–districts (or *thana*) show a population rise as defined by the ≥ 0.5 standard deviation (Std. Dev.), particularly in the outskirts of DMDP.

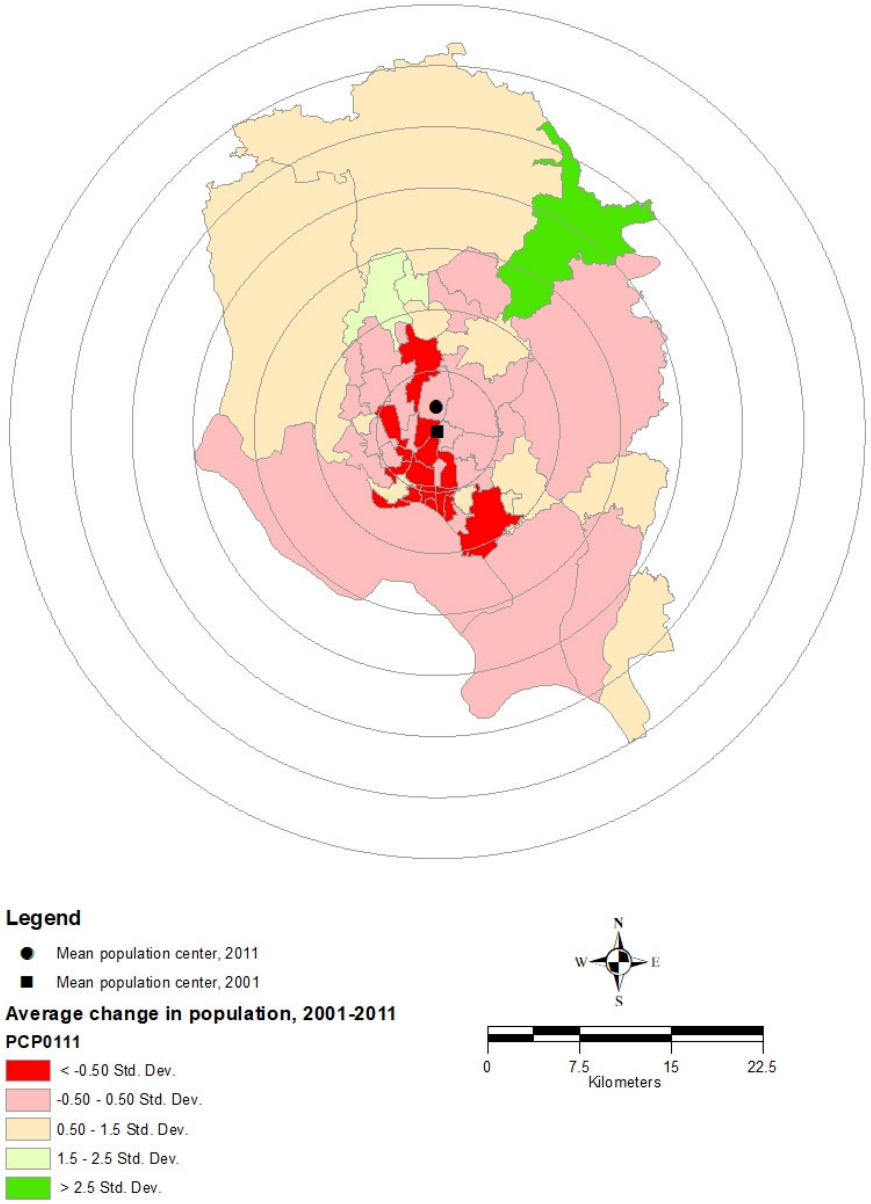

Figure 2–7 Average change in sub–district (*thana*) population, 2001–2011. Circles indicate annular buffers at 5 km intervals from mean population centre of 2001

2.5.2 Population change and built–up land dynamics

The scatterplots for individual years indicate that the relationship between population density and percent built–up area is essentially non–linear, except for the year 2010 when a linear relationship was observed (Figure 2–8, a–d). The relationship is statistically significantfor all years analysed. This means that there is obviously a relationship between urbanisation and population density, irrespective of the degree of linearity.

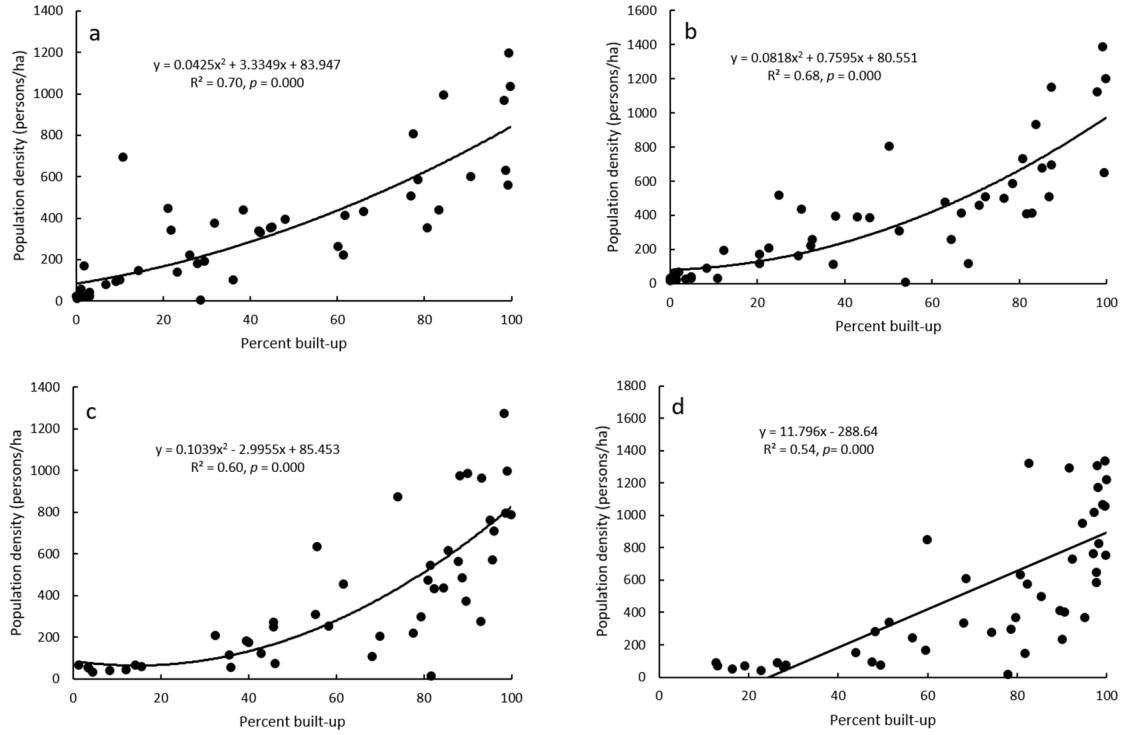

Figure 2–8 Relationship between percent of built–up land and population density: a) 2000; b) 2004; c) 2010; and d) 2017

The distribution of population density and the changing extent of built–up surfaces, as well as the day and nighttime SUHI in the DMDP, was examined. Population density per unit area of built–up surface was computed for each sub–district and then a weighted population centre (ESRI, 2012) was computed for the 2001 and 2011 census years. Using the 2001 weighted population centre, a multiple buffer ring was created, resulting in seven annual buffers with an increment of 5 km from the mean population centre to the furthest sub–district (35 km) (Figure 2–7). The population density, proportion of built–up surface and mean SUHI in day and night were calculated. The results showed that the increase of built–up area in association with population density has been substantial during recent years. The magnitude is high in zone 3 to 5 for built–up land whilst the mean population density is estimated to be very high in zone 2 as compared to the other buffer zones (Figure 2–9, a–b).

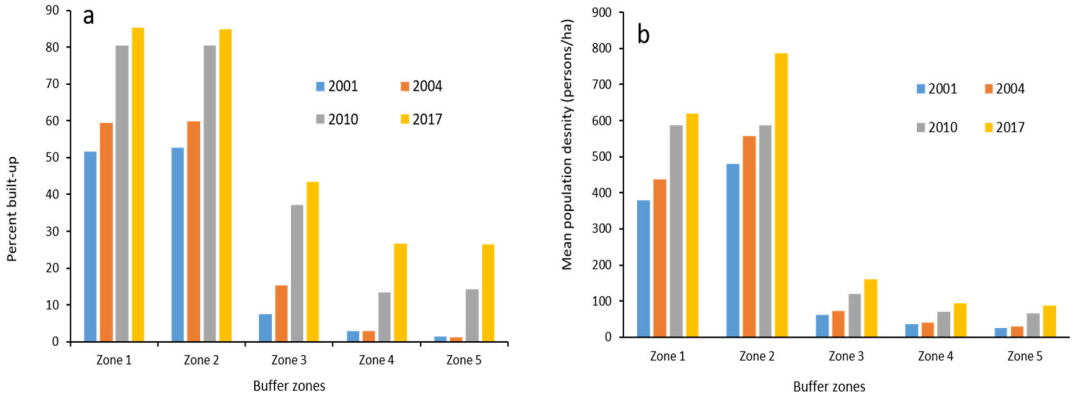

Figure 2–9 Characteristics of the five annular buffer zones from 2001 to 2017: a) percent built–up; b) mean population density

Figure 2–10 (a–b) demonstrates the mean SUHI in °C within the five annular buffer zones. One distinctive feature is that mean SUHI (during both day and night) appears to be increasing over time in almost all zones. However, mean SUHI is distinctively high in the main urban core. Analysis of the combined effect of population density and percent built–up on mean SUHI clearly indicates that these two anthropogenic variables are related to SUHI, both during the day and at night.

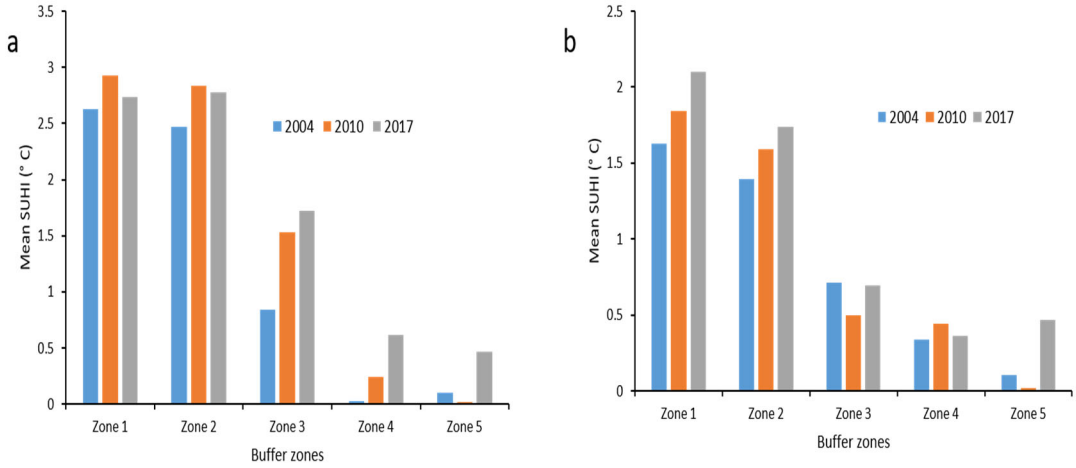

Figure 2–10 Mean SUHI of the five annular buffers: a) daytime; b) nighttime

To examine the effect of percent built–up land and population density on day and nighttime SUHI, a separate regression analysis was conducted with yearly day and night data, i.e. 2004, 2010 and 2017. Interestingly, the analysis shows statistically significant results with r^2 values ranging from 0.50 to 0.83. Table 2–9 shows regression statistics, which are considered useful in understanding the contribution of population density and percent built–up areas on day and

nighttime SUHI. The figures indicate that population density (popden) and percent built–up (pbuilt–up) are important predictors for both day and nighttime UHI in the DMDP area.

Table 2–9 Coefficients of causal factors and SUHI

Day/Night	Equation	r^2	*p*
Day 2004	SUHI = 2.1679(pbuilt–up$^{2)}$ + 14.608(pbuilt–up) + 4.3508	0.83	0.000
	SUHI = 72.26(popden$^{2)}$ – 56.529(popden) + 72.097	0.74	0.000
Night 2004	SUHI= 19.197(pbuilt–up)^2 + 11.661(pbuilt–up) – 3.1668	0.70	0.000
	SUHI = 18.514e$^{1.937\ (ppoden)}$	0.60	0.000
Day 2010	SUHI = 23.113 + 8.4605 (pbuilt–up)	0.80	0.000
	SUHI = 53.184e$^{0.6661\ (popden)}$	0.53	0.000
Night 2010	SUHI = 35.16 + 15.157 (pbuilt–up)	0.61	0.000
	SUHI = 43.396e$^{1.2985\ (popden)}$	0.66	0.000
Day 2017	SUHI = –4.1397(pbuilt–up)^2 + 40.769(pbuilt–up) + 3.8886	0.79	0.000
	SUHI = 56.277e$^{0.7746\ (popden)}$	0.50	0.000
Night 2017	SUHI = 32.015 + 22.804 (pbuilt–up)	0.82	0.000
	SUHI = 57.544e$^{1.1612\ (popden)}$	0.67	0.000

2.5.3 Response of LULC to LST

The thermal response of the dominant LULC categories (see Table 2–4) derived from combined MODIS LST data (day and night) was plotted on a box–and–whisker diagram (Figure 2–11). As snow and ice is not encountered in this area, only seven of the eight original variables were plotted. The analysis reveals that the mean annual LST for the built–up (or urban) category is considerably higher than that for all other categories during the daytime whilst waterbodies and wetland categories show minimum values. However, water and wetland categories had the opposite response during the night, which is to be expected due to their different thermal inertia. Another noticeable feature is that built–up and barren LULC show a similar type of thermal response at night. Cropland and grassland have a similar thermal response during daytime, but the nighttime temperature of grassland appears to be higher than that of cropland. Generally, the median value for the forest category is 29 °C during the day and, at night, is between 19 and 20 °C.

The urban and rural area differences in annual LST and other variables are plotted in Figure 2–12. These plots are instrumental in showing the effect of urbanisation and population growth on local temperature in the study area. Notably both day and nighttime temperatures in urban areas are considerably higher than those in the rural area.

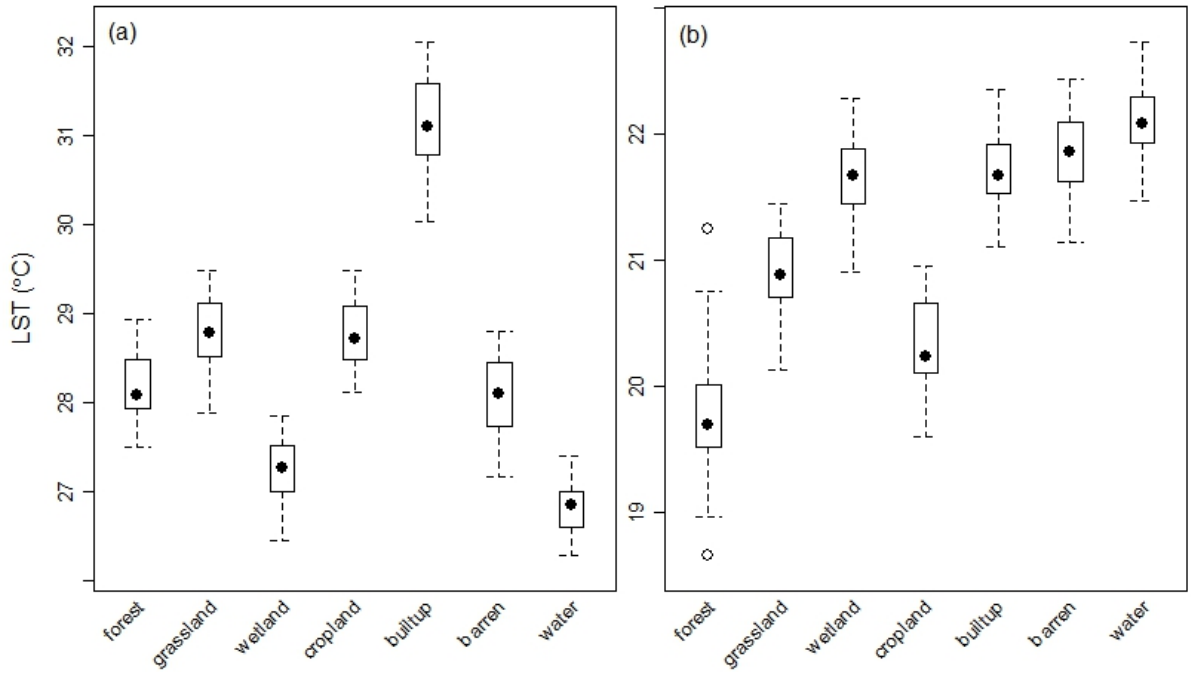

Figure 2–11 Box–and–Whisker plot, showing variation of LST between different land cover categories for: a) day; b) night

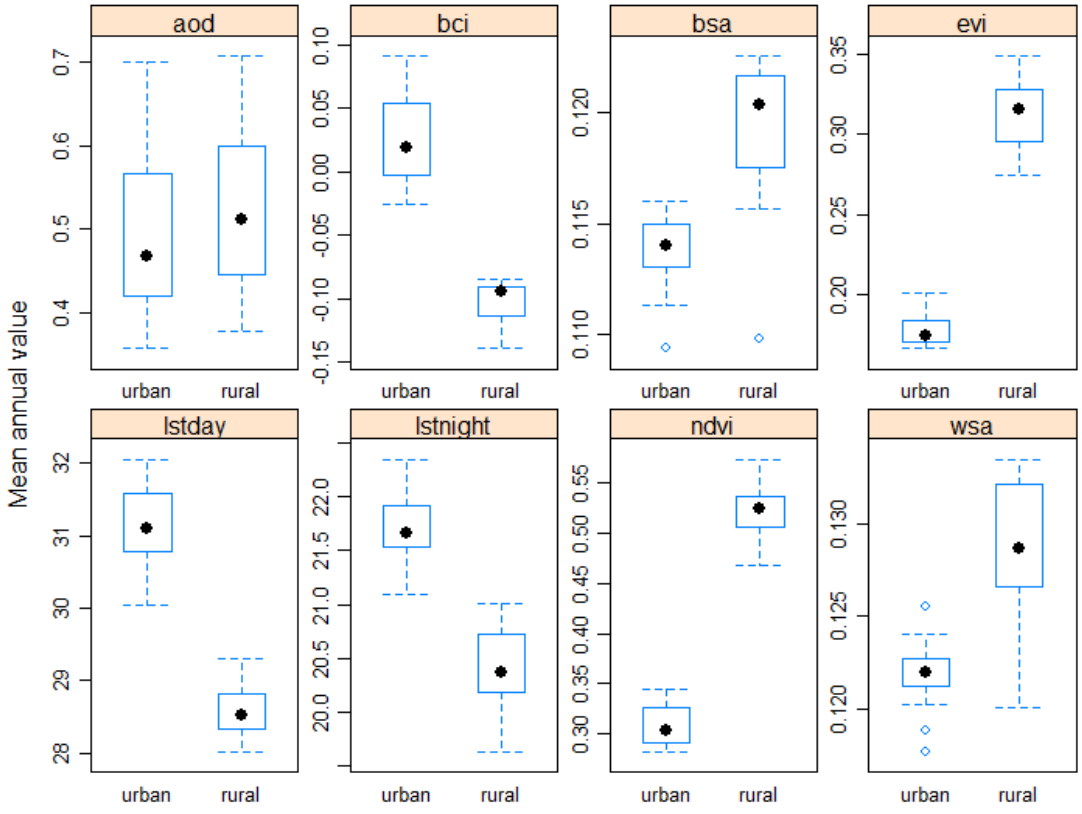

Figure 2–12 Box–and–whisker plot, showing urban and rural variation in LST and aod, bci, bsa, evi, ndvi and wsa

2.5.4 Spatio–temporal variability of SUHI

2.5.4.1 Monthly variation

Figure 2–13 shows SUHI intensity across the months. The summer month (April, 3.43 °C) exhibits the largest intensity during the daytime, followed by monsoon month of July (3.28 °C). In contrast, the winter months (December–February) show the highest nighttime intensity compared to other months. January has the maximum (2.23 °C) whilst July records a negative SUHI (–0.8 °C) during nighttime, as obtained from the time–series MODIS analysis.

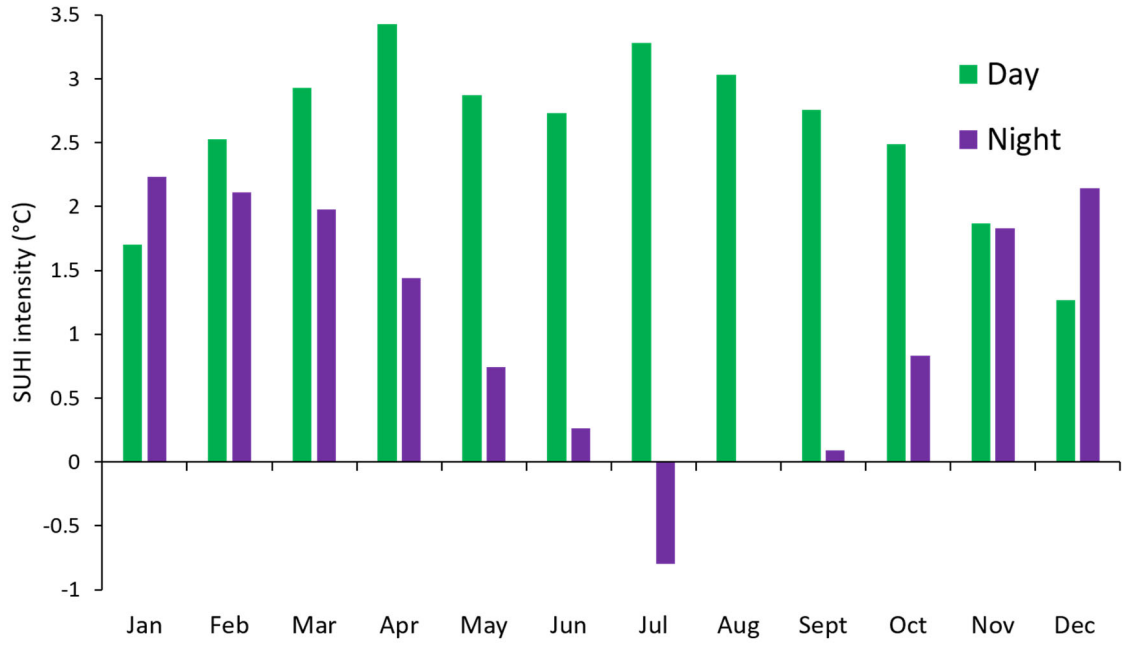

Figure 2–13 Monthly SUHI intensity in the DMDP area

Figures 2–14 and 2–15 show the spatial variation of monthly mean SUHI over the DMDP. Inspection of the two maps (day and nighttime) reveals a distinct pattern. For example, the coverage of SUHI (in terms of area), is greater during most months, except December. It gradually increases from February and continues until May–June. With the arrival of the monsoon (which brings torrential rainfall to Bangladesh territory), SUHI magnitude appears to decrease but not to a great extent, as urban areas still show a very high SUHI value (> 3° C). In contrast, nighttime SUHI is highly pronounced during the months of November to March. Interestingly, nighttime SUHI magnitude is almost absent from May to October and a few locations exhibit moderate (1–2 °C) SUHI (Figure 2–15). The months of December and January show the maximum coverage over space when considering the moderate to very high category of SUHI.

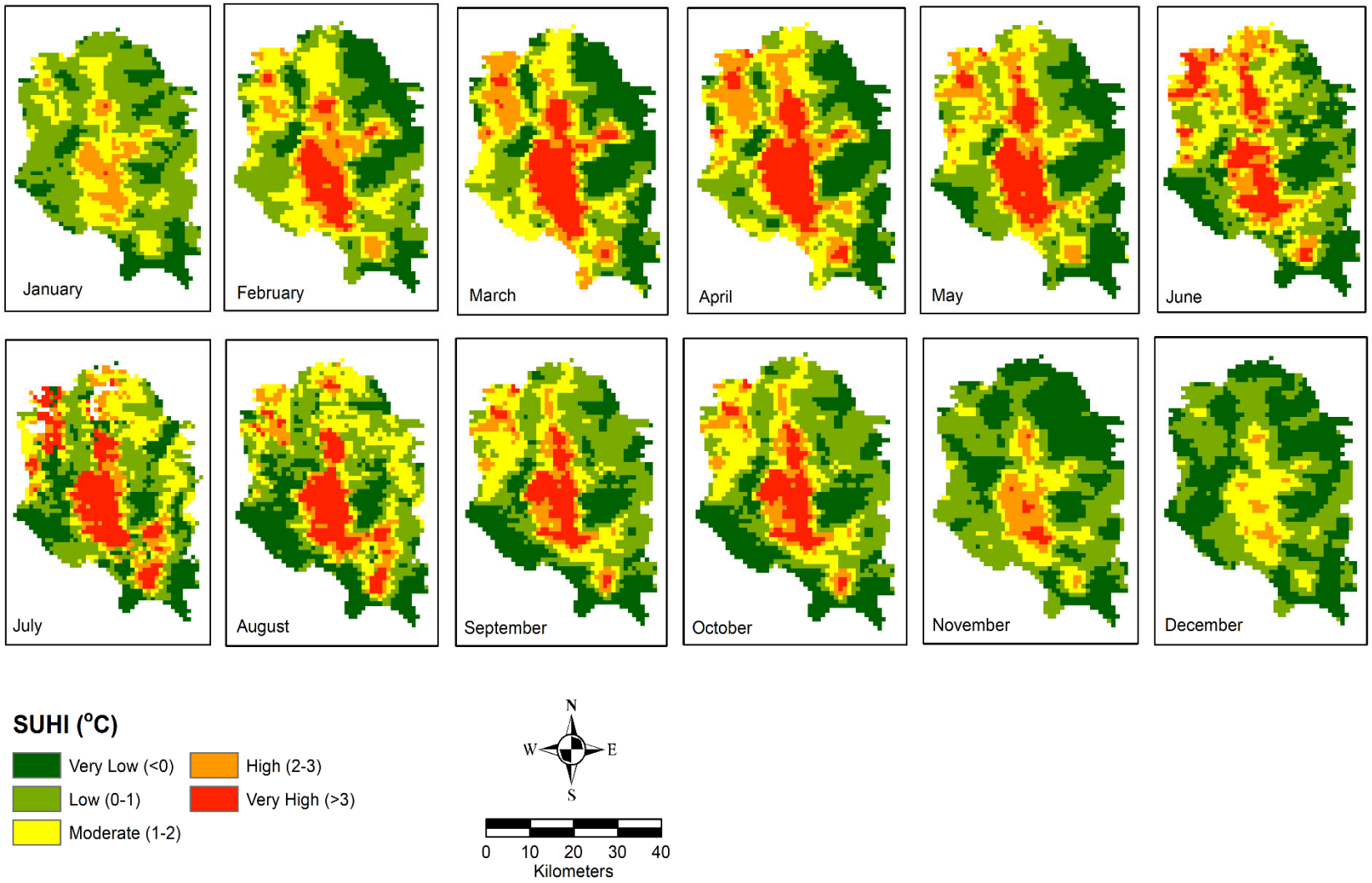

Figure 2–14 Mean monthly daytime SUHI, 2003–2018

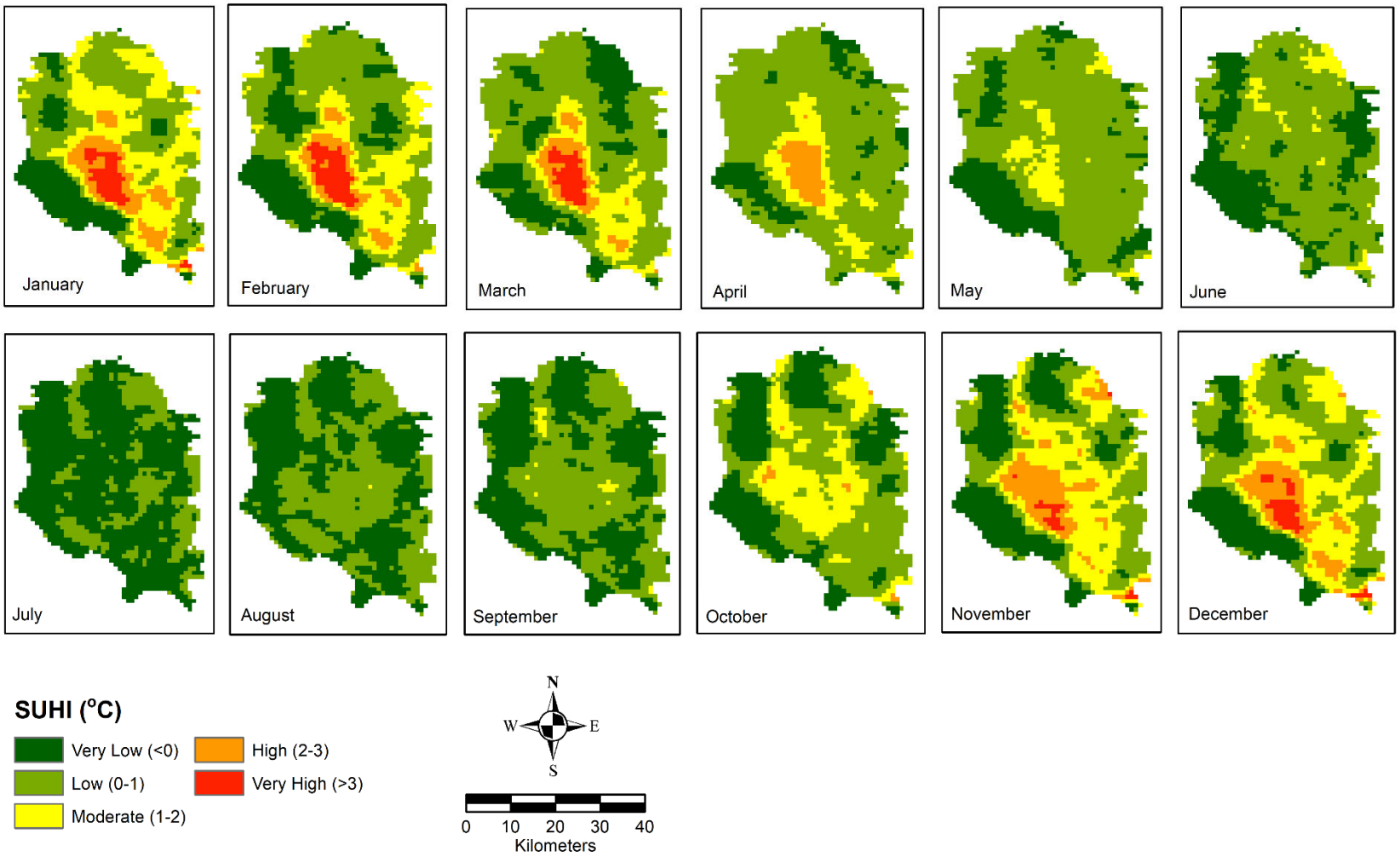

Figure 2–15 Mean monthly nighttime SUHI, 2003–2018

2.5.4.2 Seasonal variation

Figure 2–16 shows the day and nighttime seasonal SUHI trends over the study period. The pre–monsoon season daytime SUHI shows an increase from 0.60 °C in 2003 to 1.6 °C in 2015. For the monsoon period, these values are 0.69 °C (2003) and 1.59 °C in 2018, a rise of 0.9 °C in 16 years. The post–monsoon season recorded a value of 0.29 °C in 2003, which increased to 0.72 °C in 2018. During winter, the minimum of 0.25 °C in 2003 which showed a maximum of 0.87 °C in 2017. As far as the nighttime SUHI is concerned, the value ranges from 0.30 °C to 0.64 °C in the pre–monsoon season and –0.15 °C to 0.33 °C in the monsoon season. The difference seems to be low for winter when nighttime SUHI ranges from a minimum of 0.60 °C to 0.84 °C whilst the post–monsoon season had a difference of 0.34 °C (Figure 2–16). Note however that the day–night SUHI variability is high in both the monsoon and pre–monsoon seasons with a very subtle day–night variation in winter.

The spatial variation indicates that the densely developed urban areas are experiencing very high SUHI compared to the surrounding areas (Figure 2–17). For example, the daytime SUHI generally exhibits a similar distribution pattern when compared to the nighttime SUHI for the four seasons, with little variation during the post–monsoon and winter seasons. During nighttime, the winter months have the highest area coverage of SUHI distribution compared to other seasons and the spatial distribution of monsoon season SUHI is scattered and mainly located around major waterbodies (Figure 2–17). Note that the winter variability is high over space, both during the day and at night.

2.5.4.3 Annual variation

Mean annual SUHI for day and nighttime is shown in Figure 2–18, which indicates an increasing daytime temperature with a tapering off in 2017–2018. The nighttime SUHI also shows a rise, although more subdued than the daytime. Interestingly, the magnitude of daytime SUHI shows a sharper rise than the nighttime. A mean difference of 1.23 °C has been observed between nighttime and daytime SUHI between 2003 and 2018.

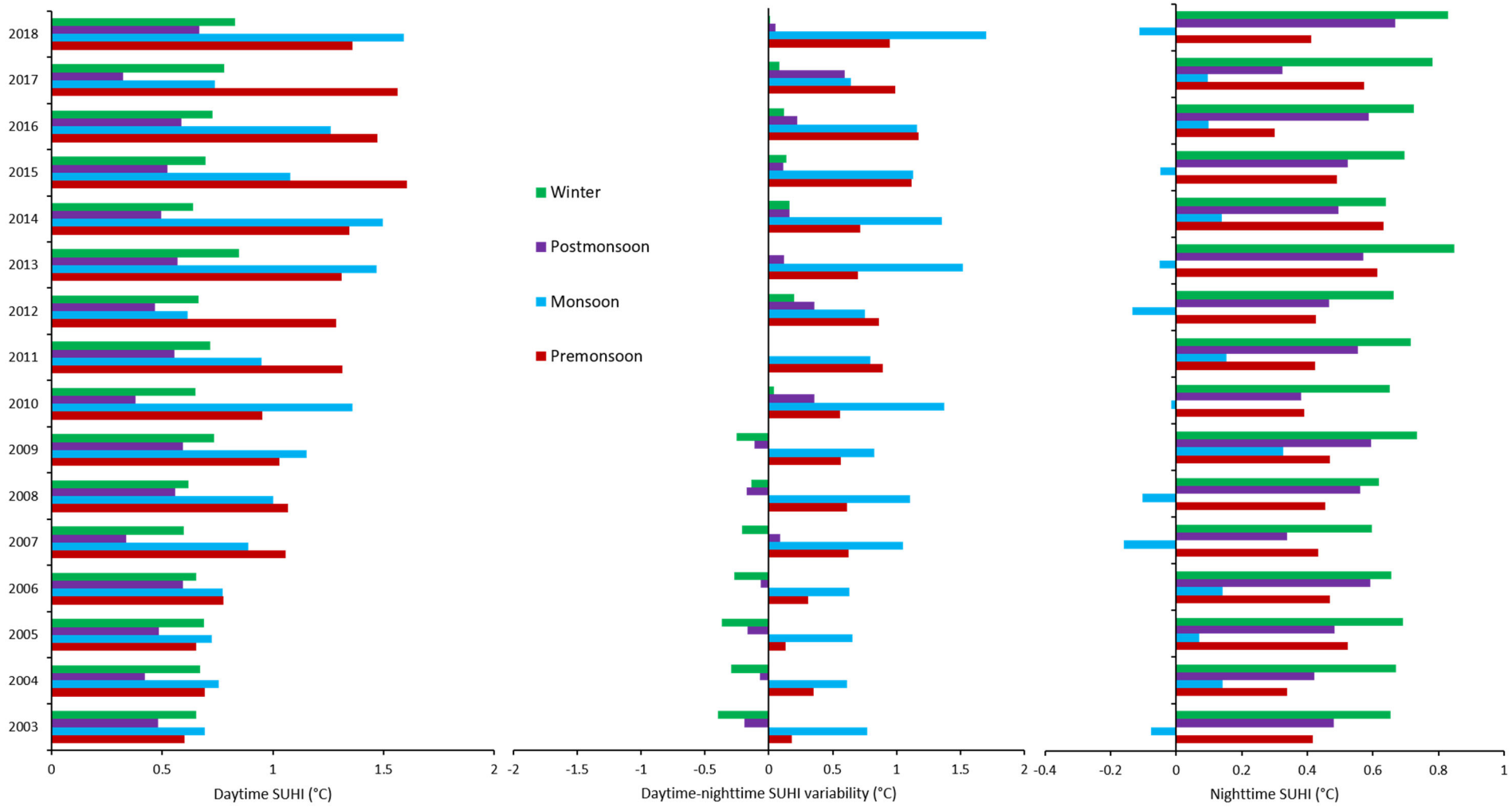

Figure 2–16 Day, night and day–night seasonal variability of SUHI

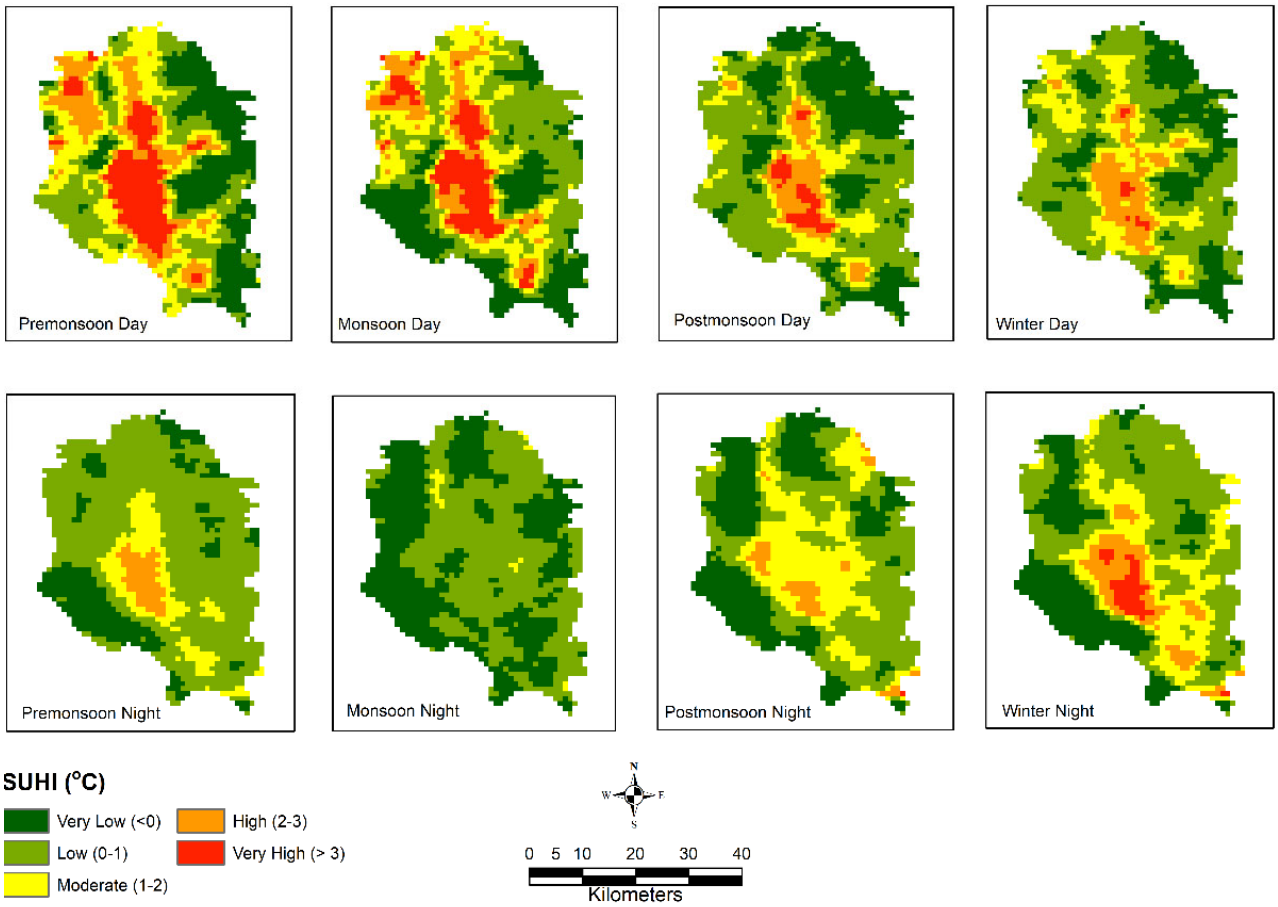

Figure 2–17 Spatial distribution of seasonal SUHI (day and night), 2003–2018

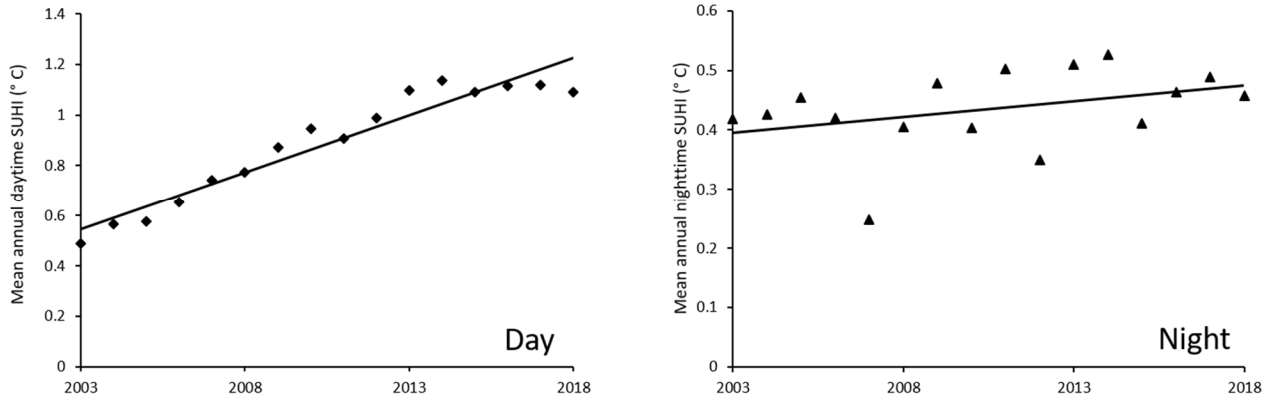

Figure 2–18 Trend of mean annual day and nighttime SUHI, 2013–2018

Examining the SUHI spatially, it is clear that the daytime SUHI is concentrated around the urban areas (Figure 2–19). Approximately 1.7 °C difference can be observed between the urban and other surfaces during the daytime, the low and high being 2.59 °C and 4.29 °C,

respectively. In contrast, the nighttime distribution of SUHI is still concentrated in the main urban core and more densely populated areas. The waterbodies within the DMDP also exhibit an elevated temperature during the night. The difference between high and low SUHI values is estimated to be in the order of 1.5 °C, indicating asymmetric warming.

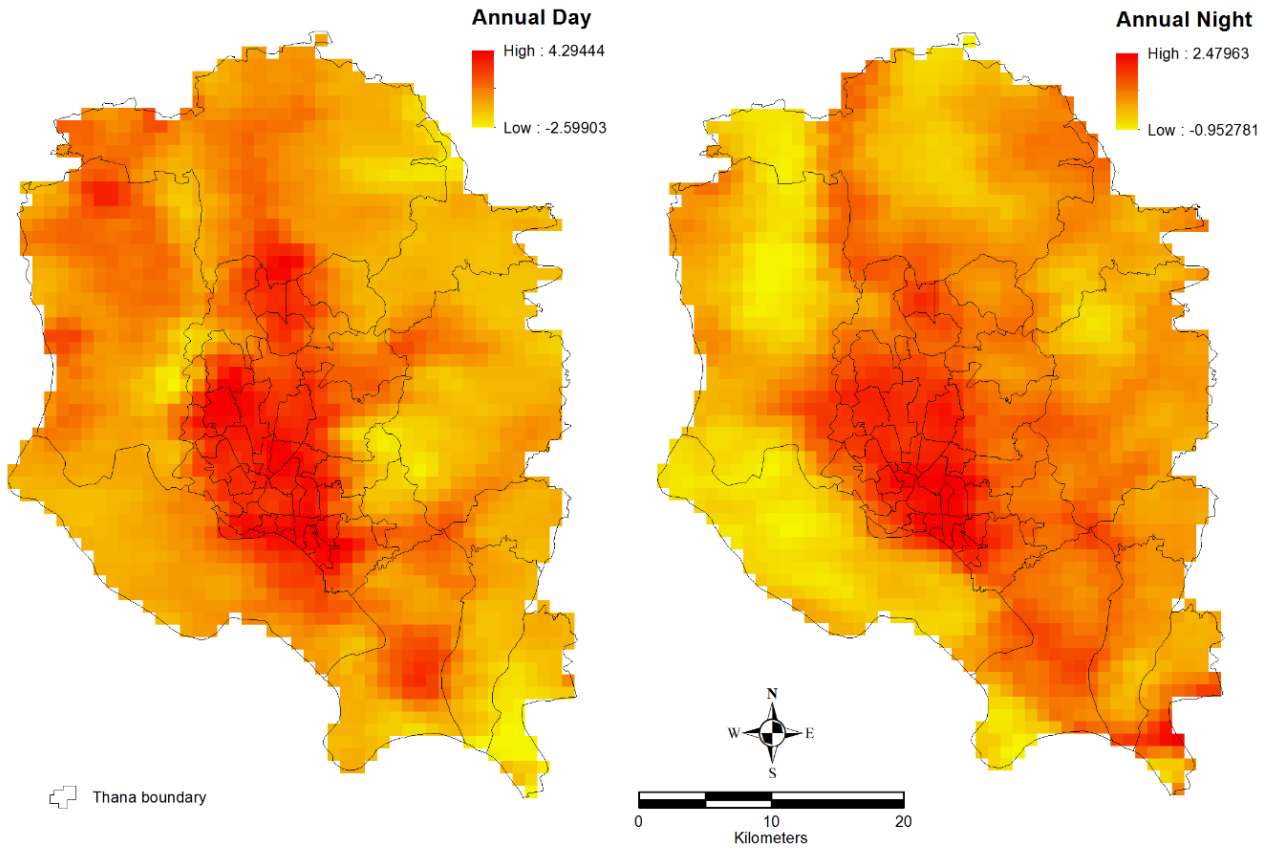

Figure 2–19 Spatial variation of annual day and nighttime SUHI

Spatiotemporal variation of annual day and nighttime SUHI over space is shown in Figures 2–20 and 2–21. Comparison of the distribution between the earliest (2003) and the latest (2018) years clearly show that, during the daytime, the very high SUHI area is increasing over time (Figure 2–20). The nighttime temperature exhibits a similar increasing trend in terms of area exposure but urban heat, categorised as high to very high (2 °C to >3 °C), seems to be concentrated only in the urban core areas of the DMDP.

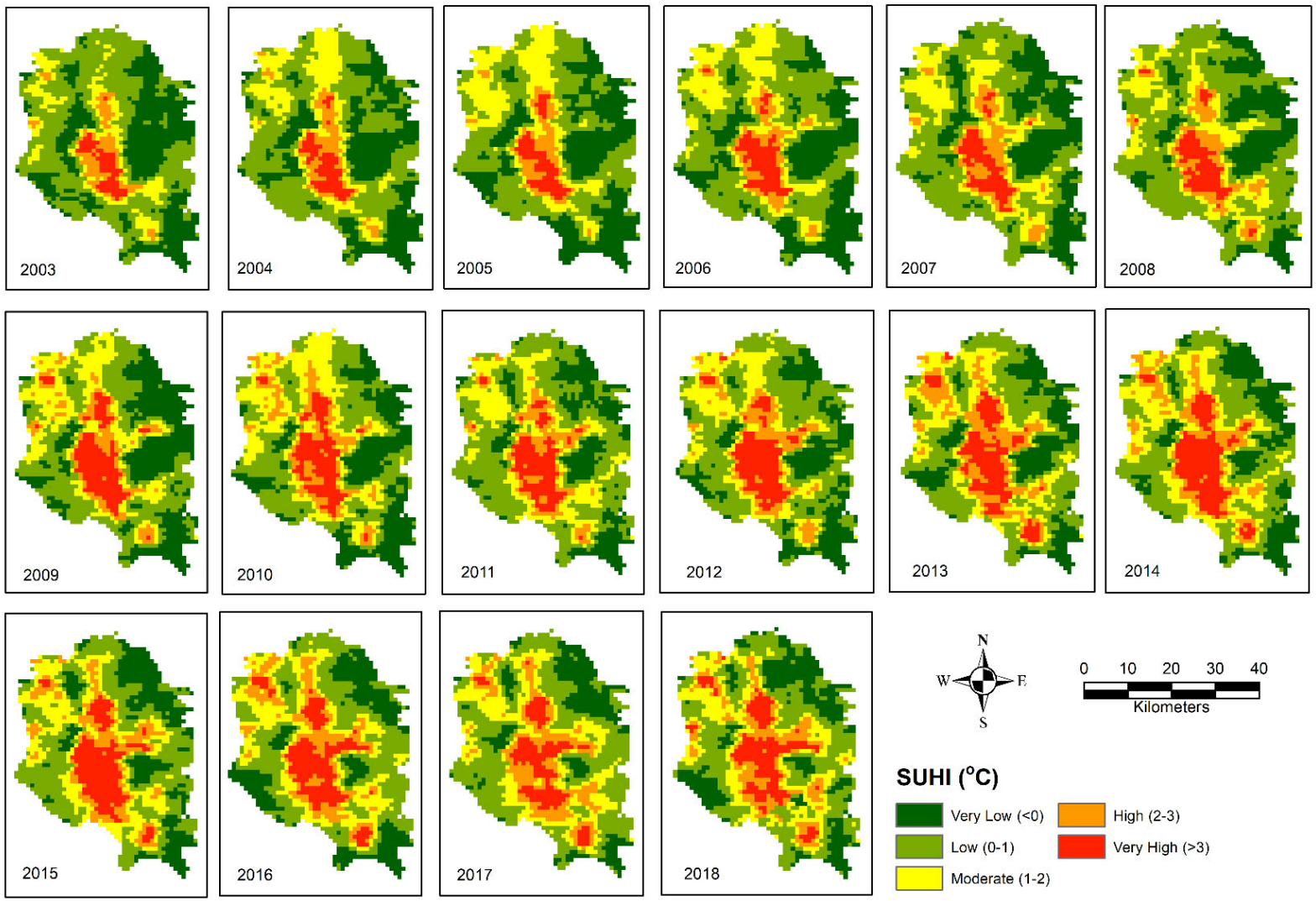

Figure 2–20 Annual daytime SUHI, 2003–2018

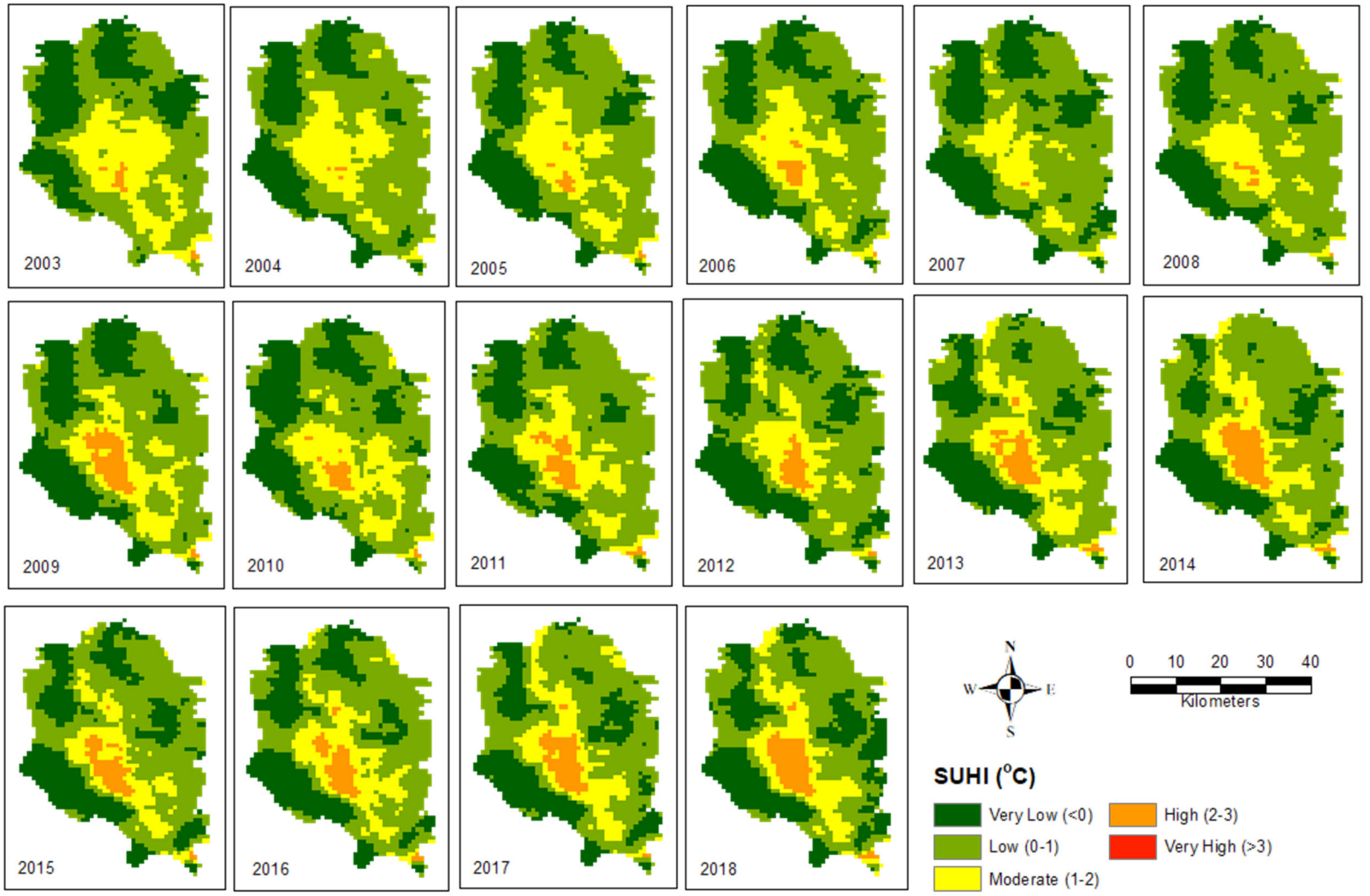

Figure 2–21 Annual nighttime SUHI, 2003–2018

In order to examine the spatial trend in more detail, pixels having >= 0.5, 1.0, 1.5, 2.0, 2.5 and 3.0 °C were mapped using annual SUHI data. The increase in areas having >= 2 °C from 2003 to 2018 is clearly evident in Figure 2–22. The daytime pattern is thus quite noticeable.

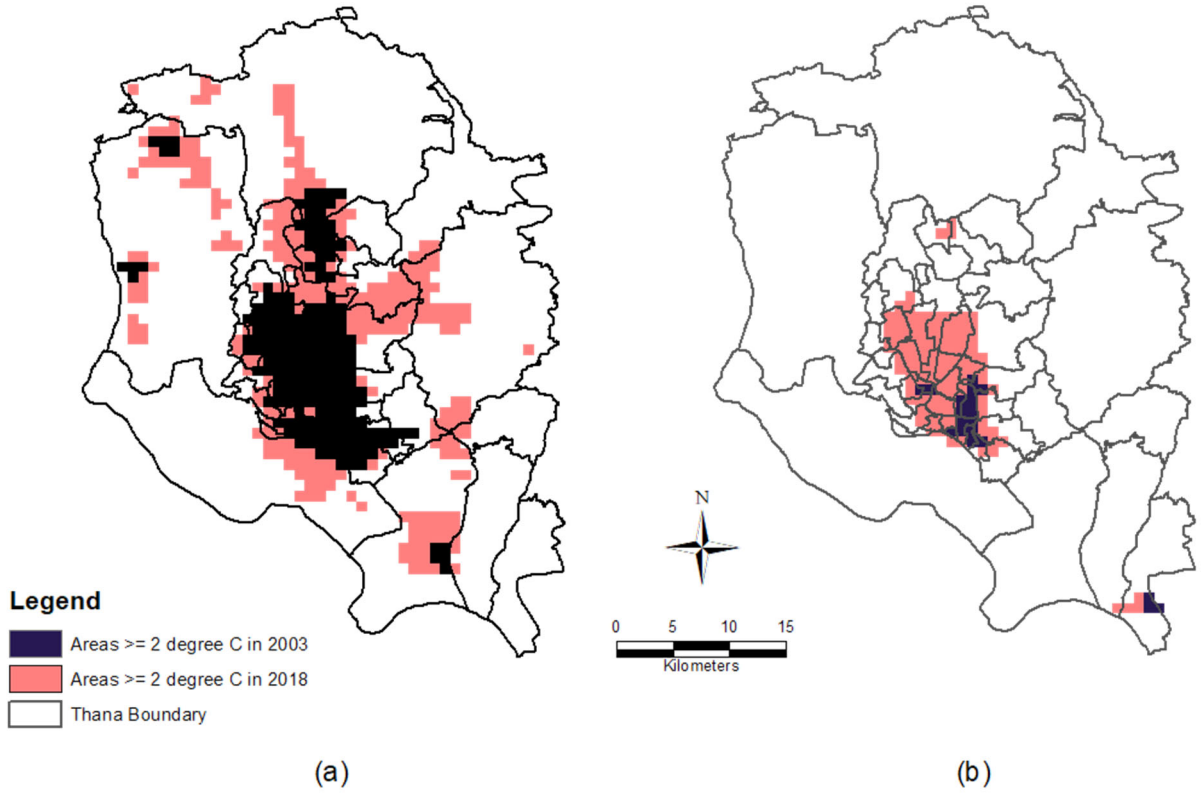

Figure 2–22 Spatial changes of annual SUHI with pixels >=2 ºC, 2003–2018: a) day; b) night

An examination of the temporal variation of areas >=2 ºC of SUHI reveals a steeper increase in the daytime SUHI when compared to the nighttime, with the night trend increase being much more subdued (Figure 2–23).

A SUHI magnitude map was produced using the average of hottest quarter of the year divided by the average of all seasons. The result is shown in Figure 2–24 (a–b). This indicates that the daytime SUHI is usually concentrated in the main urban core and newly–developed areas with a range between 0.90 °C and 3.62 °C (Figure 2–24a). Interestingly, the cooler surfaces are some distance from the main urban core and the difference of SUHI magnitude appears to be 2.72 °C between hotter and cooler surfaces. During nighttime (Figure 2–24b), the main urban core remains hot but exhibits lower SUHI values than the large waterbodies and wetlands in the area due to the differential thermal response of waterbodies. The range varies from 0.45 °C to 2.33 °C.

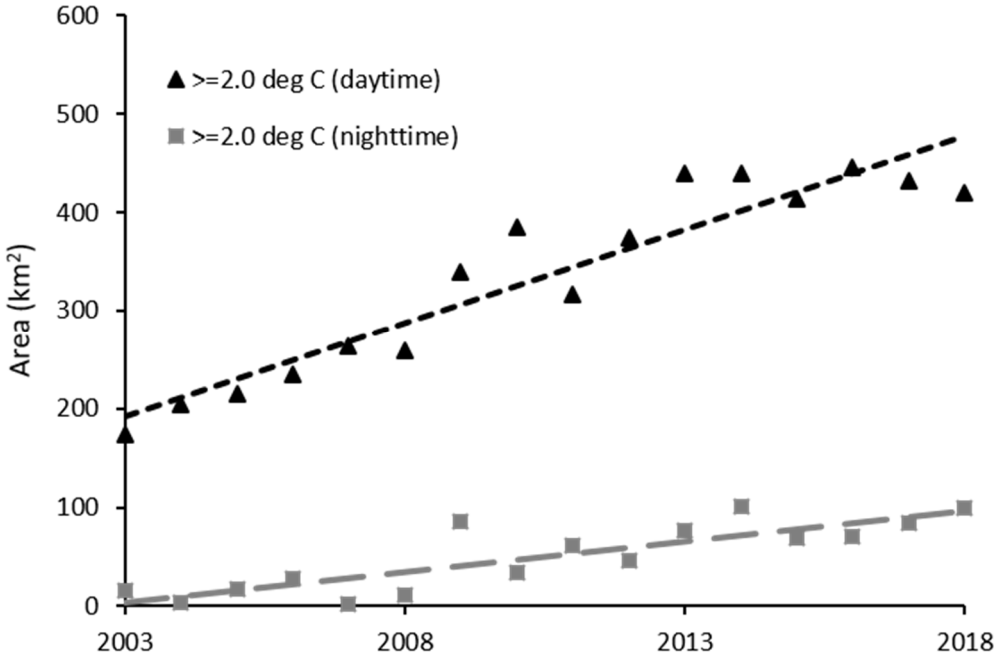

Figure 2–23 Temporal trend of area coverage of SUHI (pixels >=2 ºC)

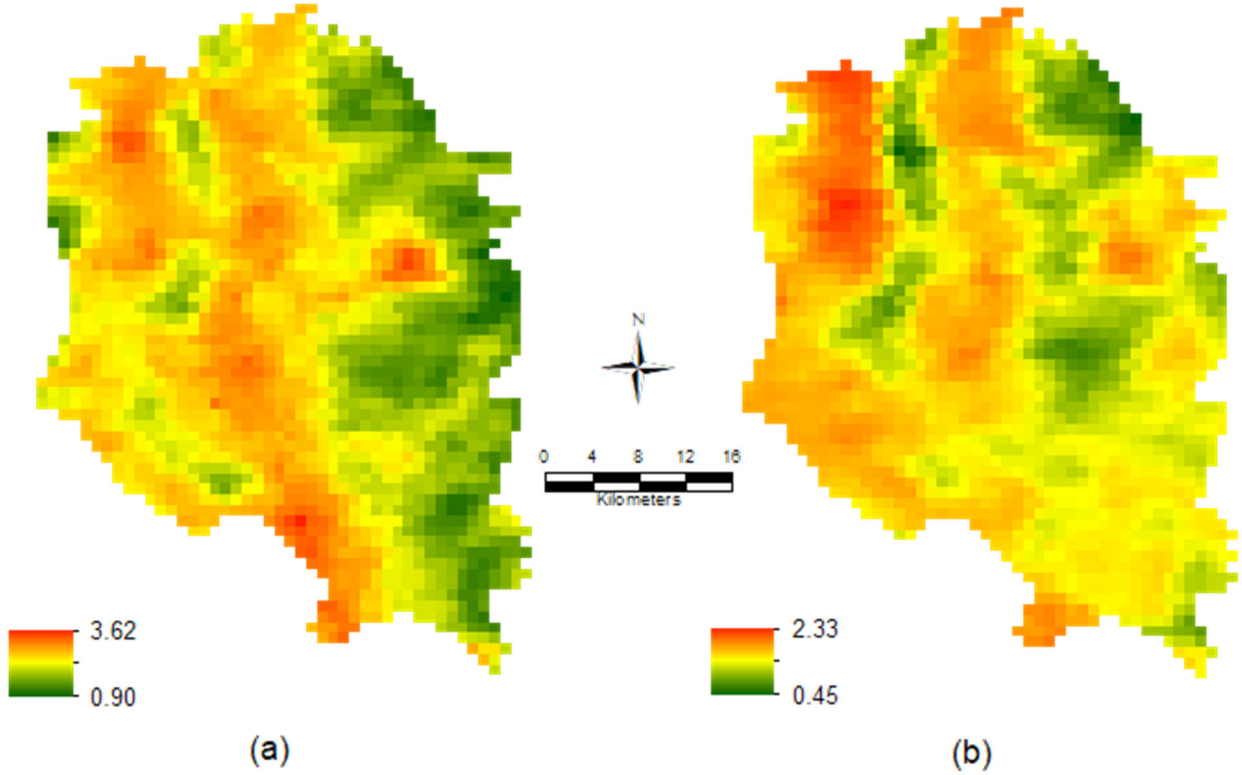

Figure 2–24 SUHI magnitude: a) day; b) night

2.6 Driving factor analysis

The following section provides the results of the statistical analysis for day and night.

2.6.1 Relationship between day/night SUHI and predictor variables

A correlation matrix was produced to assist in determining the strengths and direction of correlation of the selected variables with the daytime SUHI (Figure 2–25a). Those exhibiting a high degree of association or collinearity (such as ndvi with savi, lai and evi) were discarded in the subsequent regression models. An exception was made for some variables (e.g. ndbi) due to their importance as good predictors of SUHI. Figure 2–25b shows the seven variables (aod, bci, bsa, isabi, ndbi, popden, vcf-ptc) considered as important. These variables were used in the global and local regression models.

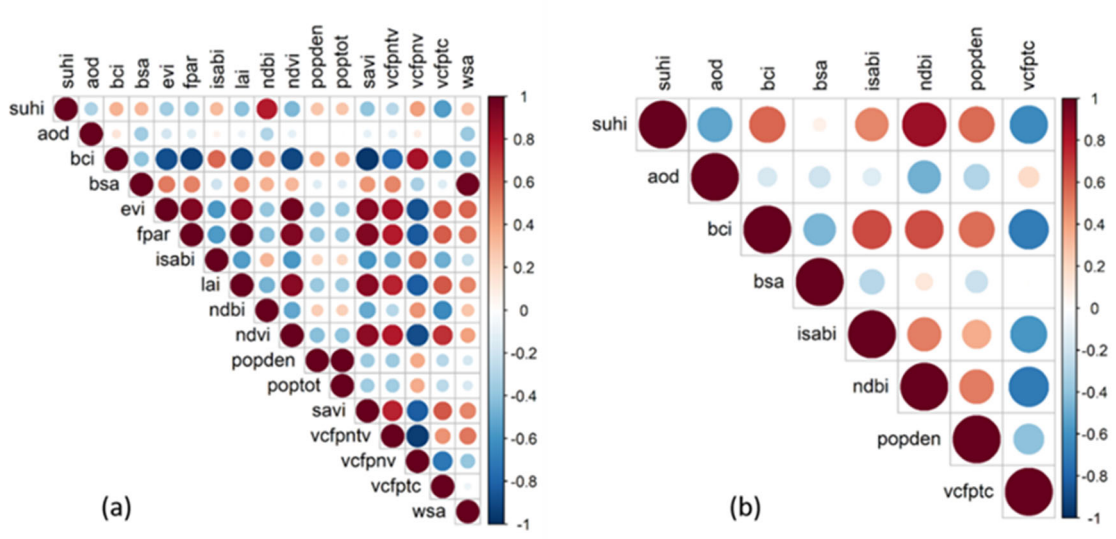

Figure 2–25 Correlation matrix between SUHI and predictor variables during the day: a) with 16 variables; b) with seven variables

Figure 26 (a–b) shows both the relationship between predictor variables and nighttime SUHI. In this case, bci was more highly associated with SUHI than ndbi, which was an important predictor for the daytime SUHI. This may be due to the differences in spectral properties and method of computation. On the other hand, SUHI was negatively correlated with vegetation indices such as vegetation continuous field – percent tree cover (vcfptc) or evi (Figure 2–26a). Figure 2–26b shows the selection of variables based on correlation matrix outputs for nighttime SUHI.

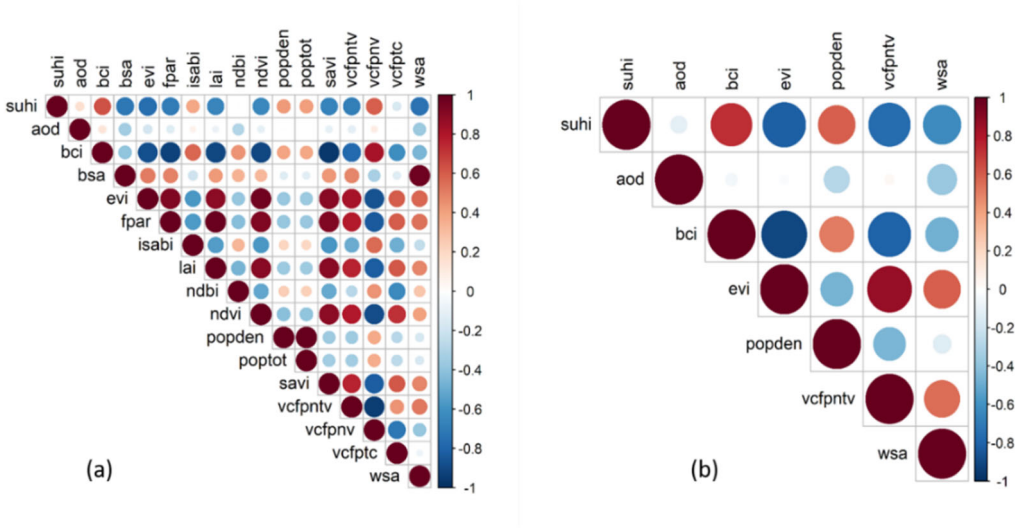

Figure 2–26 Correlation matrix between SUHI and predictor variables during the night: a) with 16 variables; b) with six variables

It is apparent that there is a positive correlation between SUHI and bci (biophysical composition index) and population density (popden). Strong negative correlation was seen between evi, vegetation continuous field and SUHI. A weaker negative relationship was also observed between aerosol (aod) and SUHI (Figure 2–26b).

Tables 2–11 and 2–12 show the performance of OLS and GWR in terms of AIC during day and night. The statistics reveal that the local model outperformed the global model and indicates that GWR is significantly better than OLS in predicting SUHI. These tables also provide detailed statistics for the two models. Based on the interquartile range of global estimates, variables greater than ±1 standard deviation were discarded (Fotheringham et al. 2003).

Table 2–10 OLS and GWR parameter estimates at daytime

Parameter	OLS					GWR				
	Estimate	Std. Err	t-stat	Sig.	VIF	Min	25% Q	Median	75% Q	Max
(Intercept)	5.17900	0.36750	14.09	0.00	-	-25.90	-0.03	3.44	7.60	35.10
aod	-4.85300	0.43060	-11.27	0.00	1.436	-32.10	-11.20	-5.78	-0.66	12.70
bci	-1.16100	0.45230	-2.57	0.01	4.939	-19.90	-1.69	0.89	3.78	21.50
bsa	-1.97300	2.15100	-0.92	0.36	2.301	-81.60	-5.85	10.80	25.80	118.00
isa-bi	0.62680	0.15960	3.93	0.00	1.908	-2.67	-0.42	0.03	0.47	4.92
Ndbi	10.08000	0.37320	27.01	0.00	3.778	-11.60	1.01	3.58	6.38	18.30
Popden	0.00001	0.00000	10.59	0.00	1.622	-0.01	0.00	0.00	0.00	0.01
vcfptc	-0.02528	0.00501	-5.04	0.00	2.914	-0.21	-0.05	-0.02	0.00	0.17
AIC	2675.0					-333.5				

Table 2–11 OLS and GWR parameter estimates at nighttime

Parameter	OLS					GWR				
	Estimate	Std. Err	t-stat	Sig.	VIF	Min	25% Q	Median	75% Q	Max
(Intercept)	6.21100	0.17390	35.73	0.00	-	-10.80	0.79	2.57	4.67	41.20
aod	-3.01000	0.19610	-15.35	0.00	1.406	-24.40	-2.91	-0.06	2.29	16.30
bci	-0.86190	0.25550	-3.37	0.00	5.835	-5.83	-1.49	-0.17	1.14	6.75
evi	-4.47100	0.28730	-15.56	0.00	8.416	-13.10	-5.29	-3.31	-1.59	6.44
popden	0.00001	0.00000	22.20	0.00	1.515	-0.02	0.00	0.00	0.00	0.00
vcfpntv	-0.00589	0.00132	-4.45	0.00	4.196	-0.02	0.00	0.00	0.01	0.03
wsa	-22.88000	0.91490	-25.00	0.00	2.036	-48.30	-18.90	-10.90	-2.67	42.10
AIC	843.4					-1661.0				

Figure 2–27 (a–b) shows the observed annual day and night SUHI and predicted SUHI from the GWR modelling which indicated strong agreement between the two with a high correlation coefficient of 0.98. Data points between observed and predicted show a good fit, again indicating the importance of the local model in predicting SUHI.

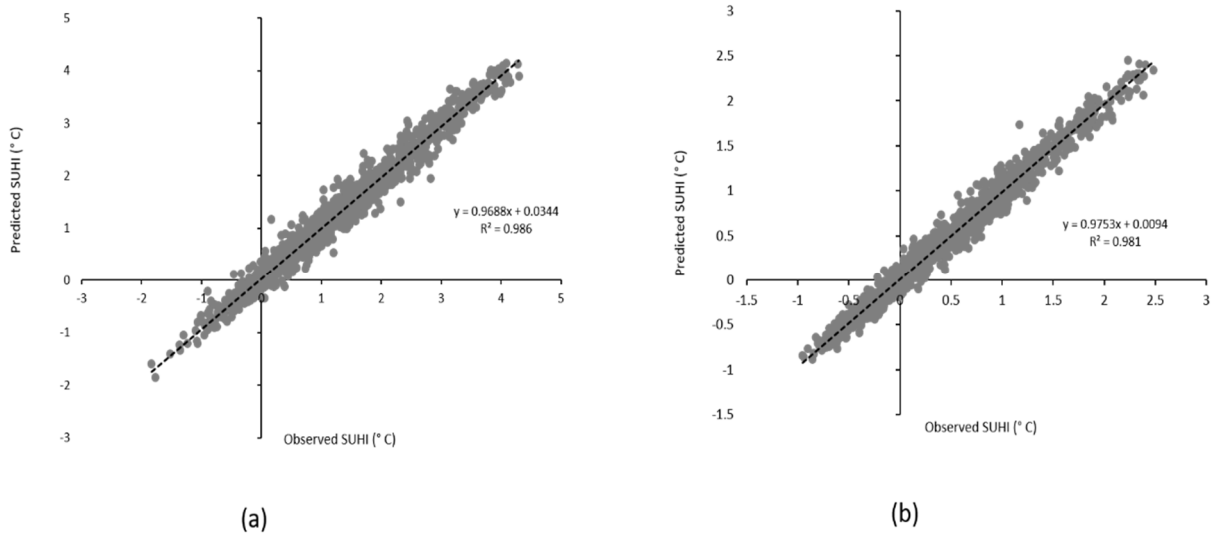

Figure 2–27 Observed versus predicted values by GWR and MODIS–derived SUHI: a) day; b) night

The spatial distribution of r^2 from the GWR model, for both annualised day and night, is shown in Figure 2–28 (a–b). The range of r^2 value is between 0.62 and 0.96 for daytime. For night, it ranges from 0.58 to 0.98. Furthermore, high daytime r^2 values (>=0.80) are distributed over the main urban core and newly developed areas where the annual SUHI is high (Figure 2–28a). An almost similar distribution of nighttime r^2 can be seen in Figure 2–28b, emphasizing that the relationship between dependent and predictor variables varies spatially and is non–stationary.

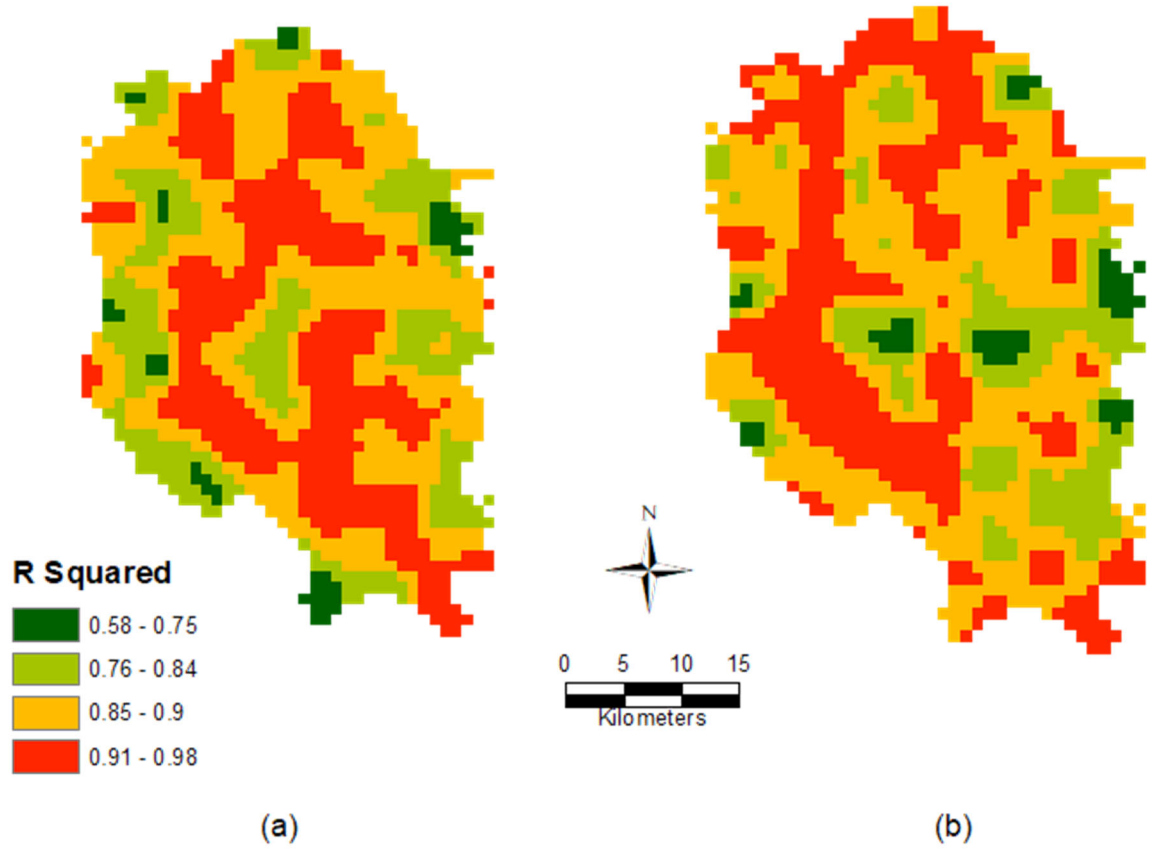

Figure 2–28 Spatial distribution of GWR–derived r^2 SUHI parameter: a) day; b) night

The impact of environmental factors on day and night SUHI are shown in Figures 2–29 and 2–30. They are instrumental in revealing that changes in the parameters lead to changes in SUHI and that they tend to vary spatially. For example, Figure 2–29 shows that aerosol (aod) has a statistically significant negative relationship with SUHI, exemplified by the domination of negative pixels during daytime. Conversely, built–up surface (e.g. ndbi) exhibited domination of statistically significant positive grids in DMDP. Figure 2–30 shows statistically positive significant grids with SUHI during the night, meaning that as population density increases so does SUHI. As expected, the majority of vegetation (e.g. evi) pixels showed negatively significant grids during the night in the study area whilst biophysical variable (e.g. bci) showed a domination of insignificant pixels (Figure 2–31). Note that only six variables were mapped for brevity, despite seven variables being used for day and six variables for nighttime modelling.

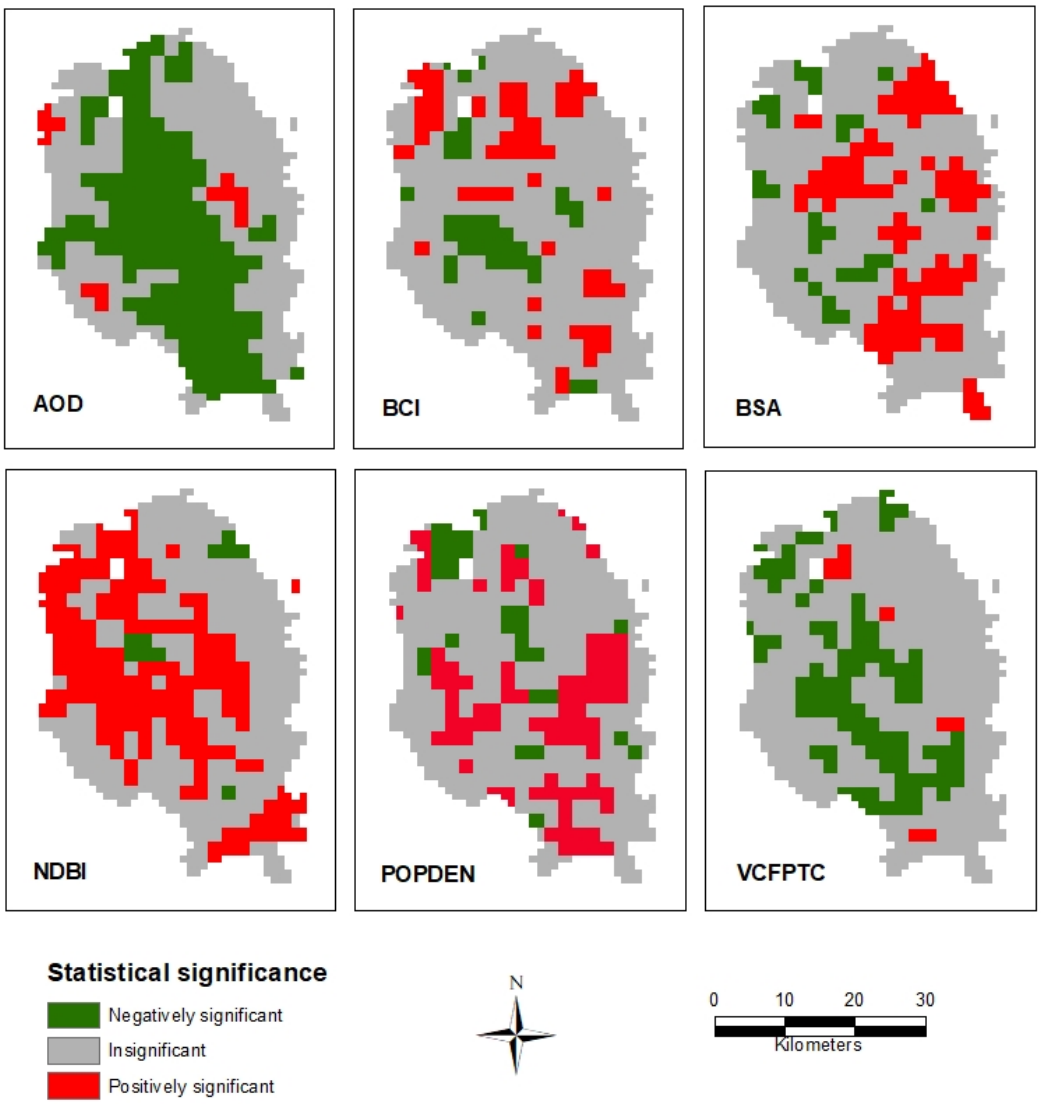

Figure 2–29 Clockwise significance maps of daytime SUHI versus aod, bci, bsa, ndbi, popden and vcfptc

2.6.2 Correlation between SUHI and predictor variables at seasonal scale

Seasonal day and night grid–based spatial correlation maps were produced using SUHI versus the explanatory variables. The correlation is based on the individual seasonal mean of the dependent (SUHI) and independent variables from 2003 to 2018. A series of maps were produced to determine the role of the predictors in regards the seasonal SUHI. Figure 2–31 (a–b) shows day and night correlation maps during the pre–monsoon season. In the daytime, aod and bci show higher positively significant pixels, whilst the majority of bsa and ndvi pixels had a negatively significant relationship throughout DMDP area (Figure 2–31a). During the night,

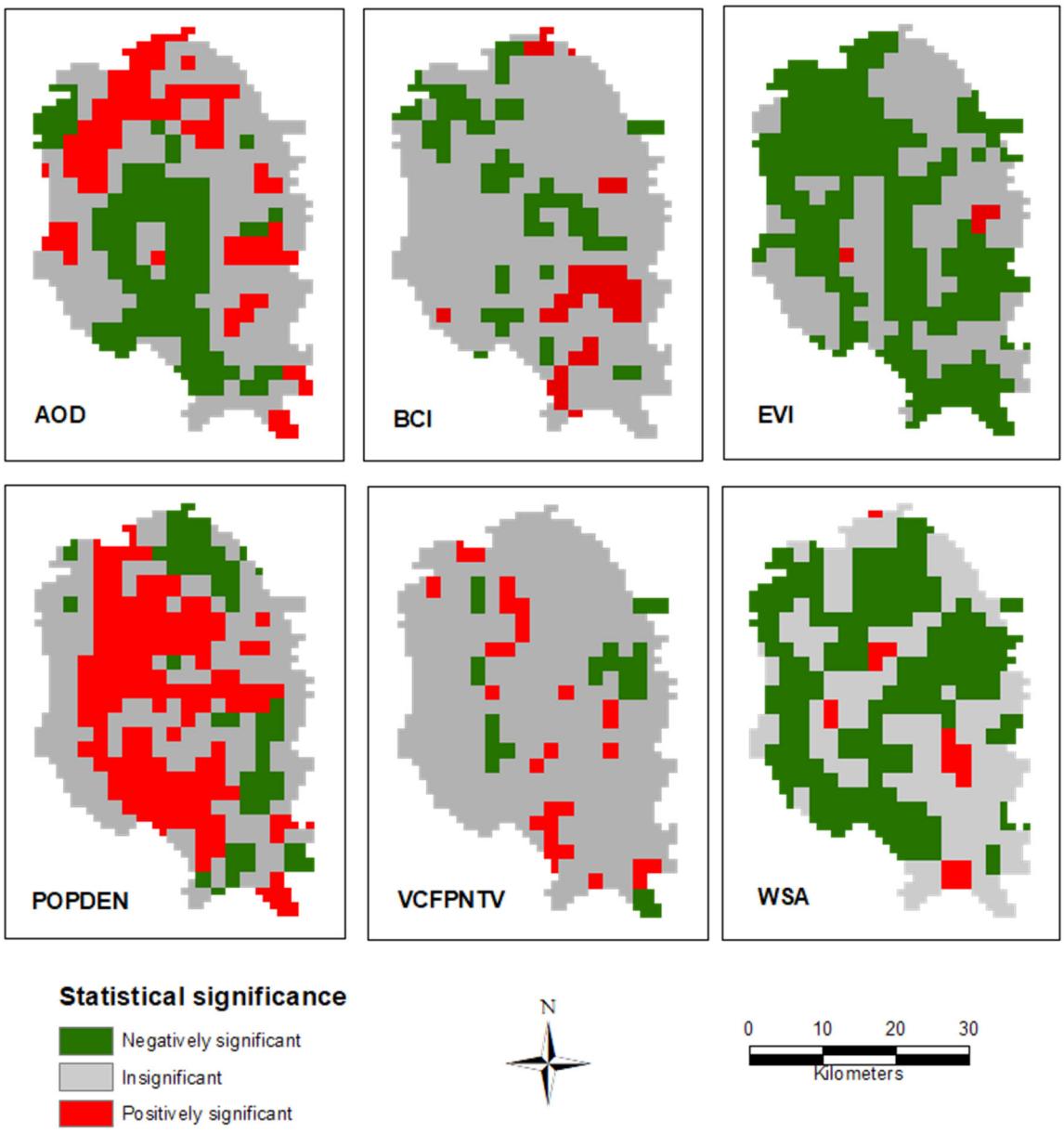

Figure 2–30 Clockwise significance maps of nighttime SUHI versus aod, bci, evi, popden, vcfpntv and wsa

however, the number of positively significant pixels was low, with many of them located near large water features within the DMDP. ndvi and bsa show a negatively significant relationship along the urban boundary (Figure 2–31b).

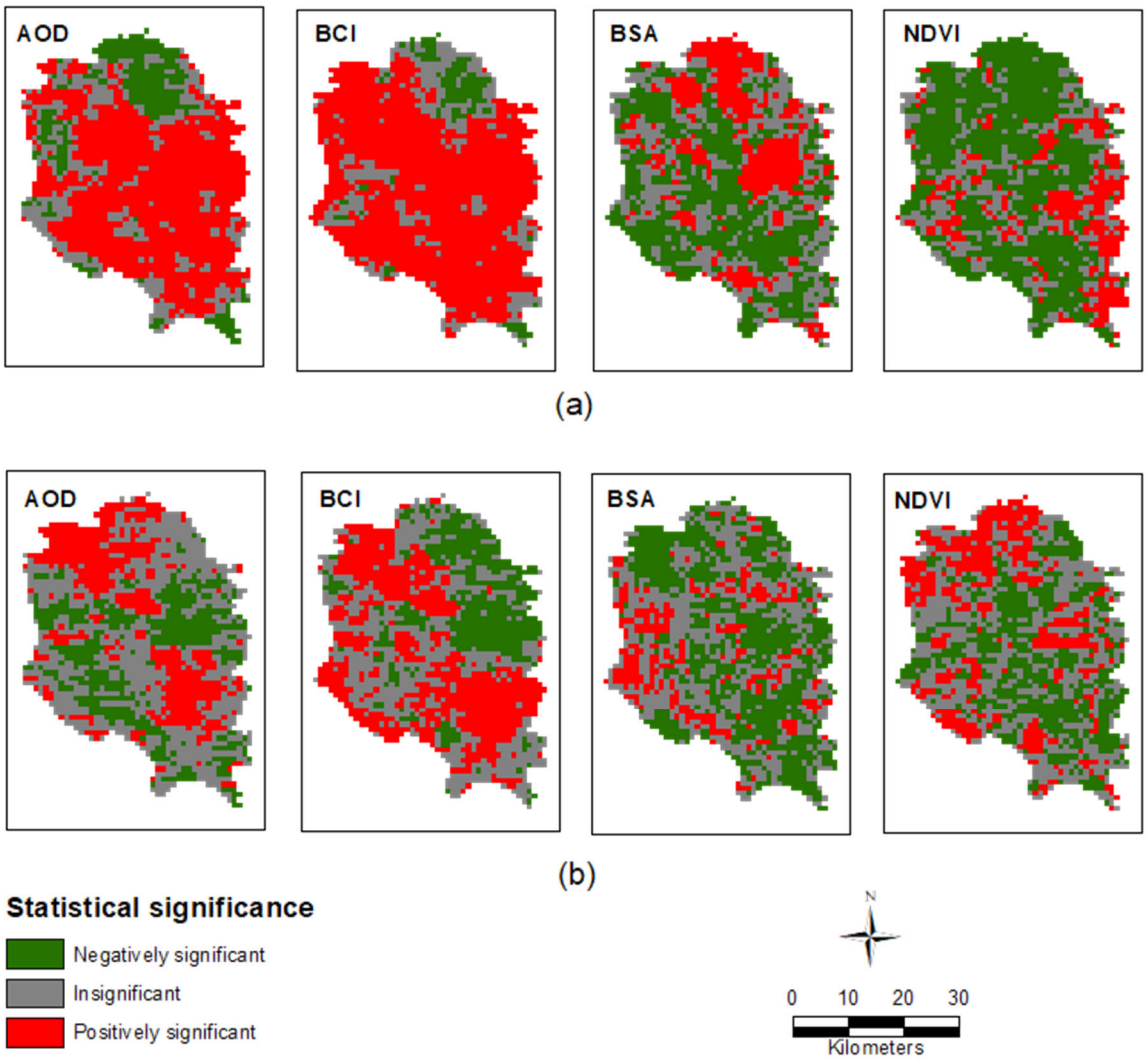

Figure 2–31 Spatial correlation maps showing: a) day; b) night SUHI versus aod, bci, bsa and ndvi during the pre–monsoon season

During the monsoon season daytime, positively significant pixels were higher for ndvi than bci or aod. Along low–lying areas and adjacent to waterbodies, a significantly positive relation was noticeable between ndvi and SUHI. However, the results were marred by missing data for bsa and bci (Figure 2–32a). During nighttime, on the other hand, bsa showed a reversal of correlation with SUHI whilst ndvi was relatively consistent in regards the significance of the relationship (Figure 2–32b). It appears that the effect of bci on SUHI was minimal as indicated by the low number of significant pixels during the day and night.

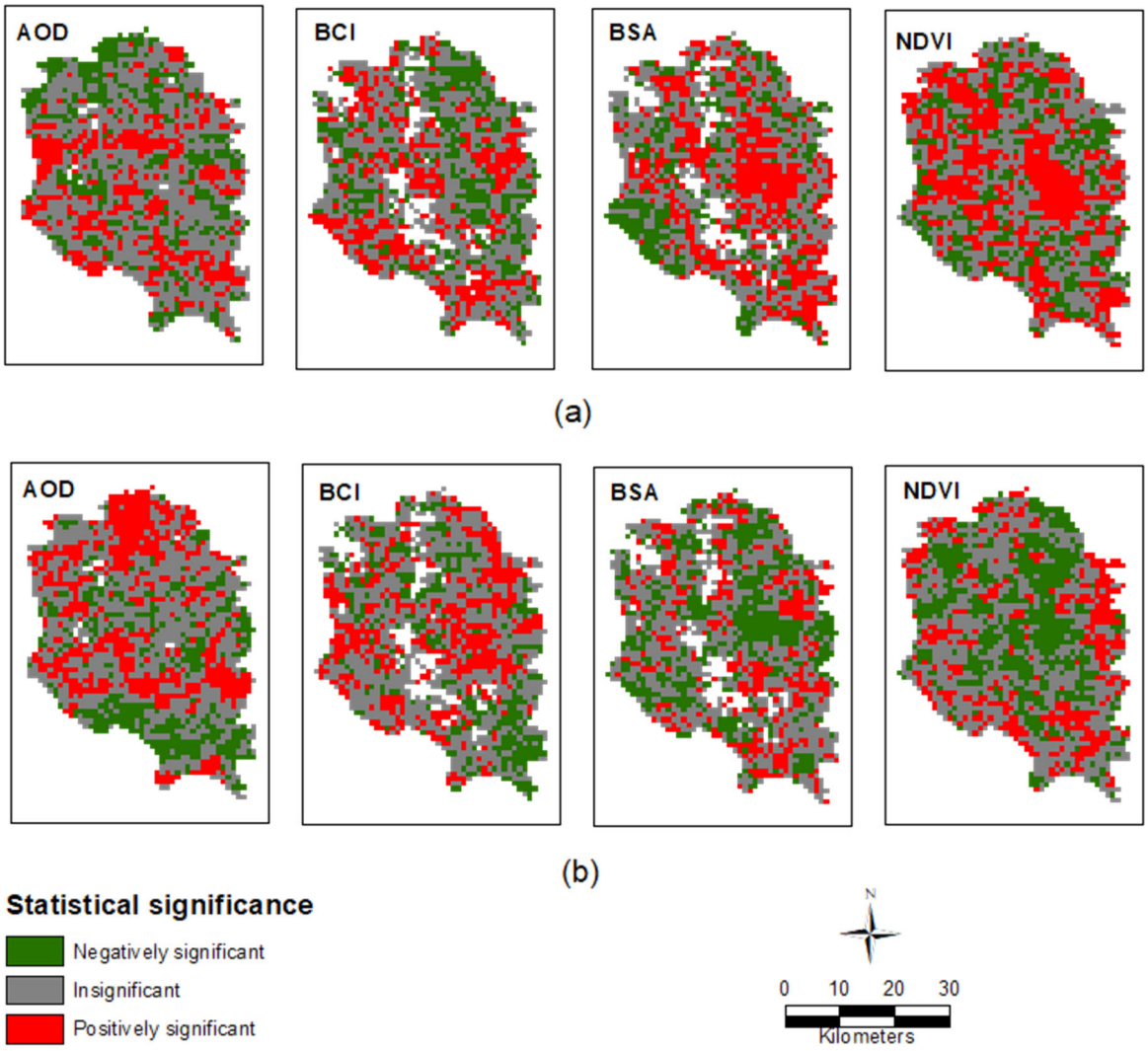

Figure 2–32 Correlation maps showing: a) day; b) night SUHI versus aod, bci, bsa and ndvi during the monsoon season. The white pixels represent no data

During the post–monsoon daytime, aod and bsa seem to play an important role in SUHI development (Figure 2–33a). The built–up area pixels exhibited a positively significant relationship between ndvi and SUHI. However, bci showed a strong association with SUHI in the north of the DMDP area. At nighttime, however, the effect of bsa on SUHI reduced substantially, although a highly pronounced spatial effect from ndvi and aod on the magnitude of SUHI can be observed (Figure 2–33b).

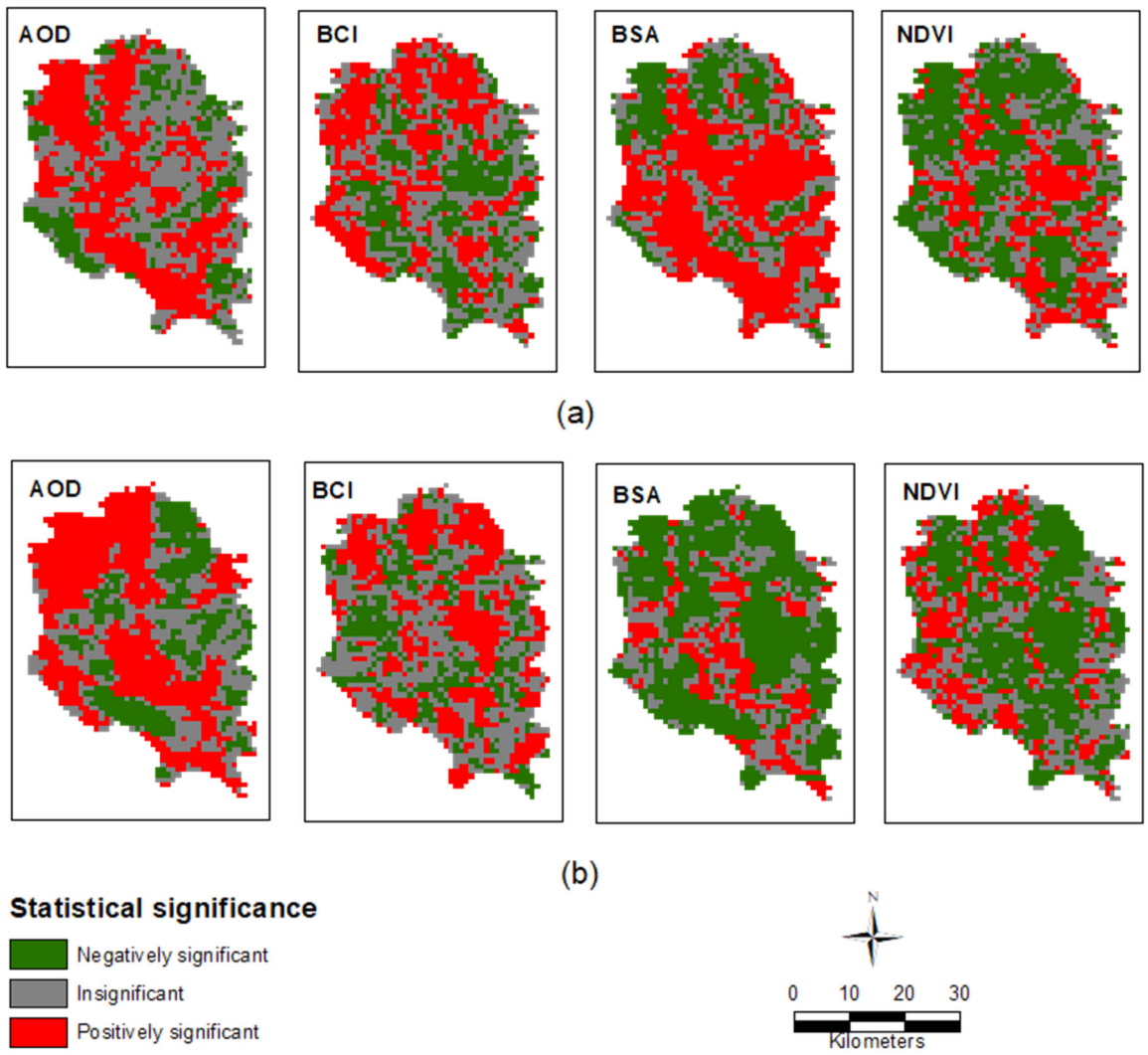

Figure 2–33 Correlation maps showing: a) day; b) night SUHI versus aod, bci, bsa and ndvi during the post–monsoon season

The spatial correlation maps of the winter season provide valuable information regarding the SUHI (Figure 2–34, a–b). Variables such as aod, bci, bsa and ndvi appear to substantially impact the generation of SUHI, as during the daytime the positively significant pixels between aod, bsa and SUHI, and the negatively significant locations between SUHI and ndvi are well distributed over the DMDP area (Figure 2–34a). On the other hand, however, a positively significant correlation exists between bci, aod and SUHI (Figure 2–34b). During the night, most of the urban pixels exhibited a negative correlation with ndvi while there appeared to be minimal effect as regards the bsa variable at night.

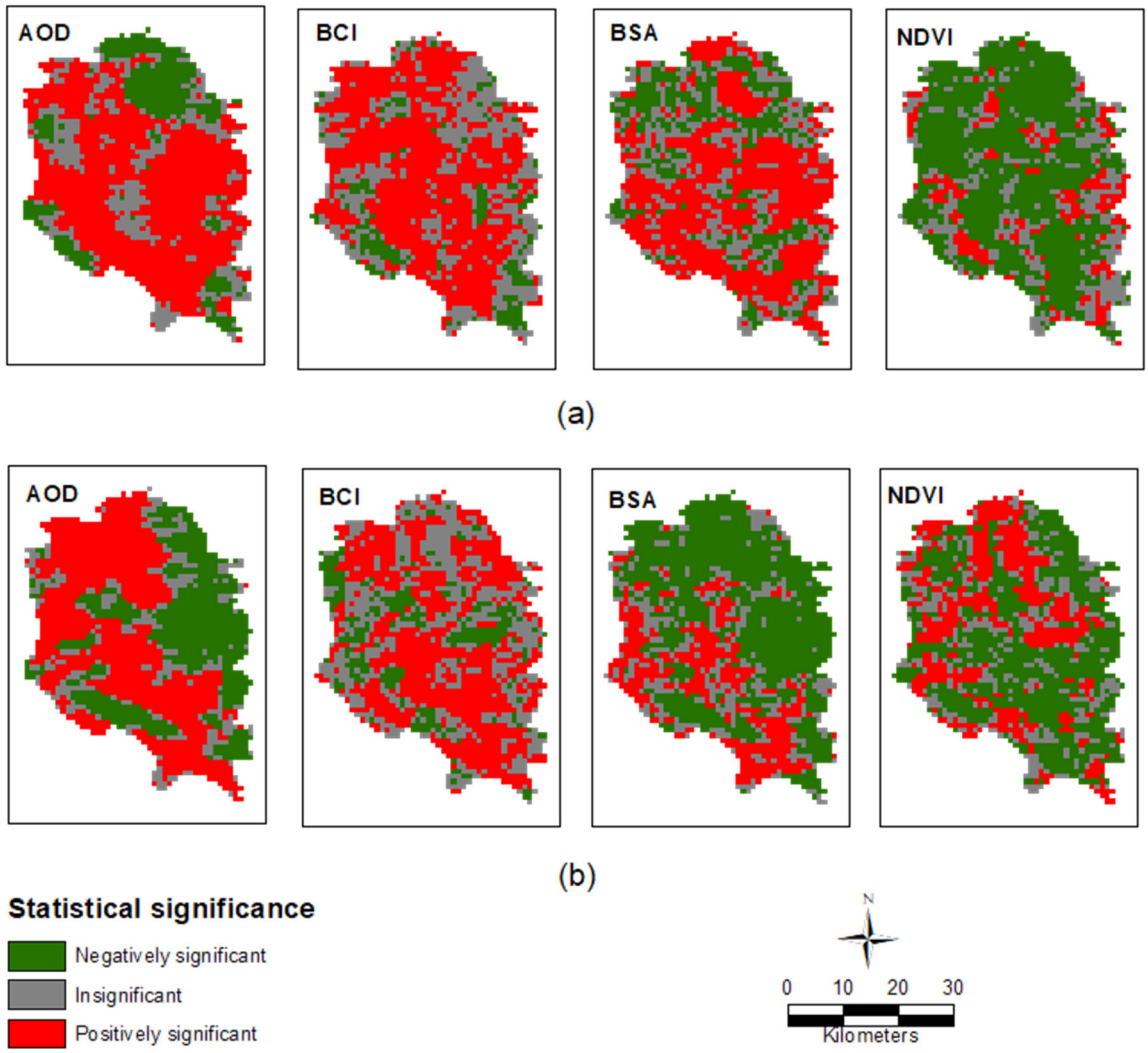

Figure 2–34 Correlation maps showing: a) day; b) night SUHI versus aod, bci, bsa and ndvi during the winter season

2.7 Discussion

Moderate resolution (30 m) cloud–free Landsat data for the 2000, 2004, 2010 and 2017 years was used to determine changes in LULC. The spatial pattern of urban growth (collectively referred to as built–up) indicated that the predominant expansion direction of the built–up areas of Dhaka were along a NNW–SSE axis, with growth occurring both north and south of the already developed urban areas. This has included expansion into areas of low–lying marshy lands south of the main urban core areas, which were originally considered a constraint to development (Dewan and Corner, 2014a). From 2010, and continuing into 2017, there is evidence of increasing urbanisation along the extensive system of major transport routes radiating out from the city proper. The area statistics indicated that built–up class increased from 6.5% to 34% of the available land area. Only cultivated land makes up a greater proportion (44%) but this also decreased from 2000 when 53% of the area was under cultivation. Similarly,

vegetation and wetland/lowland areas also decreased (Table 2–6). The map density estimation indicated a consistent increase in low and medium built–up density and a decrease in the high–density areas from 2000 to 2017 (Figure 2–6 and Table 2–8). This is consistent with the trend observed by Dewan and Corner (2014c), which showed a decline from a high of 80% in 2000 to 76% in 2011. They suggested that most high–density development is adjacent to already developed urban areas while the low and medium density development is found along the road networks and around the periphery of the city (Figure 2–6).

Regression analysis showed that percent built–up and population density variables have significant effects on both annual day and nighttime SUHI. The relationship appeared to be both linear and non–linear (Table 2–9). This finding is in accord with a study by Lazzarini et al. (2013) who noted that a rise in percent imperviousness led to an increase in surface temperature during summer and winter. Coseo and Larsen (2014) observed that a 10% increase in impervious surface area increased the nighttime air temperature by 0.74 °C in Chicago, however the current findings clearly show that the shift in demographic patterns (which led to an increase in built–up land) has also had a direct impact on the SUHI magnitude. It is also surmised that percent vegetation cover would be a very useful additional variable to include in the model. These current findings are an improvement on information documented in the existing literature (Zhang et al. 2013; Rizwan et al. 2008).

Annual MODIS LULC data was used to ensure that there was commonality in the data capture methodology and the temporal–spatial scale. Buffering was used for delineation of the rural area (at a distance of 5–10 km from the urban area boundary for each year). The annual LST data for LULC during 2003–2018 period revealed that built–up cover (urban area) had a considerably higher LST than other covers during the day, while at night various waterbodies, wetlands and grassland categories tended to have a thermal response similar to built–up areas (Figure 2–11). This differential response may be related to various physical, ecological and socioeconomic drivers within cities having a significant effect on the SUHI and influencing urban microclimatic features (Dwivedi and Mohan, 2018; Trlica et al. 2017; Li et al. 2016, Schwarz et al. 2012).

2.7.1 Analysis of SUHI over different timescales

An analysis of the SUHI indicated that April (during the pre–monsoonal period), was the hottest month and that the magnitude of SUHI could be as high as 3.43 °C during the daytime. SUHI did record the highest values during the winter month of January (2.23 °C) at nighttime. With the arrival of the monsoonal downpours, SUHI tended to decrease, but increased again in the post–monsoonal period. An important finding is that the nighttime SUHI is higher during December and January, a period when mean nocturnal temperatures also remain higher than during the day. This appears to confirm a warming trend in the winter nights. This finding is consistent with studies done elsewhere (Sun et al. 2019), suggesting an asymmetric warming

of climate (Chakraborty and Lee, 2019; Peng et al. 2013). Spatially, the daytime SUHI is well distributed over built–up surface of the DMDP area from February to November (Figure 2–14). With the arrival of the southwest monsoon, the nighttime SUHI decreases, and from July to September there is essentially no SUHI (Figure 2–15). This feature could be related to the background climate (Sun et al. 2019; Zhao et al. 2014) and requires further investigation.

Seasonally, SUHI ranges from 0.25–1.60 °C during daytime, and during the night it varies between –0.16 °C and 8.4 °C, with the pre–monsoon period having the hottest temperatures (Figure 2–16). The winter season has a consistently higher nighttime SUHI in comparison to the other seasons. In regards day–night variability, the monsoon and pre–monsoon seasons appeared to show high day and night SUHI variability (Figure 2–16). The monsoon season SUHI appears highly scattered but the other three seasons (pre–monsoon, winter and post–monsoon) showed a consistent pattern, indicating that urban surfaces had high to very high SUHI during both day and night. A similar observation was noted by Ifzhak-Ben-Shalom et al. (2017) over Dhaka for nighttime SUHI during the monsoon season. These findings also correspond with those noted by Chun and Guldmann (2018) and Yao et al. (2018a, b), highlighting the fact that the seasonality of SUHI is a crucial element that needs to be incorporated into the development of any possible mitigation measures. This factor has been largely overlooked in work conducted to date (Chun and Guldmann, 2018).

Annually the daytime SUHI showed a sharply increasing trend in comparison to the nighttime where the trend was fairly flat (Figure 2–18). This is consistent with the findings of many global studies (Chakraborty and Lee, 2019; Deilmai et al. 2018; Peng et al. 2011) and may be related to several causative factors, including urban form, geographic location and street orientation (Giridharan and Emmanuel, 2018; Drach et al. 2018; Roth, 2007). Spatially, a difference of approximately 1.7 °C in SUHI is observed between the urban and rural land covers during the daytime. At night, it is around 1.5 °C (Figure 2–19). Analysis of the trend of SUHI area coverage over annual scale indicated that pixels having SUHI of >= 2 °C are increasing at a greater rate during the day than at night (Figure 2–23).

2.7.2 Environmental factors associated with SUHI magnitude

Spatial correlation between day and nighttime SUHI and predictor variables indicated that the relationship is dependent on many factors and the strength of correlation varies between seasons. For example, during pre–monsoon season daytime SUHI, aod, bci and ndvi are important factors, while the presence of vegetation cover appears to have had significant effects on the nighttime SUHI (Figures 2–31, a–b). In the monsoonal months, ndvi appears to influence daytime SUHI to a greater extent than any other variables, whereas the effect of bci was minimal (Figures 2–32, a–b). A similar type of correlation was observed during the post–monsoon season (Figures 2–33, a–b), however aod, bci, bsa and ndvi tend to have substantial influence on day and nighttime SUHI during winter season (Figure 3–34, a–b). Although most

of the predictors had a differential effect on daytime and nighttime SUHI, the influence on vegetation pixels was generally consistent at a seasonal scale. This confirms the findings of other studies that urban heat tends to decrease with the presence of vegetation cover (Saaroni et al. 2018; Tan et al. 2016; Onishi et al. 2010), but during the winter time this effect is almost nil (Chun and Guldmann, 2018).

The GWR model clarified which environmental factors had the greatest influence on SUHI distribution during the day and night (Table 2–10, 2–11). During daytime, built–up was the prime factor affecting SUHI variability over space, followed by population density and percent tree cover. Conversely, during the nighttime, population density and evi were the most important predictors of SUHI. This may be related to the observation made by Rizwan et al. (2008) who demonstrated that direct anthropogenic heat flux during the night contributes to the maintenance of nighttime SUHI. Furthermore, dominant factors affecting LST distribution over an area vary with the seasons. This highlights the fact that any adaptation strategies must be based on local conditions (Ferreira and Duarte, 2019; Peng et al. 2018). Encroachment of waterbodies into urban development areas could also be an important factor – potentially elevating nighttime SUHI due to the fact that waterbodies affect the transformation of sensible and latent heat flux (Sun and Chen, 2012). Rapid urbanisation, intense human activity, construction of a very large number of high–rise buildings in recent times and the associated effects on air movements, the trapping of short–wave radiation, and high heat conductivity of man–made features may all be playing a significant role in SUHI development in the DMDP area (Deilami et al. 2018; Akbari et al. 2016). Urban planning requirements such as specific green cover ratios and building densities are not strictly enforced during new urban development in the area, and these issues could all have a serious influence on the observed variation in SUHI. Kakon et al. (2009) noted that the outdoor thermal comfort of Dhaka did not noticeably improve following the enactment of new building regulations, reinforcing the effect of mankind on local warming of Dhaka.

This work quantified the spatiotemporal variability of SUHI and influencing factors in the DMDP area. This is the first time this has been achieved and promises to provide some valuable pointers for planners when developing mitigation measures, specifically based on local conditions (Li et al. 2012). It has been argued that temporal aggregation (Hu and Brunsell, 2013) and urban thermal anisotropy (Li and Li, 2020; Voogt, 2008) may introduce bias in the estimation of SUHI over urban areas, however studies also revealed that compositing data at various temporal scales prior to further analysis greatly reduces any possible estimation biases (Lai et al. 2018a; Wang et al. 2017; Hu and Brunsell, 2013).

2.8 Conclusion

The objectives of the chapter were to examine spatiotemporal variability of the surface urban heat island (SUHI) and its influencing factors over the Dhaka Metropolitan Development Plan (DMDP) area. Combined MODIS LST data as well as other associated MODIS products recorded from 2003–2018, were used to investigate the relationships between SUHI or LST. In addition, multi–temporal Landsat data and population data from two decennial censuses (2001 and 2011) was used to understand the effects of demographic shift and land cover change on SUHI. Major findings of this chapter are:

- Due to population shift, changes in land use/cover have been very rapid resulting in a marked increase in SUHI. Regression models demonstrated that as the percent built–up and population density increased, SUHI also increased in response.

- The LST of urban areas was considerably higher during daytime than that associated with other land use categories, while wetlands, waterbodies and urban categories had a similar LST during the night.

- At a monthly scale, April appears to be consistently the hottest month, with daytime SUHI up to 3.43 °C greater than the rural area. The nighttime SUHI, during January and December, is higher (2.23 and 2.14 °C, respectively) than during the daytime (1.7 and 1.27 °C) and exhibited marked spatial variation.

- Seasonally, winter showed the highest area coverage with little difference between day and night SUHI. High day–night variability of SUHI is observed in the pre–monsoon and monsoon seasons but a very subtle day–night variation observed in winter.

- Annual daytime SUHI appears to be increasing with time, though the nocturnal SUHI trend is relatively flat. Since 2003, the spatial distribution of SUHI increased to a greater degree in the daytime than at nighttime. At a pixel scale, cells ≥ 2° C SUHI showed an increasing trend for the daytime as compared to the nighttime.

- Factors influencing SUHI tend to vary between day and night. The use of GWR techniques show that both anthropogenic (e.g. imperviousness) and physical (e.g. albedo) factors are responsible for elevating SUHI in the study area. Predicted versus observed SUHI using GWR modelling indicated a good model fit with a correlation coefficient of 0.98 for both day and nighttime.

3 MICROSCALE ANALYSIS – DHAKA METROPOLITAN AREA (DMA)

3.1 Introduction

In the previous chapter, high temporal resolution but low spatial resolution MODIS data was used to determine SUHI at the mesoscale. While 1 km spatial resolution data is useful for assessing SUHI at the mesoscale, such resolution appears to hinder characterising SUHI and determining causal factors at the microscale. The following microscale assessment examines the SUHI phenomenon in detail in the DMA, an area of approximately 300 km^2 located within the DMDP area (Figure 3–1).

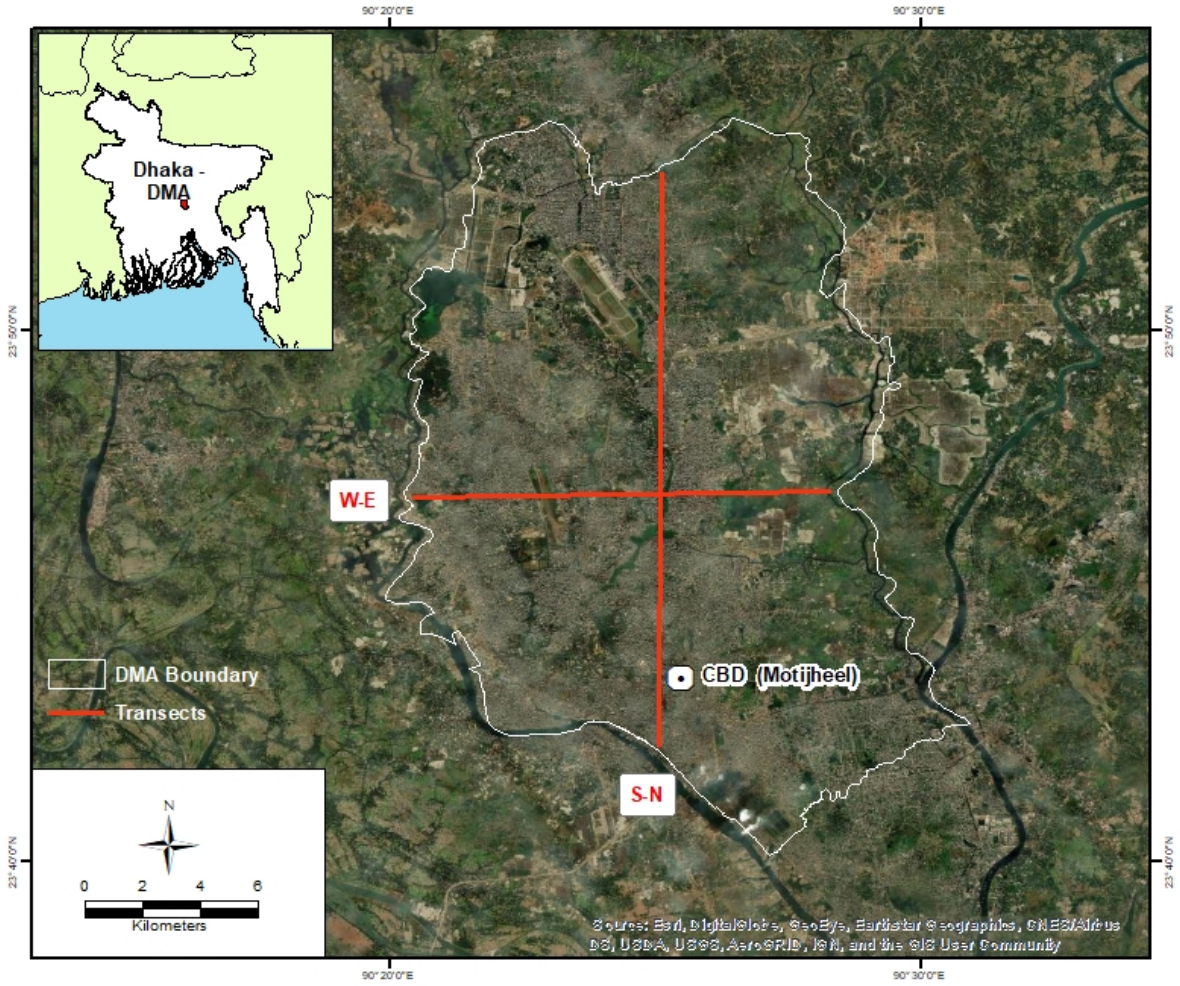

Figure 3–1 Boundary of the Dhaka Metropolitan Area (white and light grey) with transect lines orientation shown in red (*source: ESRI, DigitalGlobe, Geoeye, EarthStar Geographics, CNES/Airbus DS, USDA, USGS, AeroGrid, IGN and the GIS User Community*)

The aims of the microscale analysis are: (i) to examine spatial and temporal variation of day and nighttime SUHI using medium–resolution satellite data; and (ii) to analyse biophysical factors influencing UHI. Figure 3–2 shows the methods and overall workflow of this chapter.

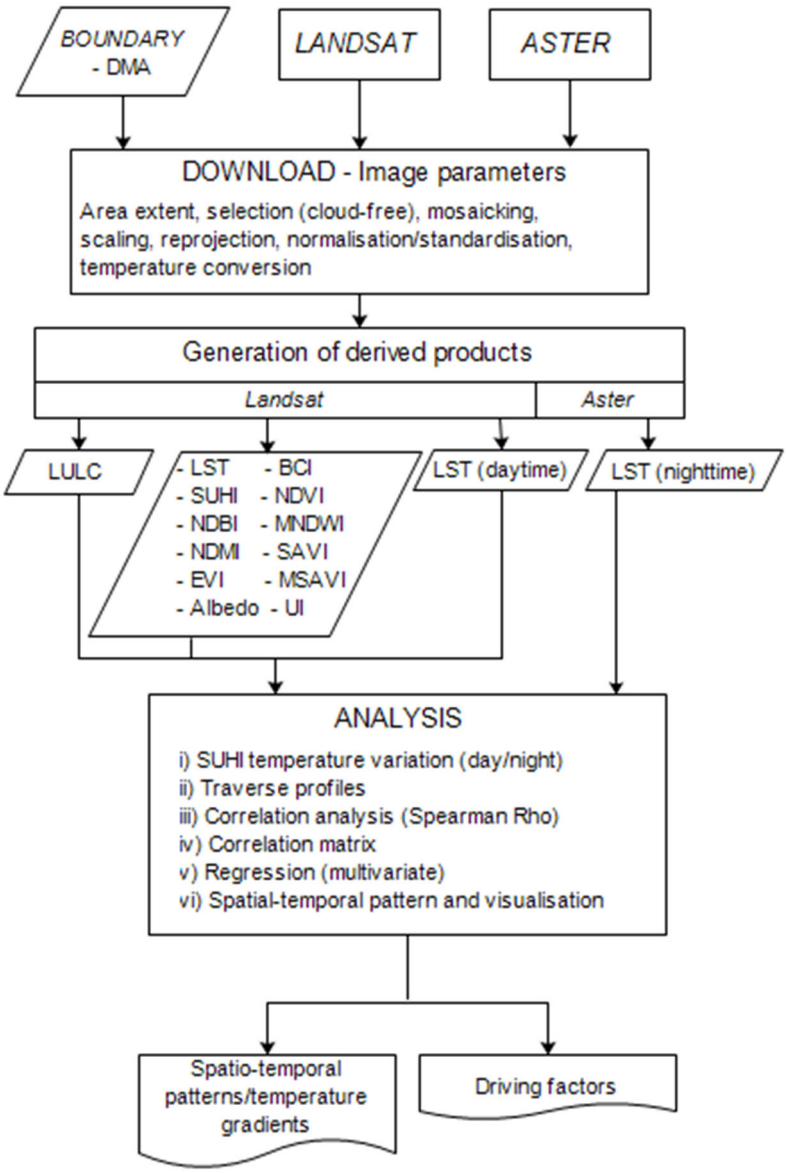

Figure 3–2 Flowchart, showing methods used in the microscale analysis

3.2 Description of the study area

The DMA is a police jurisdiction area (Dewan and Corner, 2014a) that constitutes the entire Dhaka North City Corporation (DNCC), Dhaka South City Corporation (DSCC), Cantonment Board and adjacent unions. It is bounded by four rivers, Buriganga to the south, Turag to the west, Balu to the east and Tongi Khal to the north. According to the 2011 population and housing census, the total population of DMA is 8,906,039, giving a density of 29,392 persons per km^2 (BBS, 2012). Compared with other parts of the DMDP, it has extensive administrative and infrastructure facilities together with dense transport networks. As a result, the DMA has been the major focus of urban development and economic activities. Due to unplanned urban expansion and rapid growth rates of population, however, a number of environmental issues

have become evident, including an increase in urban temperature (Trotter et al. 2017; Itzhak-Ben-Shalom et al. 2017; Ahmed et al. 2013).

3.3 Materials and methods

3.3.1 Landsat data acquisition and preparation

A total of 322 Landsat scenes of the DMA area (path 137, rows 43 and 44), comprising Landsat 5, 7 and 8 data between 2000 and 2018, were downloaded from the EarthExplorer (https://earthexplorer.usgs.gov/). Both Level 1 and Level 2 collections were selected, as the infrared thermal bands (TIRs) do not include in the Level 2 products. Four criteria were used to select Landsat data: i) less than 10% cloud cover; ii) clear–sky within the actual study area (i.e. a complete absence of clouds in any part of a scene); iii) each date must have two Landsat scenes covering the area of interest; and, iv) no Landsat 7 scene recorded after 31 May 2003 was to be used due to the Scan–Line Corrector (SLC) issue. A total of 160 scenes (from rows 43 and 44) were chosen for further processing. Two scenes of each day were geometrically rectified, mosaicked and clipped to the DMA boundary vector file, resulting in a final total of 80 mosaicked Landsat images (Appendix II).

An analysis of the seasonal distribution of the images shows that 46% cover the winter period (December–February), 30% comrpise post–monsoon (October–November) and 24% represent pre–monsoon months (March–May). No image satisfied the four criteria during the monsoonal months of June to September. It is worth noting that the original spatial resolution of TM TIR (band 6) is 120 m, ETM+ TIR (band 6) is 60 m and Landsat 8 TIRs (bands 10 and 11) are 100 m, but USGS downscales the original resolution to 30 m and provides this with the reflective bands.

3.3.2 Deriving biophysical parameters

A number of biophysical parameters were generated based on the mosaicked Landsat Level 2 products. The pre–processed Landsat 5, 7 and 8 surface reflectance products were retrieved using the two alternative algorithms. While the Landsat 4/5 and 7 use the Landsat Ecosystem Disturbance Adaptive Processing System (LEDAPS) algorithm, Landsat 8, on the other hand, utilises Surface Reflectance Code (LaSRC) to generate the surface reflectance of Landsat 8 (USGS, 2018a, b). Table 3–1 provides information on the biophysical indices derived and used. These were included in the study given their importance in understanding the relationship between land surface temperature (LST) and other biophysical parameters (Peng et al. 2019; Macarof and Statescu, 2017; Karnieli et al. 2010).

Together with biophysical parameters, multi–year albedo data was also computed from 80 Landsat mosaics. An albedo–derivation method proposed by Liang (2001) was used for the

Landsat 5 and 7 data; for Landsat 8, a method proposed by Baldinelli and Bonafoni (2017) was employed.

Table 3–1 Landsat–based spectral indices used in the microscale analysis

Indices	Formulation	Description	Reference
Normalised difference vegetation index (NDVI)	(NIR–R)/(NIR+R)	The higher the value, the greater the green vegetation cover	Rouse et al. (1974)
Normalised difference built–up index (NDBI)	(SWIR–NIR)/(SWIR+NIR)	Highlights the built–up surface	Zha et al. (2003)
Normalised difference moisture index (NDMI)	(NIR–SWIR)/NIR+SWIR)	Wetness of the land surface	Jin and Sader (2005)
Enhanced vegetation index (EVI)	G*((NIR–R)/(NIR+C1*R–C2*B+L))	Provides greater sensitivity to high biomass while minimising the influence of soil and the atmosphere	Liu and Huete (1995)
Modified normalised difference water index (MNDWI)	(Green–MIR)/(Green + MIR)	Enhances waterbodies by reducing the noise produced by non–water features	Xu (2006)
Urban index (UI)	(SWIR2–NIR)/SWIR2+NIR)	Highlights urban surface	Kawamura et al. (1996)
Soil–adjusted vegetation index (SAVI)	((NIR–RED)/(NIR + RED+L))*1+L	Distinguishes and minimizes soil brightness from canopy spectra	Huete (1988)
Modified soil–adjusted vegetation index (MSAVI)	2*s*((NIR–RED)*(NIR–s*RED))/(NIR+RED)	A more precise measurement of vegetation cover	Qi et al. (1994)
Biophysical composition index (BCI)		Isolates impervious surfaces from soil	Deng and Wu (2012)

* The bands used in specific indices computation vary between Landsat 5, 7 and 8

3.3.3 Computing daytime LST from Landsat data

Land surface temperature (LST) can vary strongly over time and space. It can differ by more than 10 Kelvin (K) over just a few centimetres or by more than 1 K in less than one minute (Tang and Li, 2014). The accuracy, and hence reliability, of any derived product depends on the method utilised for computation (Ma et al. 2010). To date several methods (comprising both single and multi–channel bands) are available to compute LST from TIRs (Li et al. 2013).

A number of these methods require ancillary information to compensate for atmospheric differences (Tang and Li, 2014). For example, the mono–window algorithm (Qin et al. 2001) is believed to produce relatively accurate LST, but its usage is limited when using historical TIRs due to the requirement of near surface air temperature and the total column water vapour content to be available for the satellite overpass period. This is usually not available (Tang and Li, 2014). Jiménez-Muñoz and Sobrino (2003) developed a generalised single channel algorithm from TIR data with a full width at half maximum (FWHM) of ~ 1 micrometre (μm). Land surface emissivity and water vapour content during data acquisition are the essential inputs. The radiative transfer equation (RTE) requires atmospheric upwelling, downwelling path radiance and transmittance information to calculate LST, but these are generally unavailable for historical data, particularly before 2000 (Yu et al. 2014; Basri et al. 2005). Likewise, a variety of split–window (SW) algorithms have been proposed following the first SW method by McMillin (1975). Even though the SW algorithms do not require atmospheric profile or radiosonde data during satellite overpass, two adjacent TIR channels are necessary to be utilised (Wan and Dozier, 1996). In the absence of atmospheric profile information, water vapour content and near–surface air temperature data during the TIRs acquisition, an image–based method has been developed (Lo and Quattrochi, 2003; Weng, 2001), which is also known as the Planck function (Ndossi and Avdan, 2016). Comparison of LST algorithms with Landsat 8 data revealed that the RTE produced reasonably accurate data with an RMSE (root mean square error) of <1 K for TIR band 10, the split–window method provides moderate accuracy, and the single channel gives low accuracy (Yu et al. 2014). In another work, Ndossi and Avdan (2016) compared four methods (e.g. RTE, mono–window, single channel and Planck function or image–based) in retrieving LST from three generations of Landsat TIRs (e.g. Landsat 5, 7 and 8). Their study showed that the image–based method produced superior results (RMSE of 1.58 °C) when compared to RTE (RMSE of 2.64 °C) for Landsat TM 5. Both RTE (RMSE of 3.75 °C) and Planck function (RMSE of 3.58 °C) are best for Landsat 7 ETM+. The Planck function (2.07 °C) has the best outcome for Landsat 8, closely followed by the single channel algorithm (RMSE of 3.06 °C).

The downloaded satellite data included both historical, single and multi–channel imageries. As a result, the availability of atmospheric profile data proved to be a major constraint in utilising the RTE, mono–window, split–window and single channel method. The Bangladesh Meteorological Department (BMD) was contacted in regards the ability to access profile information, however this was not available. The documented stray light issue, associated with the Landsat 8 TIR band 11, also increases the uncertainty in the estimation of LST and constrains the use of the split–window algorithm (Montanaro et al. 2014; https://landsat.gsfc.nasa.gov/landsat-8-thermal-data-ghost-free-after-stray-light-exorcism/).
An image–based approach, therefore, appears to be a viable alternative in retrieving LST from the multi–temporal Landsat data due to the higher degree of accuracy obtained when compared with other methods (Ndossi and Avdan 2016), and when tested in various environments

(Hammodi et al. 2019; Peng et al. 2019; Dai et al. 2018; Trotter et al. 2017; Shen et al. 2016; Chen et al. 2014; Li et al. 2012). The data consisted of single band TIR data from three Landsat sensors for multiple years, so a 3–stage custom model was used.

In the first stage, the digital number of all TIRs from the mosaicked Landsat images were converted into spectral radiance by employing the calibration coefficients (e.g. gains and bias) (Chander et al. 2009; Chander and Markham, 2003), available in the metadata. Next, Planck Law's was applied to convert spectral radiance into at–sensor brightness temperature (Tb) in K using the following equation.

$$T_b = \frac{K_2}{\ln[(K_1/L_\lambda)+1]} \quad (1)$$

L_λ is the at–sensor radiance of TM/ETM+ band 6 and Landsat 8 band 10 (W * m2 * sr * μm), and K_1 and K_2 are pre–launch calibration constants in K. For Landsat TM, K_1 = 607.76 W * m^2 * sr * μm, K_2 = 1260.56 K, for ETM+, K_1 = 666.09 W * m^2 * sr * μm, K_2 = 1282.71 K and for Landsat 8, K_1 = 774.89 W * m^2 * sr * μm and K_2 = 1321.08 K, respectively (https://www.usgs.gov/land-resources/nli/landsat/landsat-8-data-users-handbook), were used.

Finally, to retrieve LST from brightness temperature (T_b), individual images were used to obtain spectral emissivity (Artis and Carnahan, 1982). The NDVI Threshold Method utilises the following equation (Sobrino et al. 2008) and NDVI data obtained from the relevant Landsat bands (Table 3–1).

$$\text{LST} = \frac{T_b}{1+(\lambda T(\text{K})/\rho)\ln\varepsilon} \quad (2)$$

λ is the wavelength of emitted radiance in meters, ρ equals hc/σ (1.438 x 10^{-2} mK), K is the Stefan Boltzmann's constant (1.38 x 10^{-23} J K^{-1}), h is the Planck's constant (6.26 x 10^{-34} J s), c is the velocity of light (2.998 x 10^8 s^{-1}), ε is the estimated surface emissivity. Generally, the emissivity value for a vegetated surface is 0.95, for non–vegetated surface it is 0.923 and for water areas it is 0.992 (Weng et al. 2004; Artis and Carnahan, 1982). However, when a surface is covered by a mixture of soil and vegetation, defined values between 0.2 and 0.5 are applied (Avdan and Jovanovska, 2016). The vegetation fraction (P_v) is computed from each NDVI product, factoring in the emissivity of various land covers using an empirical function suggested by Gillies et al. (1997) as NDVI is dependent on the season and the atmospheric conditions of an area. The derived LST in Kelvin was then converted to degree Celsius by adding absolute zero (approximately –273.5 °C).

3.3.4 ASTER–based nighttime LST

To derive nighttime LST, the product of ASTER (AST_08) was downloaded from https://lpdaac.usgs.gov/products/ast_08v003/. The AST_08 is a surface kinetic temperature generated using the five TIR bands of ASTER, with a spectral range of 8–12 μm. The Planck's Law is used to retrieve LST, and the Temperature/Emissivity Separation (TES) algorithm is used to account for surface emissivity (Gillespie et al. 1998). The downloaded data are in 90 m spatial resolution and is widely used in urban climate studies (Sun and Chen, 2012; https://asterweb.jpl.nasa.gov/content/03_data/04_Documents/ASTERHigherLevelUserGuide Ver2May01.pdf) and has an absolute accuracy of <1.5 K (https://asterweb.jpl.nasa.gov/content/03_data/04_Documents/ASTERHigherLevelUserGuide Ver2May01.pdf).

An initial quality check found that only seven ASTER LST products could realistically be used to examine nighttime LST. Of the seven products, three were from 2018 (January 06, December 01 and 08) and there was only one each for 2016 (November 09), 2015 (November 12), 2012 (December 07) and 2005 (November 11). It should be noted that the nighttime LST data does not provide coverage for all the seasons and the majority represent only winter. Due to this incomplete coverage, the samples are not regarded as adequate to perform seasonal evaluation of nocturnal SUHI. The original imagery was mosaicked and the LST of individual years was clipped to the DMA boundary.

The final step involved aggregating the Landsat and ASTER–based LST data to annual scales. This operation resulted in a disproportionate number of samples. It should be noted that there is no Landsat coverage for 2012 available due to transitioning to Landsat 8. Previous studies across large cities of the world, however, have employed limited numbers of images to characterise SUHI (Huang et al. 2019; Yang et al. 2018) so this is not regarded as an issue. It is, therefore, reasonable to assume that any issues with the number of day and night samples should not affect the evaluation of LST and SUHI at an annual scale.

3.3.5 Computing SUHI

The land use/land cover (LULC) data represent only four years – 2000, 2004, 2010 and 2017 (see Chapter 2). It is assumed that the LULC of 2000 can be used to estimate SUHI in 2000–2003, and similarly the LULC of 2004 can be used for 2004–2008, LULC of 2010 used for 2009–2015 and LULC of 2017 can be used for the 2016–2018 period. Since the study area is small and a true rural pixel is difficult to define, the SUHI was computed by subtracting the mean temperature of the combined vegetation plus cultivated land pixels from the urban pixels, on a pixel–by–pixel. Another option was to use vegetation pixels for this calculation, however when used in the calculation, the results were very similar. The literature suggests that both categories may be useful for calculating SUHI due to their role as a cool–island feature (Zhang

et al. 2013). Prior to computing SUHI, the urban water pixels were masked out. The analysis was conducted for all years between 2000 and 2018 to map the SUHI spatio–temporal pattern.

As noted previously, the limited number of ASTER samples hindered the time series mapping of nighttime LST. Only five LST products, spanning the 2005 to 2018 period, could be used. In a similar manner to the Landsat LST data, the 2004 LULC data was overlaid with 2005 LST, 2010 LULC with 2012 and 2015 LST, and 2017 LULC cover with 2018 LST data to determine thermal response of the land use/cover categories. The nighttime SUHI was then computed based on the combined mean value of the cultivated plus vegetation cover for each year.

To derive annual–scale LST over the study period (2000–2018), the mean value of the original individual years was considered. The annual daytime SUHI was then calculated by subtracting the mean temperature of the cultivated plus vegetation pixels over this period from the annual LST. A similar procedure was used for nighttime SUHI extraction, however only five years (2005, 2015, 2015, 2016 and 2018) data were used.

LULC datasets produced from Landsat imagery are available for the years 2000, 2004, 2010 and 2017 (see Chapter 2, Figure 2–4). They all represent the month of December (winter) so use of these in estimating the SUHI of the other three seasons (pre–monsoon, monsoon and post–monsoon) could be problematic and may increase uncertainty. It is felt that the disproportionate number of day and night LST samples could affect the findings significantly, so in this chapter, the analysis of LST and SUHI has been restricted to an annual scale. This is in contrast to mesoscale (e.g. DMDP) work where entire time–series MODIS data was available, with a few exceptions.

3.3.6 Relationship between biophysical parameters and LST

A number of biophysical variables were extracted from the Landsat surface reflectance products and then aggregated to annual scale. To examine the relationship between the biophysical indicators and LST for the period 2000 to 2018, a set of 1000 random points were selected within the DMA. They were then used to extract the mean annual values of various biophysical variables and LST from each point location for each year. Instead of investigating the relationship for every year, the retrieved annual values were further averaged over the 18 years. A non–parametric bivariate correlation was carried out to measure the strength of association. The Spearman Rho correlation coefficient was used in this case. Due to the existence of high correlations between the potential variables, the development of linear regression models for predicting LST was not considered. To overcome this issue, a series of linear regression models were developed. The stepwise method was utilised and the best models were chosen based on their predictive ability and coefficient of determination (i.e. r^2).

3.3.7 Profiling of SUHI

To provide an understanding of the spatial variation of the SUHI and the various biophysical variables, two transects were defined within the DMA to provide georeferenced locations for image data extraction: a north–south (N–S) line and an east–west (E–W) line (see Figure 3–1). Points at 100 m intervals along the transects were subsequently computed. The DMA area is elongated along the N–S orientation so this transect is 21 km in length (comprising 201 points at 100 m intervals) while the E–W is 14 km in length (137 points). The transect points were overlain over the applicable aerial imagery and SUHI, and variable values were extracted from the rasters using the geographic information systems (GIS) tools. Individual variables were averaged for the entire study period and the results examined for possible causal factors. It should be noted that the N–S profile intersected the general Central Business District (CBD) or Motijheel area to allow SUHI differences between the CBD and other locations in the study area to be visualised.

3.4 Results

3.4.1 Daytime variation

The mean of LST according to LULC is presented in Figure 3–3a. This demonstrates that the temperature of the built–up category was consistently higher when compared with the natural surface (essentially the vegetation cover). The spatial distribution of yearly LST (day and night) can be found in Appendix III and IV. Plotting the mean LST between built–up and cultivated plus vegetation categories shows that the LST of urban or built–up locations is higher (Figure 3–3b). The analysis further indicates that mean urban LST for the 18 years (2000–2018) is around 1.30 °C higher than that of the combined LULC class of vegetation plus cultivated lands. It can be seen that the urban LST shows a slight increase as compared to the combined LULC category.

Figure 3–4 shows yearly daytime SUHI. This indicates that certain parts of the DMA are prone to elevated SUHI, particularly dense urban locations such as areas close to the CBD. Examination of SUHI reveals that it tends to fluctuate considerably over time. The maximum SUHI (2.35 °C) was observed in 2011, whereas the minimum was recorded in 2001 (0.91 °C). The long–term (2000–2018) difference of mean SUHI between urban (1.36 °C) and vegetation cover (0.20 °C), for instance, indicates that the urban area has temperatures in excess of 1.1 °C. This clearly shows the existence of a daytime SUHI in the DMA, though its spatial pattern tends to vary over time (Figure 3–4). Inter–annual variation showed substantial temporal fluctuation of daytime SUHI with a clear spike in 2011 (Figure 3–5).

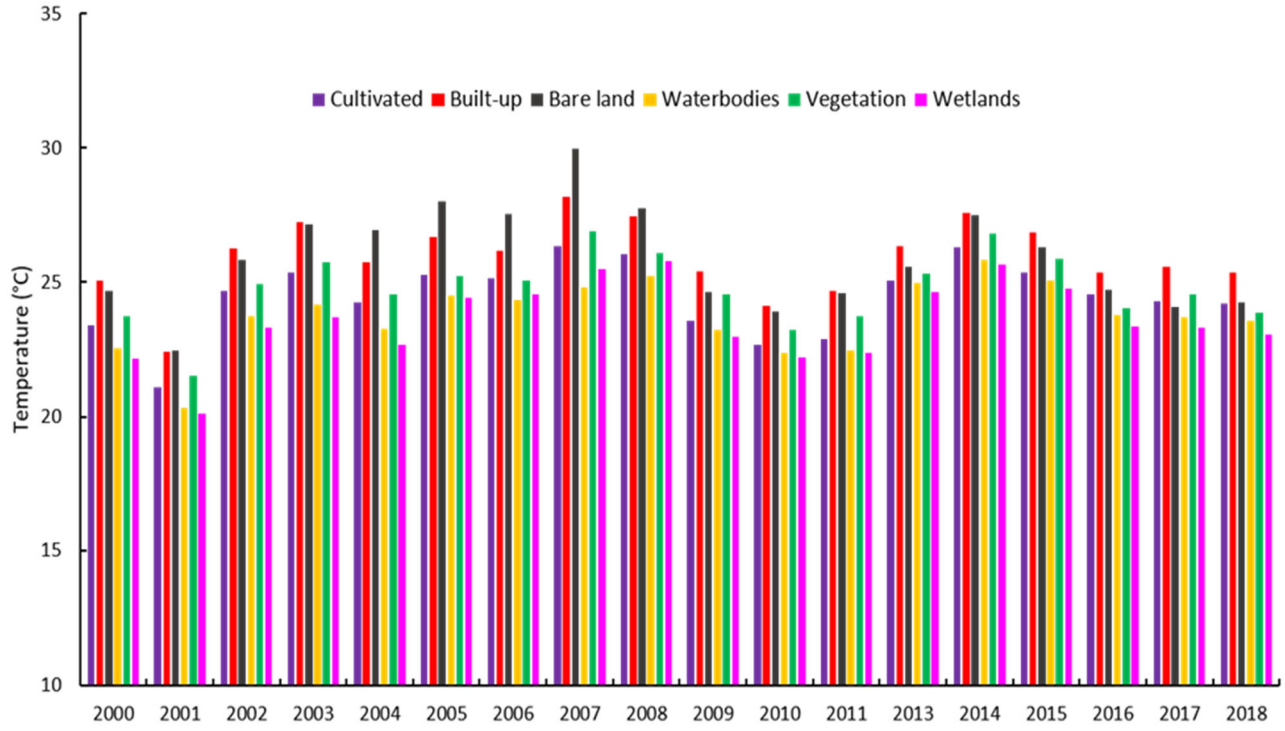

(a)

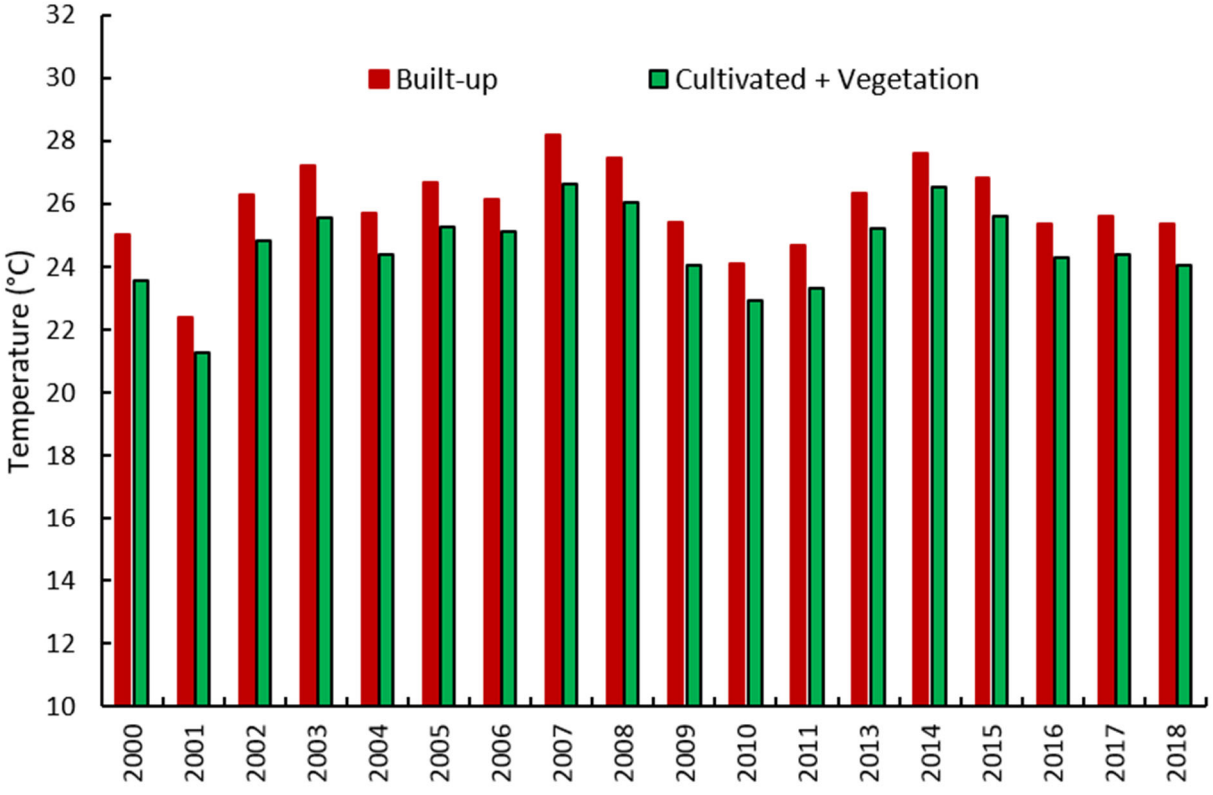

(b)

Figure 3–3 Temporal bar graph, showing mean LST against: (a) LULC categories; (b) built–up and cultivated plus vegetation

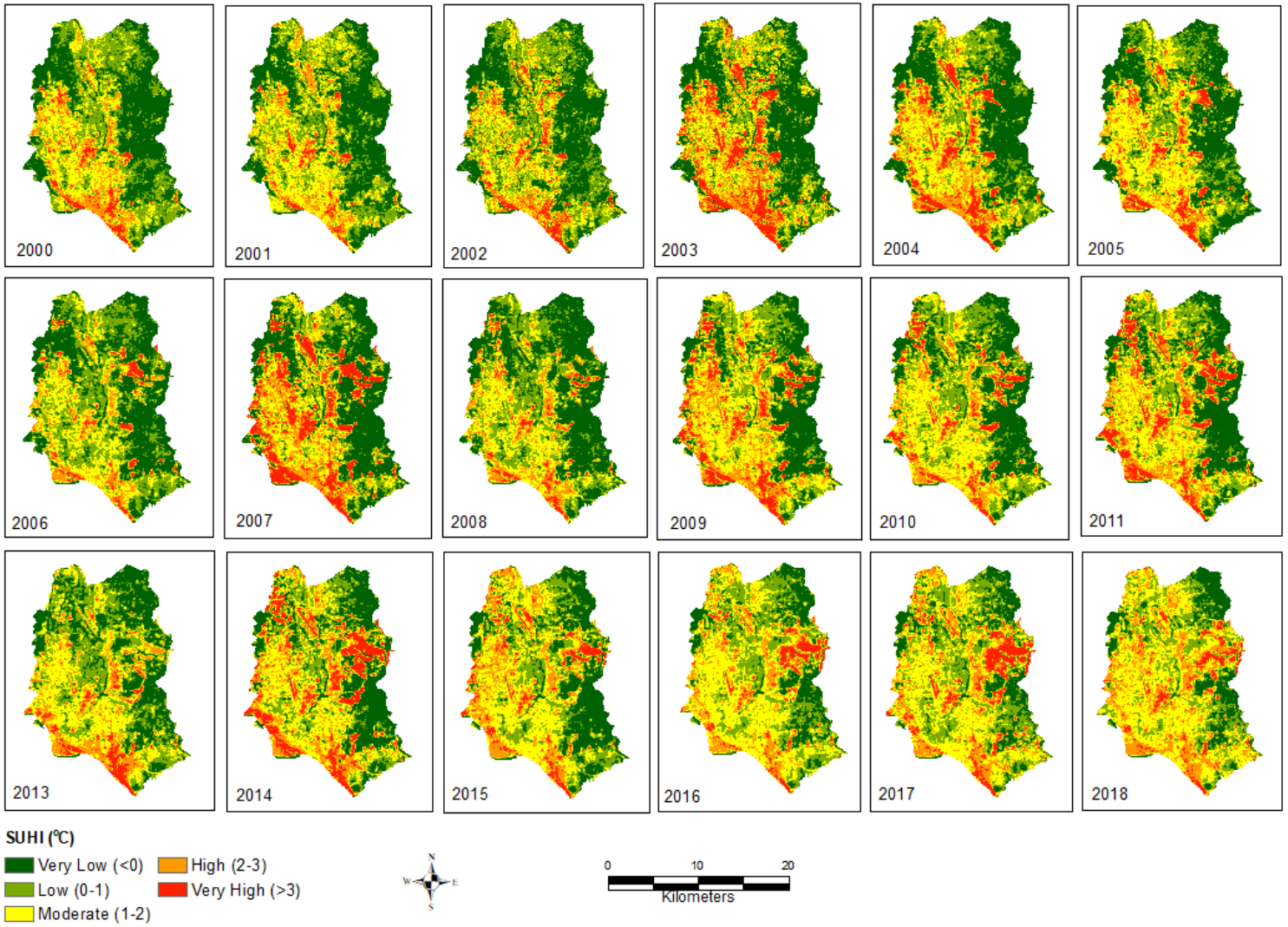

Figure 3–4 Daytime SUHI, 2000–2018

Figure 3–5 Temporal variation of daytime SUHI, 2000–2018

Plotting of LULC categories against SUHI indicates that bare land and built–up LULC had higher SUHI compared with cultivated land, for example, and this clearly points toward increasing temperature of the urban surface of the DMA (Figure 3–6). Bare land also had the elevated SUHI over the years 2000 to 2018.

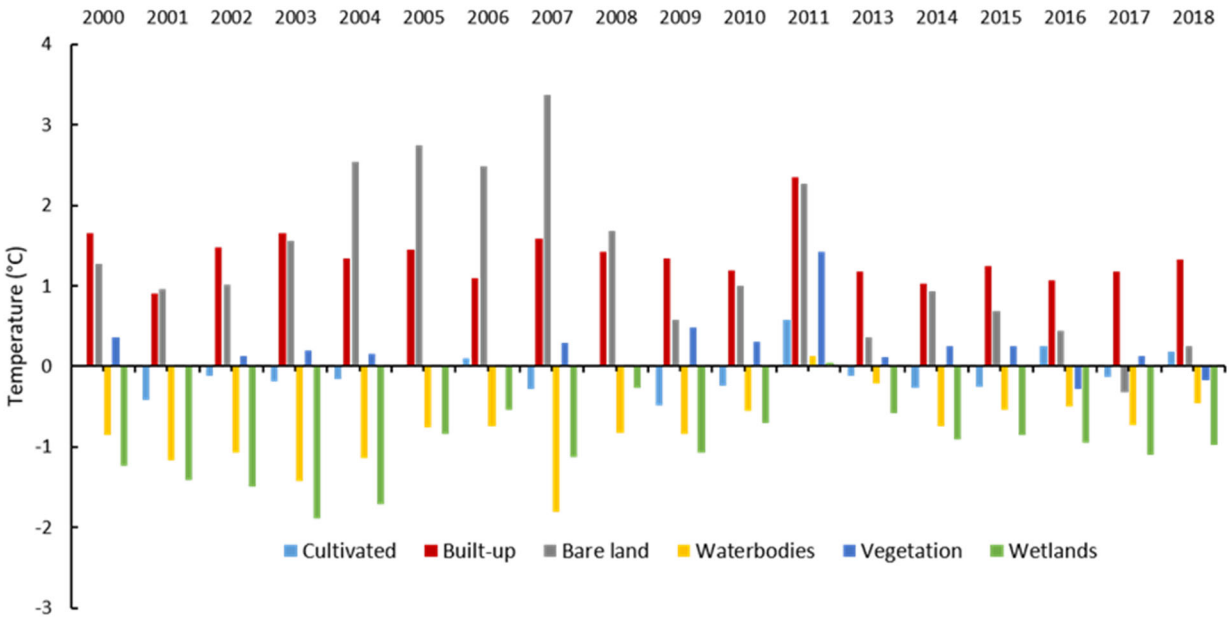

Figure 3–6 Daytime mean SUHI according to LULC categories, 2000–2018

3.4.2 Nighttime variation

Figure 3–7 shows nighttime LST distribution according to LULC categories. Out of five years, the mean LST for combined vegetation plus cultivated LULC was slightly higher during 2005 and 2015 when compared with other three years. On average, built–up (urban) surface exhibited a temperature 0.28 °C higher than the combined LULC (cultivated plus vegetation) category between 2005 and 2018.

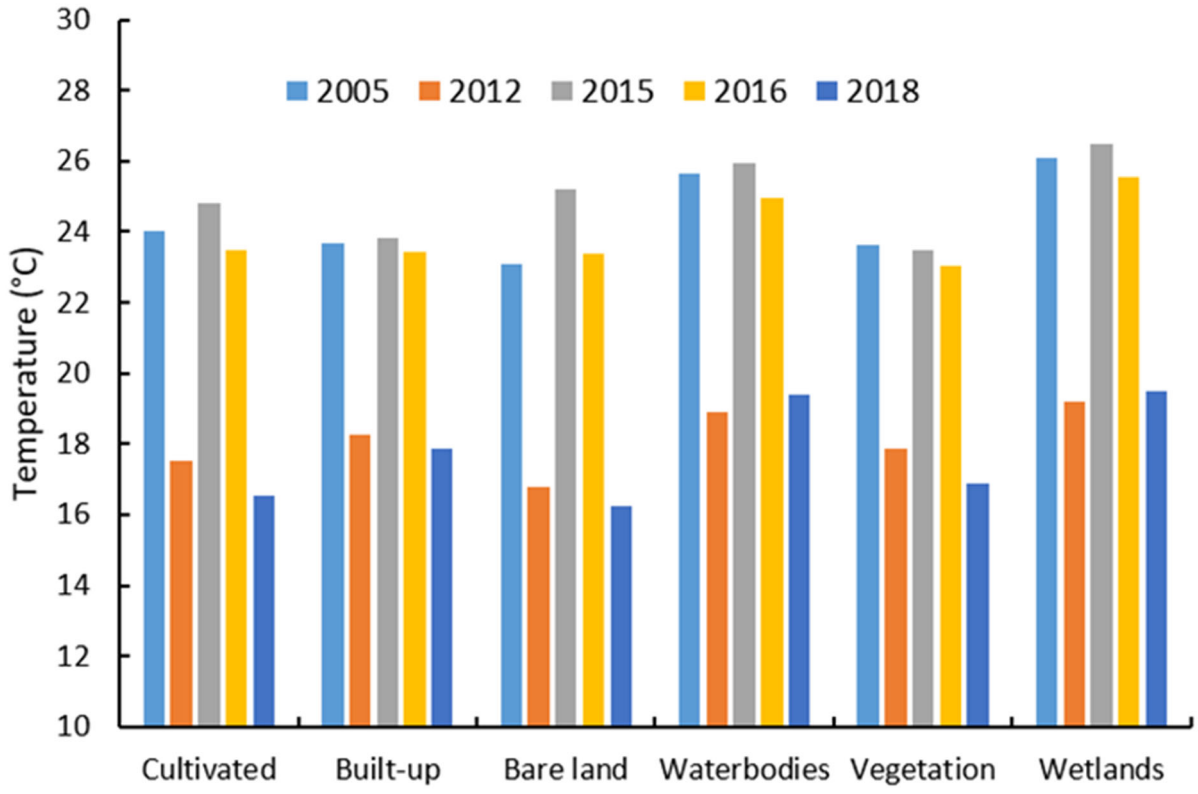

Figure 3–7 Mean LST over time according to LULC during nighttime

As expected, waterbodies and wetland categories had a higher LST than built–up cover due to the variation in the thermal inertia of differing water surfaces (Figure 3–7). The average of waterbodies and wetlands LULC were found to be 1.6 and 1.9 °C higher than the built–up category during the night. Appendix IV shows the distribution of nighttime LST in DMA.

The spatial pattern of annual nighttime SUHI is presented in Figure 3–8. This indicates that during 2012, 2015 and 2018, the SUHI was highly pronounced in the developed locations. In contrast, the magnitude during 2005 and 2016 was not as intense as other three years (e.g. 2012, 2015 and 2018), signifying high spatial variability. As expected, the temperature distribution of various water surfaces (such as a lake) is quite evident during nighttime.

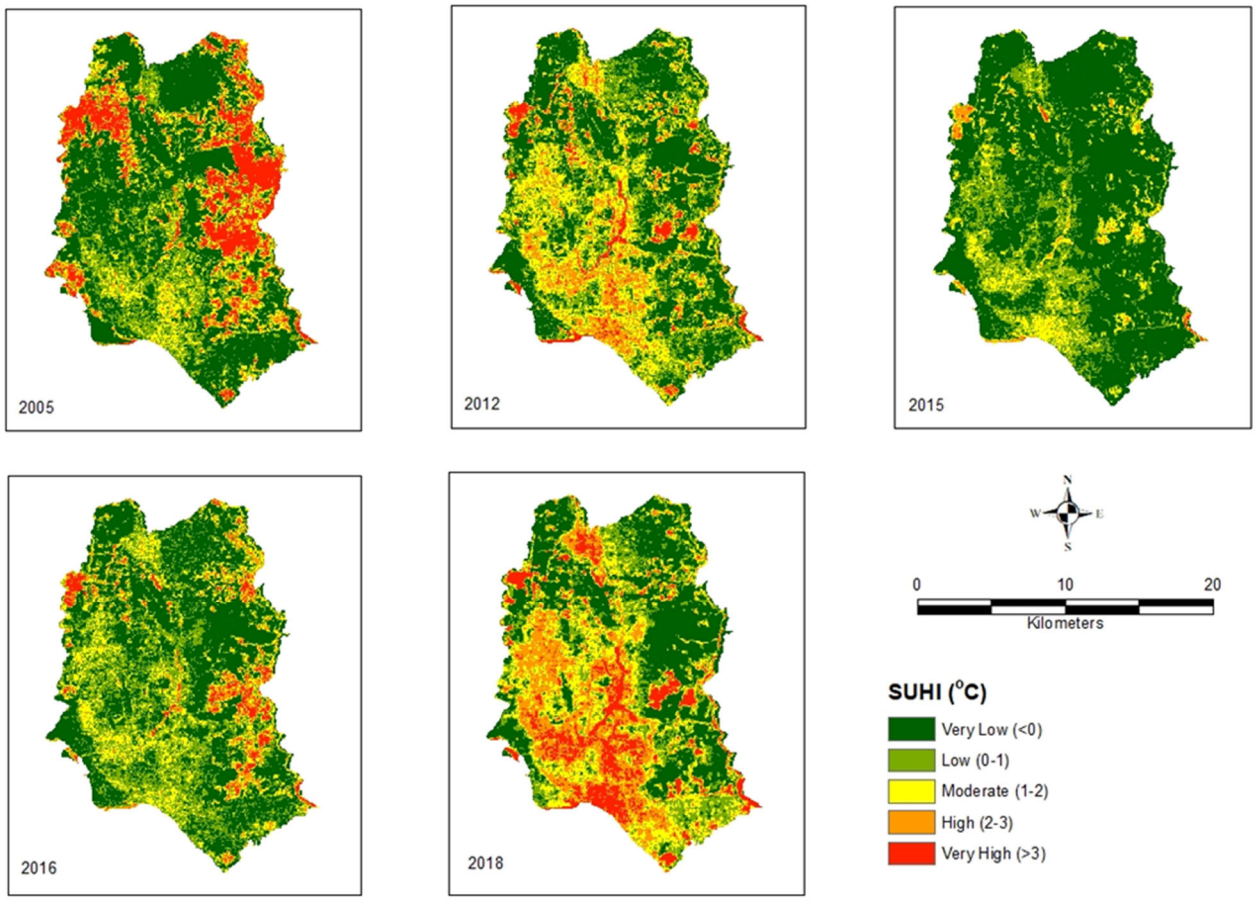

Figure 3–8 Spatial distribution of nighttime SUHI

The temporal variation of nighttime SUHI evident in the different LULC categories, reveals waterbodies and wetland cover had a positive SUHI over the 2005–2018 period for which data is available (Figure 3–9). In contrast, the built–up surface had relatively low temperatures in 2005 and 2015, but exhibited positive SUHI in the other three years. The maximum nighttime SUHI for urban surface was found to be 1.5 °C in 2018 when the mean temperature of the cultivated plus vegetation covers was subtracted from the urban pixels. Figure 3–9 further demonstrates that even though the magnitude of nighttime SUHI for combined land cover is not higher than water surface, positive SUHI during nighttime may point toward an increasing of nocturnal UHI. The arrangement, size and location of waterbodies in the proximity of dense urban areas have the potential to have a substantial impact on waterbody temperature.

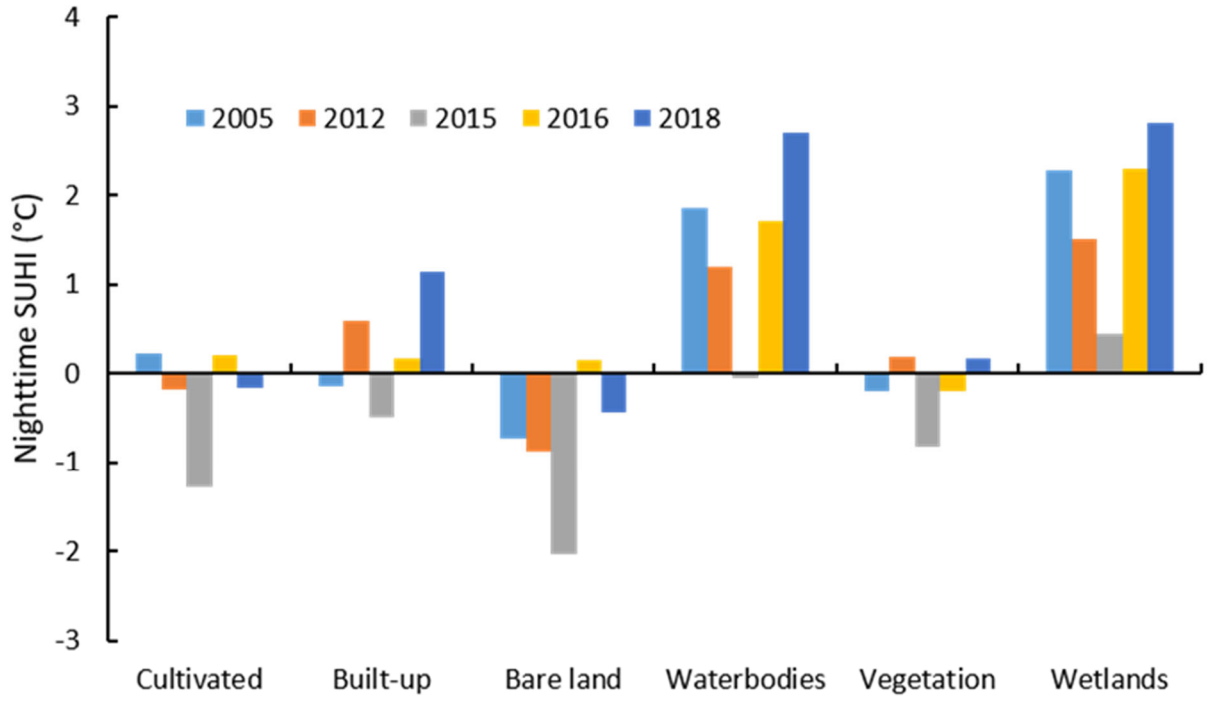

Figure 3–9 Nighttime SUHI according to different LULC categories, 2005–2018

3.4.3 Annual daytime and nighttime SUHI

The result of averaged annual daytime and nighttime SUHI is presented in (Figure 3–10). The maximum SUHI during the daytime can be as high as 6.81 °C whilst in the nighttime it is 4.33 °C, a difference of 2.48 °C, inferred from annualised SUHI data (Figure 3–10a). The analysis demonstrates that certain locations in both the new (e.g. Badda, Gulshan, Mirpur) and old towns (e.g. Wari, Motijheel, Ramna, Jatrabari) experience elevated temperature in the daytime. Conversely, Dhanmondi, Lalmatia, Uttara of new town areas and Motijheel, Khilgaon, Lalbagh, Bangshal of old town areas have high nighttime SUHI intensity (Figure 3–10b). Small pockets of SUHI can be found during the day and night at many locations within the DMA. Landsat provides a greater number of samples than ASTER, and this may have influenced precise mapping of the nighttime SUHI. As expected, cool islands are located in areas where cultivated and vegetation coverage is higher than in the areas of built–up land cover.

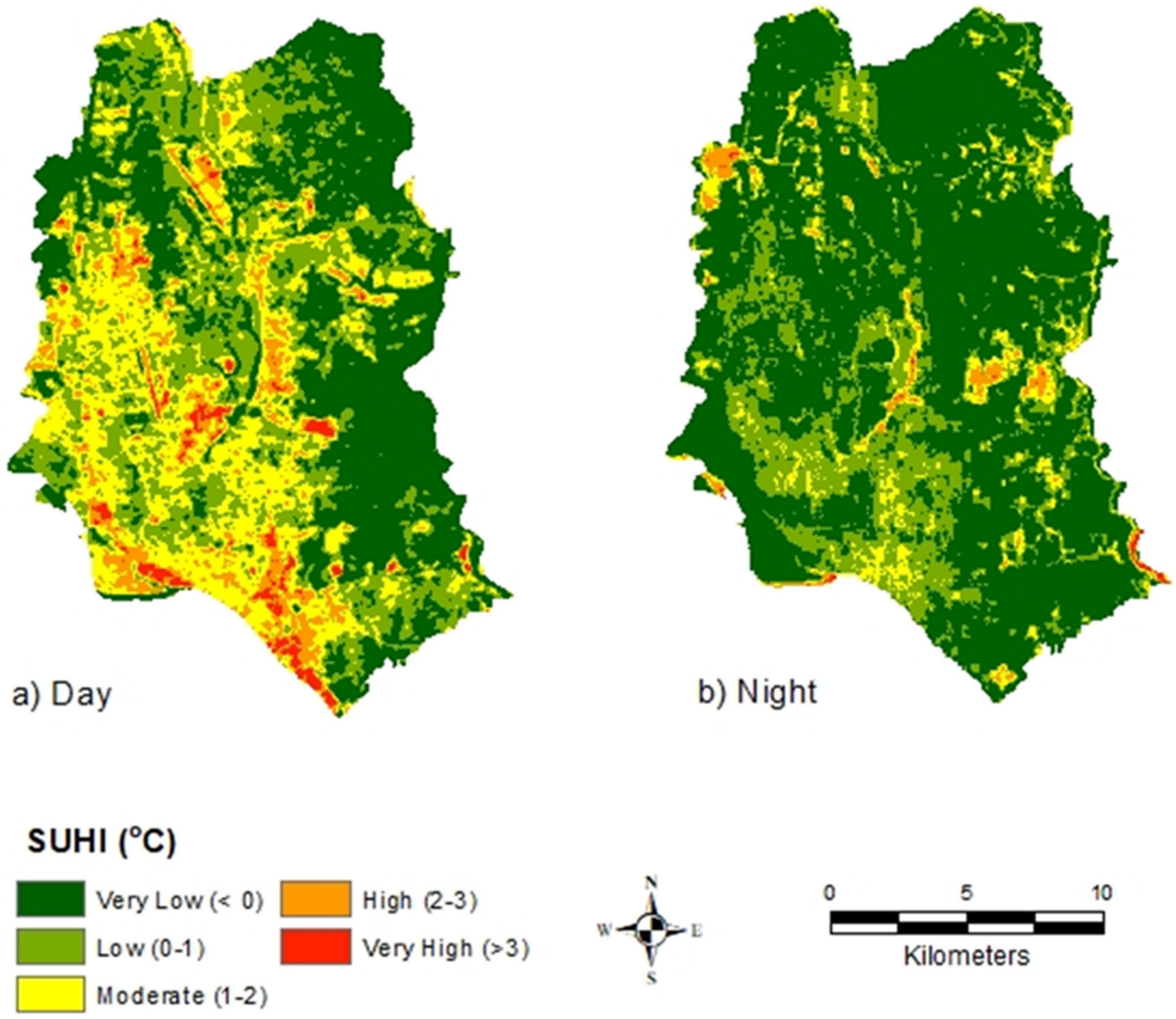

Figure 3–10 Annual day and nighttime SUHI over the DMA

3.4.4 Factors affecting LST

Table 3–2 shows the strength of the relationship between LST and the biophysical variables. It shows that the built–up index (NDBI) has a statistically significant relationship with LST. Urban index (UI), however, has a negative relationship, an observation, which is contrary to what would normally be expected. The strength of BCI, albedo with LST is low compared with normalised difference moisture index (NDMI). Vegetation indices (VI) indicate significant negative correlation, with enhanced vegetation index (EVI) showing a greater negative relationship than the more widely used NDVI. The results are considered useful in identifying factors, affecting daytime LST in the study area.

Table 3–2 Spearman correlation coefficients between LST and biophysical indicators during daytime

Variables	Correlation coefficient (r)
LST and Albedo	.325*
LST and NDBI	.868*
LST and NDMI	–.862*
LST and NDVI	–.482*
LST and UI	–.871*
LST and SAVI	–.480*
LST and EVI	–.507*
LST and MNDWI	.402*
LST and BCI	.395*
LST and MSAVI	–.495*

* Correlation is significant at the 0.01 level (2–tailed)

Although the correlation coefficient is useful in identifying the strength of the relationship between variables of interest, it does not indicate which variable(s) would be useful in predicting LST. To assist in this, multivariate linear regression models were developed to isolate important predictors. Prior to establishing the regression models, a matrix of pair–wise Pearson correlation coefficient was performed between LST and the biophysical variables.

Analysis of the correlation matrix (Table 3–3) reveals that average NDVI has high positive correlation with other vegetation indices (VI) such as SAVI (r = .982), EVI (r = .971) and MSAVI (r = .972). This means they essentially contain the same information, and therefore, dropped in the regression model. Conversely, all VI had significantly negative correlations with LST. Built–up index (NDBI) was positively related to LST with an r value of .849 but UI was negatively correlated (r = -.860). NDMI had a statistically negative relationship (r = .844) while albedo showed weaker correlation (r = .376). The water index (MNDWI) also showed positive relationship.

Table 3–3 Correlation matrix between LST and biophysical variables

	ALBEDO	NDBI	NDMI	NDVI	SAVI	EVI	MNDWI	BCI	MSAVI	UI	LST
ALBEDO	1.000										
NDBI	.522*	1.000									
NDMI	–.519*	–.987*	1.000								
NDVI	.258*	–.397*	.396*	1.000							
SAVI	.363*	–.387*	.384*	.982*	1.000						
EVI	.353*	–.425*	.421*	.971*	.996*	1.000					
MNDWI	.760*	.716*	–.705*	.342*	.349*	.305*	1.000				
BCI	.091**	.142*	–.146*	.053**	.041**	.030**	.173*	1.000			
MSAVI	.363*	–.408*	.405*	.972*	.998*	.998*	.323*	.033**	1.000		
UI	–.406*	–.974*	.962*	.572*	.560*	.590*	–.556*	–.120*	.577*	1.000	
LST	.376*	.849*	–.844*	–.458*	–.448*	–.474*	.519*	.106*	–.461	–.860*	1.000

* Statistically significant at 99% confidence interval (2-tailed); ** Not significant

Linear regression analysis indicates that NDBI has a strong correlation (r = .849) with LST. The r^2 indicates that 72% variation in the dependent variable (LST) could be explained by the independent variable (NDBI). In the second model, the analysis suggests that 73% of the total variation of LST can be explained by two variables, NDBI and EVI, whilst in the third model NDBI, EVI and NDMI are shown to have a significant influence on LST (Table 3–4). Note however, that there is little difference between the second and third models in terms of r^2, therefore, it can be concluded that NDBI and EVI have the greatest influence on LST. In this context, NDBI represents the degree of built–up surface or imperviousness and EVI illustrates vegetation abundance.

Table 3–4 Summary of multivariate linear regression models

Predictor(s)	**Equation**	**r**	**r^2**	**Adj. r^2**
NDBI	LST = 25.820 + 7.752(NDBI)	.849	.721	.721
NDBI and EVI	LST = 26.152 + 7.216(NDBI) – 2.302 (EVI)	.858	.737	.736
NDBI, EVI and NDMI	LST = 26.154 + 5.237(NDBI) – 2.293(EVI) – 2.051(NDMI)	.859	.738	.737

In investigating the relationship between nighttime LST and biophysical variables, a Spearman rank correlation was performed. The results are presented in Table 3–5. This reveals that none of the variables has any influence on nighttime surface temperature. Albedo appears to have a very weak relationship, but this is statistically insignificant.

Table 3–5 Spearman correlation coefficients between LST and biophysical indicators

Variables	**Correlation coefficient (r)**
LST and Albedo	0.11**
LST and NDBI	–.015**
LST and NDMI	.012**
LST and NDVI	.023**
LST and UI	.019**
LST and SAVI	.025**
LST and EVI	.026**
LST and MNDWI	.014**
LST and BCI	–.012**
LST and MSAVI	.026**

** Not Significant

A linear regression model was attempted but nothing of value was determined due to the fact that the coefficient of determination was too low (r^2 = .007). It is assumed that other factors such as population density, urban form or building density may affect the distribution of the nighttime LST.

N–S and E–W profiles were used to examine the variation of SUHI and biophysical variables and show how they varied over space during day (Figures 3–11 (a–c) and 3–12 (a–c)).

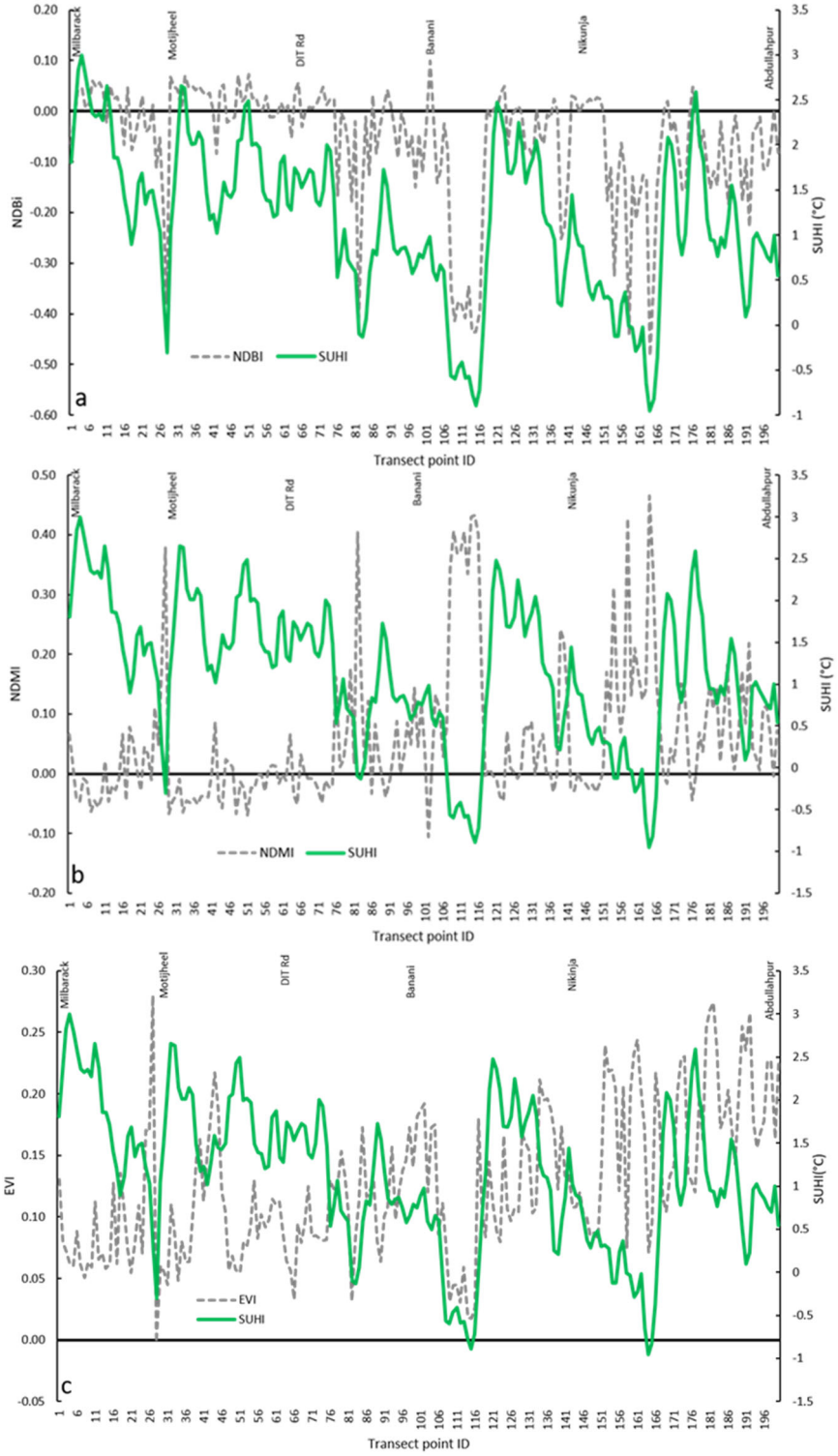

Figure 3–11 SUHI profile plotted against: (a) NDBI; (b) NDMI; and (c) EVI along a N–S transect. Place names are shown above the graphs

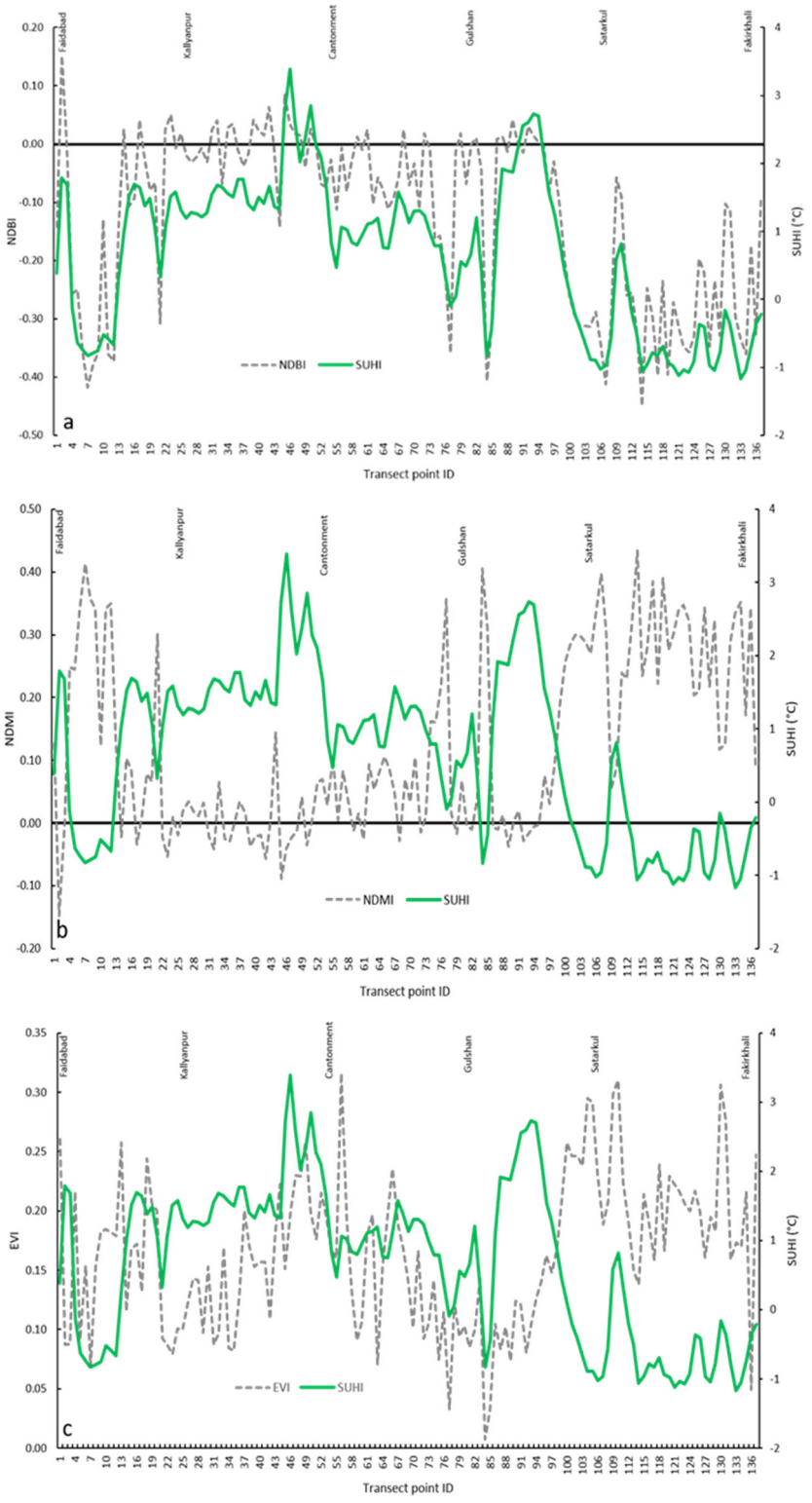

Figure 3–12 SUHI profile plotted against: (a) NDBI; (b) NDMI; and (c) EVI along E–W transect. Place names are shown above the graphs

Only NDBI, NDMI and EVI against SUHI were plotted. Generally, the relationship between these three variables seemed to be consistent along the transects, however, there are locations

where the expected relationship does not appear to hold true. This may be related to other factors such as building density, amount of waste heat generation, urban morphology and the existence of green and blue spaces that assist in moderating the local climate.

3.5 Discussion

An important learning from the current work is that the use of a large number of samples over many years may possibly reveal different LST/SUHI patterns as compared to the patterns produced using only selected years. For instance, if only years that had shown high SUHI were selected and used (Figures 3–4, 3–5), then the results could be significantly different and somewhat misleading. Therefore, the number of sampling appears to have a substantial effect on the ability to accurately characterise LST/SUHI (de Faria Peres et al. 2018). Methodological differences in extracting LST and subsequent SUHI also need to be considered. While MODIS uses a split–window (SW) algorithm, Landsat 5 and 7 have only one TIR band, and therefore, the use of SW techniques was not possible. Though Landsat 8 has two thermal channels, the use of band 11 with band 10 in a SW process could lead to significant uncertainty due to the stray light issue of band 11 (Wulder et al. 2019; Montanaro et al. 2014). As noted by Li et al. (2013), a universally–accepted method of accurately estimating LST is lacking. A confounding factor is that the environmental condition of an area seriously affects any LST computations. Kerr et al. (2004) made a similar observation, noting that the selection of the best analytical method depends on the availability of any water vapour content data captured during data acquisition and precise surface emissivity data. The use of many input parameters could also increase uncertainty when using the SW algorithm (Sòria and Sobrino, 2007). Hence, sensor characteristics and availability of atmospheric information during satellite overpass needs to be seriously considered when selecting between the various methods for LST retrieval (Tang and Li, 2014). As atmospheric profile data were not available for the current study due to the historic nature of the data used, an image–based approach was considered as a viable option for retrieving LST information from Landsat. Previous work has shown this approach to be reasonably accurate (Ndossi and Avdan, 2016). In addition, the generation of SUHI is believed to be significantly impacted by background climatic factors (Sun et al. 2019; Zhao et al. 2014). This means SUHI computation requires the use of a number of parameters, some of which are nearly impossible to obtain for a megacity like Dhaka. Furthermore, concurrency of datasets are useful in accurately estimating SUHI (Zhao et al. 2016). In case of the microclimatic evaluation of DMA, this work was constrained by four specific years of LULC data (i.e. 2000, 2004, 2010 and 2017). Use of these four datasets to compute SUHI for the other years, between 2000 and 2018, may have affected the results described in this chapter.

Despite the caveats noted above, an analysis of the spatial–temporal variation of LST and SUHI revealed that the DMA urban areas have a 1.2 °C higher temperature than surrounding vegetated surfaces during daytime, illustrating a local warming affect. In addition, these areas have a 1.30 °C higher temperature than the combined mean of cultivated and vegetation covers.

TIR data recorded during afternoon or early evening could be very useful but such a thermal band option is not available over the study area with the current satellite configuration. Though SUHI appears to fluctuate considerably over time, it was possible to discern a noticeable and rising trend since 2016 in the data (Figure 3–5). Although there were few nighttime LST samples, the observed spatial pattern indicated SUHI intensity in three years (2005, 2015 and 2018) (Figure 3–8).

An analysis of possible driving factors suggested that a combination of built–up index (NDBI), EVI and NDMI do influence daytime SUHI as shown by the multivariate linear regression plots (Table 3–4). Similar observations (notably increased LST values) have also been reported in other large cities where urban growth has been rapid and the loss of vegetation has been substantial (Jia and Zhao, 2020; Huang et al. 2019; Peng et al. 2018; Dwivedi and Khire, 2018; Estoque et al. 2017; Katpatal et al. 2008). Although UI was reported to be the best predictor for LST elsewhere (Mushore et al. 2017), this work revealed a negative value during daytime and very weak relation during nighttime. This possibly relates to the fact that generation of urban heat islands depends on geographic location as well as being city specific (see Giridharan and Emmanuel, 2018). Another important finding is that the widely–used vegetation index NDVI appears to be less effective than EVI in predicting LST. This may be related to saturation of NDVI, to the differing vegetation types and possibly to development density influencing the surface temperature of vegetation in the urban area (Li et al. 2011). The current work could not isolate any variable influencing the nighttime SUHI which could be related to the DMA's biophysical composition and neighbouring environment (Song and Wu, 2016). The inclusion of anthropogenic factors such as the amount of waste heat released, urban form, building density, and other similar factors into the modelling could prove useful.

3.6 Conclusion

Medium resolution remotely–sensed data was used to provide an assessment of the DMA microclimate. Landsat and ASTER–based LST were the major data sources used to define the day and night SUHI variability at an annual scale. The major findings are:

- The daytime LST of urban area is 1.30 °C higher than the combined cultivated and vegetation land covers.

- Although a marked variation was observed in the spatio–temporal distribution of daytime SUHI, the urban core has a 1.2 °C higher temperature than the surrounding vegetation cover, and a sharply rising trend of daytime SUHI can be observed since 2016.

- During the nighttime, the spatial and temporal variability is very high, however the built–up surface exhibited a 0.28 °C greater temperature than the cultivated plus vegetation land cover categories. This estimation, however, was seriously impacted by the low number of samples obtained from the ASTER LST products.

- Annual day and nighttime SUHI computation indicated that SUHI is well–distributed over the entire DMA, but a number of locations in both old and new towns have recorded elevated LST. There is a 2.48 °C difference between annual day and nighttime SUHI.

- NDBI, NDMI and EVI are the main factors affecting SUHI at the microscale as inferred from the regression analysis undertaken.

4 FIELD–BASED MICROCLIMATE ASSESSMENT

4.1 Introduction

This chapter provides details on a microclimate assessment conducted in Dhaka Metropolitan Area (DMA). Fixed weather stations and traverse surveys were used to record local climatic data across the four different seasons. The collection of microclimatic data included parameters such as temperature, humidity, wind speed, wind direction and solar radiation. To determine the role of green and blue spaces in alleviating temperature, multiple data loggers were installed at various locations within the vicinity of a park and lake. The cooling effect of different vegetation species was recorded and analysed. The thermo–physical behaviour of various urban features was analysed via thermographic assessment. Site locations are shown in Figure 4–1 and the use of individual instruments in the subsequent microclimate analysis is described in the relevant sections.

4.2 Fixed station monitoring

Two weather stations were installed and data were collected for a year to demonstrate seasonal variations of surface urban and canopy layer heat islands. The locations of the two weather stations were:

- Lalbagh Fort (23.72° N, 90.39° E), representing an urban location
- Isapura village (23.82° N, 90.49° E), representing a rural site

A site close to the CBD was proposed but due to various security concerns, it was determined that this was not going to be realistically feasible. Images of the weather station environments are shown in Figure 4–2. Each weather station is equipped with five smart sensors to measure air temperature, humidity, surface temperature, solar radiation, leaf wetness index, wind speed and wind direction. A multi–channel HOBO micro station data logger (model: H21–USB) is used for data collection in the outdoor locations. The smart sensors height was set at around 2.5 m from the ground to minimise the effects of any vertical temperature gradient on the analysis of UHI (Oke, 1982). Details of the five sensors are given in Table 4–1.

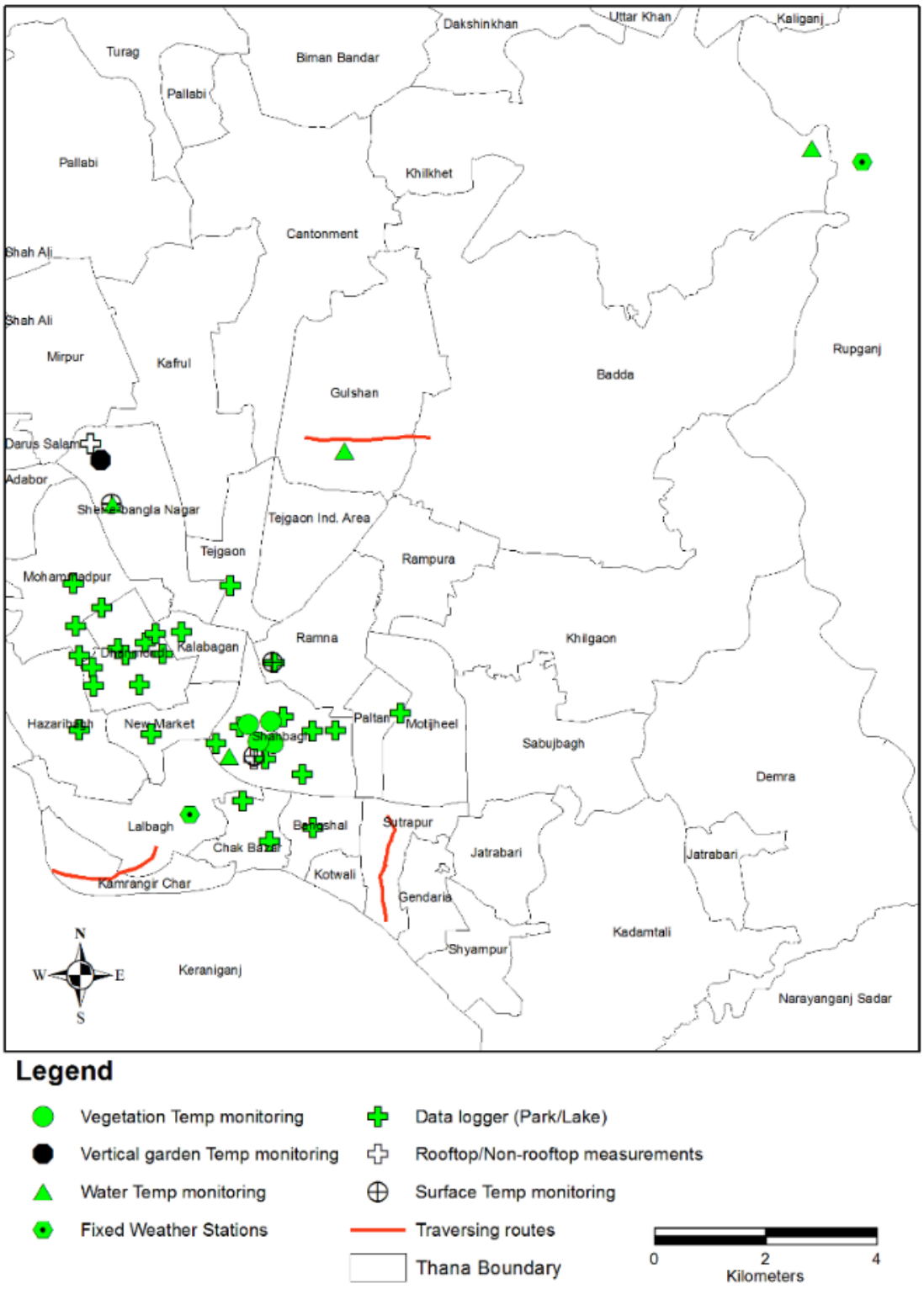

Figure 4–1 Location of fixed weather stations, data loggers and traverse routes in DMA

Lalbagh Fort (urban) Isapura (rural)

Figure 4–2 Fixed weather stations installed in Lalbagh Fort and Isapura village, denoting an urban and rural locations

Table 4–1 Specification of smart sensors used in the fixed weather stations

Device	Variables	Accuracy
S–THB–M002	Air temperature, humidity	± 0.2 °C, at 0–50 °C ± 2.5%, from 10%–90% RH
S–WCF–M003	Wind speed/direction	± 1.1 m/s or 4%, whichever is higher ± 5 grades
S–LIB–M003	Solar radiation	± 10 W/m^2 or ± 5%, whichever is higher
S–LWA–M003	Leaf wetness	± 5%
S–TMB–M002	Surface temperature	<± 0.2 °C

Prior to commencement of the study, all instruments were calibrated and checked to ensure recording accuracy. All the recorded calibration values were cross–checked with data from a local weather station operated by the Bangladesh Meteorological Department (BMD). This revealed a very subtle difference in temperature and relative humidity readings (ranging between 0.1 and 0.2%). Measurements were set to be recorded at 15–minute intervals, with the data to be periodically downloaded. The data was then averaged at seasonal diurnal and monthly scales to allow further analysis.

4.3 Traverse surveys

Three survey routes were selected for the microclimate assessment (Figure 4–1). Selection criteria for these routes were based on urban form, housing conditions, socioeconomic

characteristics, magnitude of temperature distribution (obtained from satellite data, see Chapters 2 and 3) and land use types. The following areas were defined:

- Planned – an area with a high density of commercial and residential buildings and close proximity to a lake. The traverse starts at Bir Uttam AK Khandakar road (23.46° N and 90.24° E) and finishes in Bir Uttam Rafiqul Islam Avenue (23.46° N and 90.25° E)

- Unplanned – an area with a high density of residential buildings and mostly unplanned development. The route starts at Tikatuli (23.43° N and 90.25° E) and finishes in Malakartola lane (23.42° N and 90.25° E)

- Mixed – an area with low socioeconomic status, predominantly mixed land use type and close to a large river, the Buriganga. It starts at Gabtoli road (23.43° N and 90.23° E) and finishes in Madrasha road (23.42° N and 90.21° E)

Samples were collected three times a day; morning (0900), afternoon (1500) and evening (2100). The samples consisted of air and surface temperature, wind speed, solar radiation and relative humidity. The traverses were conducted on foot, as vehicle or bicycle use was not practical due to the severe traffic congestion. The measurements were conducted at 100 m intervals, and on average, each traverse took around two hours to complete. For each traverse survey, a week of measurements were recorded and averaged. Table 4–2 details the handheld devices used to obtain the urban canyon–level measurements.

Table 4–2 Devices used in traversing the three sites

Device	Model	Variables	Accuracy
Pyranometer	MP–100	Solar radiation	± 5%
Anemometer	Windmate 350	Wind speed	± 3%
TinyTag	TGP–4500	Air temperature and relative humidity	±3%
TinyTag	TGP–4020	Surface temperature	±6 °C
Thermal camera	Testo 865	Thermal infrared image	±2 °C
Infrared thermometer	Testo 835–T–1	Surface temperature of urban features	± 1%

To determine the spatial distribution of CUHI and SUHI along the three transect routes, the mean value of each observation point (7–day average) was subtracted from the corresponding transect mean. This was determined for the three time periods (e.g. morning, afternoon and evening) and is considered useful for separately identifying the deviation of temperature from the mean temperature of each site (Basara et al. 2008).

4.3.1 Thermo–physical behaviour of urban features

Two thermal cameras (Table 4–2) were used to produce infrared images along the three transects and enable a subsequent evaluation of the temperature variations between various urban features. A typical thermal camera has a resolution of 160 x 120 pixels with an instantaneous field–of–view (IFOV) of 2.1 mrad (https://www.testo.com/en-AU/testo-865/p/0560-8650). The spectral range is nominally 7.5–14 μm.

Images of various objects were acquired, taking care to ensure that weather conditions were essentially identical at all times (e.g. without precipitation, low wind speed, clear sky). The type and colour of coatings (e.g. green) and the structure types (e.g. brick, concrete surface) of each feature were also recorded. The thermography was obtained on the first day of the site traverse and a total of 20 sites (at nominal 100 m intervals), were covered in the 2 km traverse. To ensure consistency in the recording process, a dedicated person was tasked with recording all the thermal images. To achieve and maintain maximum accuracy, the camera commenced recording 10 minutes after being activated. Thermal images were taken once in the morning and once in the evening. This was due to the fact that taking an image three times a day was logistically extremely difficult (the result of rapid power failure in the thermal camera). The recording of two images per day (one in the morning and one in the evening) were deemed to be sufficient to accurately determine the cooling rate of the various urban features which was one of the objectives of the assessment. Visible images of the respective thermal data were also recorded by a digital camera at the same time. The ideal scenario to reduce any possible recording errors would be to take simultaneous thermography recordings of the sites (Hartz et al. 2006) but due to time constraints this was not possible.

During the thermographic survey, wind speed, air temperature, surface temperature and relative humidity of each site was recorded. An infrared device (model: Testo 835-T1 equipped with a 4–point laser) was also used to crosscheck and calibrate the thermal cameras. A variety of images were captured at the three traverse routes and over 100 thermal images were recorded from three sites. After quality checking, however, only 88 images (taken twice daily, for winter, pre–monsoon and monsoon), were utilised. At each site, at least five unique object types were captured, though it was possible to produce duplicates by combining data from the three zones. An example of a typical thermal image and the corresponding photograph are shown in Figure 4–3. Normally a thermal camera can capture images in both normal and super–resolution modes. For this study, the latter type was used due to the high production quality and ease of ground feature identification (https://www.testo.com/en-AU/thermalimaging/irsoft).

Two types of analytical methods were used. They were:

- Use of the TwinPix tool embedded in the IR software (https://www.testo.com/en-AU/thermalimaging/irsoft). This was used to overlay both thermal and visible images,

and helps pinpoint objects of interest (Figure 4–4). During the data collection, the surveyor marked all features targeted on the visible images, which aids in the subsequent image analysis. In addition, a rectangle was drawn on each image to extract the temperature of individual features. The lower limit of temperature was nominally set to 15 °C to limit the effect of cloud cover and visible sky.

- Retrieval of the area average temperature (AAT) from each thermal image. This included delineating a polygon shape over an image while excluding cloud cover or visible sky. Post–processing operations comprised adjustment to ambient temperature, emissivity, relative humidity and distance. Appendix V shows examples of the process of computing surface temperature from thermal images.

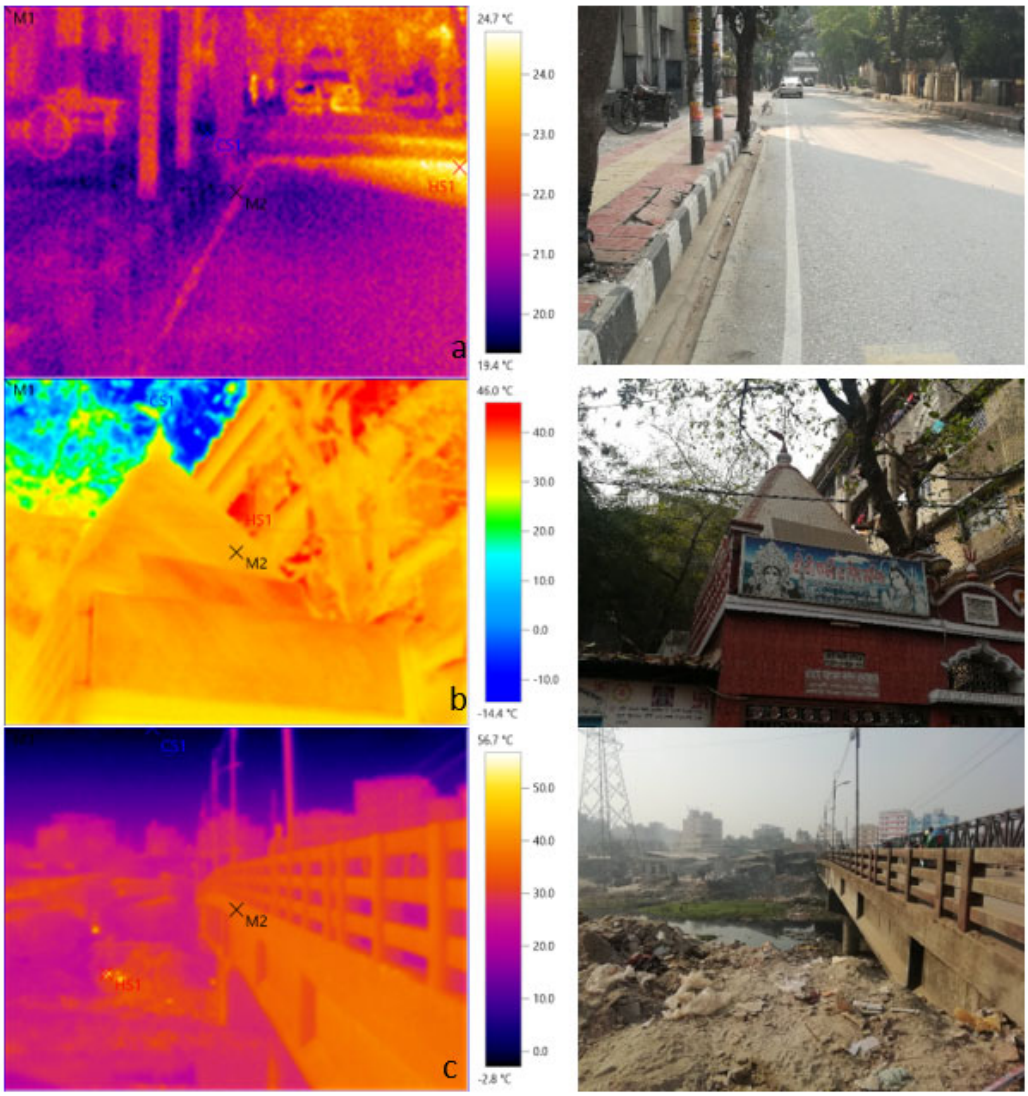

Figure 4–3 Representative thermal and corresponding visible images of the three traverse sites during morning: (a) Planned; (b) Unplanned; and (c) Mixed

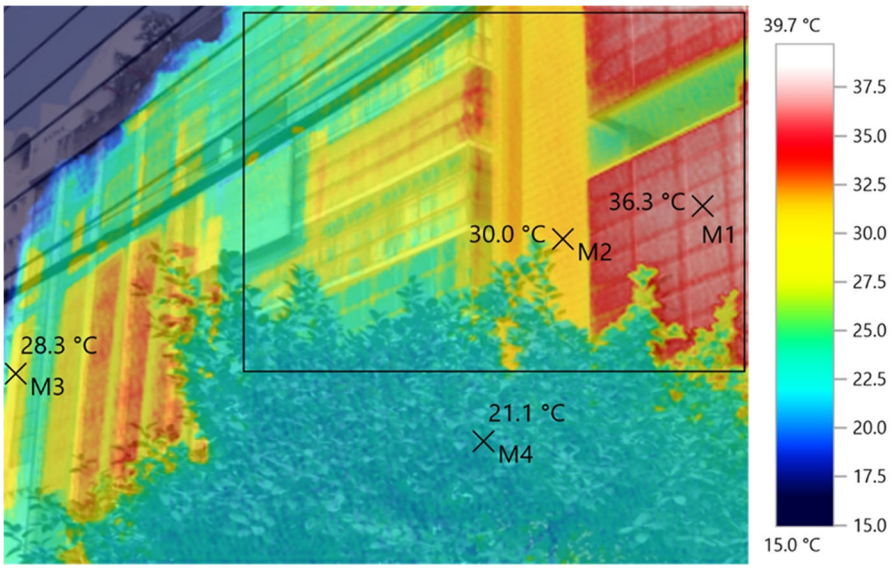

Figure 4–4 An overlay of thermal and visible images via TwinPix. M1, M2, M3 and M4 denote extraction of features temperature from a thermal image

The final analysis was conducted separately for each of the three transects, and for each season. The aim was to capture as diverse range of objects as possible during the thermographic recording. The temperature difference (ΔT) was then obtained by subtracting the morning value (early image) from the evening (late image) value to determine the cooling potential/rate of the features. Based on the two capture times and their respective temperature differences, two delta values were computed (Δtime and ΔT) so that the hourly cooling rate of each object could be estimated. The cooling rate (CR) equals (T1–T2)/change)*60 (Hartz et al. 2006). The higher the value, the more rapid the CR.

4.4 Impact of rooftop gardens on surface and air temperature

To gain an understanding of the effectiveness of rooftop gardens in reducing urban heat, measurements were recorded for three seasons (e.g. winter, pre–monsoon and monsoon). Rooftops, both with and without gardens, were considered. Data was collected only on sunny days. Air temperature was measured at three different heights (e.g. 1, 2 and 3 m) while the surface temperature of the roof was measured at the surface of the rooftop. The devices used for this purpose can be found in Table 4–3, and they were calibrated every time, prior to deploying for data collection.

4.5 Thermal response of rooftop vegetation types

To determine the cooling potential of rooftop vegetation types, five dominant vegetation species identified as being grown by the residents of DMA, were selected for investigation. The species were Guava (*Psidium Guajava*), Malta (*Maltes*), Bagan–bilash (*Bougainvillea*),

Madhobi–lata (*Combretum indicum*) and Lemon (*Citrus Limon*) (Appendix VI). The temperature data logger (Table 4–3) was calibrated and then placed at breast height in the individual trees and the measurements taken over a six–day period in three seasons. The data were then averaged according to the diurnal cycle.

Table 4–3 Devices used in measuring temperature of vegetation types, rooftop garden, vertical green wall and water features

Device	Model	Variables	Accuracy
TinyTag	TGP–4500	Air temperature and relative humidity	0.5 °C and ±3% RH
TinyTag	TGP–4020	Surface temperature	±6 °C
Easy logger	EL–USB–2PLS	Air temperature and relative humidity	0.45 °C and 2.05% RH
HOBO	MC–2201	Temperature	±0.5 °C

4.6 Cooling effect of open space plants

The Suhrawardi Uddyan (23.44° N, 90.23° E) is one of the largest parks in the DMA and is situated approximately 1.9 km (air distance) away from the Motijheel (23.43° N, 90.25° E) or Central Business District (CBD). This park area was used to examine the cooling effect of open–space plants. Four plots were chosen (relative from the park centre), with each 40 x 40 m, covering an area of approximately 1600 m^2. Within each plot, the dominant species, canopy cover and crown depths were evaluated, and then the dominant plant types from each plot were identified. A total of 15 vegetation species were selected: Cylon ironwood (*Mesua ferrea*), Earleaf acacia (*Acacia auriculiformis*), False ashok (*Polyathia longifolia*), Teak (*Tectona grandis*), Mimusops (*Mimusops elengi*), Banyan (*Ficus benghalensis*), Mahogany (*Swietenia mahagoni*), Beharda (*Terminalia balerica*), Royal Poinciana (*Delonix regia*), Loha kat (*Xylia dolabiformis*), Barringtonia (*Barringtonia acutangula*), Chambal (*Artocarpus chaplasha*), Mango (*Mangifera indica*), Coconut (*Cocos nucifera*) and Palm tree (*Arecaceae*).

The Lascar temperature and humidity data loggers (Table 4–3), with solar radiation shield (model: EL–USB–CASE), were calibrated and used to record the temperature and humidity of five species in each plot for a day (between 0900 and 1800). The loggers were set up in each plant around 1.5 m above the ground. To cover all plots, the loggers were moved from one plot to another the following day. It took four days to record temperature and humidity for each species in each season, with one day at each plot. Dominance of species was the main criteria so it was possible to have the same plant in four plots. Where the same species had been used, an average temperature value was determined. The data were then analysed using the hours of the day to explore any temporal variation when estimating the cooling potential of individual species. Average wind speed and solar radiation data recorded with a mobile weather station

(model: HOBO multi–channel micro station) during the measurement period is detailed in Appendix VII.

4.7 Variation in temperature of urban water features

Five waterbodies of different sizes were selected in order to examine the impact of land surface conversion on temperature variation. These included lakes, ponds and rivers. Five data loggers (Table 4–3) were calibrated and installed between 0.30 and 0.45 m below the water surface and programmed to capture data at hourly intervals. During the first few weeks of installation, however, two devices were swept away by river currents and one started malfunctioning (from 25th December, 2018). This malfunctioning device was replaced, however due to security and safety issues it was not possible to replace the other two. All available data for the period has been used in this study. During processing, any outliers in the data were removed, and the data summarised and adjusted to a diurnal cycle for every season. The acceptance criteria used for the data was based on all values falling within the physical temperature range of water (i.e. 0 °C and 100 °C).

4.8 Cooling potential of a green vertical wall

A vertical greening system, or hanging wall, appears to be an effective strategy which can be used to reduce the temperature in cities (Tan et al. 2014; Wong et al. 2010). An experimental method documented by Wong et al. (2010) is adopted for use in this study. An illustration of the experimental procedure is shown in Figure 4–5.

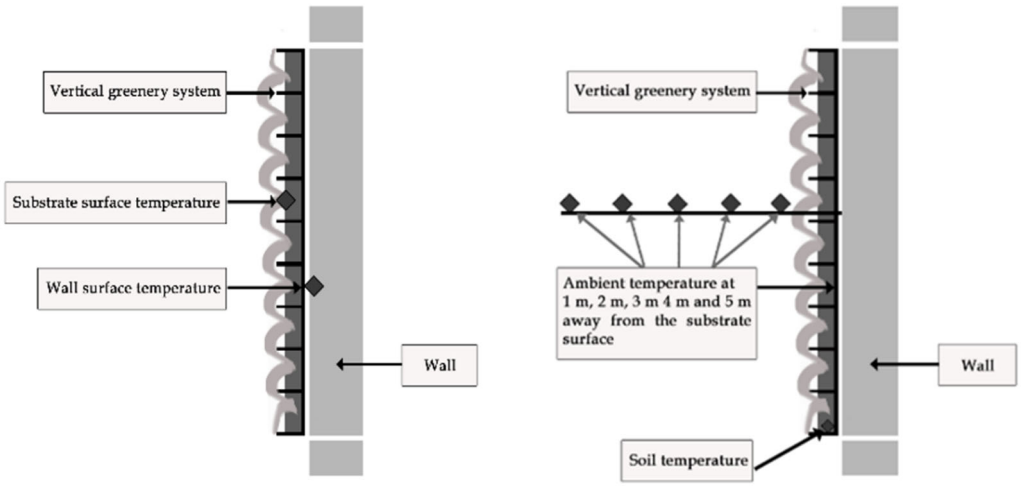

Figure 4–5 Position of devices for measuring surface and ambient temperatures of a hanging green wall system (after Wong et al. 2010)

A Tinytag surface thermistor with probe (model: PB–5003–1M5) was used to measure the surface temperature of soil, wall and the substrate (Table 4–3). Five temperature/humidity data

loggers (EL–USB–2PLS) were used to measure the ambient temperature. These were placed on a long wooden stick (at 1 m spacing) and positioned with one end at the substrate and the other extending outwards. All of the data loggers were housed in a protective casing to avoid the effects of direct solar radiation, and calibrated at regular intervals. Six clear days, during pre–monsoon, monsoon and winter, were used to measure air and surface temperatures. The data were then averaged according to the hours of operation and used to analyse and report the ambient and surface temperatures of a representative green hanging wall. Appendix VIII also shows the experimental set up of a green hanging wall system.

4.9 Cooling potential of greenspace/blue space

A greenspace is defined as an area designated by local government as a public park/place and with a vegetation cover of ≥ 80% of the total area. This criterion has been used in the selection of Suhrawardi Uddyan (23.44° N, 90.23° E) as an identified green space (Figure 4–1). A total of thirty low–cost data loggers (https://bluemaestro.com/products/product-details/bluetooth-temperature-humidity-sensor-beacon, model: Tempo Disc) were installed; fifteen around the park and fifteen around the lake. The Tempo Disc has an accuracy of 0.3 °C with maximum 0.4 °C at –10 °C to +75 °C, while the relative humidity accuracy is 3% for a range of 0–80%. The average height of logger placement was 2 m from the ground surface. The units were tested and calibrated prior to installation. The logging interval of each device was set to 1 hour.

One of the aims of the study was to determine the directional effect of greenspaces, a research question that appears to be generally missing in the scientific literature. Data loggers were installed in areas aligned to the four compass points (north, south, east and west) in relation to relative centre of the defined green area (Appendix IX). A 2–km radius from the centre of the park was first defined. The original idea was to install each device at a 100 or 200 m interval from the park centre but two major issues were encountered. The first was the inability to obtain suitable/secure siting locations for use. The second related to equipment security issues. One logger was removed by the Bangladeshi intelligence authority immediately after installation and another was withdrawn by the Dhaka University authority. Both organisations expressed security concerns regarding the devices. The data from the remaining loggers was downloaded periodically and aggregated to diurnal scale of each season. A day was nominally divided into the following local time periods: early morning (0000–0559), late morning (0600–1159), afternoon (1200–1759) and evening (1800–2355).

To evaluate the impact of blue space on temperature, the same procedure and methodology as that employed for the greenspace was used. Fifteen data loggers were installed around the Dhanmondi Lake (23.44° N and 90.22° E) (Appendix X).

4.10 Analysis of urban planning indicators (UPI) and temperatures

Previous research indicated that urban planning indicators can play a significant role in modulating urban heat islands in various cities (Guo et al. 2016; Petralli et al. 2014; Zhao et al. 2011), particularly when spatial heterogeneity and urban morphology result in a large difference in intra–urban temperature (Shiflett et al. 2017; Konaska et al. 2016). Though there are many indicators which have been utilised by the studies noted above, in this work six UPI's have been defined using the 2017 structure and land use data obtained from RAJUK (the Capital Development Authority). The six indicators consisted of street cover ratio (SCR), building cover ratio (BCR), building volume density (BVD), green cover ratio (GCR), water cover ratio (WCR) and aspect (building height/width). The definitions for these indicators can be found in Petralli et al. (2014) and Sharmin et al. (2017). Five buffer zones were defined for a point at 50, 100, 150, 200 and 250 m intervals along the three traverse routes. To avoid overlapping of values at the individual points, five sample points (at 100m, 600m, 1100m, 1600m and 2000m) along each traverse were used. A Pearson product–moment correlation coefficient (r) analysis was then conducted using temperatures (air and surface) recorded during the traversing and the six UPI.

4.11 Results

4.11.1 Winter season

4.11.1.1 Urban–rural gradient of air and surface temperature

A plot of the diurnal cycle of surface temperature is provided in Figure 4–6a. This shows that the urban temperature is consistently higher than the rural temperature across the diurnal cycle in winter. On average, the urban temperature was 1.41 °C higher than that recorded in the rural landscape, although the difference in temperature tended to vary depending on the time of recording. For example, the urban surface temperature can have a reading of 25.98 °C at 1400 hours, while the rural temperature was 23.07 °C.

The average diurnal air temperature during winter between the urban and rural locations reveals an interesting pattern (Figure 4–6b). Air temperature in the urban area is higher than rural over two periods (00:00–0900 and 1700–2300), however from 1000 to 1600 the rural air temperature was higher. Across the diurnal cycle, urban areas had an average of 1.72 °C higher temperature, when compared to rural location.

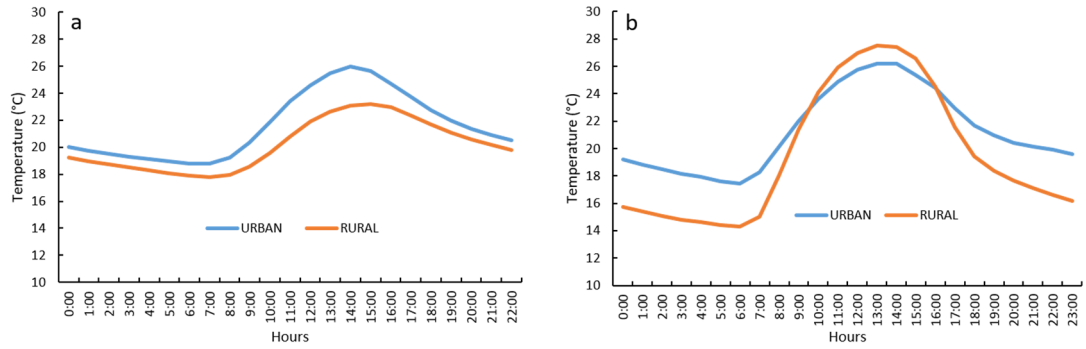

Figure 4–6 Diurnal variation of temperature between urban and rural sites in winter: (a) surface; (b) air

The SUHI and CUHI (defined by the difference between the urban and rural temperatures), is shown in Table 4–4. Analysis of the entire diurnal cycle reveals that air temperature starts

Table 4–4 Differences in surface and air temperature during the winter season

	Surface temperature (°C)			Air temperature (°C)		
Hours	Urban	Rural	SUHI	Urban	Rural	CUHI
0:00	19.99	19.22	0.77	19.21	15.74	3.46
1:00	19.75	18.96	0.79	18.81	15.41	3.40
2:00	19.52	18.72	0.80	18.47	15.10	3.38
3:00	19.31	18.49	0.83	18.16	14.81	3.36
4:00	19.13	18.27	0.86	17.96	14.60	3.35
5:00	18.97	18.08	0.90	17.60	14.42	3.19
6:00	18.82	17.90	0.92	17.45	14.31	3.14
7:00	18.77	17.77	1.00	18.29	15.00	3.29
8:00	19.25	17.94	1.31	20.13	18.04	2.10
9:00	20.37	18.59	1.79	22.01	21.41	0.59
10:00	21.88	19.59	2.29	23.62	24.13	–0.51
11:00	23.42	20.80	2.62	24.90	25.94	–1.04
12:00	24.61	21.91	2.70	25.76	26.96	–1.20
13:00	25.50	22.64	2.86	26.22	27.50	–1.28
14:00	25.98	23.07	2.91	26.19	27.41	–1.22
15:00	25.66	23.21	2.45	25.36	26.60	–1.24
16:00	24.72	22.96	1.76	24.44	24.52	–0.08
17:00	23.76	22.38	1.37	22.96	21.57	1.39
18:00	22.76	21.69	1.07	21.71	19.42	2.28
19:00	21.95	21.07	0.88	20.96	18.39	2.57
20:00	21.35	20.57	0.78	20.41	17.66	2.75
21:00	20.89	20.17	0.73	20.15	17.12	3.03
22:00	20.53	19.82	0.71	19.89	16.64	3.25
23:00	20.24	19.50	0.73	19.57	16.15	3.42

decreasing in the urban area from 1000 and continues until 1600. From 1700 hours, the air temperature tends to increase and can be more than 2 °C higher, on average, than the rural site (Table 4–4). Interestingly, the rural area exhibited a higher temperature than the urban site between 1000 and 1600 hours, with the greatest difference being observed around noon (1300). In contrast, the surface temperature remains consistently high in the urban area during the entire diurnal cycle in winter. The intensity and magnitude of SUHI is therefore meaningful.

To examine the causes of air and surface temperature variation, solar radiation was averaged and analysed over the same diurnal cycle. The data indicates a normal distribution (Figure 4–7). On average, it appears that the rural area receives 8.0 W/m^2 greater solar radiation than the urban area over the three winter months (December to February). It is, therefore, reasonable to speculate that high solar radiation can account for the canopy layer heat island effect in the rural site during the 1000–1600 period, whereas urban morphology, building density and intense anthropogenic activities may be responsible for the higher magnitude of SUHI in urban areas.

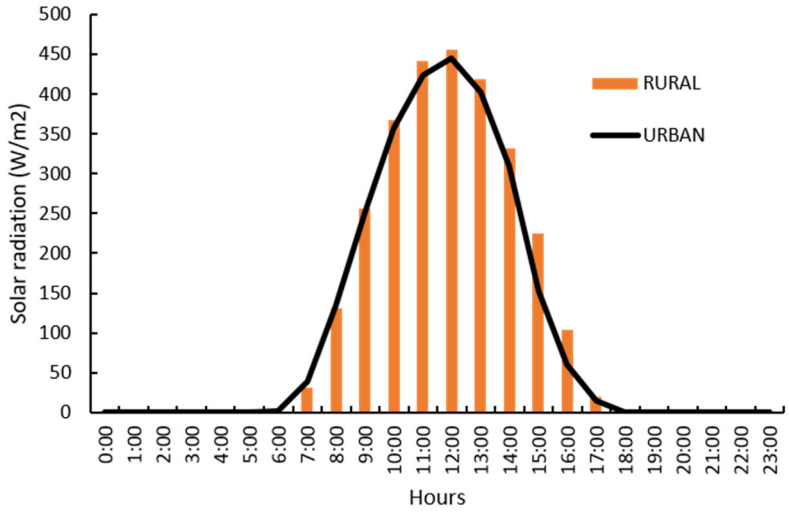

Figure 4–7 Diurnal variation of average solar radiation in urban and rural areas

Wind rose diagrams, averaged diurnally, have been generated for the winter season. While wind direction was predominantly from the NNW in the urban area, WNW were dominant at the rural site (Figure 4–8). Average wind speed for urban area was 0.59 m/s as opposed to 0.057 m/s at rural site.

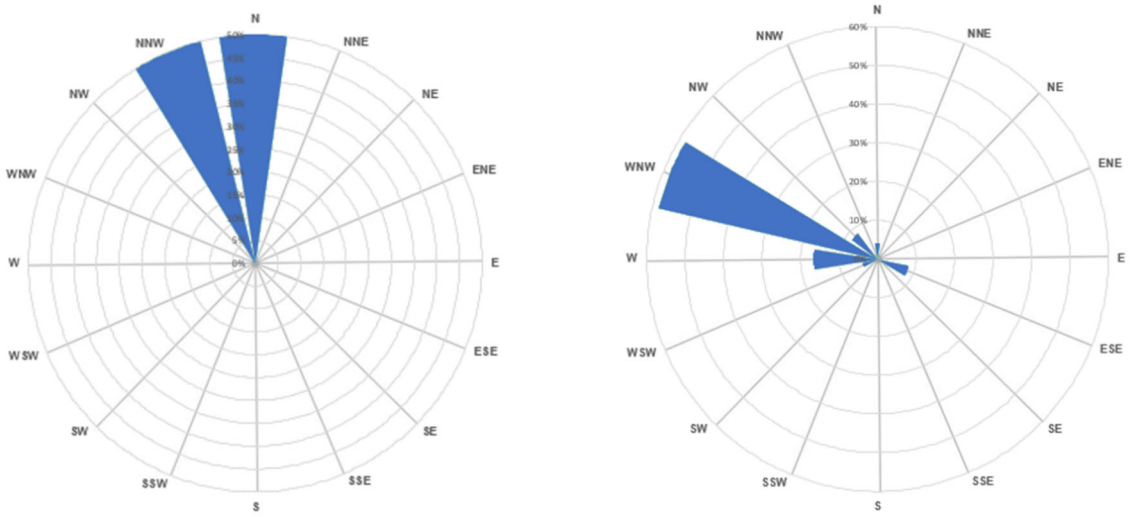

Figure 4–8 Wind rose diagrams (urban and rural) during winter (calm conditions = 0.30 m/s)

Descriptive statistics of surface and air temperatures during the winter season indicate that the average surface and air temperatures is higher in urban area than rural site (Table 4–5). The magnitude of mean air temperature, however, was slightly higher (1.72 °C) than surface temperature (1.41 °C).

Table 4–5 Descriptive statistics related to air and surface temperature in urban and rural locations

	Air temperature (°C)		**Surface temperature (°C)**	
	Urban	Rural	Urban	Rural
Maximum	26.22	27.50	25.98	23.21
Minimum	17.45	14.31	18.77	17.77
Mean	21.26	19.54	21.55	20.14
Std. Dev.	2.96	4.80	2.41	1.84

The monthly average of surface and air temperatures (along with a number of other parameters) recorded between the two locations, is shown in Table 4–6. This indicates that during December, January and February, the urban area had 0.55, 1.64 and 2.19 °C higher surface temperatures than the rural site. The differences in air temperatures were also higher than the rural area. The difference was 1.48, 1.96 and 1.74 °C, respectively during the three winter months. The results therefore signify warming of urban microclimate.

Table 4–6 Monthly mean temperatures, relative humidity, solar radiation, wind speed in urban versus rural location

	Urban					Rural				
Months	ST (°C)	AT (°C)	RH (%)	SR (W/m^2)	WS (m/s)	ST (°C)	AT (°C)	RH (%)	SR (W/m^2)	WS (m/s)
Dec	20.71	20.28	77.72	80.33	0.67	20.16	18.80	87.76	89.71	0.01
Jan	20.95	20.97	57.94	115.13	0.76	19.31	19.01	79.81	126.61	0.02
Feb	22.98	22.53	62.94	129.45	0.35	20.94	20.79	52.24	132.25	0.15

ST: surface temperature; AT: air temperature; RH: relative humidity; SR: solar radiation; WS: wind speed

4.11.1.2 Analysis of traverse surveys

The results of air temperatures recorded during the traverse surveys is shown in Figure 4–9 (a–c). This indicates that the planned land use type had a higher temperature than the mixed zone during the morning (Figure 4–9a). In the afternoon, however (Figure 4–9b), the situation is reversed, with the air temperature being >2 °C higher in the mixed land use type when compared to the other two zones (e.g. unplanned and planned). This may be due to the existence and influence of large waterbodies in that zone. During nighttime (2100 hrs), the mixed land use cooled more rapidly than the other two land use zones (Figure 4–9c), possibly due to differences in land use and socioeconomic conditions. Both planned and unplanned zones had elevated temperatures in the evening, recording values nearly 1 °C higher than the mixed land use zone.

Surface temperature plots of the three zones are shown in Figure 4–10 (a–c). In the morning, the average temperature of the three zones was 27.3 °C (unplanned), 27.8 °C (planned) and 26.0 °C (mixed), respectively (Figure 4–10a). In the afternoon, however, the average temperature was >3 °C higher in the mixed zone than other two traverse locations (Figure 4–10b). Interestingly, the average temperature of the three sites was quite similar in the evening, however small variations in intra–urban differences are noticeable among the twenty measuring locations along the routes (Figure 4–10c).

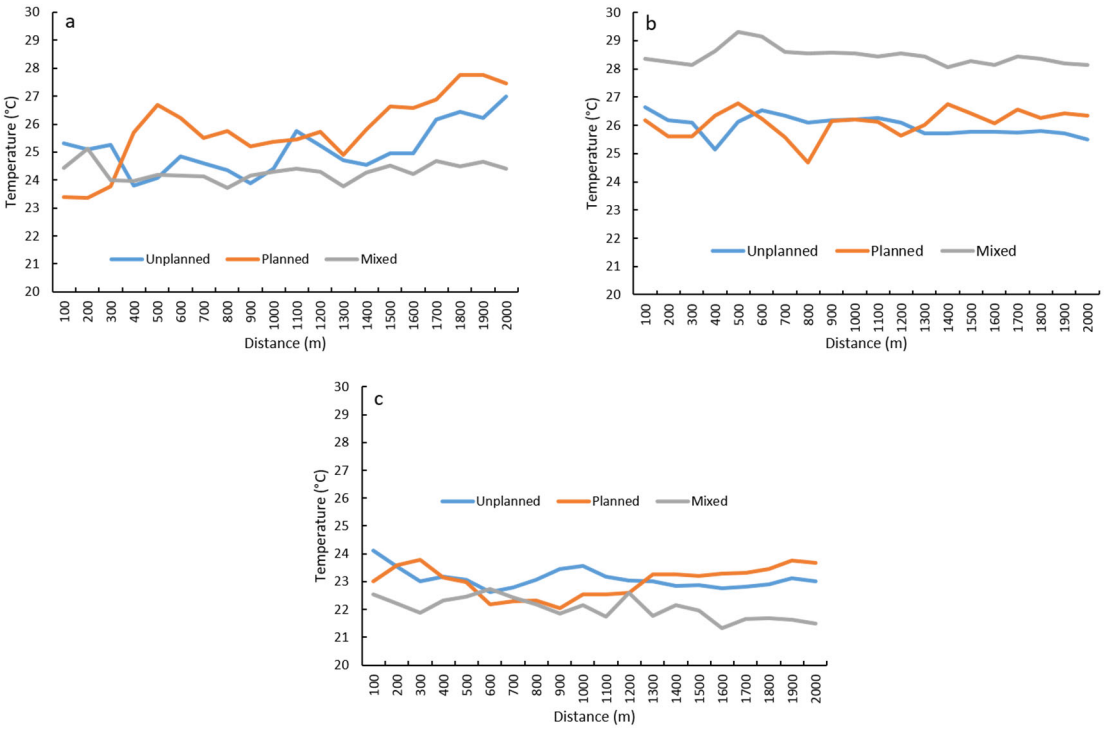

Figure 4–9 Variation of air temperature in three zones: (a) morning; (b) afternoon; and (c) evening

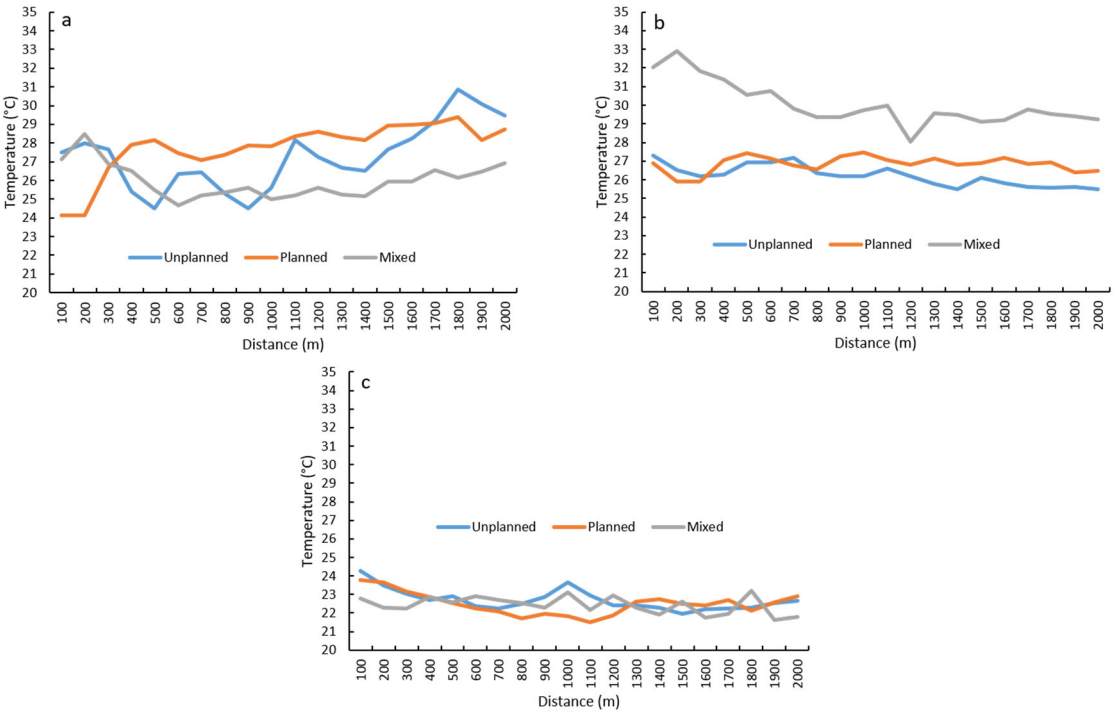

Figure 4–10 Variation of surface temperature in three zones: (a) morning; (b) afternoon; and (c) evening

Table 4–7 Spearman rank correlation between air/surface temperatures and relative humidity, wind speed and solar radiation in three traverse locations

	Air temperature (°C)						Surface temperature (°C)					
Unplanned	WS	Sig.	RH	Sig.	SR	Sig.	WS	Sig.	RH	Sig.	SR	Sig.
Morning	.023	.924	–.666**	.001	.462*	.040	.119	.616	–.797**	.000	.386	.092
Afternoon	.037	.876	–.683**	.001	.651**	.002	.260	.268	–.892**	.000	.819**	.000
Evening	.073	.760	–.633**	.003	–	–	.332	.153	–.702**	.001	–	–
Planned												
Morning	.055	.817	–.797**	.000	.304	.193	.106	.657	–.755**	.000	.538*	.014
Afternoon	.039	.872	–.726**	.000	–.122	.609	.156	.512	.171	.470	.245	.298
Evening	–.122	.608	–.866**	.000	–	–	-.153	.519	–.749**	.000	–	–
Mixed												
Morning	–.129	.588	–.430	.058	.244	.300	.247	.293	–.325	.162	.063	.791
Afternoon	–.118	.619	–.171	.471	.016	.946	.093	.695	.093	.696	.712**	.000
Evening	–.123	.604	–.475*	.034	–	–	-.276	.239	–.413	.071	–	–

** Significant at the 0.01 level (2–tailed); * Significant at the 0.05 level (2–tailed)

An analysis of the relationship between air/surface temperatures and the other three variables (wind speed, relative humidity and solar radiation) was conducted using the Spearman rank correlation technique. This method was used due to the non–normality of the data distribution. The results are presented in Table 4–7. The analysis indicates that relative humidity was the most important variable in essentially all of the three traverse routes. Solar radiation was of secondary importance.

Figure 4–11 (a–c) shows the spatial distribution CUHI in the three traverse routes during the winter season. They indicate a variation in both heat island phenomena (either warmer or cooler), primarily resulting from the different urban features (e.g. building density) and natural surfaces (e.g. green areas).

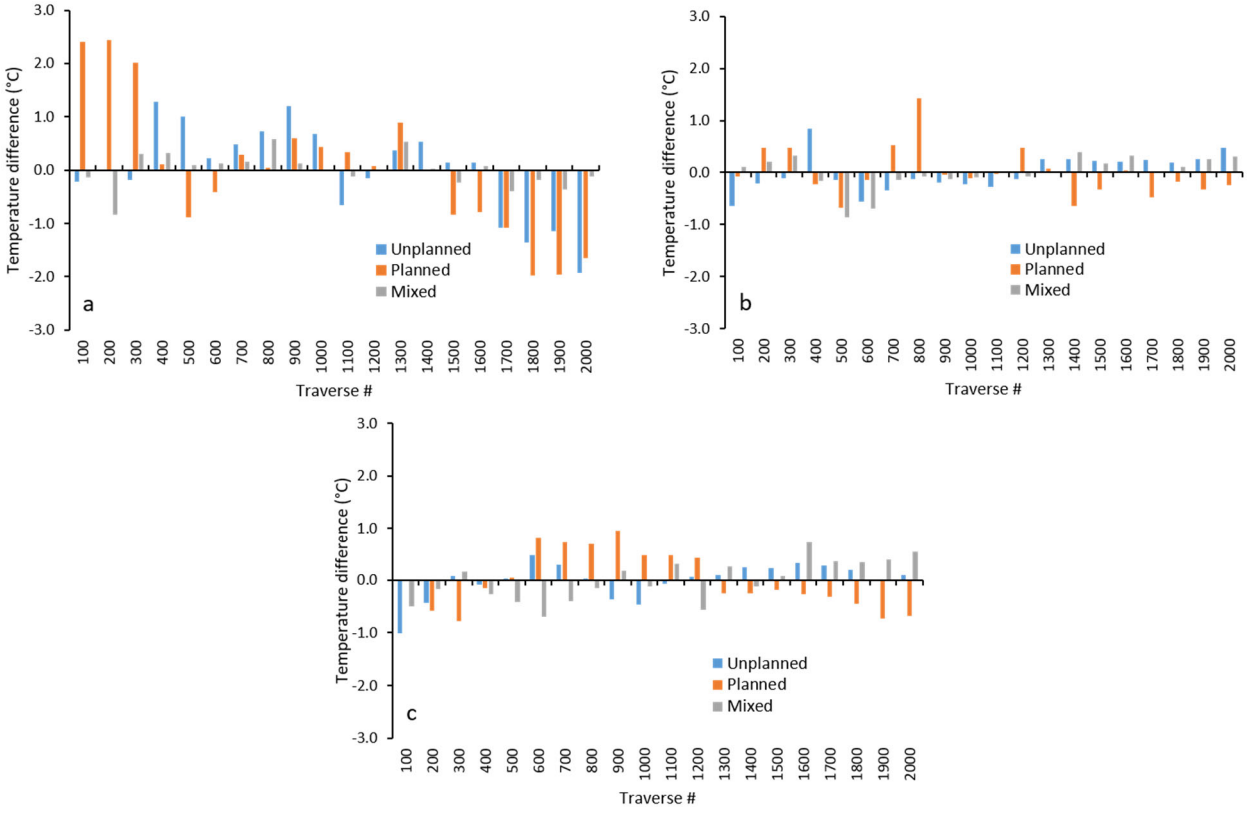

Figure 4–11 Spatial distribution of the mean air temperature differences: (a) morning; (b) afternoon; and (c) evening. Sites warmer than the mean transect value are positive and sites cooler than the mean are negative

An analysis of the surface temperature distribution, on the other hand, reveals a similar warmer and cooler pattern (Figure 4–12, a–c) which indicates the existence of SUHI. During morning hours, the unplanned areas had 9 warmer as opposed to 11 cooler sites, the planned zone had 7 warmer and 13 cooler sites whereas the mixed zone had 12 warmer and 8 cooler locations (Figure 4–12a). In the afternoon, warmer locations were higher in the mixed (14 positives and 6 negatives) and unplanned zones (12 positives and 8 negatives), whilst the planned zone had

9 warmer and 11 cooler locations (Figure 4–12b). In the evening, however the mixed land use zone had a greater number of warmer locations (13) than the other two traverse routes (Figure 4–12c). The cooler locations are referred to Urban Cool Islands (UCI).

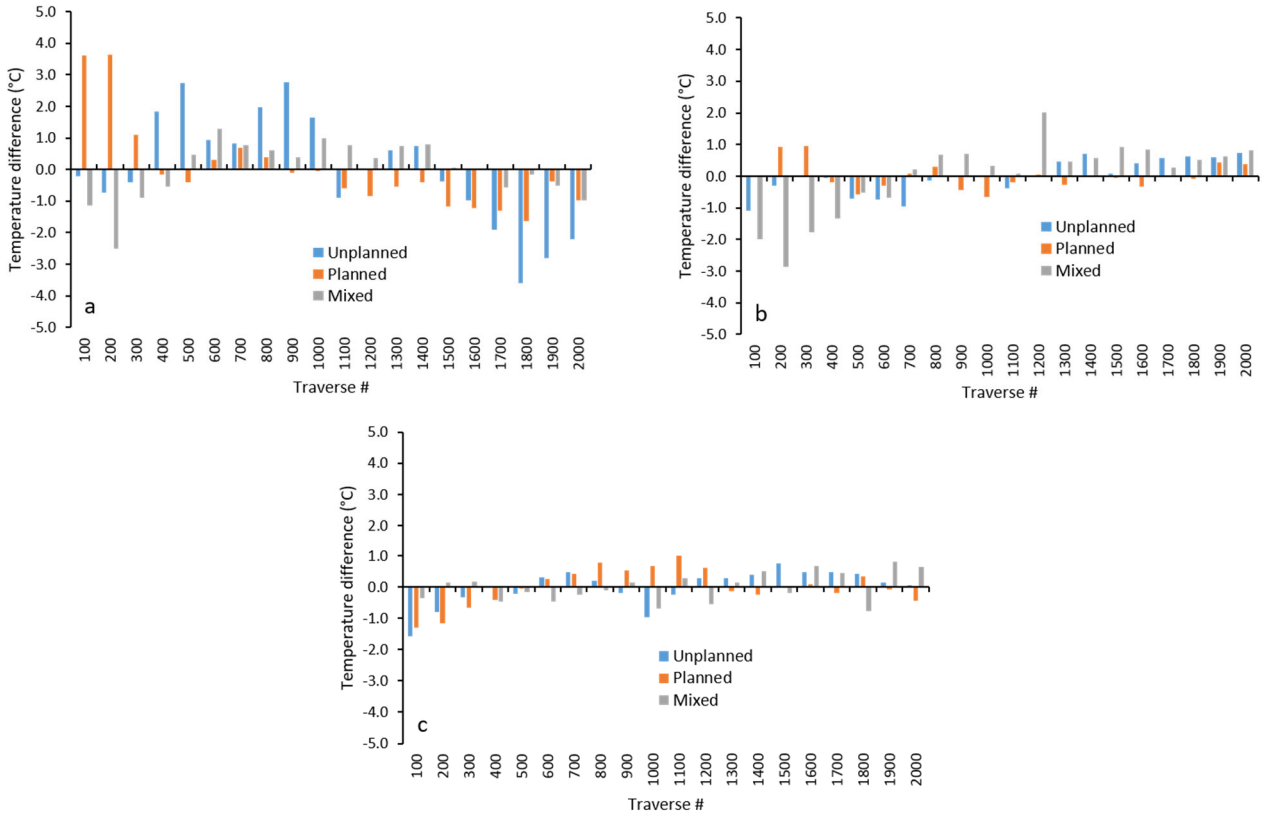

Figure 4–12 Spatial distribution of the mean surface temperature differences: (a) morning; (b) afternoon; and (c) evening. Sites warmer than the mean transect value are positive and sites cooler than the mean are negative

4.11.1.3 Thermo–physical behaviour of urban features

A summary of air temperature, surface temperature and relative humidity recorded at the three traverse sites (an average of 20 recording locations), is presented in Table 4–8. This indicates that the planned zone has a slower cooling rate than the other two zones, potentially caused by the low cooling rate (CR) of air temperature and the use of numerous air conditioners, which were identified during the survey. Even though there is little difference in terms of the CR of air and surface temperatures between planned and unplanned zones (Table 4–8), the mixed location shows a relatively higher CR for both temperatures. Because the mixed zone is located in a low socioeconomic area and in close proximity to large waterbodies, these factors may have influenced both air and surface temperatures to a greater degree than in the other two zones. Average wind speed (m/s) in these sites in the morning were 0.12 (planned), 0.04 (unplanned), 0.28 (mixed), respectively. In the evening, they were 0.22 (planned), 0.19

(unplanned) and 0.42 (mixed). It is therefore plausible to assume that airflow may have a significant impact on the CR of the microclimate at individual sites.

Table 4–8 Average of air temperature (AT), surface temperature (AAT), relative humidity (RH) of three traverse sites during morning and evening in winter. Temperature values are in °C and relative humidity is in percentage (%). Area average temperature (AAT) is taken from selected areas on the thermal images and are the average of 88 infrared photographs from 20 sites within each zone. CR is the cooling rate per hour in °C

Traverse site	AT_M	AT_E	ΔAT	CR/h	AAT_M	AAT_E	ΔAAT	CR/h	RH_M	RH_E
Planned	25.97	22.42	3.54	0.30	24.55	18.31	6.23	0.54	45.20	55.74
Unplanned	29.56	25.05	4.54	0.31	30.22	21.5	8.72	0.55	42.95	56.19
Mixed	25.80	20.92	4.89	0.48	27.34	18.49	8.85	0.87	35.61	42.89

M = morning; E = evening

The results of the thermographic assessment of various urban features are shown in Tables 4–9–11. These show that, in general, coating materials and colour, along with feature types and their locations, are important determinants in the estimation of the cooling potential. It should be noted that temporal variances during image capturing might also have affected the calculation of CR of individual objects. As mentioned previously, the use of simultaneous photography would have been useful. Note also that CR is also time dependent.

The top five objects (as defined by their CR) were chosen for each zone (bold–faced in Tables 4–9 to 4–11). This demonstrates that buildings with green glass cool faster (2.98 °C/h) than windows with grey glass (2.13 °C/h). These glass–influenced structures are followed by plastic billboards with a navy–blue colour (1.66 °C/h), mirage tin rooftop (1.60 °C/h) and building walls made of plaster (1.58 °C/h) in the planned area. In the unplanned zone, a steel electric pole with silver coating has a rapid CR (2.10 °C/h), a cemented wall with a grey coloration (1.96 °C/h), ash–coloured marble wall (1.61 °C/h), plastic advertising board with mixed colour (1.45 °C/h) and window glass with black colour (1.44 °C/h). In contrast, the cooling rate of materials is generally higher in the mixed zone. A plaster–coated building with grey colour has the highest cooling rate (9.88 °C/h). This is followed by a green plastic billboard (3.59 °C/h), black plastic house wall (3.49 °C/h), plaster building with moss (3.01 °C/h) and concrete street with grey colour (2.37 °C/h). Conversely, the lowest cooling rate was found in a brick building with green colouration (–0.25 °C/h) in the planned zone, a steel transmission pole (0 °C/h) in the unplanned zone and a plastic billboard with red colour (–1.3 °C/h) in the mixed area.

Table 4–9 Planned zone – object surface temperature (°C) and cooling rate (°C/h)

Feature type	Make	Colour	Early T (°C)	Late T (°C)	ΔT (°C)	CR/hr
Tree branch	–	–	19.2	18.2	1.0	0.09
Bld. wall	Brick	Green	20.1	23.1	-3.0	-0.25
Billboard	Plastic	White	20.2	22.6	-2.4	-0.20
Bld. wall	Glass	Blue	27.3	20.5	6.8	0.60
Bld. window	Glass	Transparent	19.8	20.2	-0.4	-0.04
Brick wall	Tile	Orange	20.3	20.4	-0.1	-0.00
Tree trunk	–	–	19.4	18.0	1.4	0.12
Bld. wall	Glass	Grey	36.3	20.8	15.5	1.38
Bld. pillar	Concrete	Red	30	20.6	9.4	0.83
Bld. wall	Concrete	Off-white	28.3	21.1	7.2	0.64
Tree foliage	–	–	21.1	18.6	2.5	0.22
Water tank	Iron	Light yellow	25.4	17.9	7.5	0.68
Tank pillar	Iron	Light yellow	22.2	18.4	3.8	0.34
Tree foliage	–	–	26.2	17.9	8.3	0.75
Tank body	Iron	Cast skin	30.5	15.7	14.8	1.34
Mosque	Brick	Red	29.8	17.5	12.3	1.14
Stair	Tile	Off-white	24.7	17.3	7.4	0.68
Grass	–	–	20.9	13.3	7.6	0.70
Tree trunk	–	–	20.9	16.4	4.5	0.42
Shaded walkway	Asphalt	Black	21.7	15.6	6.1	0.56
Waterbody	–	–	22.7	16.9	5.8	0.54
Rooftop	**Tin**	**Mirage**	**35.5**	**18.4**	**17.1**	**1.60**
Health veg.	–	–	30.5	14.3	16.2	1.52
Unhealthy veg.	–	–	31.1	16.3	14.8	1.39
Shaded street	Asphalt	Black	21	19.4	1.6	0.15
Shaded walkway	Tile	Yellow	20.2	18.9	1.3	0.12
Shaded walkway	Tile	Red	20.3	20.	0.6	0.05
Electric pole	Steel	Silver	21.7	20.1	1.6	0.15
Unshaded street	Asphalt	Black	24.7	24.6	0.1	0.00
Painted bld. wall	Concrete	Yellow	27.8	20.1	7.7	0.74
Tree foliage	–	–	25.8	17.2	8.6	0.83
Window	**Glass**	**Grey**	**38.5**	**16.2**	**22.3**	**2.13**
Tree trunk	–	–	26.5	19.3	7.2	0.69
Bld. wall	Brick	Brown	28.7	18.6	10.1	0.99
Building	**Glass**	**Green**	**38.9**	**15.5**	**23.4**	**2.98**
Bld. side wall	Brick	Plaster	23.3	20.1	3.2	0.31
Bld. front wall	Glass	Transparent	35.0	19.1	15.9	1.56
Waterbody	–	–	18.5	20.8	-2.3	-0.23
Rubbish	–	–	36.8	17.7	19.1	1.9
Speedboat	Steel	White	33.6	20.6	13.0	1.30
Shrub	–	–	24.7	15.5	9.2	0.92
Billboard	**Plastic**	**Navy blue**	**37.4**	**21.0**	**16.4**	**1.66**
Bld. wall	**Plaster**	**Mirage**	**32.8**	**17.2**	**15.6**	**1.58**
Bld. wall	Glass	Blue	28.8	16.7	12.1	1.23
Building	Glass	Green	21.5	19.0	2.5	0.26
Rooftop	Tile	Silver	29.6	18.8	10.8	0.50
Fence	Iron	–	29.7	20.7	9.0	0.42
Passenger shade	Iron	White	31.0	18.0	13.0	0.60
Wall	Brick	Red	30.7	20.3	10.4	0.48
Bld. wall	Concrete	Brown	35.6	20.3	15.4	0.72
Bld. wall	Concrete	Yellow	33.0	20.4	12.6	0.59
Bld. front wall	Concrete	Grey	31.5	18.1	13.4	0.62

Table 4–10 Unplanned zone – object surface temperature (°C) and cooling rate (°C/h)

Feature type	Make	Colour	Early T (°C)	Late T (°C)	ΔT (°C)	CR/hr
Billboard	Plastic	Red	40.0	30.0	10.0	0.84
Window	Glass	Hue	33.2	19.8	13.4	1.13
Balcony	Plaster	–	26.6	19.2	7.4	0.62
Raw brick	–	Red	35.4	23.4	12.0	1.01
Bld. wall	**Marble**	**Ash**	**41.1**	**22.0**	**19.1**	**1.61**
Electric pole	**Steel**	**Silver**	**43.8**	**19.0**	**24.8**	**2.10**
Window	Glass	Grey	26.5	20.7	5.8	0.19
Shaded fence	Concrete	White	21.4	20.9	0.5	0.04
Dense veg canopy	–	–	5.7	3.4	2.3	0.20
Painted fence	Brick	Yellow	24.4	21.3	3.1	0.27
Dense vegetation	–	–	21.8	6.8	15.0	1.33
Vegetated wall	Brick	–	24.2	20.8	3.4	0.32
Bld. wall	**Cement**	**Grey**	**42.0**	**21.1**	**20.9**	**1.96**
Bld. entrance	Concrete	White	28.5	22.4	6.1	0.57
Old fence	Brick	Red	22.6	20.8	1.8	0.18
Dome	Brick	Yellow	28.0	21.0	7.0	0.71
Elevated fence	Plaster	White	23.1	22.2	0.9	0.09
Tree trunk	–	–	23.5	23.2	0.3	0.03
Cornice	Iron	Yellow	26.0	23.3	2.7	0.27
Building	Tile	Mixed	25.5	22.4	3.1	0.32
Window	**Glass**	**Black**	**34.6**	**20.5**	**14.1**	**1.44**
Neon sign	**Plastic**	**Mixed**	**33.9**	**19.7**	**14.2**	**1.45**
Bld. entrance	Brick	Black	38.3	20.6	17.7	0.81
Rooftop	Tin	Silver	35.1	15.6	19.5	0.89
Bld. wall	Plaster	Brown	24.2	20.4	3.8	0.17
Bld. wall	Plaster	White	24.1	22.2	1.9	0.09
Cornice	Brick	Moss	37.1	22.5	14.6	0.67
Plastic wall	Plastic	Blue	34.6	26	8.6	0.40
Rooftop	Tin	Silver	25.6	21.7	3.9	0.18
Cornice	Iron	–	36.5	19.2	17.3	0.79
Degraded fence	Brick	Yellow	24.1	21.8	2.3	0.10
Rooftop	Concrete	No paint	25.6	21.7	3.9	0.33
Transmission pole	Steel	Silver	34.4	34.4	0.0	0.00
Billboard	Steel	Silver	35.0	20.3	14.7	0.67
Bld. wall	Brick	Red	27.5	22.6	4.9	0.23
Window	Iron	Mirage	23.8	21.1	2.7	0.12
Window	Glass	Blue	24.0	16.5	7.5	0.38
Degraded bld.	Brick	Mirage	46.6	22.2	24.4	1.22

Table 4–11 Mixed zone – object surface temperature (°C) and cooling rate (°C/h)

Feature type	Make	Colour	Early T (°C)	Late T (°C)	ΔT (°C)	CR/hr
Bridge	Concrete	–	33.6	23.9	9.7	0.86
Waterbody	–	Turbid	27.7	13.2	14.5	1.28
Grass	–	–	20.2	17.2	3.0	0.26
Electric pole	Steel	Silver	24.0	23.3	0.7	0.06
Rooftop	Tin	Silver	27.3	19.2	8.1	0.71
Bare soil	–	Brown	25.4	20.2	5.2	0.46
Bld. wall	Raw brick	Red	16.9	13.1	3.8	0.34
Bld. wall	Brick	Brown	25.5	16.3	9.2	0.82
Street	Asphalt	Black	26.6	16.7	9.9	0.88
Roof with garden	Concrete	–	19.6	22.0	-2.4	0.21
House wall	Tin	Silver	25.9	20.5	5.4	0.48
Balcony	Iron	Brown	35.6	21.9	13.7	1.22
Shop shutter	Tin	Silver	37.5	18.7	18.8	1.67
Billboard	Plastic	Red	37.5	52.1	-14.6	-1.30
Tree foliage	–	–	23.1	19.6	3.5	0.34
Window	Glass	Green	20.5	15.7	4.8	0.46
Bld. wall	Brick	Yellow	21.9	19.5	2.4	0.23
Shop shutter	Tin	Silver	32.3	20.3	12.0	1.17
Bld. wall	Raw brick	Red	20.3	18.5	1.8	0.18
Bld. wall	Tile	White	13.8	18.2	-4.4	-0.43
Shop	Tin	Grey	24.0	19.1	4.9	0.48
Window	Glass	Blue	25.1	18.1	7.0	0.68
Bld. front wall	Brick	Yellow	34.3	21.6	12.7	1.23
Open balcony	Plaster	Off-white	26.9	23.2	3.7	0.36
Shutter	Tin	Silver	39.6	22.0	17.6	1.71
Signboard	Plastic	White	35.7	21.6	14.1	1.37
Tree trunk	–	–	39.0	20.5	18.5	1.80
Bld. pillar	Raw brick	Red	26.8	21.4	5.4	0.52
Bld. wall	Brick	Yellow	25.4	18.1	7.3	0.71
Bld. front wall	Raw brick	Red	36.6	20.3	16.3	1.59
Street	Asphalt	Black	25.4	21.1	4.3	0.42
Electric pole	Steel	Silver	37.2	21.5	15.7	1.53
Bld. wall	Brick	Blue	37.9	20.0	17.9	1.73
Window	Glass	Black	34.4	22.7	11.7	1.13
Rooftop	Raw brick	Red	38.5	14.8	23.7	2.29
Billboard	**Plastic**	**Green**	**54.9**	**18.9**	**36.0**	**3.59**
Bld. front wall	Plaster	Grey	36.8	20.8	16.0	1.59
Coconut T. foliage	–	–	30.1	18.3	11.8	1.18
Rooftop wall	Raw brick	Red	37.6	18.0	19.6	1.95
Tree trunk	–	–	25.0	19.1	5.9	0.59
Bld. wall	Brick	Orange	35.3	20.2	15.1	1.52
Bld. side wall	Cement	Grey	26.3	20.4	5.9	0.59
Bld. wall	**Plaster**	**Grey**	**35.2**	**17.0**	**18.2**	**9.88**
Rooftop	Concrete	Grey	35.3	20.6	14.7	1.49
Billboard	Plastic	Red	40.3	17.6	22.7	2.30
Road	Concrete	Ash	29.7	16.3	13.4	1.37
Bld. wall	Raw brick	Red	32.5	14.9	17.6	1.80
Window	Glass	Transparent	23.2	14.6	8.6	0.88
Bld. wall	Brick	Purple	23.8	16.2	7.6	0.77
Bld. wall	Plaster	Grey	42.3	17.5	24.8	2.53
Tree	–	–	27.2	14.9	12.3	1.25
Water tank	**Plastic**	**Black**	**53.7**	**19.6**	**34.1**	**3.49**
Bld. wall	**Plaster**	**Moss**	**47.4**	**18.0**	**29.4**	**3.01**
Street	**Concrete**	**Grey**	**40.0**	**16.8**	**23.2**	**2.37**

4.11.1.4 Thermal response of rooftop with/without garden

An analysis of the surface temperature for both a rooftop with a garden and without a garden reveals that the surface temperature of a non–vegetated rooftop was around 4.7 °C higher than for a roof with vegetation (Figure 4–13). The temperature of the roof with vegetation was low across the measurement periods, showing the effectiveness of a rooftop garden in reducing the temperature of the immediate surroundings. It appears there may be potential for a significant reduction in heat flux from outdoors to indoors due to the presence of vegetation on the roof. This would result in reduced energy consumption and increased human comfort levels.

Figure 4–13 Diurnal variation of surface temperature of rooftop with garden and rooftop without garden in winter

It appears that rooftop gardens are effective in reducing air temperature at a height of 1 m, whereas the results are mixed for 2 m and 3 m heights (Figure 4–14, a–c). At the 1 m height level, on average, a rooftop with associated garden appears to reduce air temperature by around 3.45 °C when compared with a rooftop without garden. The other two categories had a varied response, depending on the time of a day. At 2 m, for instance, reduction of afternoon temperature is high, while at the 3 m height level, the benefit of a roof garden is apparent from the early morning into the late afternoon (Figure 4–14c).

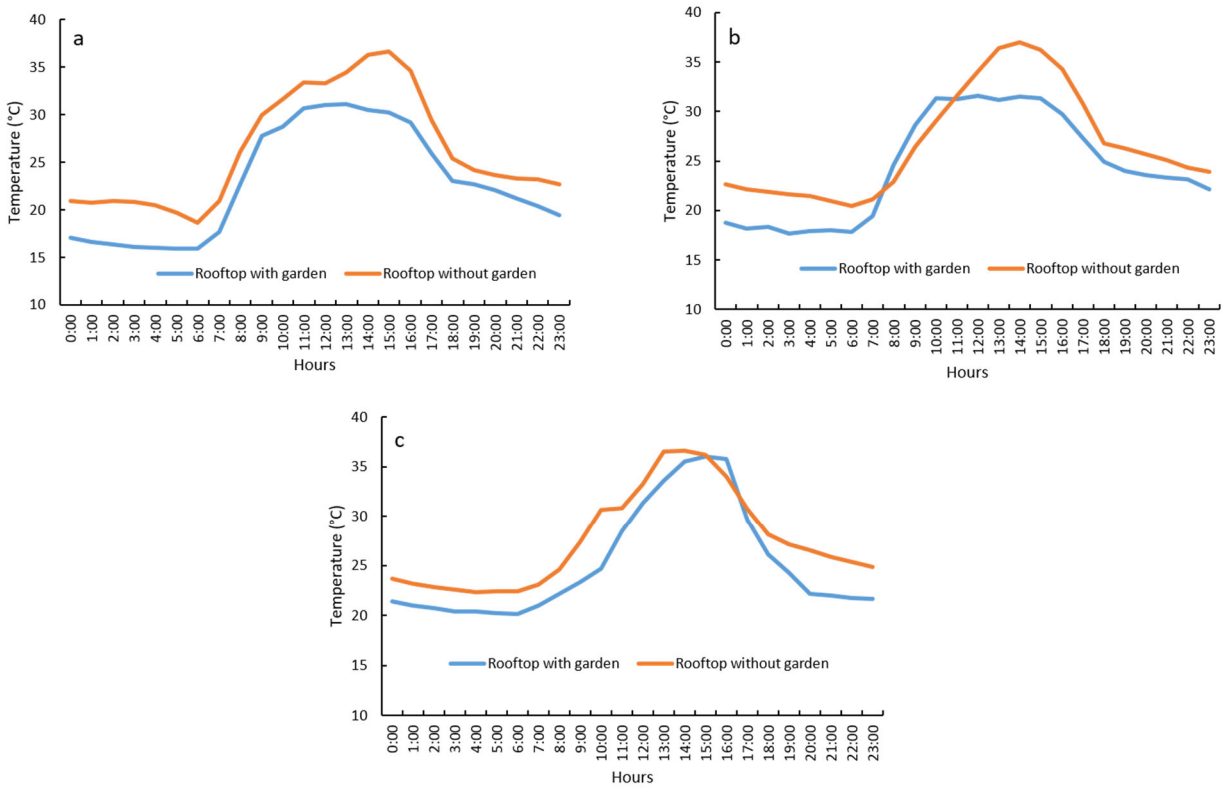

Figure 4–14 Diurnal response of rooftop and non–rooftop gardens on air temperatures at three different heights: (a) 1 m; (b) 2 m; and (c) 3 m

4.11.1.5 Response of dominant rooftop plants

The study indicates that *Combretum indicum* has the greatest environmental air temperature reduction potential (Figure 4–15). Species such as *Bougainvillea*, *Psidium Guajava*, *Maltes*

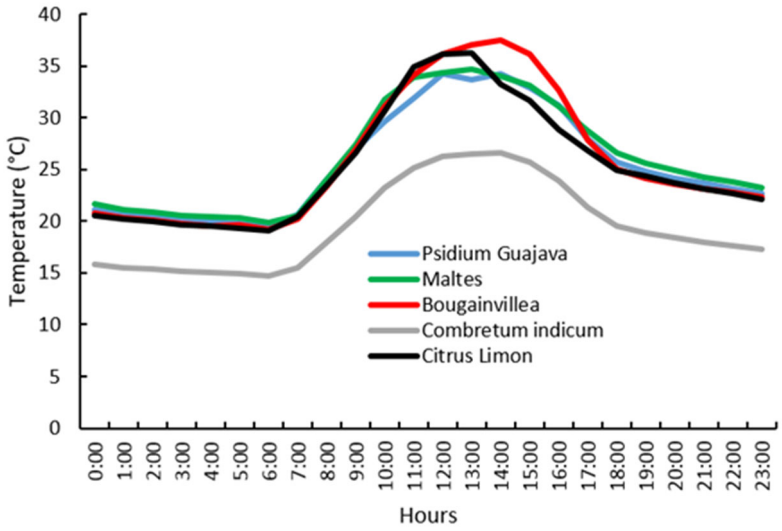

Figure 4–15 Thermal response of dominant rooftop vegetation types

and *Citrus Limon* have an almost identical thermal response, though *Bougainvillea* did appear to have an elevated thermal response during the afternoon (1300–1600). *Combretum indicum* species recorded a temperature approximately 5–6 °C lower than the other species over the diurnal cycle. These are the types of vegetation which may be useful in rooftop gardens to assist in reducing the temperature of the surrounding environment.

4.11.1.6 Cooling potential of open space vegetation

The thermal response of the dominant plants in open space areas is plotted with a box–and–whisker diagram (Figure 4–16). This indicates that *Barringtonia* has the highest cooling potential whilst the *Earleaf acacia* has the lowest potential. Average wind speed for four measurement days was 1.22 m/s whilst solar radiation was 193.28 W/m^2. Both wind speed and solar radiation were high at noon (1.59 m/s and 380 W/m^2, respectively) (Appendix VII).

A threshold value of 30 °C (the red horizontal line in Figure 4–16) has been used to identify open space plants considered useful in reducing ambient heat. *Barringtonia* ranks top followed by *Beharda*, *Teak*, *Cylon ironwood*, *Mimusops* and *Chambal*. *Barringtonia* is a mangrove species, therefore it is possible that this is a reason for the high evapotranspiration rate of this plant. The next useful species is *Beharda* followed by *Teak*, both of which are local species and may have the added advantage of being economically beneficial.

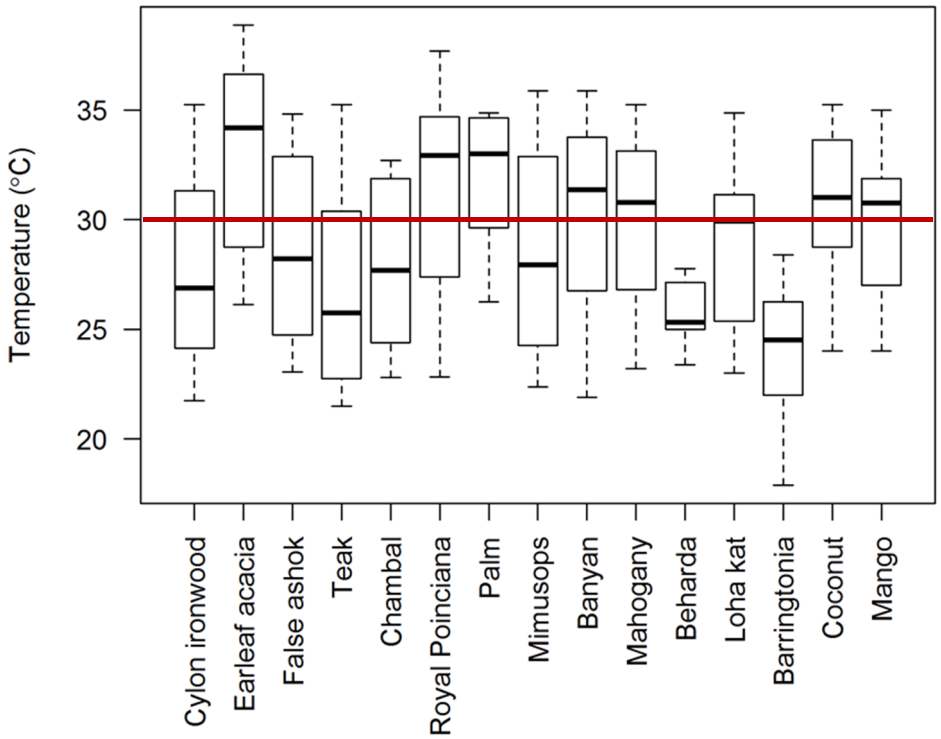

Figure 4–16 Box–and–whisker plot, showing variation of thermal response between open space plant species. The red horizontal line defines the 30 °C threshold value

The temperature of vegetation species was further categorised into morning–early afternoon (0900–1300) and afternoon–early evening (1400–1800), based on their average temperature (Table 4–12). The results indicated that *Barringtonia* appears the most effective plant in reducing the air temperature of the external environment in the morning to early evening period, as its temperature is significantly lower than other species examined.

Table 4–12 Average temperature (°C) of open space plants

Plant types	Morning (9:00–13:00)	Afternoon (14:00–18:00)
Cylon ironwood	26.30	27.53
Earleaf acacia	34.58	31.73
False ashok	26.00	27.65
Teak	26.58	27.70
Chambal	24.43	27.03
Royal Poinciana	32.33	28.90
Palm	33.53	30.33
Mimusops	29.30	27.55
Banyan	32.35	27.85
Mahogany	29.38	27.75
Beharda	25.08	26.23
Loha kat	29.03	28.88
Barringtonia	22.35	25.13
Coconut	30.78	30.80
Mango	30.38	29.13

4.11.1.7 Temperature variation of urban waterbodies

Figure 4–17 shows the response of two water features, namely a river and a pond. This indicates that the temperature of the river starts to increase from the early morning and peaks at around noon. On the other hand, the temperature of the pond fluctuates over the diurnal cycle. The pond has a low temperature at noon, but this increases during the late afternoon, suggesting a possible contribution of heat to the immediate surroundings during the night. Although a detailed analysis of such responses by waterbodies is beyond the scope of this work, we speculate that the temperature variation of waterbodies may be influenced by location and size, as well as by the degree of any turbidity.

4.11.1.8 Thermal response of a green hanging wall

Measurements of a green hanging wall feature indicates that the average surface temperature of the soil is lower than the substrate and wall. The surface temperature of wall and substrate tend to follow the same pattern from 1100 to 1500 and then decrease afterwards (Figure 4–18). The substrate temperature decreases more rapidly than the wall temperature from 1500, indicating a possible effectiveness in lowering the nocturnal heat of buildings. The ambient temperature recorded at various distances from a green hanging wall shows that the cooling

effect is high between 1 m and 3 m, and reduces at greater distances. The diurnal cycle of the first 3 m indicated that the system could be effective at lowering the temperature of the immediate surrounds from 0900 to 1600. After 1600, all distances had a reduced cooling potential (Table 4–13).

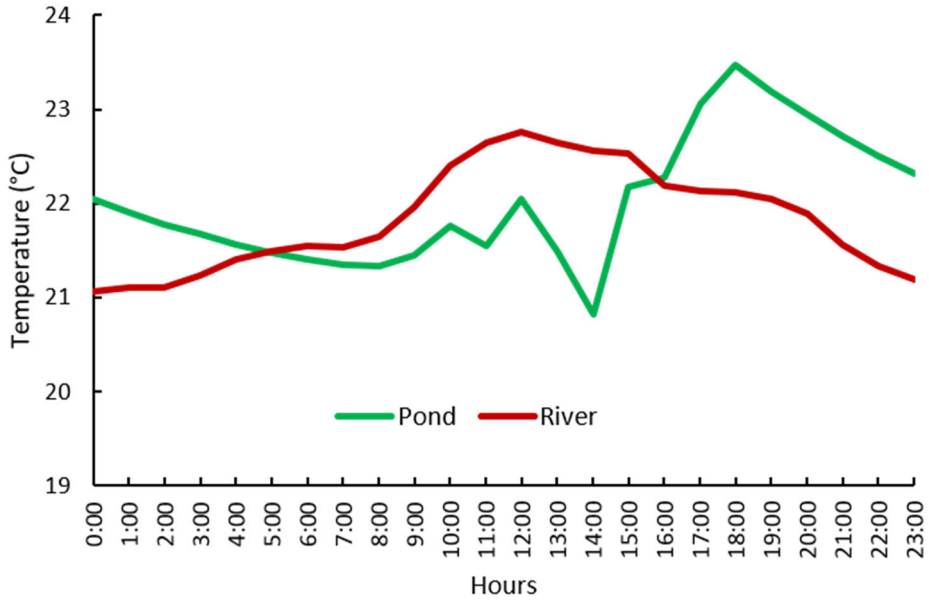

Figure 4–17 Diurnal variation of river and pond temperature

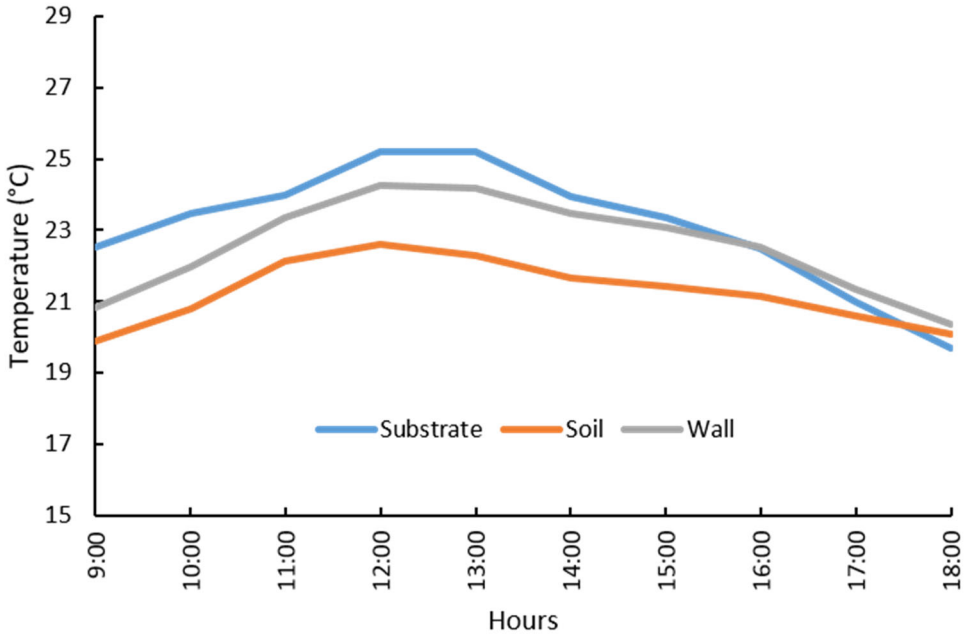

Figure 4–18 Average soil, wall and substrate temperature of a green hanging wall

Table 4–13 Ambient temperature of a green hanging wall at distances from the substrate

	Temperature (°C)				
Hours	**1 m**	**2 m**	**3 m**	**4 m**	**5 m**
9.00	21.46	21.90	21.00	22.08	25.87
10.00	23.54	23.67	22.83	23.56	27.43
11.00	25.58	25.10	24.63	25.19	30.41
12.00	26.67	27.17	26.10	26.69	29.15
13.00	26.21	27.08	27.04	27.38	28.21
14.00	25.06	25.63	25.79	25.77	27.14
15.00	23.92	24.35	24.44	24.56	25.19
16.00	23.13	23.19	23.54	23.52	23.78
17.00	21.40	21.52	21.90	21.81	21.98
18.00	19.88	19.85	20.13	20.04	19.94

4.11.1.9 Cooling potential of green and blue space

An analysis of the cooling effects of green space indicates orientation and distance from the park can influence any cooling effects (Figure 4–19). An inspection of the temperature gradient

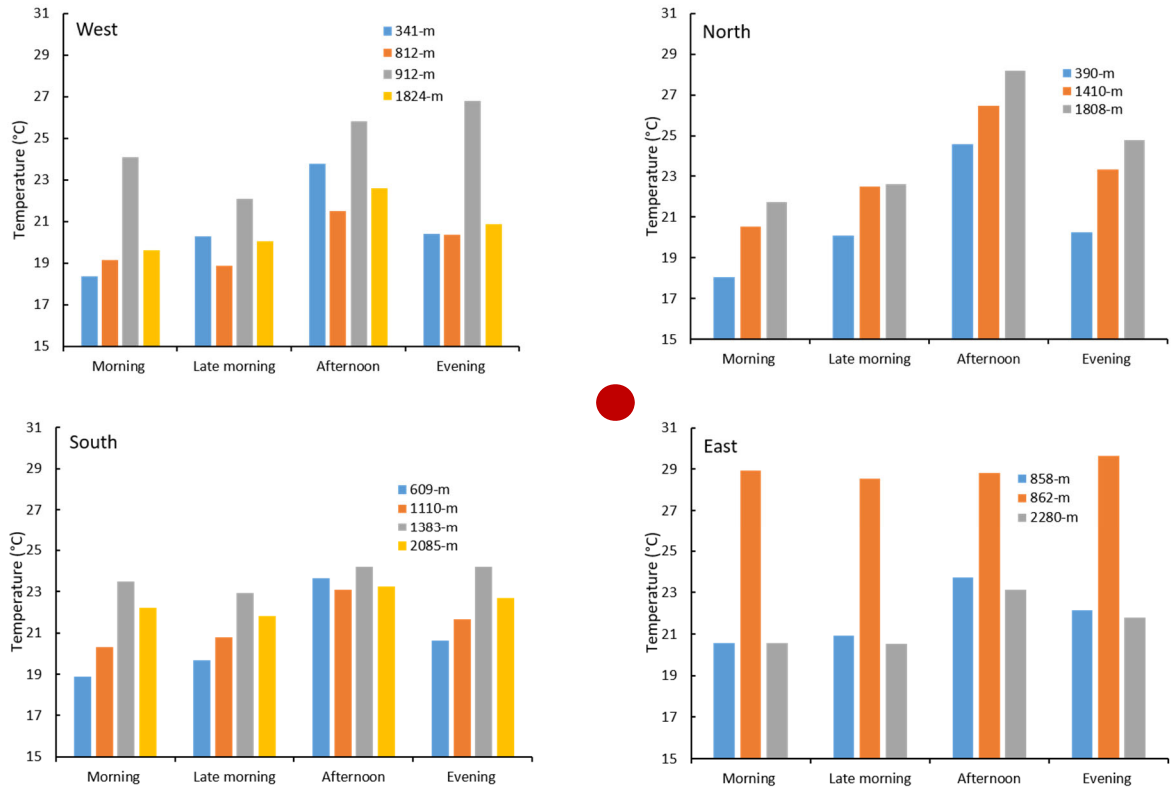

Figure 4–19 Cooling effect of a greenspace at various distances and in four directions. The dark red circle denotes the centre of the park relative to measuring points

from the park's centre, in terms of the diurnal cycle of winter, showed that distance from a greenspace appears to have little effect to the east. An increase in temperature at 862 m distance can be observed from morning to evening, however, at this direction malfunctioning of a device in February was noted (Appendix IX). The effect of the greenspace to the west can be observed at 314 m distance, particularly during the late morning to afteroon. At a distance of 912 m the temperature can be seen to increase from morning to evening, except for a period in the late morning (Figure 4–19). To the north, the distance to the greenspace appears to have signifcant impact on reducing temperature during the entire diurnal cycle in winter. A low cooling effect is noticeable at the proximity to the park to the south, especially in the late morning and evening.

The blue space response results are presented in Figure 4–20, which indicate that the possibility of blue spaces mitigating increased urban temperatures is inconclusive. Although a shorter distance has had an impact in southerly and westerly directions, distance and directional effects to the north and east seem to diminish considerably. It is, therefore, unclear as to how waterbodies could potentially reduce urban warming.

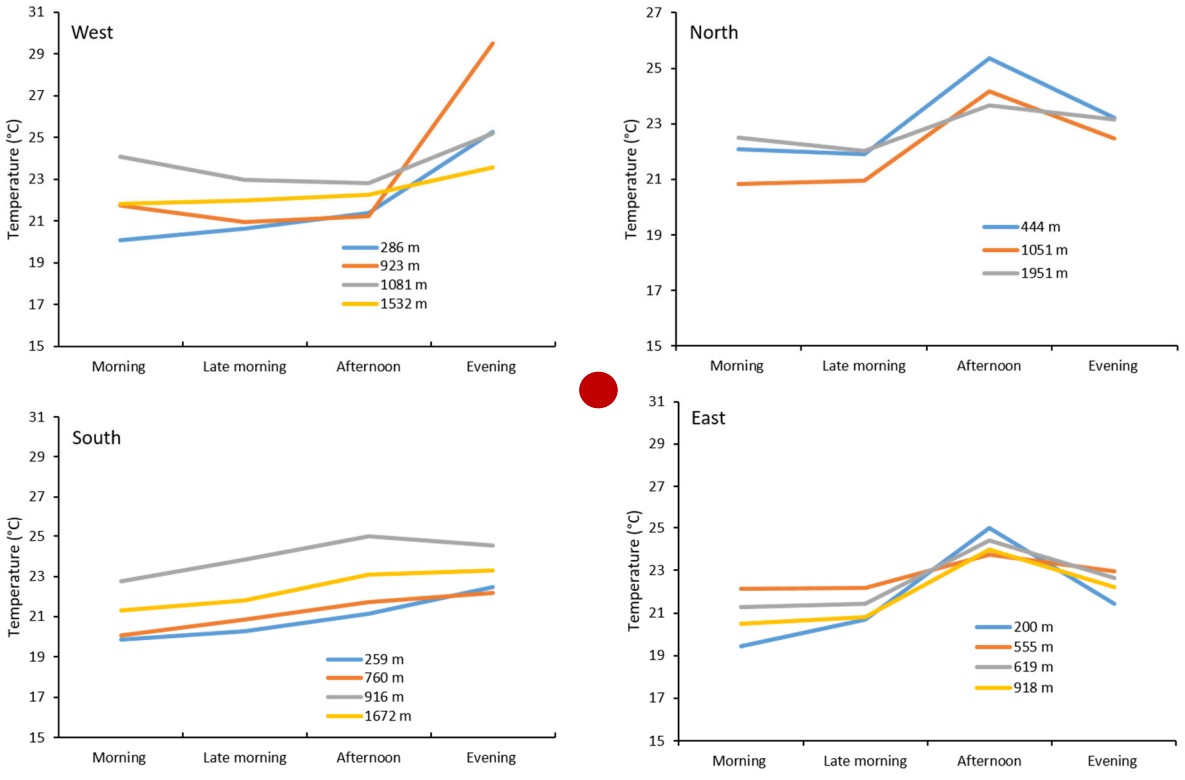

Figure 4–20 Cooling effect of a blue space at various distances and directions. The dark red circle denotes the centre of the lake relative to measuring points

4.11.2 Pre–monsoon season

A microclimatic assessment was conducted for the pre–monsoon, monsoon and post–monsoon seasons using the same data collection techniques and methods specified above (see sections 4–2 to 4–9). The following sections detail the results of the pre–monsoon season.

4.11.2.1 Urban–rural gradient of surface and air temperatures

During the pre–monsoon months (March–May), the analysis indicates that surface temperature remains consistently high over the diurnal cycle at the urban site, but the intensity appears to be the greatest at night (Figure 4–21a). During winter, average surface temperature of the diurnal cycle in urban areas was 1.23 °C higher than the rural area. The air temperature between urban and rural locations, on the other hand, exhibits a subtle deviation (Figure 4–21b). On average, the air temperature was 1.24 °C higher in urban areas than rural site across the diurnal cycle.

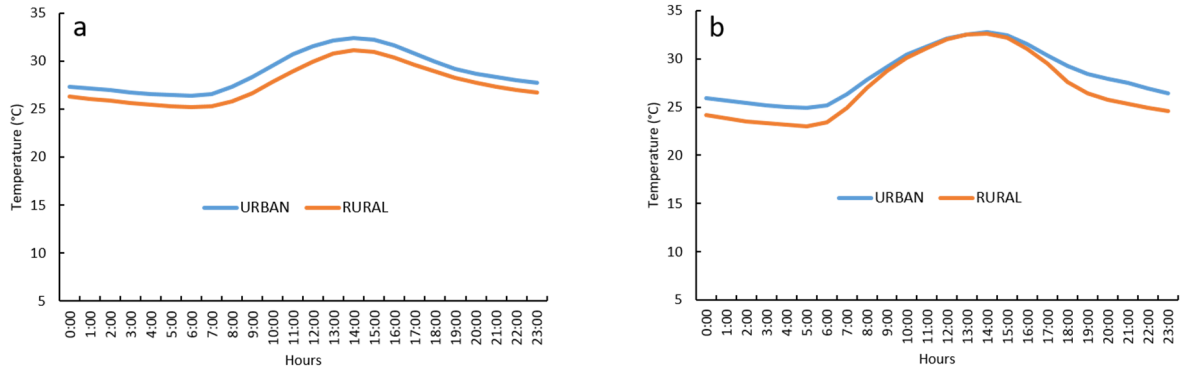

Figure 4–21 Diurnal variation of temperature during pre–monsoon season: (a) surface; (b) air

An analysis of the intensity of CUHI, defined as the urban temperature minus the rural temperature, reveals that the average urban area temperature tends to be 1.24 °C higher over the entire diurnal cycle (Table 4–14) with the greatest difference being observed between 1900 and 2200 (ranging from 1.65 to 2.01 °C). This indicates the magnitude of the CUHI. A somewhat different pattern emerges for the SUHI, where the urban site recorded an average temperature of 1.23 °C higher than the rural site. These results provide further evidence that the SUHI is markedly higher during the nighttime (except 1900–2100), a common phenomenon in large cities around the world.

To better understand the observed differences in both air and surface temperatures between the urban and rural locations, incoming solar radiation was averaged and plotted in Figure 4–22. Although the solar radiation average recorded almost the same intensity between the two sites

(177.18 and 177.91 W/m^2), the SUHI was particularly pronounced in the urban area, possibly linked with factors like sky view, building density and urban morphology.

Table 4–14 Differences in surface and air temperature during pre–monsoon

	Surface Temperature (°C)			Air Temperature (°C)		
Hours	Urban	Rural	SUHI	Urban	Rural	CUHI
0:00	27.34	26.31	1.03	25.93	24.13	1.80
1:00	27.14	26.07	1.07	25.69	23.82	1.88
2:00	26.95	25.86	1.09	25.43	23.54	1.89
3:00	26.77	25.66	1.10	25.18	23.31	1.87
4:00	26.59	25.48	1.11	24.99	23.12	1.86
5:00	26.44	25.32	1.12	24.90	23.04	1.86
6:00	26.36	25.21	1.16	25.16	23.38	1.78
7:00	26.60	25.30	1.30	26.37	24.89	1.48
8:00	27.29	25.79	1.51	27.84	26.97	0.88
9:00	28.34	26.67	1.67	29.16	28.76	0.40
10:00	29.52	27.82	1.70	30.40	30.11	0.29
11:00	30.68	28.93	1.75	31.23	31.09	0.15
12:00	31.51	29.90	1.61	32.08	32.02	0.06
13:00	32.18	30.75	1.42	32.54	32.53	0.01
14:00	32.43	31.14	1.29	32.76	32.60	0.17
15:00	32.25	30.92	1.33	32.44	32.18	0.26
16:00	31.64	30.40	1.23	31.53	31.00	0.53
17:00	30.78	29.64	1.14	30.39	29.48	0.91
18:00	29.97	28.94	1.03	29.23	27.58	1.65
19:00	29.22	28.26	0.96	28.41	26.38	2.03
20:00	28.70	27.75	0.95	27.95	25.80	2.15
21:00	28.33	27.35	0.98	27.47	25.34	2.13
22:00	28.01	27.00	1.01	26.95	24.94	2.01
23:00	27.72	26.69	1.03	26.45	24.62	1.83

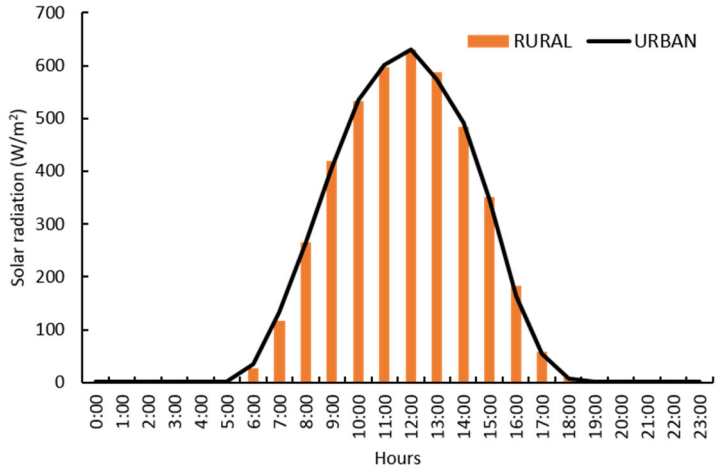

Figure 4–22 Diurnal variation of average solar radiation in urban and rural locations

Diurnally averaged wind rose diagrams of the two locations are presented in Figure 4–23. These indicate that constrasting wind direction prevail in the two sites during the pre–monsoon

season. In the urban location, it is predominantly from the southeast, with a mean wind speed of 1.60 m/s. However, the wind direction recorded in the rural area was almost diametrically opposite (e.g. WNW), and the mean air velocity was in the order of 0.85 m/s.

Comparing the recorded wind direction with those detailed in the weatheronline website (https://www.weatheronline.co.uk/) reveals similar wind directions to those seen in the urban wind rose. There is no rural site in Dhaka that measures wind data, so no validation was possible in regards the rural recordings. Despite relatively high wind speeds in urban areas, the overall ventilation in urban areas appears poorer than at the rural site. As a result, average of both temperatures, across the diurnal cycle, remained consistently high in the urban areas.

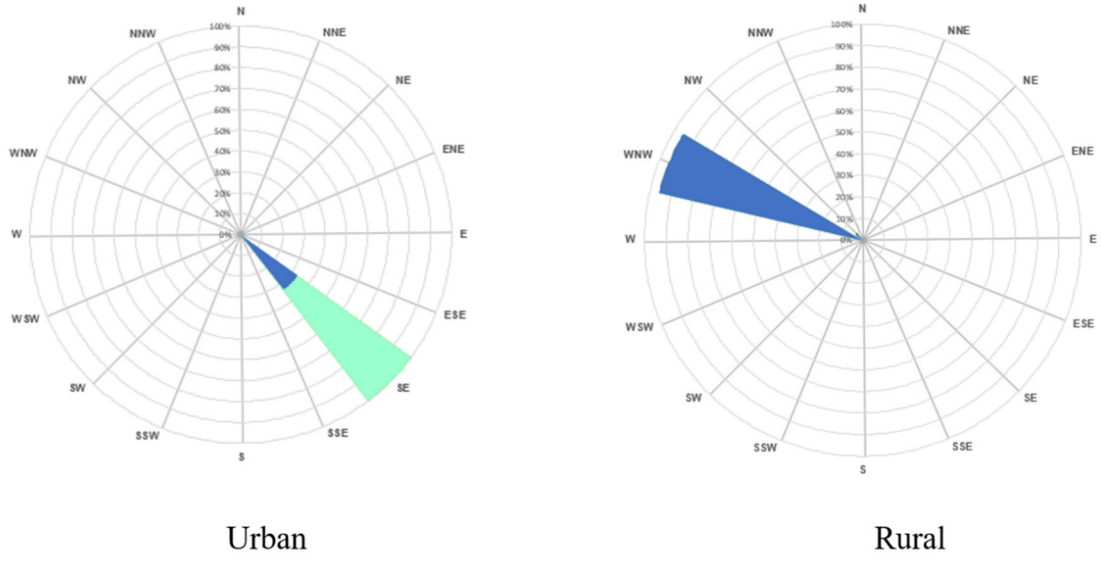

Figure 4–23 Wind rose during pre–monsoon (calm conditions = 0.30 m/s)

Descriptive statistics related to surface and air temperatures between urban and rural locations are shown in Table 4–15. This clearly demonstrates the existence of both CUHI and SUHI during the hot summer months. An interesting feature is that the difference between air and surface temperatures in both locations (urban vs rural), is subtle if one considers the average of the three months of pre–monsoon (e.g. 1.24 vs 1.23 °C).

Table 4–15 Descriptive statistics related to air and surface temperature in urban vs rural

	Air Temperature (°C)		Surface Temperature (°C)	
	Urban	Rural	Urban	Rural
Maximum	32.76	32.60	32.43	31.14
Minimum	24.90	23.04	26.36	25.21
Mean	28.35	27.11	28.86	27.63
Std. Dev.	2.73	3.44	2.08	2.00

Mean monthly surface and air temperatures between the two locations, along with solar radiation, wind speed and relative humidity is shown in Table 4–16. The relative humidity sensor at the rural site appeared to malfunction, so the humidity data from this site was not used. The analysis shows that both the surface and air temperature in the urban area is higher than at the rural site. Though wind speed was higher across the three pre–monsoon months in the urban areas, both recorded temperatures were high, reinforcing the impacts of anthropogenic influence on the UHI. April recorded the greatest difference in surface temperature (1.45 °C) whilst March had the greatest difference (1.63 °C) in air temperature in the urban areas relative to the rural location.

Table 4–16 Monthly mean temperatures, solar radiation, wind speed and relative humidity – urban versus rural

	Urban					Rural				
Months	ST (°C)	AT (°C)	SR (W/m^2)	WS (m/s)	RH (%)	ST (°C)	AT (°C)	SR (W/m^2)	WS (m/s)	RH (%)
March	26.10	26.32	173.18	0.76	63.89	24.93	24.69	176.44	0.33	NA
April	29.50	28.62	177.13	1.51	74.70	28.05	27.32	176.70	0.67	NA
May	30.99	30.12	181.22	2.61	82.32	29.92	29.32	180.58	1.54	NA

ST = surface temperature; AT = air temperature; RH = relative humidity; SR = solar radiation; WS = wind speed

4.11.2.2 Analysis of traverse surveys

Figure 4–24 (a–c) shows the results of traverse surveys at three locations. The same traverse routes were employed as in the winter months. During the morning, both the planned and unplanned areas recorded an air temperature at least 2 °C higher than the mixed, low socio–economic zone (Figure 4–24a). A distinct thermal pattern can be observed during the afternoon when the planned area exhibited a temperature approximately 2 °C higher than the other two sites (Figure 4–24b). This is possibly related to the contribution of anthropogenic heat from commercial, transportation networks and residential buildings. The same pattern can be found during the evening hours at the three survey sites. The planned location recorded higher temperatures than both the unplanned and mixed sites (Figure 4–24c).

The three locations also exhibit distinct thermal patterns in regards surface temperature, most notably during the morning and evening hours in the pre–monsoon (Figure 4–25, a–c). In the morning, the planned area recorded a temperature approximately 8 °C higher than the other two sites (unplanned and mixed), however this difference decreases during the afternoon. During the evening, the planned location average temperature (33.89 °C) was 3 °C greater than at the unplanned location (30.13 °C), but more than 5 °C higher than the mixed land use (28.46 °C).

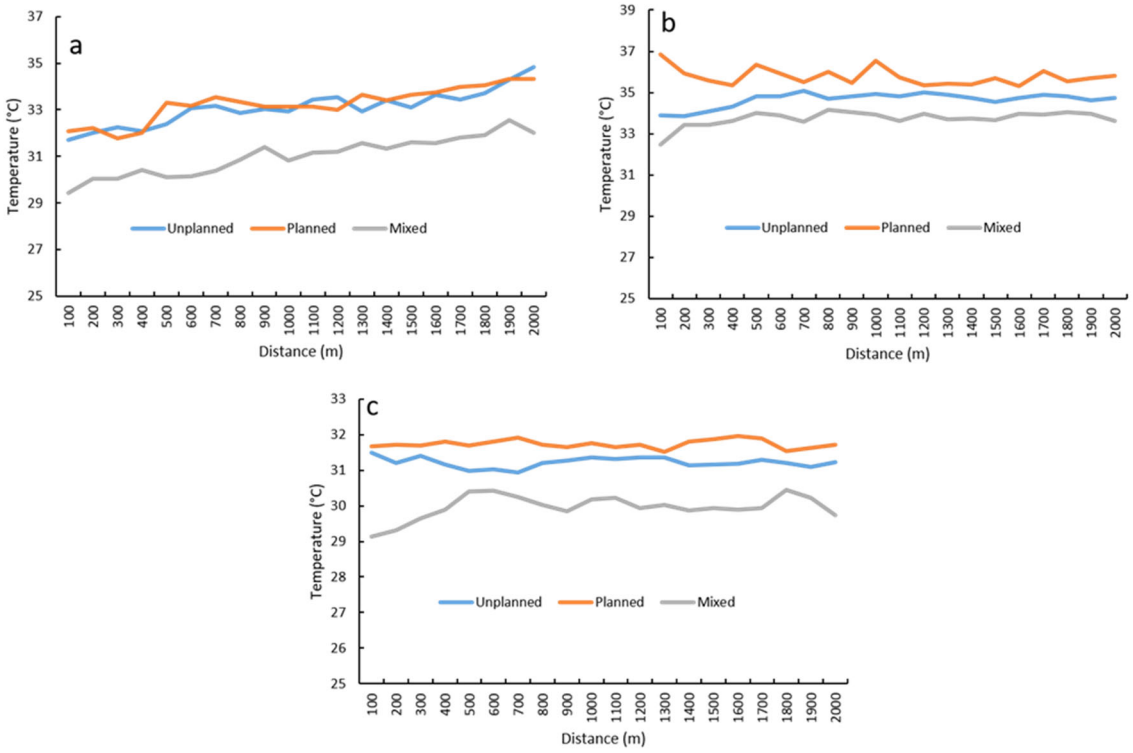

Figure 4–24 Variation of air temperature in three zones: (a) morning; (b) afternoon; and (c) evening

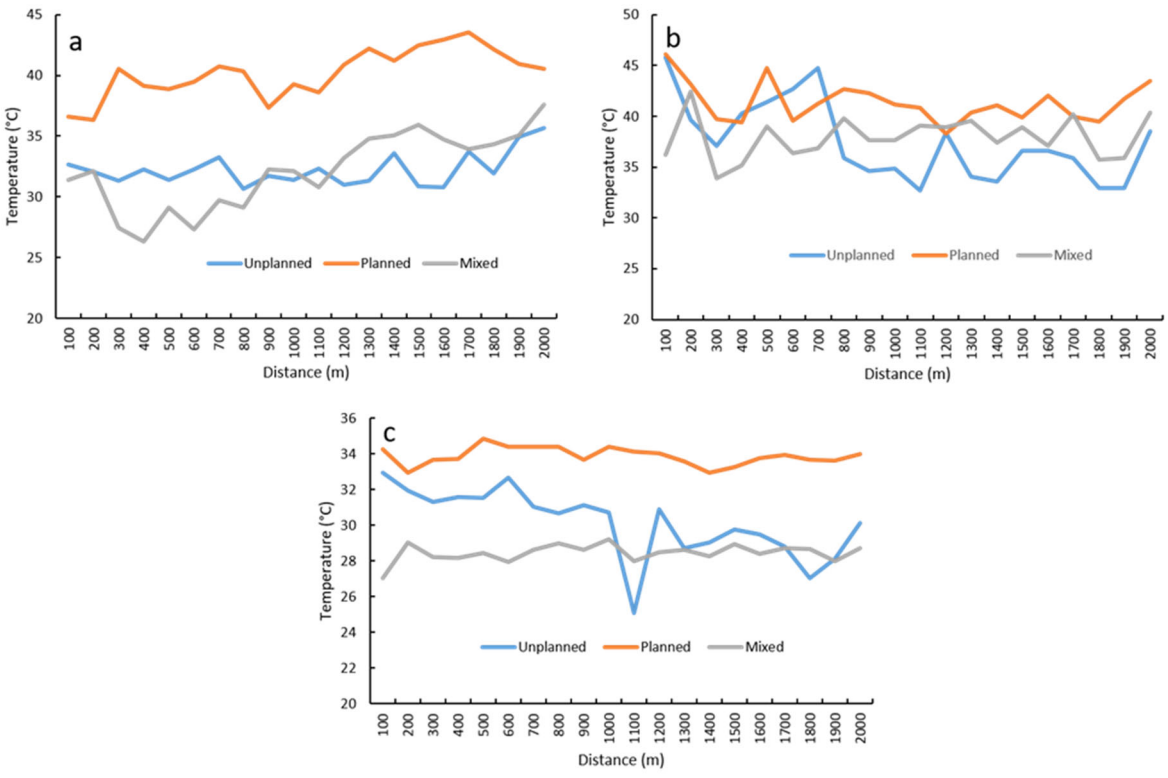

Figure 4–25 Variation of surface temperature in three zones: (a) morning; (b) afternoon; and (c) evening

Table 4–17 Spearman correlation coefficient between air/surface temperatures and relative humidity, wind speed and solar radiation in three traverse locations

	Air temperature (°C)						**Surface temperature** (°C)					
Unplanned	WS	Sig.	RH	Sig.	SR	Sig.	WS	Sig.	RH	Sig.	SR	Sig.
Morning	–.435	.055	–.730**	.000	.460*	.041	–.219	.353	–.050	.835	.293	.211
Afternoon	–.295	.207	–.298	.202	.359	.120	.583**	.007	–.334	.150	.485*	.030
Evening	.159	.504	–.211	.371	–	–	.247	.293	–.675**	.001	–	–
Planned												
Morning	–.006	.980	–.733**	.000	.185	.435	–.182	.442	–.583**	.007	.424	.062
Afternoon	.273	.244	–.044	.853	–.175	.462	.005	.982	.152	.523	–.078	.743
Evening	.080	.738	–.217	.359	–	–	–.527*	.017	–.476*	.034	–	–
Mixed												
Morning	–.142	.551	–.938**	.000	.561	.010	.262	.264	.794**	.000	–.785**	.000
Afternoon	–.648**	.002	–.439	.053	–.045	.002	–.154	.515	–.326	.160	.665**	.001
Evening	–.150	.528	–.247	.295	–	–	–.010	.967	–.186	.431	–	–

** Significant at the 0.01 level (2–tailed); * Significant at the 0.05 level (2–tailed)

A Spearman rank correlation test was undertaken on the recorded temperatures and other selected meteorological variables (Table 4–17). The results indicate that factors affecting the temperature vary between the zones and during the measurement times. At the planned site, relative humidity seems to have a substantial effect on air temperature during the morning and on the surface temperature in the afternoon, while wind speed and relative humidity appear to be more important in the evening hours. At the unplanned location, relative humidity appears to be important in the morning and evening, while wind speed plays a statistically significant role in influencing surface temperature during the afternoon.

A significant relationship was also noticed between relative humidity and air temperature in the morning hours, while both relative humidity and solar radiation have an influence on surface temperature during the morning/afternoon hours at the mixed land use site (Table 4–17).

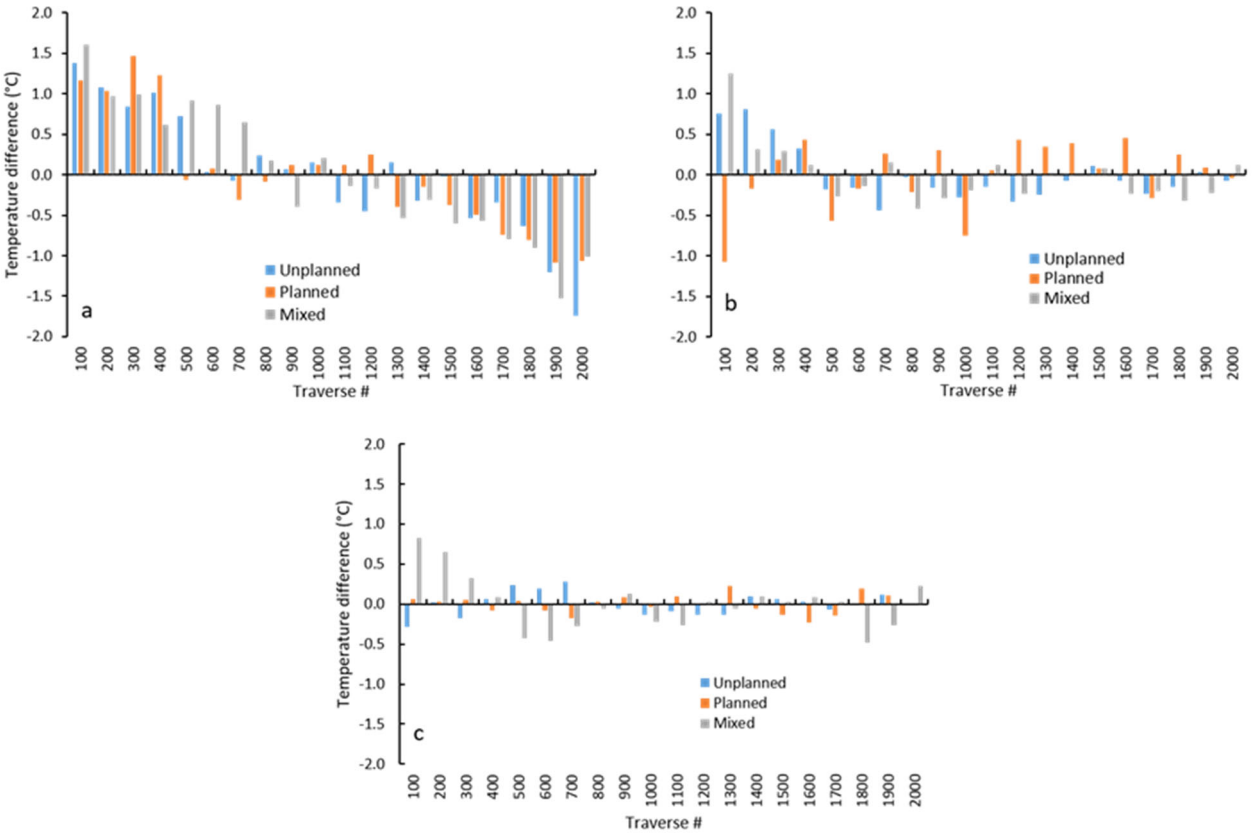

Figure 4–26 Spatial distribution of mean air temperature differences: (a) morning; (b) afternoon; (c) evening. Sites warmer than the mean transect value are positive and sites cooler than the mean are negative

The spatial distribution of the CUHI along the three transects was quantified by subtracting the mean value of each observation point (7–day average) from the corresponding transect mean.

The resulting air temperature plots are shown in Figure 4–26 (a–c). In general, 50% of the measured points along each transect recorded either a warmer or cooler temperature as indicated by the corresponding positive or negative values from the transect mean.

In terms of surface temperature, the deviation of temperature from the transect mean shows almost the same pattern (Figure 4–27, a–c). Both SUHI and urban cool island (UCI) exist along the 2 km surveyed transect. In the unplanned zone during the morning hours, 12 locations were warmer and 8 were cooler, while in the planned zone, 9 locations were warmer and 11 were cooler. The cooler sites clearly show a UCI effect. In the afternoon, both the planned and mixed zones recorded 12 warmer and 8 cooler sites, while the unplanned zone had 11 warmer sites as opposed to 9 cooler sites. During the evening, however, the number of SUHI and UCI sites between the transects was the same (9 and 11 for each) but the variation of SUHI appears higher in the unplanned zone compared with the other two, with a maximum SUHI value of 5 °C at traverse location 11 (Figure 4–27, a–c).

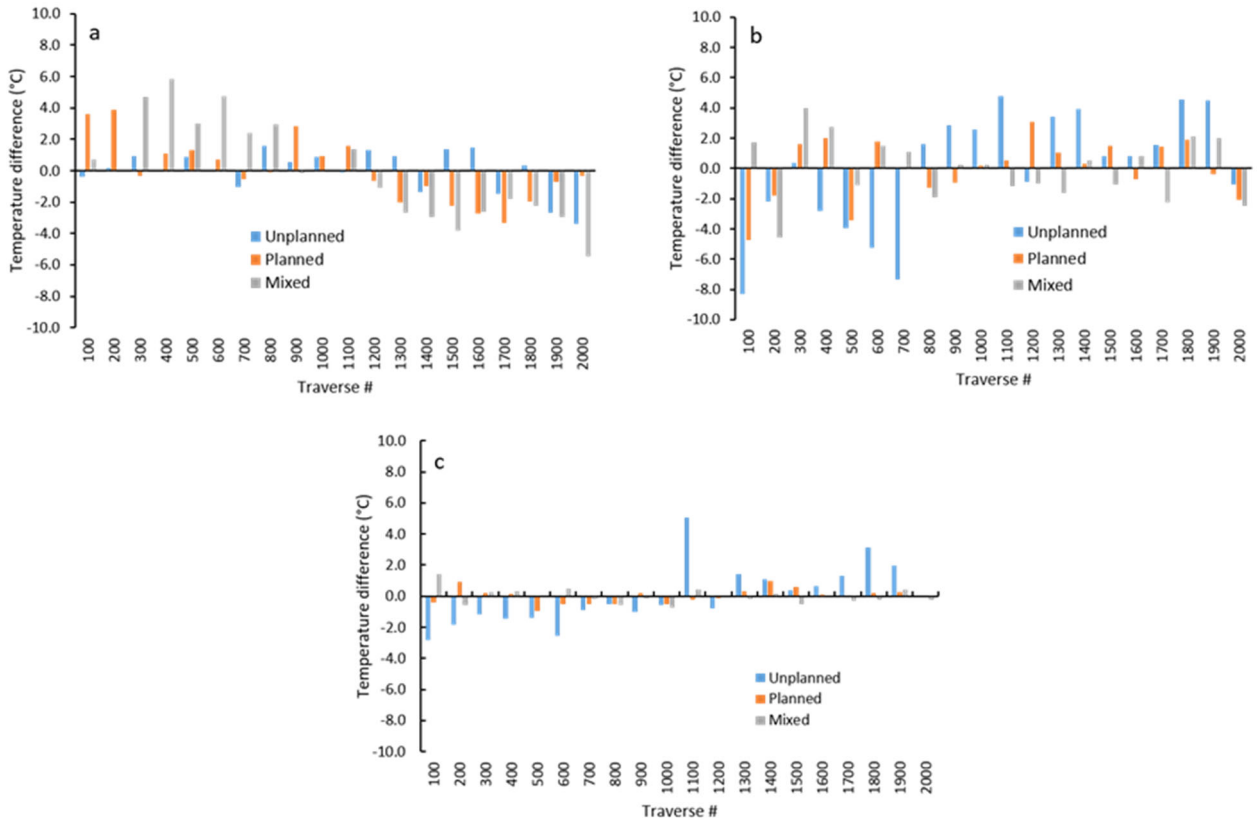

Figure 4–27 Spatial distribution of the mean surface temperature difference: (a) morning; (b) afternoon; (c) evening. Sites warmer than the mean transect value are positive and sites cooler than the mean are negative

4.11.2.3 Thermo–physical behaviour of urban features

Table 4–18 depicts the air and surface temperature of the three zones determined from 88 thermal infrared images and field surveys. The cooling rate of the air temperature between the planned and unplanned zones is almost the same (0.23 vs 0.25 °C/h), while the rate is higher in the mixed zone. The same pattern can be seen for the area average surface temperature (AAT), indicating the differential thermal gradients and cooling rates of the three traverse locations. An interesting feature is that relative humidity is higher in the planned and mixed zones when compared with the unplanned location (Table 4–18). The average solar radiation recorded during the pre–monsoon months in the three zones was 450.57 W/m^2 (planned), 340 W/m^2 (unplanned) and 162 W/m^2 (mixed). This indicates a possible reason for the higher air and surface temperatures and lower cooling rate recorded in the planned zone compared to the values recorded in the other two zones.

Table 4–18 Average air temperature (AT), surface temperature (ST) and relative humidity (RH) of three traverse routes during the morning (M) and evening (E) in the pre–monsoon. Temperature values are in °C and relative humidity is in percentage (%). Area average temperature (AAT) is taken from selected areas on the thermal images and are the average of 88 infrared photographs from 20 sites of three zones. CR is the cooling rate per hour in °C

Traverse site	AT_M	AT_E	ΔAT	CR/h	AAT_M	AAT_E	ΔAAT	CR/h	RH_M	RH_E
Planned	34.68	32.20	2.48	0.23	35.18	31.18	4.0	0.35	49.62	61.34
Unplanned	33.41	30.43	2.95	0.25	33.94	29.4	4.54	0.39	41.42	55.41
Mixed	25.8	27.89	–2.0	–0.18	23.43	24.81	–1.38	–0.11	63.54	65.34

An assessment of the thermographic analysis, along with details of the colour coating and construction materials of different urban features, is shown in Tables 4–19 to 4–21. It is important to note that the same objects were used in all seasons to aid in a comparative evaluation. The cooling rate of the top five features are shown in bold face.

In the planned zone, the top feature was identified as a water tank (2.10 CR/h) constructed of cast iron, followed by a light–yellow coloured iron water tank (1.49 CR/h), an iron fence (1.37 CR/h), a white coloured speedboat constructed of steel (1.15 CR/h), and tree foliage (1.10 CR/h) (Table 4–19).

In the unplanned zone, the cooling rate is highest for building walls constructed of grey cement (1.62 CR/h). Next is rooftop tin with a silver colouration (1.38 CR/h), followed by a grey glass window (1.30 CR/h), a marble building wall (1.29 CR/h) and a steel, silver–coated electricity pole (1.21 CR/h) (Table 4–20). Interestingly, a few objects had negative cooling rates. These included a plastic neon sign (–0.35 CR/h) and vegetation canopy (–0.84 CR/h). Previous work showed that vegetated surfaces tend to reduce heat in urban areas, therefore, the vegetation canopy results are anomalous and require further investigation.

The thermo–physical behaviour of urban objects in the mixed zone was very different to those seen in the other two zones. The majority of objects showed both negative and low cooling rates (Table 4–21). The top–ranked cooling rate objects were a building wall with moss (0.34 CR/h), a grey concrete street (0.32 CR/h), a plastic billboard with green colour coating (0.22 CR/h), and a grey plaster building wall (0.10 CR/h). A possible explanation for the negative cooling rates recorded in this area may be the proximity to a large waterbody such as the Buriganga River. Differential thermal conductivity may also have a significant effect on the cooling potential of features located in this zone.

4.11.2.4 Thermal response of rooftop with/without gardens

The positive effect of a rooftop garden in reducing heat was observed during the winter season. Surprisingly, this effect appeared to diminish in the pre–monsoon months (Figure 4–28). The rooftop with a garden recorded a higher surface temperature than those without a garden. Specifically, a rooftop with garden had recorded a higher temperature twice during the diurnal cycle; from 0400 to 1900; and again at 0000. On average, surface temperature was 1.46 °C higher than rooftop without garden. This is not what would generally be expected. It is likely that the widespread use of air conditioners in surrounding buildings may be a factor in this elevated temperature observation. As noted previously, the UHI is most pronounced at night, and so to increase the comfort levels within homes, residents commonly activate their air conditioners. This adds artificial heat to the immediate environment, potentially increasing the temperature of the rooftop garden.

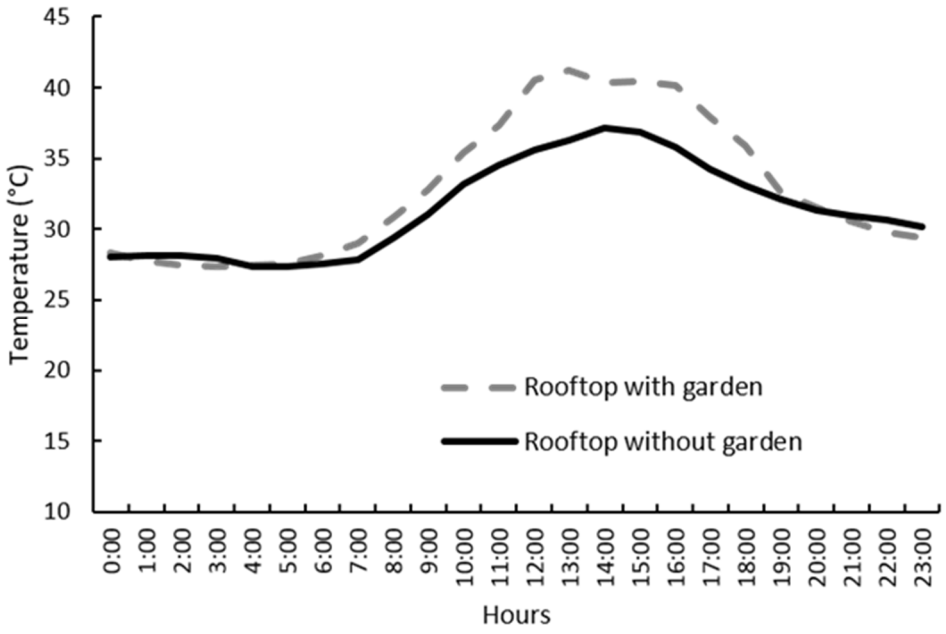

Figure 4–28 Diurnal variation of surface temperature of rooftop with/without garden

Table 4–19 Planned zone – object surface temperature (°C) and cooling rate (°C/h)

Feature Type	Make	Colour	Early T (°C)	Late T (°C)	ΔT (°C)	CR/hr
Tree branch	–	–	32.0	32.3	-0.3	-0.02
Bld. wall	Brick	Green	31.1	32.5	-1.4	-0.11
Billboard	Plastic	White	32.9	33.3	-0.4	-0.03
Bld. wall	Glass	Blue	38.6	32.3	6.3	0.54
Bld. window	Glass	Transparent	33.6	32.4	1.2	0.10
Brick wall	Tile	Orange	34.9	32.2	2.7	0.23
Tree trunk	–	–	32.5	33.1	-0.6	-0.05
Bld. wall	Glass	Grey	37.2	31	6.2	0.48
Bld. pillar	Concrete	Red	35.1	29.9	5.2	0.40
Bld. wall	Concrete	Off-white	34.1	31.1	3.0	0.23
Tree foliage	–	–	33.9	30.1	3.8	0.30
Water tank	**Iron**	**Light yellow**	**44.3**	**27.1**	**17.2**	**1.49**
Tank pillar	Iron	Light yellow	42.2	29.8	12.4	1.07
Tree foliage	–	–	**36.7**	**23.9**	**12.8**	**1.10**
Tank body	**Iron**	**Cast skin**	**50.5**	**26.2**	**24.3**	**2.10**
Mosque	Brick	Red	33.4	29.9	3.5	0.30
Stair	Tile	Off-white	38.0	31.0	7.0	0.60
Grass	–	–	34.0	29.2	4.8	0.42
Tree trunk	–	–	32.1	30.9	1.2	0.10
Shaded walkway	Asphalt	Black	32.8	31.3	1.5	0.13
Waterbody	–	–	32.4	31.2	1.2	0.10
Rooftop	Tin	Mirage	43.5	31.1	12.4	1.08
Health veg.	–	–	38.5	28.9	9.6	0.83
Unhealthy veg.	–	–	33.6	29.4	4.2	0.36
Shaded street	Asphalt	Black	32.1	33.4	-1.3	-0.11
Shaded walkway	Tile	Yellow	31.5	35.5	-4.0	-0.35
Shaded walkway	Tile	Red	30.7	32.3	-1.6	-0.14
Electric pole	Steel	Silver	32.1	32.8	-0.7	-0.06
Unshaded street	Asphalt	Black	38.0	34.7	3.3	0.29
Painted wall	Concrete	Yellow	34.2	31.6	2.6	0.23
Tree foliage	–	–	33.8	30.7	3.1	0.27
Window	Glass	Grey	36.7	30.3	6.4	0.56
Tree trunk	–	–	34.7	31.3	3.4	0.30
Bld. wall	Brick	Brown	34.0	30.6	3.4	0.30
Building	Glass	Green	36.4	32.4	4.0	0.35
Bld. side wall	Brick	Plaster	34.4	32.0	2.4	0.21
Bld. front wall	Glass	Transparent	33.3	32.3	1.0	0.09
Waterbody	–	–	33.0	29.2	3.8	0.34
Rubbish	–	–	36.9	30.8	6.1	0.54
Speedboat	**Steel**	**White**	**49.2**	**36.3**	**12.9**	**1.15**
Shrub	–	–	31.3	30.8	0.5	0.04
Billboard	Plastic	Navy blue	45.0	34.5	10.5	0.98
Bld. wall	Plaster	Mirage	38.7	32.5	6.2	0.58
Bld. wall	Glass	Blue	40.0	32.1	7.9	0.74
Building	Glass	Green	39.1	28.8	10.3	0.96
Rooftop	Tile	Silver	37.0	32.1	4.9	0.46
Fence	**Iron**	–	**47.3**	**32.6**	**14.7**	**1.37**
Passenger shade	Iron	White	36.0	32.5	3.5	0.33
Wall	Brick	Red	37.9	31.7	6.2	0.58
Bld. wall	Concrete	Brown	40.8	31.3	9.5	0.89
Bld. wall	Concrete	Yellow	38.8	32.3	6.5	0.61
Bld. front wall	Concrete	Grey	36.4	31.8	4.6	0.43

Table 4–20 Unplanned zone – object surface temperature (°C) and cooling rate (°C/h)

Feature Type	Make	Colour	Early T (°C)	Late T (°C)	ΔT (°C)	CR/hr
Billboard	Plastic	Red	39.3	32.3	7.5	0.63
Window	Glass	Hue	42.2	26.6	15.6	1.32
Balcony	Plaster	–	38.4	29.7	8.7	0.74
Raw brick	–	Red	34.9	28.4	6.5	0.55
Bld. wall	**Marble**	**Ash**	**43.9**	**28.7**	**15.2**	**1.29**
Electric pole	**Steel**	**Silver**	**41.4**	**27.1**	**14.3**	**1.21**
Window	**Glass**	**Grey**	**39.6**	**24.3**	**15.3**	**1.30**
Shaded fence	Concrete	White	30.7	31.1	-0.4	-0.03
Dense veg canopy	–	–	17.7	27.6	-9.9	-0.84
Painted fence	Brick	Yellow	29.0	28.2	0.8	0.07
Dense vegetation	–	–	17.6	21.9	-4.3	-0.36
Vegetated wall	Brick	–	29.9	29.1	0.8	0.07
Bld. wall	**Cement**	**Grey**	**46.4**	**27.4**	**19.0**	**1.62**
Bld. entrance	Concrete	White	30.9	30.5	0.4	0.03
Old fence	Brick	Red	33.2	32.8	0.4	0.03
Dome	Brick	Yellow	31.6	30.3	1.3	0.11
Elevated fence	Plaster	White	32.0	30.1	1.9	0.16
Tree trunk	–	–	31.5	30.0	1.5	0.13
Cornice	Iron	Yellow	30.9	29.8	1.1	0.09
Building	Tile	Mixed	33.3	29.8	3.5	0.29
Window	Glass	Black	31.5	30.0	1.5	0.13
Neon sign	Plastic	Mixed	32.8	37.0	-4.2	-0.35
Bld. entrance	Brick	Black	34.9	28.4	6.5	0.55
Rooftop	**Tin**	**Silver**	**47.7**	**31.4**	**16.3**	**1.38**
Bld. wall	Plaster	Brown	33.7	28.5	5.2	0.44
Bld. wall	Plaster	White	30.8	29.6	1.2	0.10
Cornice	Brick	Moss	43.2	30.2	13.0	1.10
Plastic wall	Plastic	Blue	42.3	28.8	13.5	1.14
Rooftop	Tin	Silver	37.9	29.9	8.0	0.68
Cornice	Iron	–	32.1	28.9	3.2	0.28
Degraded fence	Brick	Yellow	32.2	29.0	3.2	0.28
Rooftop	Concrete	No paint	32.2	28.2	4.0	0.34
Transmission pole	Steel	Silver	42.8	41.2	1.6	0.19
Billboard	Steel	Silver	36.1	28.2	7.9	0.68
Bld. wall	Brick	Red	33.8	29.1	4.7	0.40
Window	Iron	Mirage	33.0	28.3	4.7	0.41
Window	Glass	Blue	34.0	25.7	8.3	0.72
Degraded bld.	Brick	Mirage	39.6	29.0	10.6	0.92

Table 4–21 Mixed zone – object surface temperature (°C) and cooling rate (°C/h)

Feature Type	Make	Colour	Early T (°C)	Late T (°C)	ΔT (°C)	CR/hr
Bridge	Concrete	–	23.5	31.6	-8.1	-0.59
Waterbody	–	Turbid	21.8	27.1	-5.3	-0.38
Grass	–	–	21.4	28.9	-7.5	-0.54
Electric pole	Steel	Silver	24.2	29.8	-5.6	-0.41
Rooftop	Tin	Silver	24.9	29.0	-4.1	-0.30
Bare soil	–	Brown	25.8	28.1	-2.3	-0.17
Bld. wall	Raw brick	Red	21.1	22.1	-1.0	-0.09
Bld. wall	Brick	Brown	23.0	23.4	-0.4	-0.04
Street	Asphalt	Black	24.1	25.0	-0.9	-0.08
Roof with garden	Concrete	–	23.2	24.4	-1.2	-0.11
House wall	Tin	Silver	23.0	25.1	-2.1	-0.19
Balcony	Iron	Brown	22.7	24.4	-1.7	-0.15
Shop shutter	Tin	Silver	22.3	24.7	-2.4	-0.21
Billboard	Plastic	Red	22.3	34.3	-12.0	-1.06
Tree foliage	–	–	22.5	24.0	-1.5	-0.13
Window	Glass	Green	23.0	22.3	0.7	0.06
Bld. wall	Brick	Yellow	24.1	23.9	0.2	0.02
Shop shutter	Tin	Silver	26.0	30.6	-4.6	-0.41
Bld. wall	Raw brick	Red	23.1	29.4	-6.3	-0.56
Bld. wall	Tile	White	21.3	28.6	-7.3	-0.65
Shop	Tin	Grey	21.7	24.0	-2.3	-0.20
Window	Glass	Blue	23.0	23.9	-0.9	-0.08
Bld. front wall	Brick	Yellow	23.5	23.6	-0.1	-0.01
Open balcony	Plaster	Off-white	21.5	24.1	-2.6	-0.23
Shutter	Tin	Silver	22.5	24.3	-1.8	-0.16
Signboard	Plastic	White	22.0	24.9	-2.9	-0.26
Tree trunk	–	–	21.6	24.8	-3.2	-0.28
Bld. pillar	Raw brick	Red	21.8	24.2	-2.4	-0.21
Bld. wall	Brick	Yellow	23.3	35.8	-12.5	-1.10
Bld. front wall	Raw brick	Red	23.9	24.6	-0.7	-0.06
Street	Asphalt	Black	22.9	24.4	-1.5	-0.13
Electric pole	Steel	Silver	24.8	25.2	-0.4	-0.04
Bld. wall	Brick	Blue	22.4	24.5	-2.1	-0.18
Window	Glass	Black	23.2	25.0	-1.8	-0.16
Rooftop	Raw brick	Red	20.0	21.3	0.7	0.06
Billboard	**Plastic**	**Green**	**26.3**	**23.8**	**2.5**	**0.22**
Bld. front wall	Plaster	Grey	24.4	23.7	0.7	0.06
Coconut T. foliage	–	–	22.7	23.6	-0.9	-0.08
Rooftop wall	Raw brick	Red	23.3	23.6	-0.3	-0.03
Tree trunk	–	–	22.6	25.3	-2.7	-0.24
Bld. wall	Brick	Orange	23.6	23.8	-0.2	-0.02
Bld. side wall	Cement	Grey	23.1	24.8	-1.7	-0.15
Bld. wall	**Plaster**	**Grey**	**25.4**	**24.3**	**1.1**	**0.10**
Rooftop	Concrete	Grey	25.9	23.3	2.6	0.28
Billboard	Plastic	Red	24.9	25.4	-0.5	-0.05
Road	Concrete	Ash	24.5	23.9	0.6	0.06
Bld. wall	Raw brick	Red	25.1	24.3	0.8	0.09
Window	Glass	Transparent	23.7	24.1	-0.4	-0.04
Bld. wall	Brick	Purple	24.2	24.0	0.2	0.02
Bld. wall	Plaster	Grey	25.5	23.5	2.0	0.21
Tree	–	–	24.5	23.8	0.7	0.07
Water tank	**Plastic**	**Black**	**25.0**	**25.0**	**0.0**	**0.00**
Bld. wall	**Plaster**	**Moss**	**27.2**	**24.0**	**3.2**	**0.34**
Street	**Concrete**	**Grey**	**27.9**	**24.9**	**3.0**	**0.32**

To examine how the vertical temperature varied on the rooftop areas with or without a garden, measurements of air temperature were taken at three different heights (Figure 4–29). The results demonstrate that at a height of 1 m, the overall air temperature is actually higher on the roof with garden (Figure 4–29a). At 2 m, the positive effects of the garden can be observed from 1000–2300, with the temperature of the rooftop, on average, being 3.2 °C lower than the rooftop without garden (Figure 4–29b). At a height of 3 m, the positive effect of the rooftop garden over the diurnal cycle can be seen (Figure 4–29c). This shows that the rooftop with garden has an average temperature 2.8 °C lower than the rooftop without garden. Note that at 1 m height data for rooftop garden is missing from 0000 to 0800.

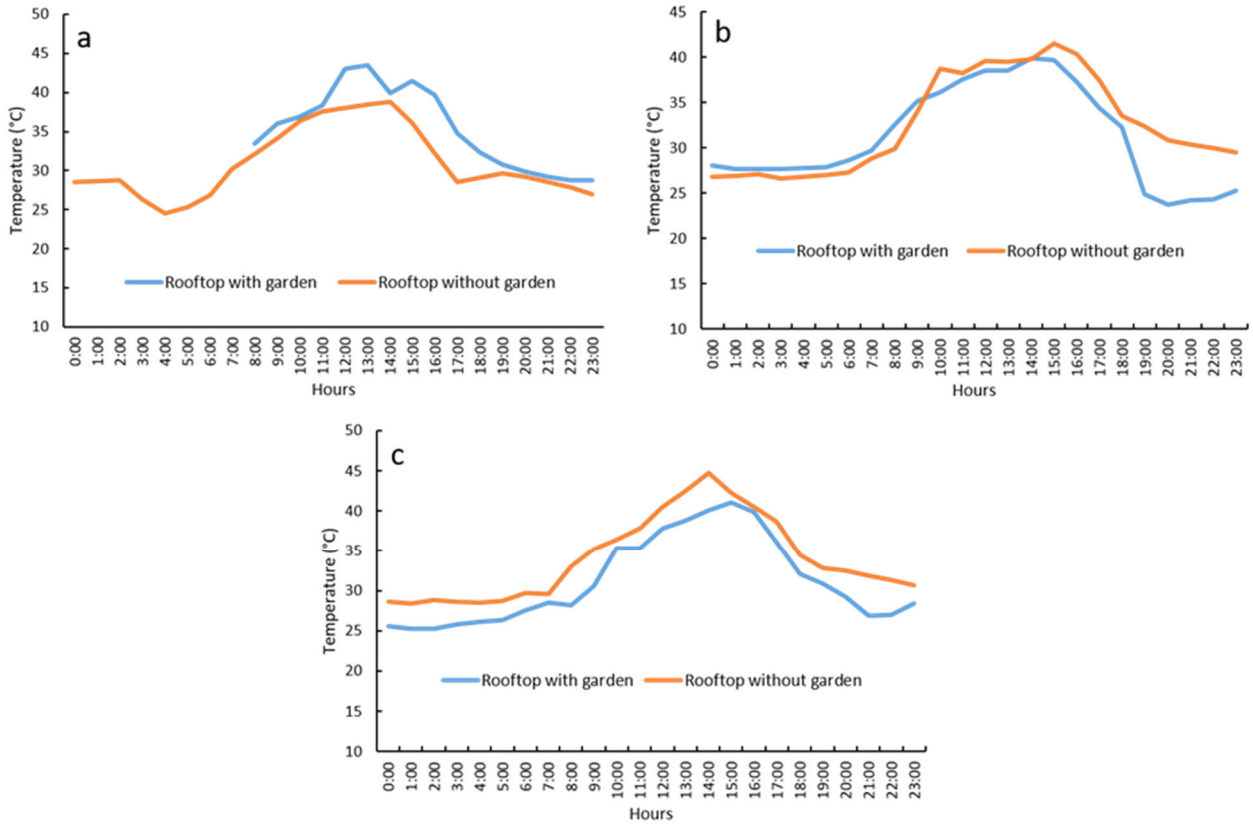

Figure 4–29 Diurnal response of the rooftop and non–rooftop garden on air temperature at selected heights: (a) 1 m; (b) 2 m; and (c) 3 m

4.11.2.5 Response of dominant rooftop plants

An examination of the potential of dominant rooftop vegetation in reducing temperature indicates that *Combretum indicum* is the most effective plant in this regard. This is followed by *Maltes* and *Pisidum red* (Figure 4–30).

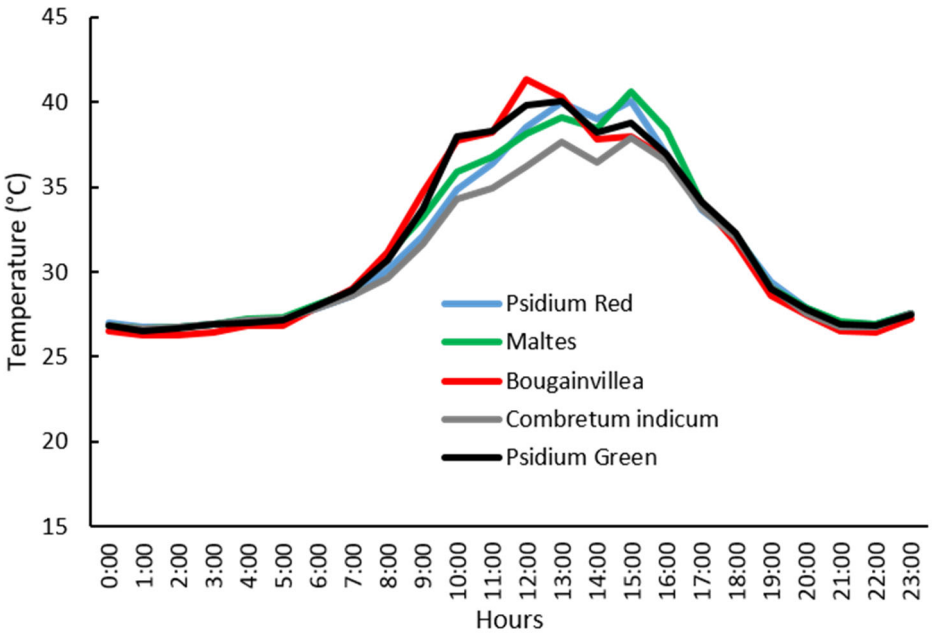

Figure 4–30 Thermal response of dominant rooftop plants

It should be noted that the thermal response of *Citrus Lemon,* which had been measured in winter, could not be measured in the pre–monsoon as it had died. *Combretum indicum* species appeared to be effective from 1000 to 1600 when solar radiation is at its peak. This plant appears to have an average diurnal cycle temperature 1 °C lower than the other plant types examined. As *Combretum indicum* also had an effective thermal response during the winter period, there is potential for this plant to be effective in mitigating rising temperatures.

4.11.2.6 Cooling potential of open space plants

The cooling potential of open space plants (with the exception of *Loha kat* and mango species), was examined during the pre–monsoon. The results indicate that *Earleaf acacia* appears to have the highest cooling potential while *Mahogony* has the lowest potential (Figure 4–31). The average wind speed and solar radiation recorded on the four measurement days was 1.7 m/s and 160.7 W/m^2, respectively (Appendix VII). Using 32 °C as a threshold value (red horizontal line in Figure 4–31), the analysis indicates that *Earleaf acacia* has the greatest potential, followed by *Teak* as indicated by the box–and–whisker plot.

To understand the thermal behaviour and response of plants, the average temperature of each plant was selected and the entire diurnal cycle categorised into morning–early afternoon (0900–1300) and afternoon–early evening (0200–0600), for each plant (Table 4–22). The results show that *Earleaf acacia* and *Teak* have the lowest temperature among the different vegetation types, both in the morning and in the afternoon. In contrast, *Coconut* appears to have the lowest potential in regards reducing the ambient temperature.

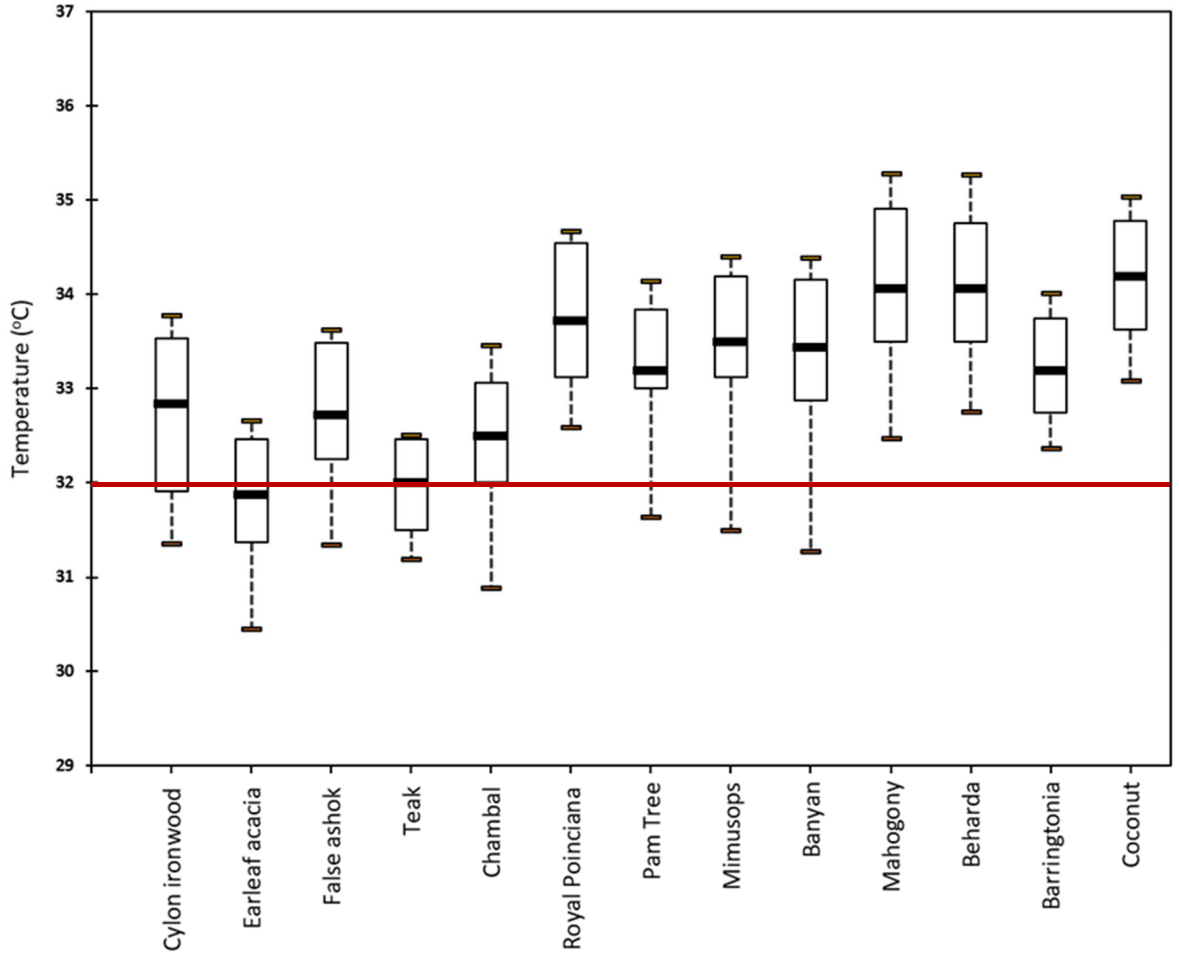

Figure 4–31 Box–and–Whisker plot, showing the thermal response of the open space plants

Table 4–22 Average temperature (°C) of open space plants

Plants	Morning (9:00–13:00)	Afternoon (14:00–18:00)
Cylon ironwood	31.95	33.19
Earleaf acacia	31.25	32.18
False ashok	31.79	33.28
Teak	31.38	32.18
Chambal	31.74	32.78
Royal Poinciana	33.28	34.01
Palm	32.55	33.48
Mimusops	32.60	33.80
Banyan	32.25	33.90
Mahogany	33.88	34.13
Beharda	33.38	34.30
Loha kat	–	–
Barringtonia	32.85	33.50
Coconut	34.03	34.18
Mango	–	–

4.11.2.7 Temperature variation of urban waterbodies

The striking thermal response of the urban water features (pond and river) over the diurnal cycle in the pre–monsoon can be seen in Figure 4–32. This indicates that the pond water temperature was consistently greater than the river temperature over the 24–hour period. This may be related to factors such as location and size, turbidity, and velocity of water flow. Another feature evident in the thermal response comparison between these two waterbodies is that the pond temperature tends to fluctuate more than the river, with a recorded temperature > 2 °C higher than the river temperature between 1600 and 2200. Due to a malfunctioning sensor, no data was recorded for May, so the values for March and April of the pre–monsoon period were used in the thermal response analysis of urban water features.

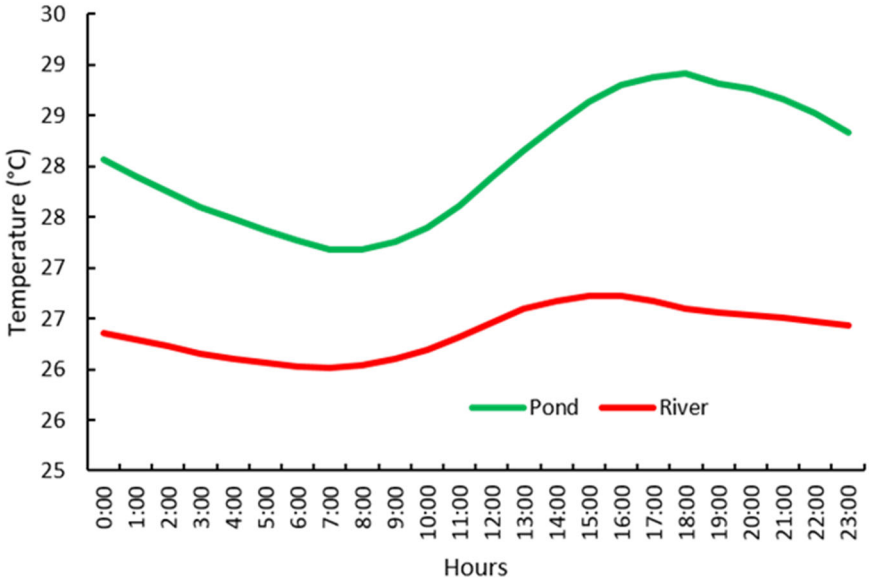

Figure 4–32 Variation in water temperature of a river and a pond

4.11.2.8 Thermal response of a green hanging wall

The diurnal surface temperature variation of the soil, wall and substrate features making up a green hanging wall, is shown in Figure 4–33. This indicates that the substrate temperature was much lower than the other two features. The thermal pattern of the substrate was consistent across the period of measurement (0900–1700), and did not vary much compared with the wall temperature, an indicator of the efficacy of the vegetation covered vertical wall. Conversely, the wall temperature was higher than the soil temperature over the diurnal cycle. In theory, the substrate system should record a lower temperature than the wall but this was not the case during the pre–monsoon months. This is possibly related to the materials used in construction, as well as surrounding environmental characteristics.

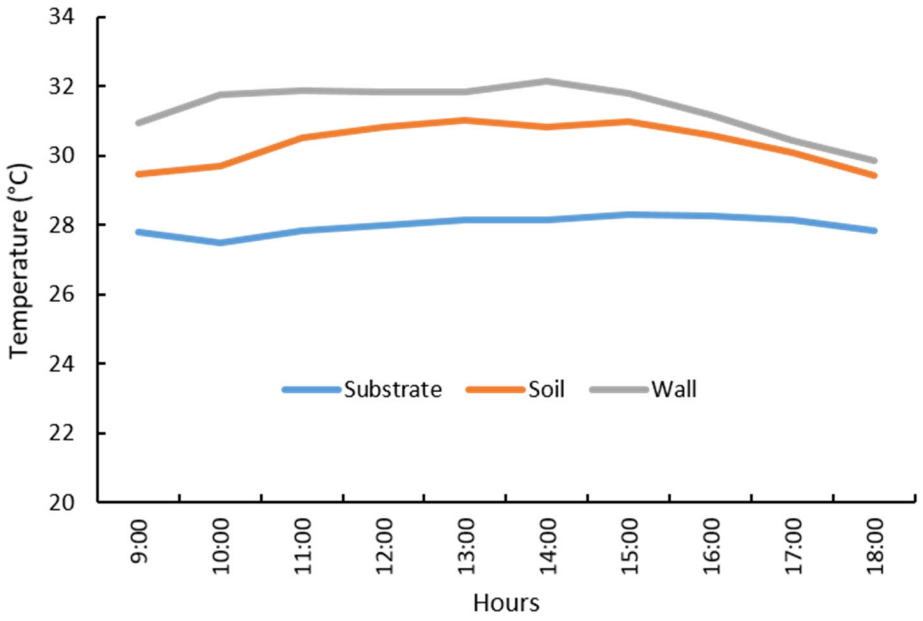

Figure 4–33 Average soil, wall and the substrate temperatures of a green hanging wall

Details of the ambient air temperature, recorded at varying distances from the substrate, are shown in Table 4–23. This indicates that, overall, the air temperature was relatively cooler at a distance of 3 m from the substrate during the 0900 to 1800 time period when compared with other distances. The deviation of air temperature from the mean, obtained at every defined distance from the substrate, revealed that the ambient temperature was 0.9 °C higher between 1000 and 1500, reflecting the warmer time of the day. In contrast the early morning (0900), and late afternoon (1600–1800) periods exhibited cooler temperatures. Since UHI tends to develop in the late afternoon and continues overnight, a vertical greening system could be an effective measure in counteracting this warming periodicity.

Table 4–23 Ambient temperature of a green hanging wall at different distances from the substrate

	Temperature (°C)				
Hours	**1 m**	**2 m**	**3 m**	**4 m**	**5 m**
9.00	30.38	31.21	29.42	30.71	30.92
10.00	31.48	32.88	30.60	32.25	32.85
11.00	32.10	33.77	31.81	33.42	34.31
12.00	32.27	33.58	31.88	33.21	33.79
13.00	31.96	33.52	31.71	33.10	33.48
14.00	31.77	33.04	30.71	32.31	32.40
15.00	31.75	32.67	30.29	32.13	32.06
16.00	31.27	31.73	29.77	31.46	31.13
17.00	30.40	30.56	29.02	30.35	29.92
18.00	29.40	29.58	28.33	29.40	29.00

4.11.2.9 Cooling potential of green and blue spaces

The recorded temperature of different locations and distances from the centre of a park during the pre–monsoon months are shown in Figure 4–34. Depending on the measurement direction (east, west, south or north), a large variability in temperature can be observed. In a westerly direction, locations nearer to the park centre tend to have a lower ambient temperature during the morning, however this effect tends to reduce with distance and time of day. The same phenomenon generally holds true for the east, though at a distance of 862 m the results seem to differ significantly. Measurements taken in a northerly direction appear to indicate a minor heat mitigation effect. To the south, it is difficult to determine any effects in reducing temperature. Due to various reasons, including equipment malfunction, some of the sensors did not record consistent observations during the pre–monsoon period. Nevertheless, the effectiveness of greenspace to turn down the heat is inconclusive.

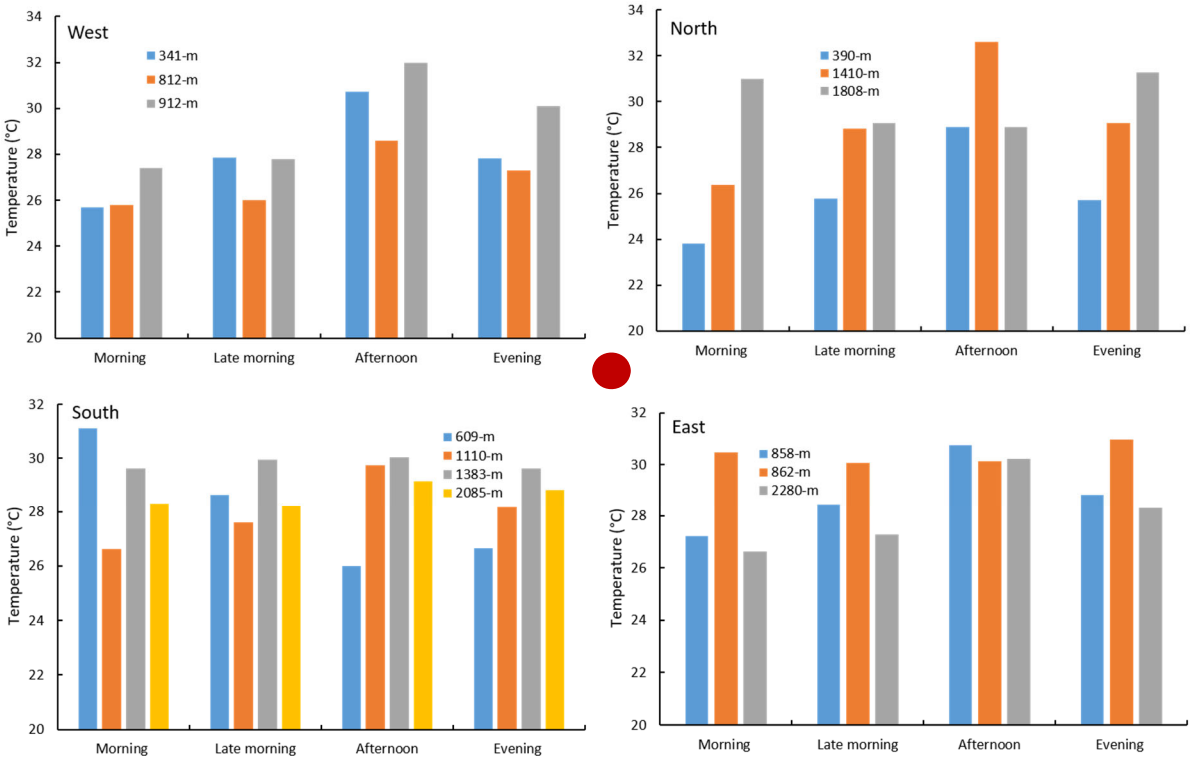

Figure 4–34 Cooling effect of a large greenspace at various distances and directions from a central point. The dark red circle denotes the centre of the park relative to the measuring points

An analysis similar to that carried out for the greenspace was conducted to examine the effect of a blue space on the surrounding environment. The results are presented in Figure 4–35. This shows the response of waterbodies in reducing temperature and is again largely inconclusive. Proximity to the lake appeared to have some kind of effect in three directions from the lake centre (east, west and south), however the effect is minimal to the north direction. The results also indicate that the cooling potential of the lake diminishes considerably with increasing

distance during the four time periods, i.e. the higher the distance from the lake, the greater the temperature. Apart from the differential thermal conductivity of waterbody, both physical (e.g. albedo) and anthropogenic (e.g. building density) factors may have a significant role to play in determining the cooling potential of the lake.

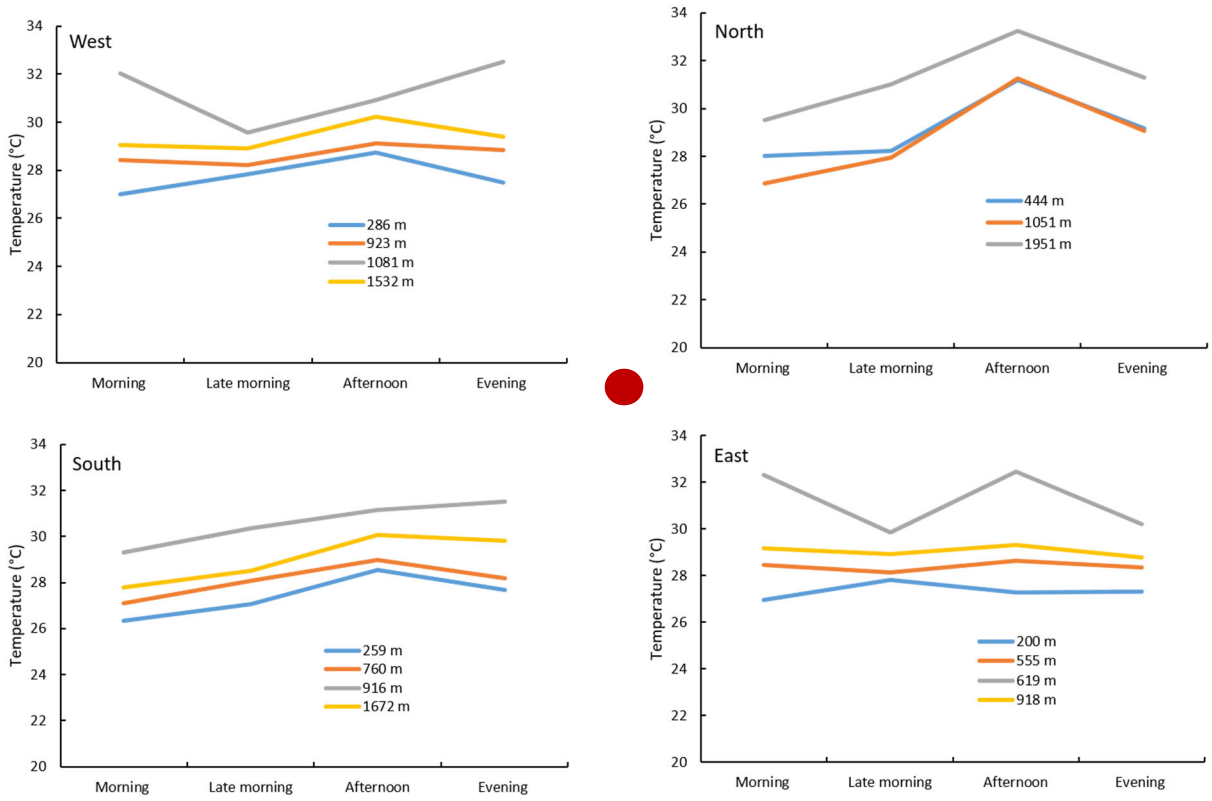

Figure 4–35 Cooling effect of a lake at various distances and directions. The dark red circle denotes the centre of the lake relative to the measuring points

4.11.3 Monsoon season

4.11.3.1 Urban–rural gradient of surface and air temperatures

The magnitude of both SUHI and CLHI is weakened during the monsoon period, partly due to the arrival of the southwest monsoon, which delivers substantial amounts of rain to the Bangladesh territory. Figure 4–36 shows the surface and ambient air temperatures at the urban and rural locations. The entire diurnal cycle of surface temperature during monsoon months shows that the urban location has a consistently higher temperature relative to the rural site (Figure 4–36a). On average, it was 0.70 °C higher but lower than during the pre–monsoon. Little difference in air temperature readings can be observed between the two sites, particularly between 1200 and 1500. In regards the average air temperature across the diurnal cycle, the urban areas exhibited a temperature that was 0.53 °C higher than the rural (Figure 4–36b).

The SUHI, which develops in the DMA tends to intensify from the late afternoon (from approximately 1600) and continues until morning (1000). This is a phenomenon also found in other big cities. The greatest effect can be seen between 1900 and 2100 hours, when the urban temperature is (on average), 0.9 °C higher than the rural temperature (Table 4–24). Even though the urban air temperature is higher across the diurnal cycle in the monsoon, it can be seen that between 1400–1500 hours, the air temperature is marginally lower at the rural site.

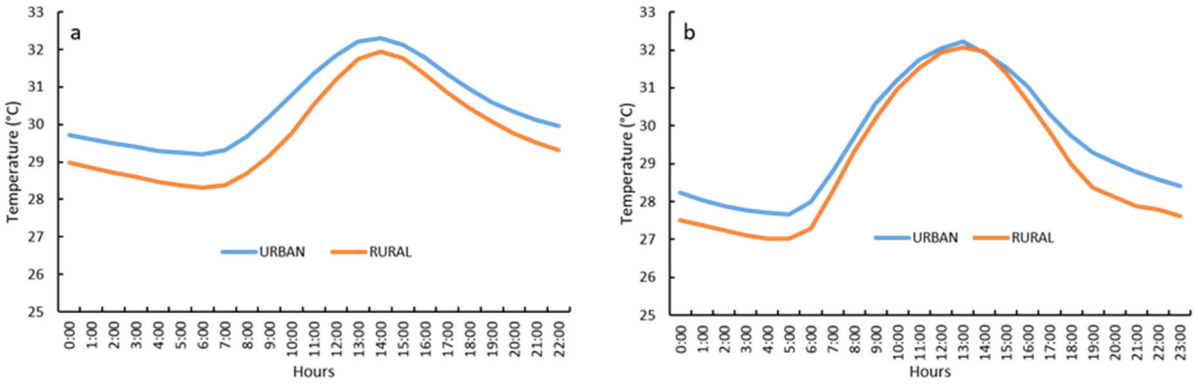

Figure 4–36 Diurnal variation of temperature during monsoon months: (a) surface; (b) air

Table 4–24 Differences in air and surface temperature during the monsoon season

Hours	Air Temperature (°C)			Surface Temperature (°C)		
	Urban	Rural	SUHI	Urban	Rural	CLHI
0:00	29.71	28.98	0.73	28.24	27.50	0.74
1:00	29.61	28.85	0.76	28.04	27.37	0.67
2:00	29.49	28.72	0.77	27.88	27.23	0.65
3:00	29.39	28.60	0.80	27.77	27.11	0.66
4:00	29.30	28.47	0.83	27.70	27.03	0.68
5:00	29.24	28.39	0.85	27.67	27.01	0.66
6:00	29.20	28.31	0.88	27.99	27.29	0.70
7:00	29.31	28.38	0.93	28.78	28.25	0.53
8:00	29.68	28.70	0.98	29.69	29.31	0.38
9:00	30.20	29.15	1.06	30.59	30.20	0.39
10:00	30.79	29.76	1.03	31.20	30.96	0.25
11:00	31.37	30.54	0.83	31.73	31.51	0.22
12:00	31.83	31.19	0.63	32.04	31.93	0.11
13:00	32.21	31.73	0.47	32.22	32.06	0.16
14:00	32.31	31.95	0.35	31.91	31.97	–0.05
15:00	32.11	31.76	0.35	31.54	31.39	0.15
16:00	31.80	31.34	0.46	31.04	30.63	0.41
17:00	31.34	30.85	0.49	30.31	29.84	0.47
18:00	30.93	30.43	0.50	29.72	28.99	0.73
19:00	30.59	30.06	0.53	29.28	28.37	0.92
20:00	30.33	29.75	0.57	29.03	28.12	0.91
21:00	30.13	29.51	0.61	28.79	27.87	0.91
22:00	29.95	29.31	0.64	28.57	27.79	0.79
23:00	29.81	29.13	0.68	28.40	27.62	0.78

The distribution of solar radiation at the two sites, over the diurnal cycle, clearly indicates that rural areas receive more solar radiation than the urban areas (Figure 4–37). The average urban radiation load was 142.2 W/m^2, while for the rural areas it was 148.3 W/m^2. Despite the higher solar radiation amounts received by the rural site, both surface and air temperature were higher in the urban areas. This again reflects the effect of increased anthropogenic activities causing the trapping of heat by buildings and other structures.

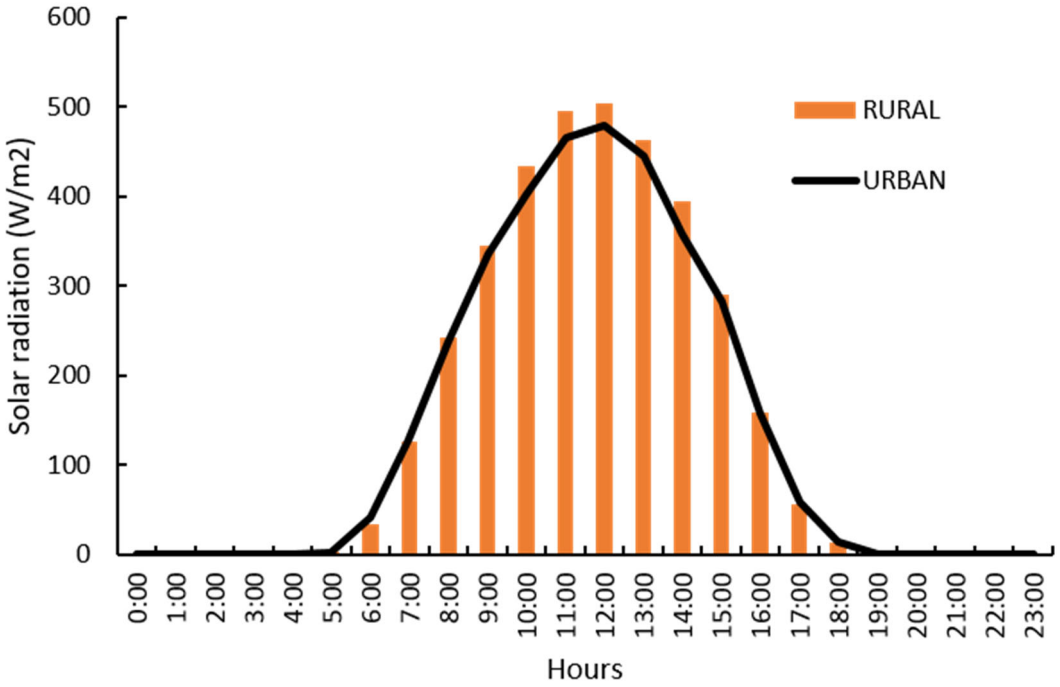

Figure 4–37 Distribution of solar radiation during the monsoon in urban and rural locations

Wind rose diagrams for the monsoon season for both sites are presented in Figure 4–38. These show that the dominant wind direction in urban locations was mainly southeastly with a mean speed of 2.14 m/s while winds from the west dominated in rural areas with an average speed of 0.84 m/s. As noted in the data analysis for the pre–monsoon months (see sub–section 4.11.2.1), the surface wind direction in the rural location is somewhat different to what would generally be expected, however, there is no independent data available to verify this.

Table 4–25 provides descriptive statistics of the monsoonal temperatures. This indicates that the mean surface and air temperatures were 0.7 and 0.54 °C higher (respectively) in the urban areas, suggesting local warming. Although the mean of the maximum for both parameters shows little difference (0.36 °C for surface and 0.16 °C for the air temperatures), the mean of the minimum between the two locations was larger (0.89 ° C for the surface and 0.67 °C for the air temperature).

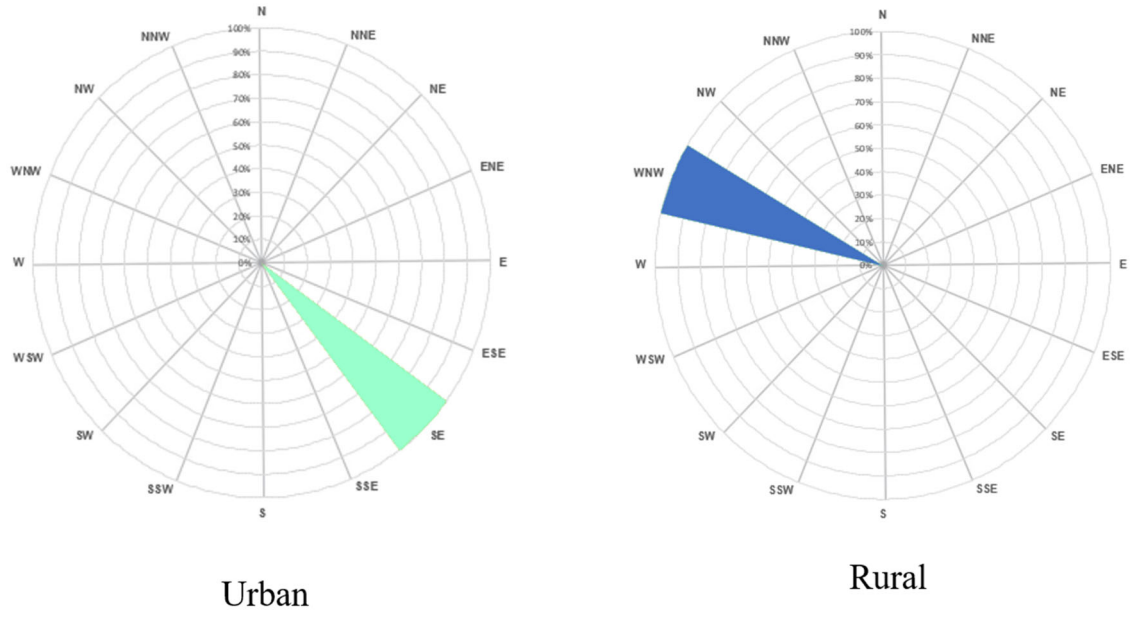

Figure 4–38 Wind rose diagrams (urban and rural) during monsoon (calm conditions = 0.30 m/s)

Table 4–25 Descriptive statistics related to air and surface temperatures in urban and rural locations

	Air Temperature (°C)		**Surface Temperature (°C)**	
	Urban	Rural	Urban	Rural
Maximum	32.31	31.95	32.22	32.06
Minimum	29.20	28.31	27.67	27.00
Mean	30.44	29.74	29.59	29.05
Std. Dev.	1.05	1.20	1.58	1.82

Mean monthly climate parameters recorded during the monsoon season are shown in Table 4–26. This shows that the average wind speed was greater in urban areas than in the rural area. Mean solar radiation was also higher in the rural area than in the urban counterpart. The difference in the monthly air and surface temperatures over the two areas indicate that, in every month of the monsoon season, the temperature at the urban location surpassed the rural temperature. The greatest difference can be seen in July when the surface temperature was 1.06 °C higher. Air temperature was also higher between these two locations. The CUHI however was higher than rural in June and September (0.64 and 0.63 °C, respectively). Note that relative humidity in the rural location was not available from June to August due to the anomalous behaviour of the sensor.

Table 4–26 Monthly mean temperatures, solar radiation, wind speed and relative humidity – urban versus rural locations

	Urban					Rural				
Months	ST (°C)	AT (°C)	SR (W/m^2)	WS (m/s)	RH (%)	ST (°C)	AT (°C)	SR (W/m^2)	WS (m/s)	RH (%)
Jun	30.32	29.87	153.24	2.01	88.37	29.81	29.23	147.65	0.90	NA
July	30.52	29.33	134.63	2.59	91.14	29.46	28.86	136.49	1.20	NA
Aug	30.95	29.84	149.25	2.22	88.87	30.08	29.45	162.85	0.75	NA
Sept	29.97	29.31	131.55	1.71	87.90	29.63	28.68	146.06	0.50	59.73

ST = surface temperature; AT = air temperature; RH = relative humidity; SR = solar radiation; WS = wind speed

4.11.3.2 Analysis of traverse surveys

Traversing surveys were conducted to determine microclimatic conditions at the three locations during the monsoon season. The results of the air temperature analysis are shown in Figure 4–39 (a–c). The unplanned locations had a higher air temperature than the planned locations, both in the morning and evening, however both locations recorded a similar temperature profile during the afternoon. The mixed land–use zone recorded lower temperatures across all the three measurement times. The average air temperature of the unplanned zone was 3.52 °C higher than the mixed during the morning hours, which showed 1.06 °C in the afternoon and 1.87 °C in the evening. The planned zone, on the other hand, had an average temperature higher than mixed zone during the three measurement periods.

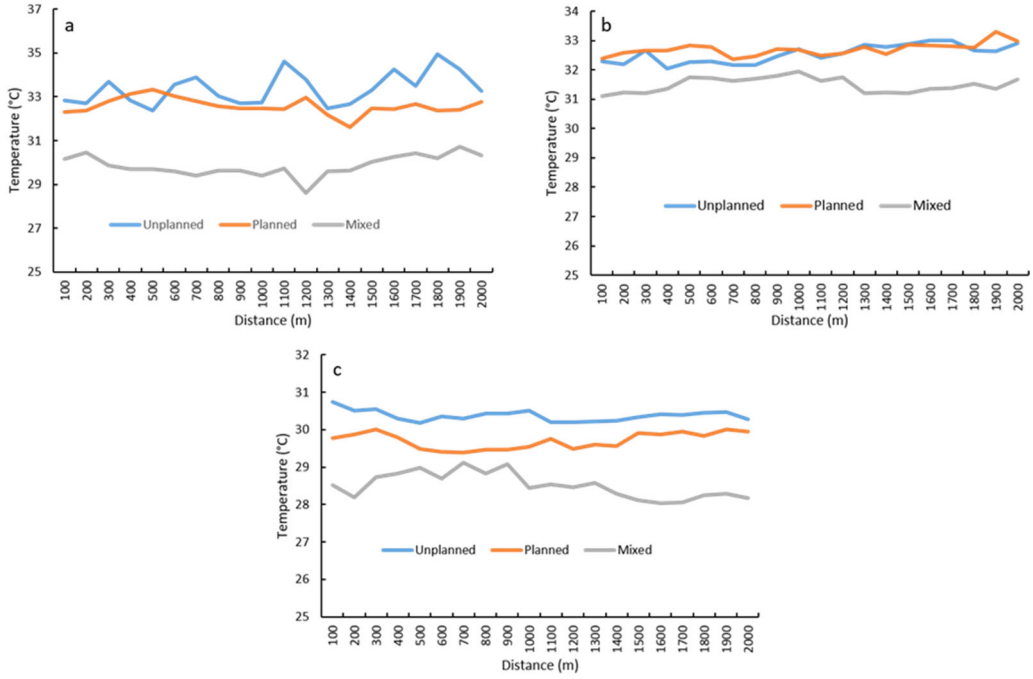

Figure 4–39 Variation of air temperature in three zones: (a) morning; (b) afternoon; and (c) evening

A notable fluctuation in surface temperature during the morning can be seen in the three locations during the monsoon (Figure 4–40a). The average temperature between these locations was large (32.13 ° for unplanned, 36.74 ° for planned, and 29.65 °C for the mixed zone) in the morning. During the afternoon, the planned location recorded a higher temperature than other two sites (Figure 4–40b), but little variation is noticeable between unplanned and planned sites during the evening in terms of their average surface temperature (28.29 and 28.41 °C, respectively). Compared to these locations, the mixed zone had a much lower surface temperature during the evening (Figure 4–40c) and the difference in mean temperature between the mixed and the other two sites was greater than 2 °C.

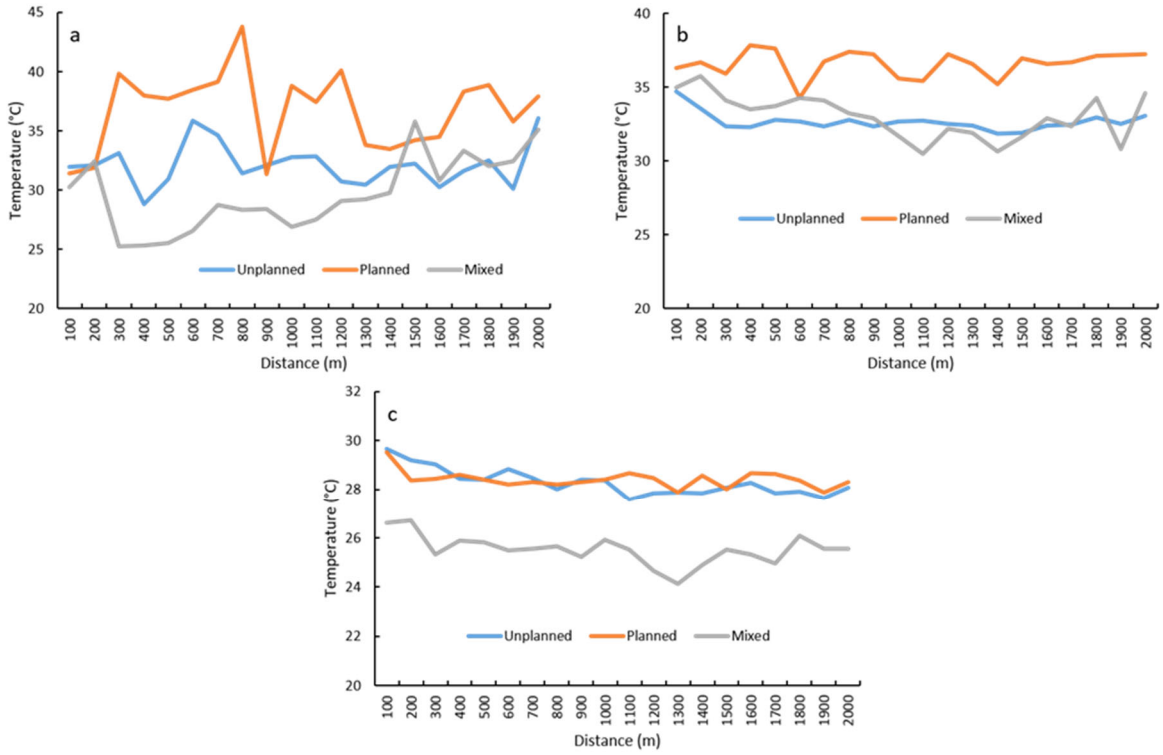

Figure 4–40 Distribution of surface temperatures in three zones: (a) morning; (b) afternoon; and (c) evening

The results of the correlation analysis, between air/surface temperature and the other recorded parameters, indicates that relative humidity has had a statistically significant influence on the air temperature of the three zones (Table 4–27).

Solar radiation also exhibits a significant relationship with air temperature during the morning at two of the three sites. The relative humidity data also shows a significant correlation in regards the surface temperature in the unplanned areas. Both relative humidity and solar radiation have had an effect on the planned zone surface temperature during the morning. In

Table 4–27 Spearman correlation coefficient between air/surface temperatures and relative humidity, wind speed and solar radiation in three traverse locations

	Air temperature (°C)						Surface temperature (°C)					
Unplanned	WS	Sig.	RH	Sig.	SR	Sig.	WS	Sig.	RH	Sig.	SR	Sig.
Morning	–.289	.217	–.642**	.002	.331	.154	.066	.781	.859**	.000	–.048	.840
Afternoon	–.253	.282	–.417	.068	–.536*	.015	.443	.050	.361	.118	.020	.935
Evening	.095	.692	–.192	.418	–	–	.370	.109	–.382	.097	–	–
Planned												
Morning	.044	.855	–.740**	.000	.774**	.000	.389	.090	–.535*	.015	.731**	.000
Afternoon	–.237	.314	–.559*	.010	–.123	.605	–.266	.256	–.284	.224	.017	.945
Evening	–.051	.832	–.754**	.000	–	–	.176	.459	–.352	.128	–	–
Mixed												
Morning	.208	.380	.503*	.024	–.722**	.000	.520*	.019	–.394	.086	.907**	.000
Afternoon	.106	.658	–.299	.200	–.033	.890	.268	.254	.409	.073	.683**	.001
Evening	–.047	.845	–.792**	.000	–	–	.346	.135	.048	.840	–	–

** Significant at the 0.01 level (2–tailed); * Significant at the 0.05 level (2–tailed)

the mixed zone, solar radiation and wind speed seem to be correlated, as revealed by the statistically significant relationship identified during both the morning and afternoon.

To determine the relative numbers of hotter and cooler sites along the three traverse routes, the individual location air/surface temperature values were subtracted from the mean traverse temperature data to obtain a site temperature, which could be compared with other sites. The results are shown in Figures 4–41 (air temperature) and 4–42 (surface temperature).

In regard to air temperature at the 20 sampled sites along each of the three transects during the morning hours, 11 were warmer and 9 were cooler in the unplanned zone, 12 were warmer and 8 were cooler in the planned zone, while 11 were warmer and 9 were cooler in the mixed location. During the afternoon, the three locations had an equal number of warmer and cooler spots (10 warmer, 10 cooler). Half of the locations were warmer/cooler in the unplanned and mixed zones, while 9 locations were warmer and 11 sites were cooler in the planned zone during the evening (Figure 4–41). With respect to surface temperature, the unplanned zone had a greater number of warmer sites (12), than those in the planned (9) and mixed (11) zones in the morning. A greater number of UCI locations were found in the planned zone (12) during the afternoon, while the comparable values were 8 for the unplanned and 10 in the mixed zones (Figure 4–42). In the evening, however the planned zone had a greater number (12) of warmer locations than the other two locations (9 in unplanned and 10 in mixed zones).

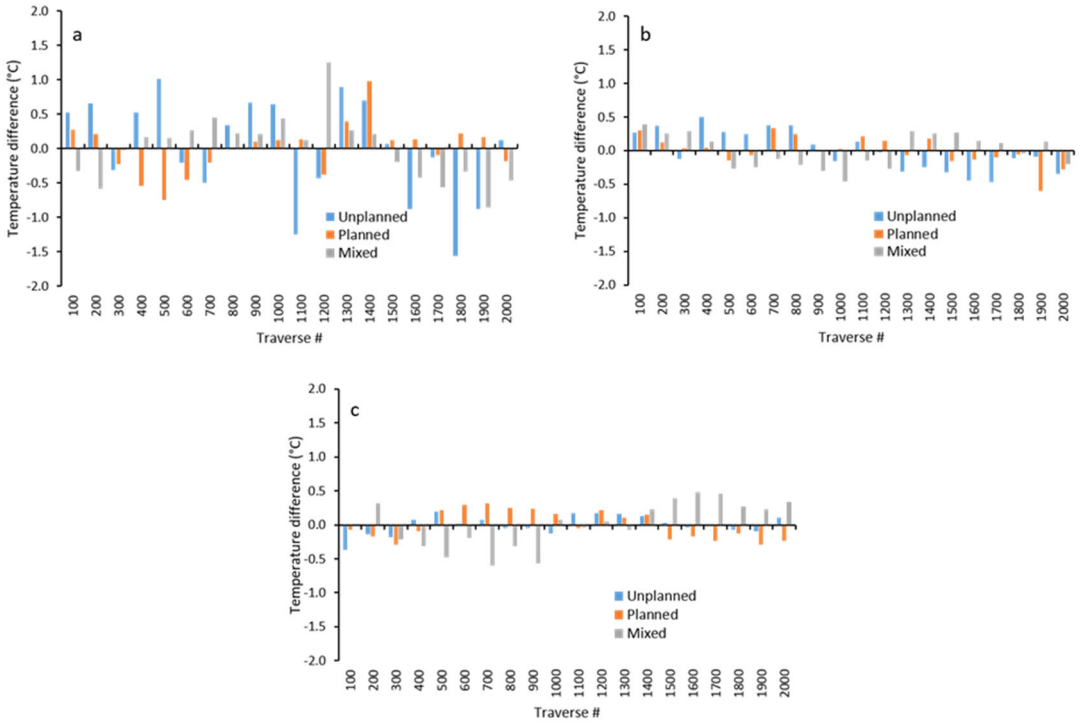

Figure 4–41 Mean air temperature difference at three locations: (a) morning; (b) afternoon; (c) evening. Sites warmer than the mean transect temperature are positive and sites cooler than the mean transect temperature are negative

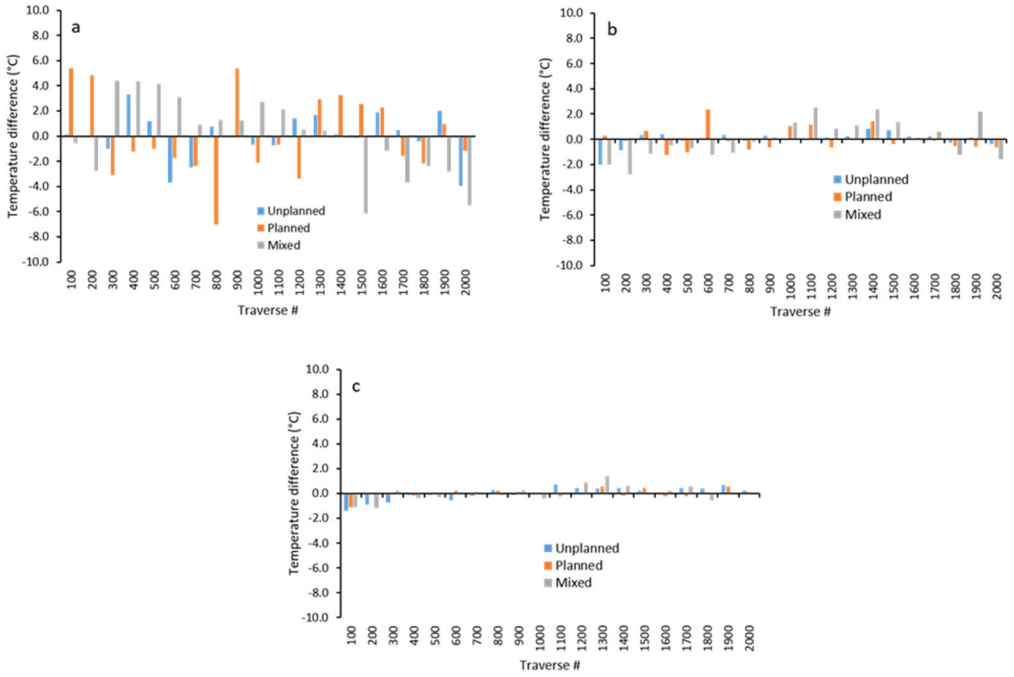

Figure 4–42 Mean surface temperature difference at three locations: (a) morning; (b) afternoon; (c) evening. Sites warmer than the mean transect value are positive and sites cooler than the mean transect value are negative

4.11.3.3 Thermo–physical behaviour of urban features

The results obtained from an examination of the thermo–physical properties of urban features are shown in Table 4–28. These results indicate that the cooling rate of air temperature is similar for both planned and unplanned sites (0.15 CR/h), with a higher rate recorded for the mixed zone during the morning (0.23 CR/h). The area average temperature (AAT), derived from the handheld thermal images, exhibited a higher cooling rate for the mixed zone (0.52 CR/h) when compared to the other two sites. Relative humidity, however, varied substantially between the three locations during the evening, though very similar relative humidity values were recorded during the morning hours (Table 4–28).

Table 4–28 Average of air temperature (AT), surface temperature (AAT), relative humidity (RH) of three traverse sites during morning (M) and evening (E). Temperature values are in °C and relative humidity is in percentage (%). Area average temperature (AAT) is taken from selected areas on the thermal images and are the average of 88 infrared photographs from 20 sites within three zones. CR is the cooling rate per hour in °C

Traverse site	AT_M	AT_E	ΔAT	CR/h	AAT_M	AAT_E	ΔAAT	CR/h	RH_M	RH_E
Planned	34.28	32.55	1.73	0.15	35.14	31.67	3.46	0.31	59.93	65.76
Unplanned	32.67	31.03	1.64	0.15	33.41	29.96	3.45	0.32	65.12	75.51
Mixed	31.51	29.00	2.51	0.23	33.25	27.43	5.82	0.52	64.93	77.72

The cooling rate of various urban features within the planned zone was determined by analysing 88 thermal images. The results indicate varied cooling rates among the objects. The five top–ranked features (in bold face) were a water tank with iron body (1.62 CR/h), healthy vegetation (1.36 CR/h), a building wall with grey glass (1.00 CR/h), a shaded walkway with asphalt (0.96 CR/h) and tree foliage (0.91 CR/h) (Table 4–29). Note however that, at another spot, tree foliage showed a negative cooling rate, reinforcing the locational effect together with proximity to other features, and the type and arrangement of vegetation.

In the unplanned zone, the top five objects (bold faced in Table 4–30), based on their cooling potential, were a tin rooftop (1.18 CR/h), a degraded building with mirage brick (0.89 CR/h), a rooftop of bare concrete (0.70 CR/h), a building wall with brown plaster (0.69 CR/h), and a blue plastic wall (0.62 CR/h). Note that some features such as a painted fence and electricity pole exhibited negative cooling rates, but their CR was too low to obtain a reliable value (Table 4–30).

Table 4–31 shows the cooling potential in the mixed zone during the monsoon season. In this area, a bare concrete rooftop had the highest cooling rate (CR 1.57/h) followed by a green coated plastic billboard (1.40 CR/h), plaster building wall with grey colour (1.21 CR/h), red brick building wall (1.11 CR/h), and finally, shop shutter with tin ranked five with a CR of 1.05 per hour (boldfaced). In addition, a building wall of raw brick exhibited a negative cooling rate (-0.01 CR/h) in the mixed site.

Table 4–29 Planned zone – object surface temperature (°C) and cooling rate (°C/h)

Feature Type	Make	Colour	Early T (°C)	Late T (°C)	ΔT (°C)	CR/hr
Tree branch	–	–	34.5	31.3	3.2	0.27
Bld. wall	Brick	Green	33.8	33.2	0.6	0.05
Billboard	Plastic	White	36.0	32.6	3.4	0.28
Bld. wall	Glass	Blue	41.7	32.1	9.6	0.81
Bld. window	Glass	Transparent	34.4	32.7	1.7	0.14
Brick wall	Tile	Orange	34.4	32.7	2.0	0.17
Tree trunk	–	–	34.0	31.3	2.7	0.23
Bld. wall	**Glass**	**Grey**	**42.3**	**30.5**	**11.8**	**1.00**
Bld. pillar	Concrete	Red	37.2	32.4	4.8	0.41
Bld. wall	Concrete	Off-white	35.0	30.7	4.3	0.36
Tree foliage	–	–	33.1	34.1	-1.0	-0.08
Water tank	Iron	light yellow	41.5	33.1	8.4	0.71
Tank pillar	Iron	light yellow	39.0	35.3	3.7	0.31
Tree foliage	–	–	**37.5**	**26.8**	**10.7**	**0.91**
Tank body	**Iron**	**Cast skin**	**50.5**	**31.4**	**19.1**	**1.62**
Mosque	Brick	Red	40.1	32.0	8.1	0.69
Stair	Tile	Off-white	38.0	30.1	7.9	0.67
Grass	–	–	32.5	29.7	2.8	0.24
Tree trunk	–	–	32.3	31.2	1.1	0.09
Shaded walkway	**Asphalt**	**Black**	**41.7**	**30.4**	**11.3**	**0.96**
Waterbody	–	–	33.2	29.6	3.6	0.31
Rooftop	Tin	Mirage	39.3	30.8	8.5	0.73
Health veg.	–	–	**43.8**	**27.9**	**15.9**	**1.36**
Unhealthy veg.	–	–	39.3	29.4	9.9	0.85
Shaded street	Asphalt	Black	33.5	32.1	1.4	0.12
Shaded walkway	Tile	Yellow	33.5	31.9	1.6	0.14
Shaded walkway	Tile	Red	33.4	32.7	0.7	0.06
Electric pole	Steel	Silver	34.0	32.2	1.8	0.15
Unshaded street	Asphalt	Black	37.1	32.5	4.6	0.40
Painted bld. wall	Concrete	Yellow	35.8	31.7	4.1	0.36
Tree foliage	–	–	29.8	31.6	-1.8	-0.16
Window	Glass	Grey	38.3	30.2	8.1	0.70
Tree trunk	–	–	33.2	31.3	1.9	0.17
Bld. wall	Brick	Brown	38.2	32.9	5.3	0.47
Building	Glass	Green	38.2	31.9	6.3	0.56
Bld. side wall	Brick	Plaster	34.3	30.9	3.4	0.30
Bld. front wall	Glass	Transparent	34.7	32.0	2.7	0.24
Waterbody	–	–	31.5	30.9	0.6	0.05
Rubbish	–	–	35.3	31.0	4.3	0.38
Speedboat	Steel	White	39.1	29.9	9.2	0.81
Shrub	–	–	33.0	30.8	2.2	0.19
Billboard	Plastic	Navy blue	35.3	32.9	2.4	0.23
Bld. wall	Plaster	Mirage	35.7	32.2	3.5	0.33
Bld. wall	Glass	Blue	36.0	31.3	4.7	0.44
Building	Glass	Green	32.4	31.4	1.0	0.11
Rooftop	Tile	Silver	34.7	30.1	4.6	0.49
Fence	Iron	–	33.0	31.7	1.3	0.14
Passenger shade	Iron	White	34.6	32.0	2.6	0.27
Wall	Brick	Red	36.0	32.7	3.3	0.35
Bld. wall	Concrete	Brown	37.4	32.1	5.3	0.56
Bld. wall	Concrete	Yellow	36.0	33.1	2.9	0.31
Bld. front wall	Concrete	Grey	36.0	32.9	3.1	0.33

Table 4–30 Unplanned zone – object surface temperature (°C) and cooling rate (°C/h)

Feature Type	Make	Colour	Early T (°C)	Late T (°C)	ΔT (°C)	CR/hr
Billboard	Plastic	Red	32.2	30.8	1.4	0.12
Window	Glass	Hue	31.7	33.4	-1.7	-0.14
Balcony	Plaster	–	33.0	30.1	2.9	0.25
Raw brick	–	Red	31.7	30.3	1.4	0.12
Bld. wall	Marble	Ash	33.5	30.5	3.0	0.26
Electric pole	Steel	Silver	32.0	30.7	1.3	0.11
Window	Glass	Grey	32.0	28.0	4.0	0.34
Shaded fence	Concrete	White	31.6	31.1	0.5	0.04
Dense veg canopy	–	–	30.0	29.8	0.2	0.02
Painted fence	Brick	Yellow	30.5	30.6	-0.1	-0.01
Dense vegetation	–	–	28.6	29.6	-1.0	-0.09
Vegetated wall	Brick	–	32.9	28.0	4.9	0.44
Bld. wall	Cement	Grey	34.5	29.9	4.6	0.41
Bld. entrance	Concrete	White	35.2	30.0	5.2	0.46
Old fence	Brick	Red	35.4	31.0	4.4	0.40
Dome	Brick	Yellow	34.5	31.3	3.2	0.29
Elevated fence	Plaster	White	31.2	29.4	1.8	0.17
Tree trunk	–	–	31.1	30.4	0.7	0.06
Cornice	Iron	Yellow	30.6	30.2	0.4	0.04
Building	Tile	Mixed	32.1	31.3	0.8	0.07
Window	Glass	Black	32.4	30.6	1.8	0.17
Neon sign	Plastic	Mixed	31.5	30.1	1.4	0.13
Bld. entrance	Brick	Black	34.7	28.5	6.2	0.58
Rooftop	**Tin**	**Silver**	**38.3**	**25.6**	**12.7**	**1.18**
Bld. wall	**Plaster**	**Brown**	**35.1**	**27.7**	**7.4**	**0.69**
Bld. wall	Plaster	White	33.8	28.5	5.3	0.49
Cornice	Brick	Moss	36.1	31.3	4.8	0.45
Plastic wall	**Plastic**	**Blue**	**36.5**	**29.9**	**6.6**	**0.62**
Rooftop	Tin	Silver	33.3	29.2	4.1	0.38
Cornice	Iron	–	34.2	28.3	5.9	0.55
Degraded fence	Brick	Yellow	32.7	27.9	4.8	0.45
Rooftop	**Concrete**	**No paint**	**35.6**	**28.2**	**7.4**	**0.70**
Transmission pole	Steel	Silver	46.4	49.3	-2.9	-0.27
Billboard	Steel	Silver	36.8	31.2	5.6	0.53
Bld. wall	Brick	Red	37.4	31.3	6.1	0.58
Window	Iron	Mirage	34.1	29.7	4.4	0.42
Window	Glass	Blue	35.2	29.7	5.5	0.53
Degraded bld.	**Brick**	**Mirage**	**39.0**	**29.7**	**9.3**	**0.89**

Table 4–31 Mixed zone – object surface temperature (°C) and cooling rate (°C/h)

Feature Type	Make	Colour	Early T (°C)	Late T (°C)	ΔT (°C)	CR/hr
Bridge	Concrete	–	38.3	28.6	9.7	0.82
Waterbody	–	Turbid	31.8	25.3	6.5	0.55
Grass	–	–	32.2	25.0	7.2	0.61
Electric pole	Steel	Silver	38.7	27.1	11.6	0.98
Rooftop	Tin	Silver	37.2	27.7	9.5	0.80
Bare soil	–	Brown	33.5	25.8	7.7	0.65
Bld. wall	Raw brick	Red	35.0	27.9	7.1	0.60
Bld. wall	Brick	Brown	33.4	28.2	5.2	0.44
Street	Asphalt	Black	31.4	27.4	4.0	0.34
Roof with garden	Concrete	–	29.2	25.7	3.5	0.30
House wall	Tin	Silver	37.9	26.4	11.5	0.99
Balcony	Iron	Brown	38.0	26.8	11.2	0.96
Shop shutter	**Tin**	**Silver**	**39.6**	**27.4**	**12.2**	**1.05**
Billboard	Plastic	Red	32.3	27.0	5.3	0.46
Tree foliage	–	–	30.5	26.4	4.1	0.35
Window	Glass	Green	35.9	26.1	9.8	0.84
Bld. wall	Brick	Yellow	31.9	26.9	5.0	0.43
Shop shutter	Tin	Silver	30.0	29.0	1.0	0.09
Bld. wall	Raw brick	Red	36.0	28.2	7.8	0.67
Bld. wall	Tile	White	30.6	28.3	2.3	0.20
Shop	Tin	Grey	35.0	28.1	6.9	0.61
Window	Glass	Blue	31.2	28.7	2.5	0.22
Bld. front wall	Brick	Yellow	38.7	30.4	8.3	0.73
Open balcony	Plaster	Off-white	30.3	28.8	1.5	0.13
Shutter	Tin	Silver	34.6	28.8	5.8	0.51
Signboard	Plastic	White	29.3	28.6	0.7	0.06
Tree trunk	–	–	30.2	28.4	1.8	0.16
Bld. pillar	Raw brick	Red	28.5	28.6	-0.1	-0.01
Bld. wall	Brick	Yellow	31.1	27.9	3.2	0.29
Bld. front wall	Raw brick	Red	32.1	27.5	4.6	0.41
Street	Asphalt	Black	30.3	28.3	1.5	0.13
Electric pole	Steel	Silver	31.7	28.3	3.4	0.30
Bld. wall	Brick	Blue	33.6	27.9	5.7	0.51
Window	Glass	Black	33.3	27.9	5.4	0.49
Rooftop	Raw brick	Red	33.9	27.5	6.4	0.58
Billboard	**Plastic**	**Green**	**45.9**	**30.4**	**15.5**	**1.40**
Bld. front wall	Plaster	Grey	35.7	28.6	7.1	0.64
Coconut T. foliage	–	–	31.9	26.6	5.3	0.48
Rooftop wall	Raw brick	Red	36.4	27.9	8.5	0.77
Tree trunk	–	–	32.4	27.3	5.1	0.46
Bld. wall	Brick	Orange	35.6	26.7	8.9	0.81
Bld. side wall	Cement	Grey	32.9	27.5	5.4	0.49
Bld. wall	**Plaster**	**Grey**	**38.7**	**25.5**	**13.2**	**1.21**
Rooftop	**Concrete**	**Grey**	**42.0**	**24.9**	**17.1**	**1.57**
Billboard	Plastic	Red	43.5	30.4	13.1	1.20
Road	Concrete	Ash	34.4	26.6	7.8	0.72
Bld. wall	**Raw brick**	**Red**	**39.2**	**27.2**	**12.0**	**1.11**
Window	Glass	Transparent	32.5	27.6	4.9	0.45
Bld. wall	Brick	Purple	31.7	26.3	5.4	0.51
Bld. wall	Plaster	Grey	34.6	27.0	7.6	0.71
Tree	–	–	31.0	28.4	2.6	0.24
Water tank	Plastic	Black	32.3	28.1	4.2	0.40
Bld. wall	Plaster	Moss	37.3	28.2	9.2	0.87
Street	Concrete	Grey	38.1	28.3	9.8	0.92

4.11.3.4 Thermal response of rooftop with/without garden

The diurnal surface temperature variation of roofs, both with and without garden, during the monsoon months is shown in Figure 4–43. The roof with an included garden appears to have an overall positive effect in regards reducing roof temperature and shows potential to reduce rooftop environmental temperatures. On average, the rooftop with garden was 2 °C lower in temperature than the rooftop without garden during monsoon. In regards rooftops with/without garden, an examination of air temperature values at different heights show that at every vertical level, a rooftop garden could reduce temperature significantly (Figure 4–44). The magnitude is most noticeable at 1 m above the ground than at the heights of 2 m and 3 m.

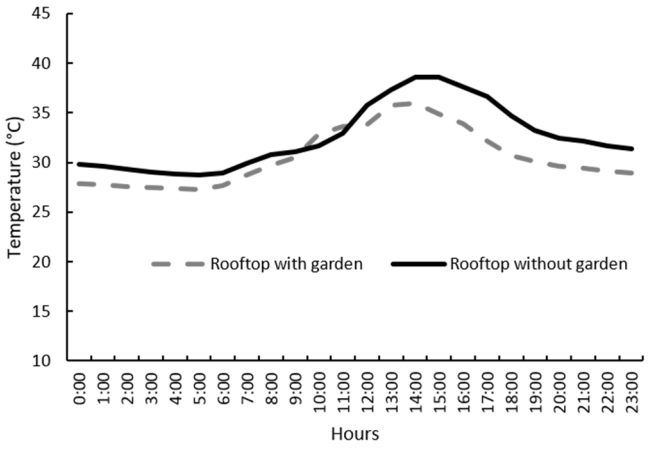

Figure 4–43 Diurnal variation of surface temperature of rooftop with/without garden

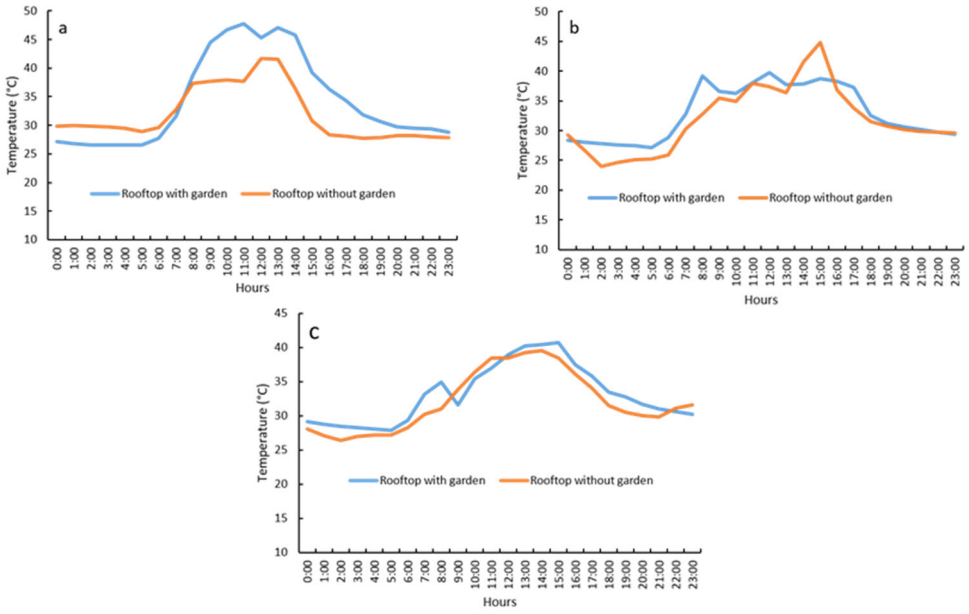

Figure 4–44 Diurnal response of rooftop with/without garden on air temperatures at different heights: (a) 1 m; (b) 2 m; and (c) 3 m

4.11.3.5 Variation of thermal pattern of rooftop plants

Combretum indicum has shown a striking ability to reduce environmental temperature values in the pre–monsoon and winter seasons and this effect is also seen in the monsoon period. The effect is most noticeable between 0700 and 1500 hours (Figure 4–45). The thermal response of dominant plants in terms of their mean value reveals that *Combretum indicum* is again ranked top followed by *Bougainvillea.* The other three plant species appear to have less of an impact in reducing surrounding environmental temperatures.

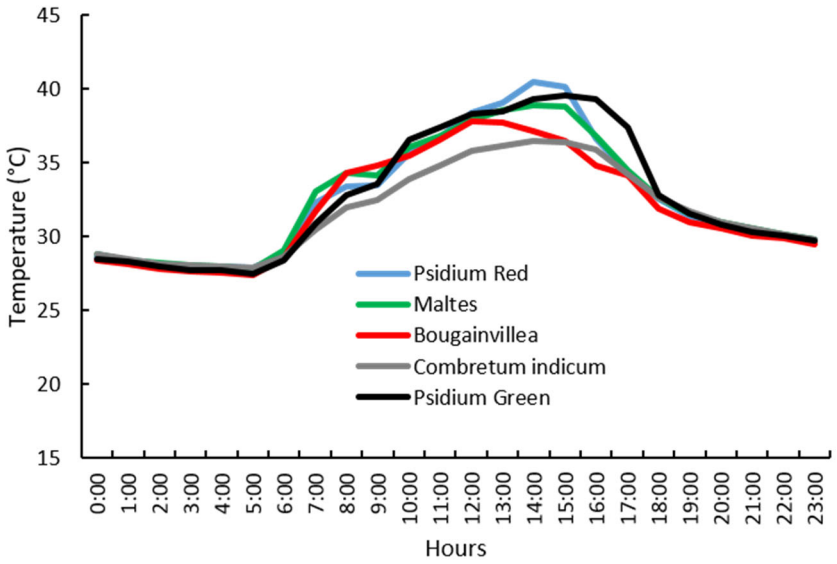

Figure 4–45 Thermal response of dominant rooftop plants

4.11.3.6 Cooling potential of open space plants

Using a threshold value, set at 28 °C, for the monsoon season, *Loha kat* shows the highest cooling potential among the species examined; this is followed by *Beharda* (Figure 4–46). Among the open space vegetation, *Coconut* had the lowest cooling potential. Since the thermal response of *Loha kat* for the pre–monsoon months is not known due to public construction work interfering in field measurements, no comparison was able to be undertaken, and thus the ability to provide a firm conclusion as to the usefulness of this plant in reducing urban temperature is not possible. The average wind speed and solar radiation during the measurement period was recorded as 2.66 m/s and 81.69 W/m^2, respectively (Appendix VII).

The average morning and afternoon temperatures recorded for each open space plant shows that *Loha kat* and *Beherda* have the potential to reduce temperature in the morning. For the afternoon period, four species, namely *Loha kat, Beharda, Pam* and *Mimusops,* could be effective in reducing local heating effects (Table 4–32). *Coconut* stood out as being the least effective temperature reduction plant during both times of the day.

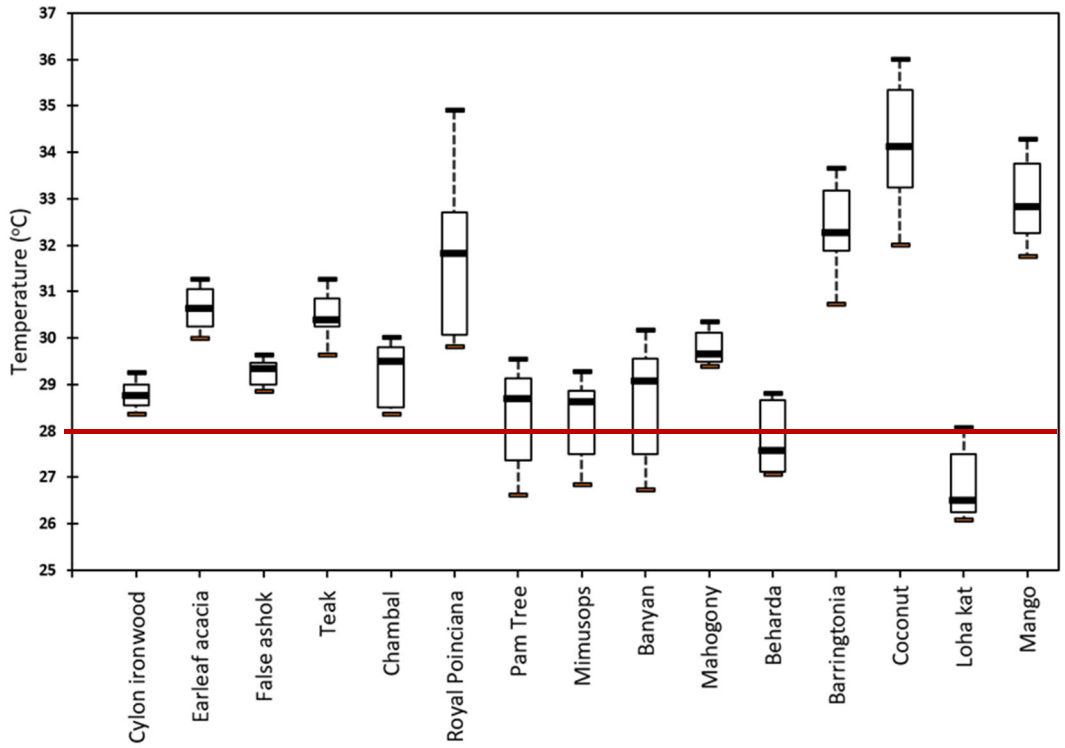

Figure 4–46 Thermal response of open space plants

Table 4–32 Average temperature (°C) of open space plants

Plant types	Morning (0900–1300)	Afternoon (1400–1800)
Cylon ironwood	29.20	28.48
Earleaf acacia	30.78	30.48
False ashok	29.61	28.94
Teak	30.75	30.18
Chambal	29.75	28.84
Royal Poinciana	33.31	30.35
Palm	29.15	27.60
Mimusops	28.88	27.63
Banyan	29.53	27.90
Mahogany	29.48	30.10
Beharda	28.30	27.38
Loha kat	27.23	26.53
Barringtonia	31.63	32.93
Coconut	33.83	34.23
Mango	32.70	33.10

4.11.3.7 Temperature variation of urban waterbodies

Water temperature data from the pond and a river was plotted (Figure 4–47) and indicated that the pond recorded a high temperature value from 1200 to 2000, with a peak (31.36 °C) at 1500 hours. On the other hand, the river had a consistent thermal pattern possibly reflecting a water velocity factor which would dissipate any heat. The difference in thermal response of these two urban water features revealed that pond temperature can fluctuate markedly. This may be related to its location, as well as any water stagnancy issues.

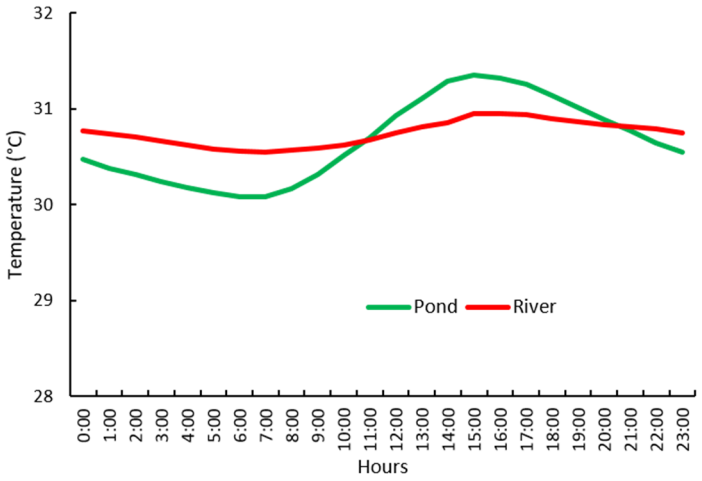

Figure 4–47 Thermal response of a river and a pond during monsoon

4.11.3.8 Cooling potential of a green hanging wall

During the monsoon months, the hanging wall soil recorded surface temperatures markedly lower than wall and substrate features (Figure 4–48). Over the measurement period

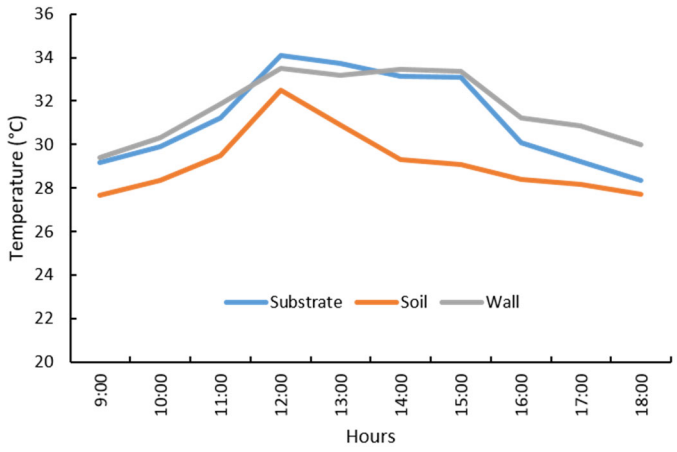

Figure 4–48 Average soil, wall and the substrate temperatures of a green hanging wall

(0900–1800), the thermal response of the substrate and wall temperature varied, with both showing a peak at 1300 and 1400 hours, respectively. Interestingly, the soil temperature peaked at 1300 but never actually overlapped the substrate and wall temperatures. The reason for this is largely unclear; however, it may have something to do with monsoonal rainfall. It is possible that the wall and substrate materials have dried out earlier than the soil with the thermal response reflecting the fact that soil moisture may be an important factor. Other factors such as the construction materials, the plant types and thermal conductivity could also influence the response of the vertical greening system studied.

Table 4–33 Ambient temperature of a green hanging wall at defined distances from the substrate

	Temperature (°C)				
Hours	1 m	2 m	3 m	4 m	5 m
09.00	32.42	33.00	32.08	37.77	32.96
10.00	34.31	33.31	33.69	40.25	34.50
11.00	35.38	34.98	35.60	41.31	36.50
12.00	36.46	38.06	38.83	42.13	40.02
13.00	34.27	36.10	36.04	40.83	36.38
14.00	32.88	36.00	34.83	38.21	34.92
15.00	31.56	34.25	32.75	35.75	32.48
16.00	30.48	31.00	31.02	33.46	30.96
17.00	29.58	29.83	29.94	31.94	29.94
18.00	28.71	28.77	28.90	30.81	28.94

Analysis of the air temperature recorded at varying heights above the green wall system indicate that at 1 m height the temperature is lower than at other heights (Table 4–33). An analysis of the deviation from the mean temperature for each hourly recording shows that at three heights (1 m, 3 m and 5 m), the temperature was cooler between 1000 and 1400 hours. An hourly lag effect is visible at 2 m. The highest overall temperature (42.13 °C) was recorded at the 4 m height at 1200 hours.

4.11.3.9 Cooling potential of green and blue spaces

Figure 4–49 illustrates the response of a specific greenspace (in this case Suhrawardy Uddyan) in reducing the environmental temperature during the monsoon season. To the west, definitive evidence of a cooling effect is missing, though data recorded for the distance category of 812 m indicates much lower temperatures than the other distance categories during the afternoon and evening. The impact that proximity to the park had on temperature seems to vary in the northerly direction, with lower temperatures recorded during the morning than were recorded at other times of the day. Looking south, the effects of both proximity and direction are also

unclear. To the east, temperatures recorded at the 2280 m distance were lower during the late morning and evening as compared to readings at the 858 m and 862 m distance.

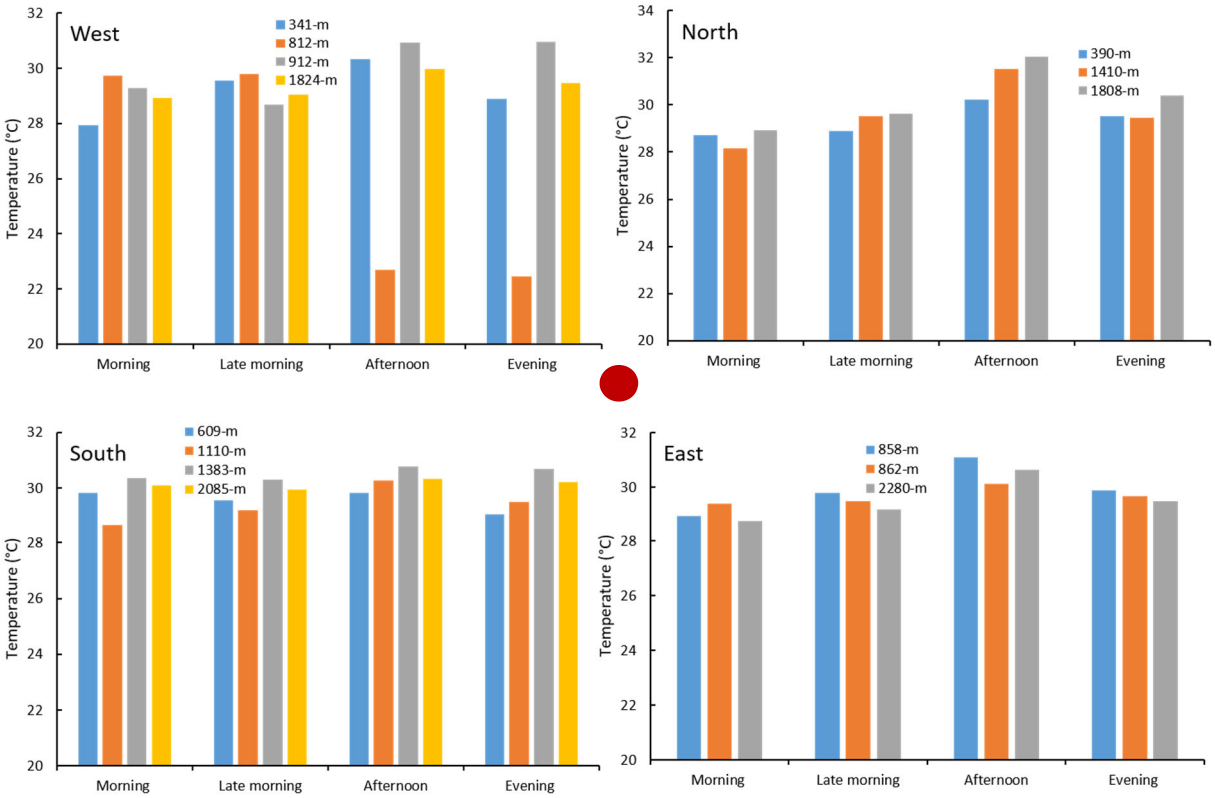

Figure 4–49 Cooling effect of a large greenspace at various distances and directions from a central point. The dark red circle denotes the centre of the park relative to the measuring points

An analysis of the data recorded for the lake (specifically, the Dhanmondi lake) shows that proximity to this water body plays a key role in the overall temperature profiles evident over the diurnal cycle in monsoon. This effect did, however, vary significantly according to the compass direction (Figure 4–50). While lower temperatures can be observed to the west, north and south directions, results are somewhat inconclusive towards the east, particularly during the afternoon and evening. Interestingly, measurements taken in an easterly direction at 555 m and 918 m distances indicate a positive effect on the ambient temperature when compared to the 619 m distance. Measurements taken at 200 m distance show a greater cooling effect during the earlier part of the day.

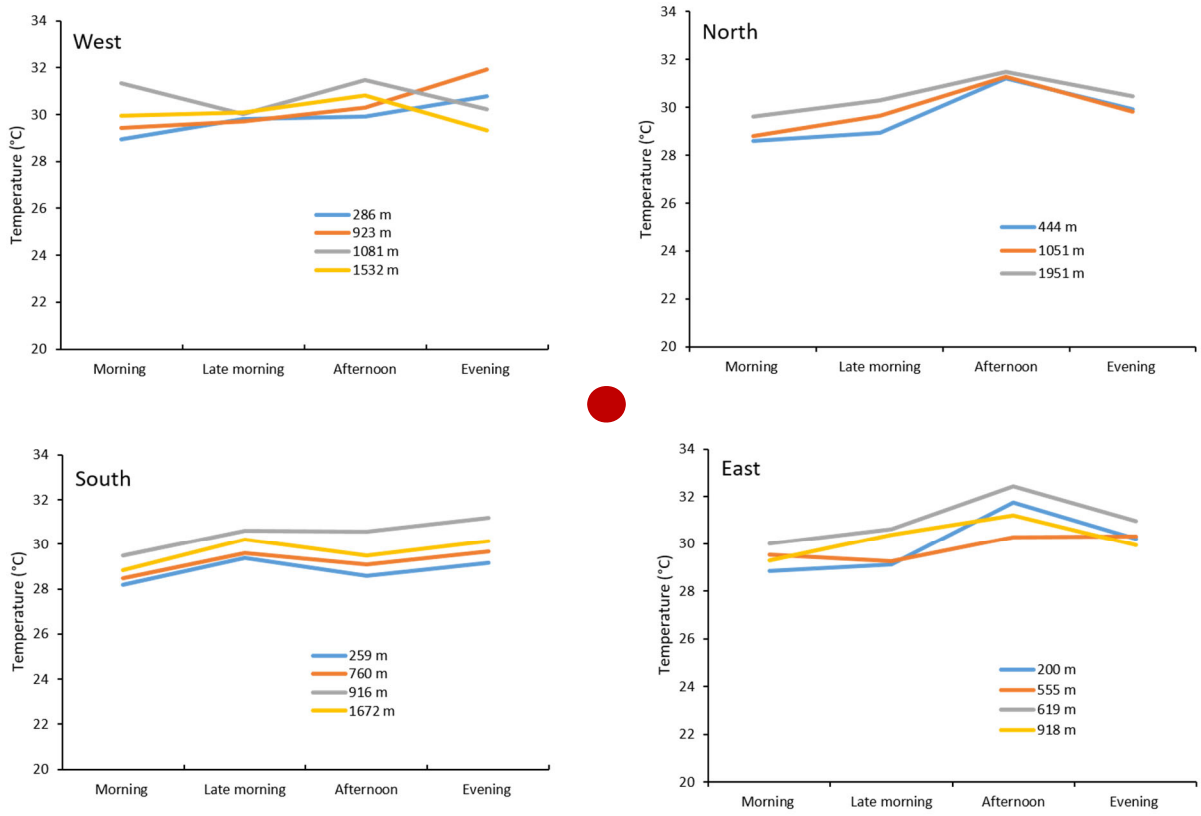

Figure 4–50 Cooling effect of a lake at various distances and directions from a central point. The dark red circle denotes the centre of the lake relative to the measuring points

4.11.4 Post–monsoon season

4.11.4.1 Urban–rural gradient of surface and air temperatures

The post–monsoon magnitude of both SUHI and CUHI is not as conspicuous as that observed during the winter, pre–monsoon and monsoon periods. Figure 4–51 (a–b) shows the surface and ambient air temperatures recorded at urban and rural locations. The graph of the entire diurnal cycle of surface temperature of this season indicates that the urban location has a higher temperature between 0000 and 1100 relative to the rural site (Figure 4–51a). The rural location, however, exhibited an elevated temperature from noon (1200) to early evening hours (2000). On average, the urban area had a 0.1 °C higher surface temperature. In contrast, air temperature readings between the two sites shows that the ambient air temperature is higher at the rural site than at the urban site, from the morning (0900) into the afternoon hours (1500). In regards the average air temperature across the diurnal cycle in the post–monsoon season, the urban area exhibits a temperature 1.18 °C higher than the rural area (Figure 4–51b).

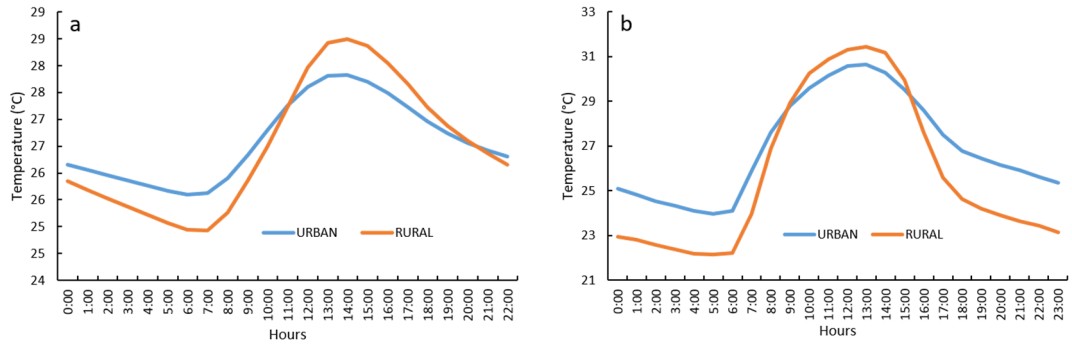

Figure 4–51 Diurnal variation of temperature during the post–monsoon season: (a) surface; (b) air

Table 4–34 Differences in air and surface temperature during the post–monsoon season

	Surface Temperature (°C)			Air Temperature (°C)		
Hours	Urban	Rural	SUHI	Urban	Rural	CUHI
0:00	26.16	25.84	0.32	25.09	22.96	2.13
1:00	26.06	25.68	0.38	24.82	22.79	2.03
2:00	25.96	25.52	0.44	24.54	22.59	1.95
3:00	25.86	25.37	0.49	24.35	22.37	1.97
4:00	25.76	25.22	0.54	24.12	22.20	1.92
5:00	25.67	25.07	0.60	23.96	22.13	1.82
6:00	25.60	24.95	0.65	24.09	22.20	1.89
7:00	25.63	24.93	0.70	25.87	23.97	1.90
8:00	25.91	25.26	0.64	27.60	26.88	0.71
9:00	26.33	25.86	0.47	28.80	28.92	–0.11
10:00	26.80	26.49	0.31	29.59	30.23	–0.64
11:00	27.25	27.23	0.02	30.16	30.89	–0.73
12:00	27.60	27.97	–0.37	30.59	31.29	–0.71
13:00	27.81	28.43	–0.62	30.66	31.44	–0.78
14:00	27.82	28.49	–0.67	30.27	31.16	–0.89
15:00	27.70	28.37	–0.67	29.51	29.95	–0.44
16:00	27.49	28.06	–0.56	28.59	27.60	0.99
17:00	27.23	27.65	–0.42	27.49	25.60	1.90
18:00	26.97	27.23	–0.26	26.78	24.63	2.16
19:00	26.74	26.88	–0.13	26.46	24.19	2.26
20:00	26.56	26.60	–0.03	26.15	23.89	2.26
21:00	26.42	26.36	0.06	25.93	23.64	2.29
22:00	26.30	26.16	0.14	25.63	23.43	2.20
23:00	26.19	25.97	0.22	25.34	23.13	2.21

The SUHI which develops in Dhaka tends to intensify in the evening (from approximately 2100) and continues into the morning hours (1000). This is a phenomenon also experienced by other big cities. The greatest effect is noted between 0500 and 0800 hours (Table 4–34). Even though the urban air temperature is elevated across most of the diurnal cycle during the post–monsoon season, the air temperature is higher from 0900 to 1500 (Table 4–34) at the rural site.

The distribution of solar radiation over the diurnal cycle at the two sites clearly indicates that rural areas receive more solar radiation than the urban areas (Figure 4–52). This may be related to the sky view factor (the fraction of the sky visible from a defined observation point). The average urban radiation load was estimated at 118.5 W/m^2, while for the rural areas it was 136.3 W/m^2. This may be a possible reason for the contrasting behaviour of the SUHI and CUHI phenomena in urban and rural locations within the DMA.

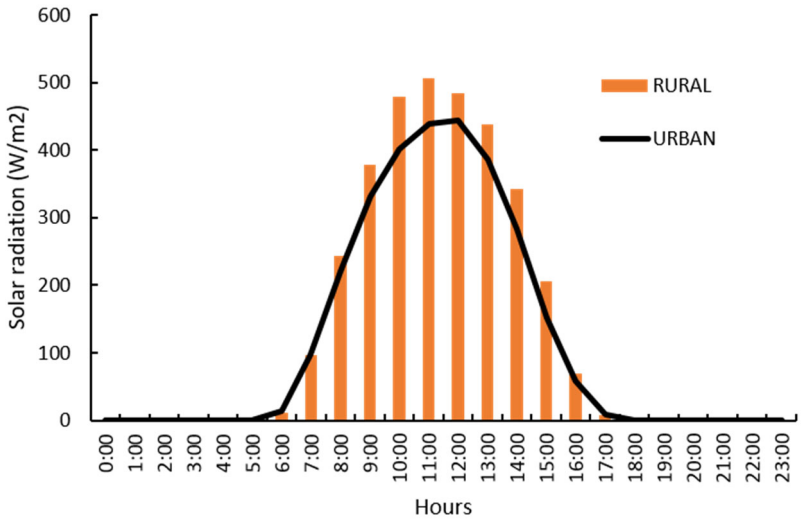

Figure 4–52 Distribution of solar radiation during the post–monsoon in urban and rural locations

Wind rose diagrams for the post–monsoon season, for both sites, are presented in Figure 4–53.

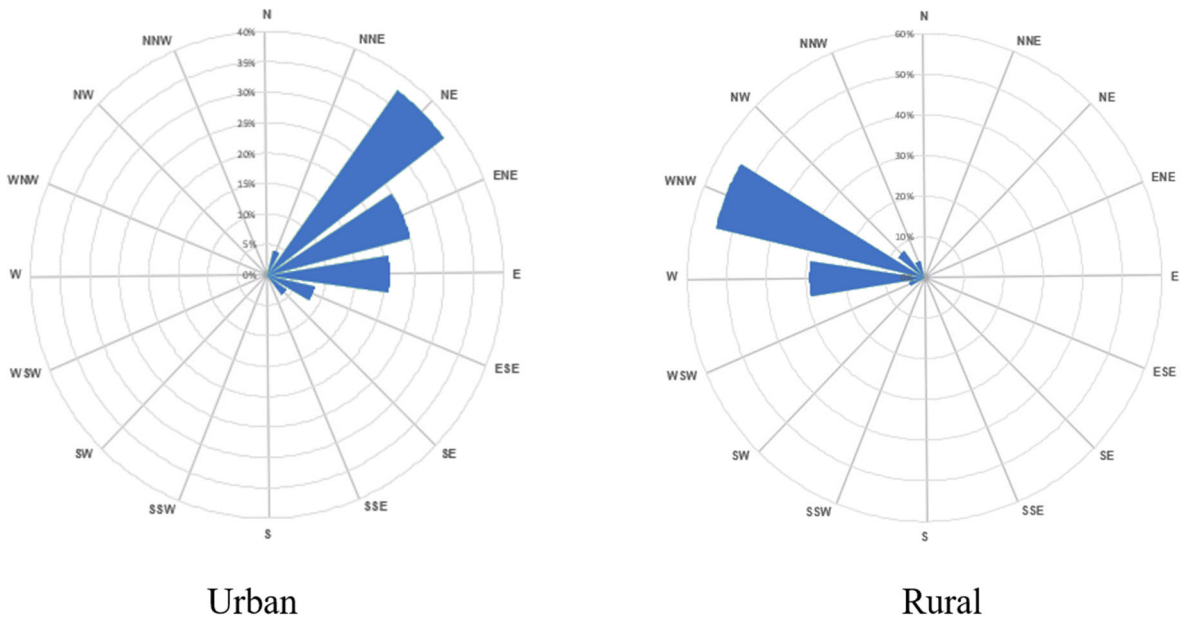

Figure 4–53 Wind rose diagram during post–monsoon (calm conditions = 0.30 m/s)

These show that the dominant wind direction in the post–monsoon period follows the same pattern like pre–monsoon and monsoon seasons, i.e. in urban locations it was mainly from the northeast, while winds from the northwest dominate in rural areas. As noted in the data analysis for the pre–monsoon months (see subsection 4.11.2.1), the low–level surface wind direction recorded at the rural location is somewhat different to what would generally be expected. As mentioned previously, there is no information available to validate these observed differences.

Table 4–35 provides descriptive statistics of the post–monsoonal temperatures. This indicates that the mean surface and air temperatures were 0.1 and 1.18 °C higher (respectively) in the urban areas. An examination of the maximum temperatures shows an interesting feature – both temperatures were higher at the rural site than the urban site during the post–monsoon months. However, a higher standard deviation was observed for both the surface and air temperatures, indicating the greater sensitivity of rural areas to temperature.

Table 4–35 Descriptive statistics related to air and surface temperatures in urban and rural sites

	Surface Temperature (°C)		**Air Temperature (°C)**	
	Urban	Rural	Urban	Rural
Maximum	27.82	28.49	30.66	31.44
Minimum	25.60	24.93	23.96	22.13
Mean	26.58	26.48	26.93	25.75
Std. Dev.	0.74	1.19	2.30	3.45

Table 4–36 Monthly mean temperatures, solar radiation, wind speed and relative humidity – urban versus rural locations

	Urban					**Rural**				
Months	ST (°C)	AT (°C)	SR (W/m^2)	WS (m/s)	RH (%)	ST (°C)	AT (°C)	SR (W/m^2)	WS (m/s)	RH (%)
October	28.18	28.17	131.33	0.36	84.41	27.85	26.90	147.25	0.04	89.92
November	24.97	25.70	105.72	0.34	78.98	25.11	24.60	125.25	0.03	88.47

ST = surface temperature; AT = air temperature; RH = relative humidity; SR = solar radiation; WS = wind speed

Mean monthly climatic parameters recorded during the post–monsoon season are shown in Table 4–36. This indicates that the average wind speed is greater in the urban areas (0.35 m/s) than in the rural area (0.04 m/s). Mean solar radiation was also higher in the rural area than in the urban counterpart. The difference in the monthly air and surface temperatures over the two areas indicates that the urban location surpassed the air temperature of the rural site during the month of October, but in November, the rural site recorded a higher surface temperature. The

relative humidity in the rural location was also higher than in the urban areas, both in October and in November.

4.11.4.2 Cooling potential of green and blue spaces

The recorded temperature of different locations and distances from the centre of a park during the post–monsoon months are shown in Figure 4–54. Depending on the measurement direction (east, west, north or south), a significant variation in temperature can be seen. In a westerly direction, locations (e.g. 341 m) nearer to the park centre tend to have a higher ambient temperature across the diurnal cycle, although this effect reduces with distance and is also affected by the time of day. To the east, park proximity appears to influence the temperature, which has lower readings than those taken at more distant locations. All distance categories, however, have elevated temperatures during the afternoon. Measurements taken in both southerly and northerly directions indicate the heat mitigation effects of greenspaces such as the park. One data logger located in the south direction recorded anomalous values during post–monsoon, and therefore, all these recordings were removed from the analysis.

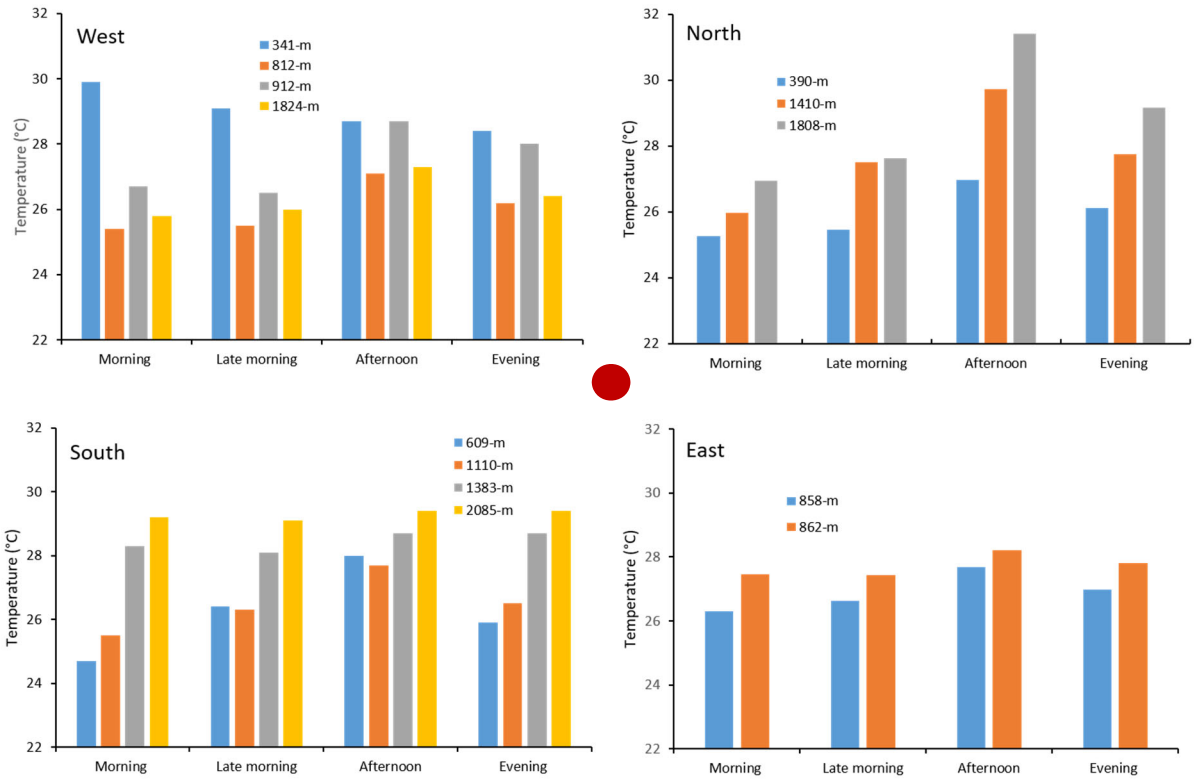

Figure 4–54 Cooling effect of a large greenspace at various distances and directions from a central point. The dark red circle denotes the centre of the park relative to the measuring points

An analysis similar to that carried out for the greenspace was conducted to examine the effect of a blue space on the surrounding thermal environment. The results are presented in Figure 4–55. Proximity to the lake appears to have some kind of heat mitigation effect in three directions

(west, north and east) from the lake centre, however, the effect is not so strong in the southerly direction, particularly at the 916 and 1672 m distance categories. The results also indicate that the cooling potential of the lake diminishes considerably with increasing distance during the four time periods, particularly to the west, east and north; that is, the higher the distance from the lake, the greater the temperature.

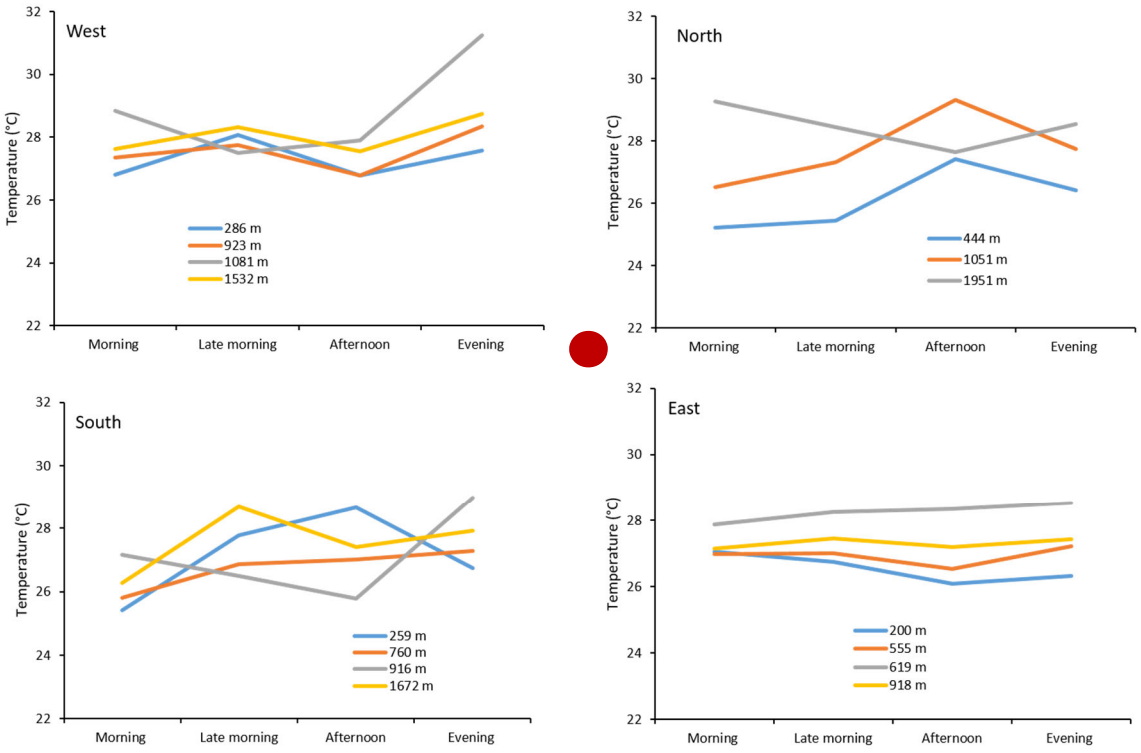

Figure 4–55 Cooling effect of a lake at various distances and directions. The dark red circle denotes the centre of the lake relative to the measuring points

4.12 Intensity of CUHI and SUHI at monthly scale

Monthly data from two fixed weather stations were analysed to determine the intensity of both UHIs (canopy layer and surface). Subtracting monthly rural temperature from urban location enabled a comparison of the magnitude of SUHI and CUHI. The results demonstrated that both UHIs existed in the DMA across the measuring period (January–December 2019), though their magnitude differs according to the months. The February data recorded the maximum (2.04 °C) SUHI intensity, whilst November had negative intensity (–0.14 °C) (Figure 4–56). In contrast, the presence of CUHI can be observed in every month, with the greatest effect being observed in the winter months (1.49, 1.96 and 1.74 °C, in December, January and February), followed by the pre–monsoon months of March (1.63 °C), April (1.31 °C) and May (0.79 °C). Among other months, June (monsoon season), records the maximum intensity (0.64 °C) and October of post–monsoon season records the largest intensity value (1.27 °C) (Figure 4–56).

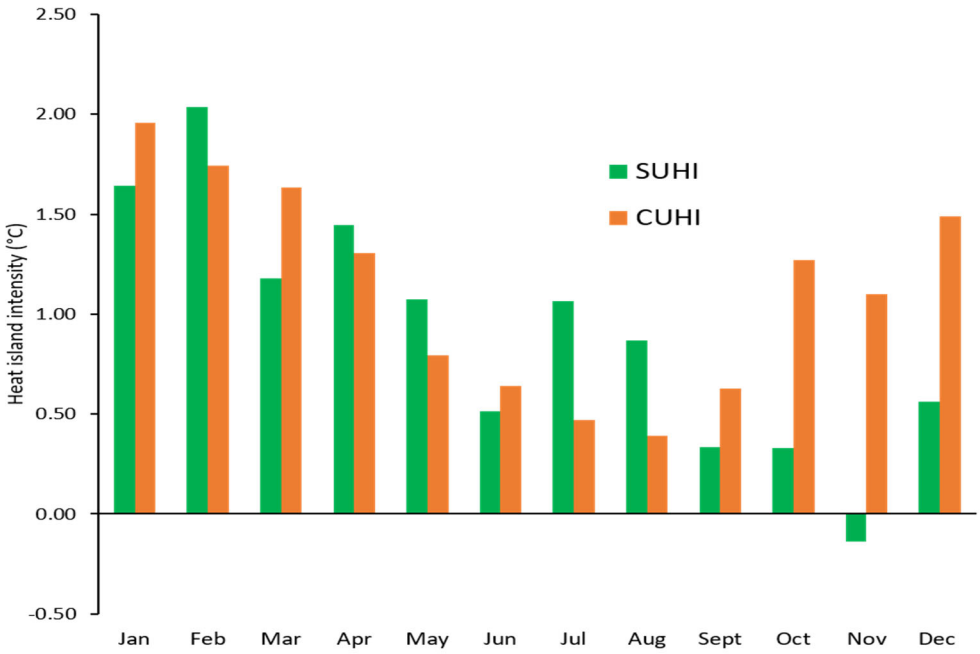

Figure 4–56 Intensity of SUHI and CUHI in the DMA, based on fixed weather stations

4.13 Correlations between UPI parameters and temperatures

Chapter 2 and 3 demonstrated the factors affecting SUHI at the mesoscale and microscale. These factors were developed using satellite–based indicators and anciallry (e.g. population) data. However, this data was unable to determine the elements affecting both canopy layer and surface urban heat islands at the microscale. To provide further information on this, six urban planning indicators were calculated and correlated with traverse–based surface and air temperatures. The results are shown in Table 4–37 (a–c) and Table 4–38 (a–c).

Generally, there appears to be an inconsistent relationship between UPI and surface temperatures measured across the seasons as inferred from bivariate correlation (r) values (Table 4–37, a–c). For example, in the planned zone the relationship between UPI and surface temperature varies depending on time and season (Table 4–37a). In this zone, BCR and BVD seem to play a greater role during winter nights than during the day. GCR shows a negative relationship with temperature during the daytime in summer, however the monsoon/winter day relationship is weakly positive, which is contrary to general expectations (Table 4–37a). BCR shows a significant negative relationship during both the day and night in three seasons in the unplanned zone. During nighttime, however, the BVD shows a positive relationship across seasons, except during monsoon daytime (Table 4–37b). On the other hand, BCR, BVD have a statistically significant negative relationship with temperature during the daytime in the three seasons analysed, but during winter night both urban indicators strongly influence surface temperature in the mixed zone (Table 4–37c). WCR is positively related with temperature

during the daytime of three seasons whereas GCR indicates a negative corelation during monsoon and winter. This analysis suggests that a combination of factors are accountable for the surface temperature variation across seasons in the DMA.

Table 4–37 Correlation coefficients (r) between surface temperature and UPI

a) Planned zone

	Pre–monsoon		**Monsoon**		**Winter**	
UPI	Day	Night	Day	Night	Day	Night
BCR	–.052	0.67	.122	.235	–.478*	.520**
BVD	–.150	0.68	–.084	.387	–.620**	.691**
Aspect	–.480*	0.26	.380	–.163	.374	–.164
SCR	–.152	0.39	–.354	.532**	–.365	.390
WCR	.276	–0.8	–.246	–.271	.359	–.501*
GCR	–.767**	0.36	.402*	.201	.454*	–.086

b) Unplanned zone

	Pre–monsoon		**Monsoon**		**Winter**	
UPI	Day	Night	Day	Night	Day	Night
BCR	–.636**	–.634**	–.409*	–.579**	–.453*	–.661**
BVD	.535**	.698**	.014	.887**	.505*	.843**
Aspect	–.080	–.417*	.279	–0.187	.563**	–.104
SCR	.417*	.124	.538**	.353	0.546**	.285
WCR	–.291	–.379	–.016	–.447*	–.400*	–.325
GCR	*.497	.452*	0.427*	.220	.071	0.264

c) Mixed zone

	Pre–monsoon		**Monsoon**		**Winter**	
UPI	Day	Night	Day	Night	Day	Night
BCR	–.537**	.214	–.785**	–.471*	–.703**	.736**
BVD	–.662**	.137	–.661**	–.308	–.646**	.780**
Aspect	.066	–.114	.187	.051	.147	–.314
SCR	–.166	–.675**	.022	.421*	.417*	.006
WCR	.468*	–.217	.675**	.471*	.692**	–.536**
GCR	.130	.154	–.087	–.410*	–.380	–.335

** Significant at the 0.01 level (2–tailed); * Significant at the 0.05 level (2–tailed)

The canopy layer heat island tends to be influenced by a number of variables in a manner similar to surface temperature, as shown in Table 4–38 (a–c). In the planned area, GCR seems to play a vital role in affecting CUHI in the pre–monsoon (night), monsoon (night) and winter (day/night), whilst other indicators such as BCR, BVD, SCR are largely inconsistent (Table 4–

38a). In the unplanned zone, GCR shows a consistently negative relationship with air temperature, whereas aspect, SCR and WCR appear to have some sort of relationship, affecting day and nighttime temperature (Table 4–38b). Conversely, the influence of UPI on air temperature demonstrates that BCR, BVD, GCR and WCR have both a positive and negative relationship with temperature in the mixed zone, which generally depends on the time of day (Table 4–38c).

Table 4–38 Correlation coefficients (r) between air temperature and UPI

a) Planned zone

	Pre–monsoon		**Monsoon**		**Winter**	
UPI	Day	Night	Day	Night	Day	Night
BCR	–.191	.267	.384	.511**	.068	–.666**
BVD	–.376	.182	.265	.379	–.078	–.583**
Aspect	–.002	–.646**	.305	–.413*	.034	–.135
SCR	–.211	–.116	–.146	.137	.103	–.625**
WCR	.210	.008	–.451*	–.324	–.052	.709**
GCR	–.351	–.779**	.016	–.640**	–.424*	–.044

b) Unplanned zone

	Pre–monsoon		**Monsoon**		**Winter**	
UPI	Day	Night	Day	Night	Day	Night
BCR	.266	–.193	.808**	–.196	.5	0.243
BVD	–.201	.762**	–.592**	.816**	–0.917	0.593
Aspect	.385	.196	–.066	–.262	0.091	0.184
SCR	.639**	.654**	–.041	.462*	–0.219	0.617
WCR	.429*	–.057	.424*	0.144	0.494	0.046
GCR	–.321	–.322	–.551*	–.236	–0.076	–0.733

c) Mixed zone

	Pre–monsoon		**Monsoon**		**Winter**	
UPI	Day	Night	Day	Night	Day	Night
BCR	.328	.318	–.534**	.634**	.004	.712**
BVD	.489*	.512**	–.477**	.792**	–.074	.712**
Aspect	–.226	–.236	.122	–.376	–.021	–.260
SCR	.086	.222	–.186	.031	–.566**	–.461*
WCR	–.218	–.201	.525**	–.432*	–.014	–.612**
GCR	–.210	–.314	–.147	–.409*	0.278	.177

** Significant at the 0.01 level (2–tailed); * Significant at the 0.05 level (2–tailed)

4.14 Discussion

Fixed station measurements of urban and rural temperatures recorded during the four seasons (winter, pre–monsoon, monsoon and post–monsoon) indicated that surface temperatures were consistently higher in the urban areas than in the rural locations (Figures 4–6, 4–21, 4–36, 4–51). This supports the findings of the satellite–based estimation, explained in Chapters 2 and 3. High surface temperatures in the urban location may result from a combination of urban morphology, building density, sky view factor, population distribution and vegetation abundance (Li and Li, 2020; Ferreira and Duarte, 2019; Son and Thanh, 2018; Mushore et al. 2017; Trlica et al. 2017; Doick et al. 2014; Zheng et al. 2014; Hathway and Sharples, 2012). The larger amounts of vegetation in the rural areas have a greater evaporative cooling potential than the small and scattered vegetated areas found in urban areas and, as a result, the SUHI is weaker in rural settings than in urban locations (Drach et al. 2018; Coseo and Larsen, 2014). Furthermore, soil moisture differs substantially between these two areas, a key factor modulating thermal interaction between surface and atmosphere, and the associated diurnal temperature range (Martilli et al. 2020; Imamura, 1993). The air temperature data for urban and rural locations also showed an interesting pattern (Figures 4–6, 4–21, 4–36, 4–51, Tables 4–6, 4–16, 4–26, 4–36). Though timing of CUHI intensity varies between seasons, generally the afternoon to late evening experiences high CUHI with an air temperature which can be 2–3 °C higher in urban areas than in rural areas. This is a feature common in South Asian cities (Kotharkar and Surawar, 2015). These results suggest that the spatio–temporal pattern of a CUHI may be another area of future research, since this phenomenon can also seriously impact energy and water consumption, and levels of human comfort (Tan et al. 2013).

Traverse surveys in the three defined zones (planned, unplanned and mixed) during winter, pre–monsoon and monsoon showed that air temperatures were higher in planned zones in winter and pre–monsoon, but lower during the monsoon (Figures 4–9, 4–24, 4–39). In the unplanned zone, pre–monsoon values recorded the highest air temperature whilst the mixed zone exhibited the lowest temperature in the three seasons compared with the other two zones. Note, however, that the intensity varies between the seasons and the specific locations measured (Figures 4–11, 4–26, 4–41). This may possibly be related to the existence of large waterbodies with differing thermal inertia characteristics in some zones. Moyer et al. (2017) observed that a river feature could enhance UHI during the nighttime by increasing local humidity levels. Hathway and Sharples (2012) note that the cooling effect of a river is usually highly pronounced during the day in close proximity to waterbodies, and tends to increase at midday. Differing land–use categories, in association with water bodies, may be another factor affecting the observed nighttime temperature of an area (Hart and Sailor, 2009). These factors may possibly be in play in the mixed land use zone. In regards surface temperature, the mixed land use zone had a higher temperature, on average, during the winter season when compared with the other two zones (Figure 4–10). In contrast, the planned zone data recorded a more elevated temperature in the pre–monsoon and monsoon seasons (Figures 4–25, 4–40) in

comparison to the other two sites. The average surface temperature across the seasons revealed that the unplanned zone experienced higher temperatures during the monsoon season (Figure 4–40).

To examine any causal factors associated with high air and surface temperatures which may influence the microclimate, three meteorological variables (wind speed, solar radiation and relative humidity) were correlated with air/surface temperatures (Tables 4–7, 4–17, 4–27). The results showed that relative humidity is the main factor affecting the general microclimate of the DMA. The relationship between relative humidity and temperature is well–known and is related to the fact that warm air can hold a greater volume of water than cool air. This factor appears to have affected temperatures significantly in the three traverse routes examined. It also appears that wind speed has a negligible impact on temperature as evidenced by the weak correlation figures (Tables 4–7, 4–17, 4–27). This study observed that wind speed is higher in urban site than rural location in every season analysed, possibly another factor accounting for the higher temperature in Dhaka and the resulting UHI. Balling and Cerveny (1987) report that atmospheric stability reduces with the growth of an UHI and, as a result, local wind speeds increase in the city area, particularly at night. A striking feature is that wind direction appeared to be diametrically opposite during three seasons, except winter, in Dhaka megacity. This may have a significant impact on the UHI growth, as opposite wind directions would not be able to dissipate heat effectively or advect rural wind (Nichol et al. 2009), an essential component in any system with the potential to reduce heating (Hsieh and Huang, 2016). Apart from these factors, others, such as urban morphology, pervious land areas, population density, vegetation cover, sky view factor, waste heat from buildings and transport sectors, factors which differ from location to location, have also been shown to influence surface temperature of a city, regardless of its size and geographic location (Rodríguez et al. 2020; Li et al. 2019; Giridharan and Emmanuel, 2018; Shiflett et al. 2017; Coseo and Larsen, 2014; Lazzarini et al. 2013; Zheng et al. 2014). All of these, in isolation or in combination, are probably accountable for SUHI and CUHI phenomena in Dhaka megacity.

Previous work identified that thermography is an effective technique for measuring the cooling rate of different urban features (Hamoodi et al. 2019; Hartz et al. 2006). The thermo–physical assessment undertaken indicated differing cooling rates for the various urban features (e.g. Tables 4–9 to 4–11 for the winter season). For example, the green glass–coated building tended to cool early. This was followed, in turn, by grey glass building, plastic billboard, mirage tin rooftop and the plastered building wall in the planned zone. Even though glass showed a high cooling rate per hour, it tended to warm faster than any other object identified in this work, a fact which may be related to the thermal conductivity of the feature (Synnefa et al. 2006). It was noted that the CR varies substantially depending on feature types and their proximity to other objects, particularly between the sites. The results are useful in understanding the variability of the cooling rates of features measured between the surveyed sites. Based on an analysis of 88 thermal images from every season, it was found that the sunlit side of a feature,

solar angle, daylight intensity, time of imaging (Chudnovsky et al. 2004), spacing/arrangement/height of buildings, abundance of vegetation, proximity to waterbodies, orientation of features and traffic load are all factors which need to be considered when determining the cooling rate of individual features. Feature capture by thermal camera may also affect the temperature of the features being imaged.

The results of analyses of the rooftop with or without garden were quite distinctive (Figures 4–13, 4–28, 4–43). The rooftop with garden appears to have a temperature more than 4 °C lower than the rooftop without garden in the winter, and 2 °C lower in the monsoon season, however its efficacy diminishes during pre–monsoon. The effectiveness of rooftop gardens in lowering temperatures in urban areas indicated that these have the potential to play a very large part in any UHI mitigation measures (Dwivedi and Khire 2018; Jim, 2015; Chatzidimitriou and Yannas, 2015; Wong et al. 2010, 2003; Hien et al. 2007). Among the vegetation types used on DMA rooftop areas, the *Combretum indicum* plant is shown to have a higher cooling potential than species like *Bougainvillea*, *Psidium Guajava, Maltes*, and *Citrus Limon* (Figures 4–15, 4–30, 4–45). The differences in thermal response, however, depends on the canopy cover and crown depth (Susca et al. 2011; Wong et al. 2010). The *Combretum indicum* species has a relatively large canopy cover with dense leaves, so this may explain the usefulness of the plant in reducing heat when compared with other plant species.

An examination of open space plant cooling potential revealed that the *Barringtonia* species has the greatest potential in regards environmental temperature reduction. This is followed in turn by *Loha kat*, *Earleaf acacia*, *Beharda*, *Teak*, (Figures 4–16, 4–31, 4–46). The *Barringtonia* is a mangrove species, so it is assumed that the evapotranspiration capacity of this species is high and can explain the observed cooling potential. However, this plant grows in close proximity to waterbodies so the widespread use of *Barringtonia* will probably not be possible in many locations in the urban environment, particularly in Dhaka. *Beharda* has a lower temperature reduction potential, followed by *Teak* plants. Including the use of these species in planning regulations could assist in mitigating the effects of increasingly–elevated urban temperatures. The amount of leaf, canopy cover and dense crown can all assist in the cooling effect of plants as shown by Feyisa et al. (2014).

An evaluation of the thermal response of a green hanging wall showed that ambient temperature varied between 1 and 3 m distance from the wall, depending on the season, but the cooling effect decreases with increasing distance from the wall as expected (Tables 4–13, 4–23, 4–33). The effectiveness of hanging wall features is documented elsewhere (Tan et al. 2014; Cameron et al. 2014). A shortcoming of the experimentation is that the methods by which circulation affected ambient temperature at various distances from the substrate could not be adequately determined. This observation needs to be examined in more detail as air circulation is said to moderate environmental temperatures (Wong et al. 2010). Other factors such as

canopy density and the materials used to construct the green wall could all affect the temperature variability of such systems.

Despite the fact that green and blue spaces have been found to be effective in reducing the temperature of the urban environment (Lin and Lin, 2016; Chang and Li, 2014; Onishi et al. 2010), the results of the current work are inconclusive. With regard to the cooling effect of green and blue spaces by direction and distance, (e.g. Figures 4–19, 4–20) urban canyons, street geometry (Shashua–Bar and Hoffman, 2003; Oke, 1988), land use of an area (Hart and Sailor, 2009), direction of the prevailing wind (Ca et al. 1998), spatial arrangement (Lin and Lin, 2016), season and timing of the day (Onishi et al. 2010) and local thermal environment (Chang and Li, 2014) may all have a significant influence on the ability to effectively cool an area. The spacing of trees, their types and patch size are other important determinants (Lin and Lin, 2016).

The relationship between UPI and air/surface temperature over the three seasons examined showed generally inconsistent results (Tables 4–37, 4–38), with a tendency to also vary between the day and night periods. Though few of the indicators showed a consistent relationship with both air and surface temperatures, this inconsistency may have resulted from variation introduced by the different traverse routes (Nichol and Wong, 2008), as well as by urban geometry and morphology (Guo et al. 2016). Traverse routes in the three locations were not uniform and spatial heterogeneity was highly variable. As a result, the landscape configuration and composition were dissimilar, which may have greatly influenced local temperatures (Li et al. 2016). Furthermore, whilst UPI variables are static, temperatures are dynamic.This may be a possibble cause of the inconsistencies found in the results, a factor which has also been reported by Nichol (1996). Local morphology (e.g. building density, materials) also appears to influence the microclimate significantly (Chandler, 1967), while factors such as dissimilar building heights, for instance, can influence wind flows in urban areas (Huang et al. 2019; Peng et al. 2019; Yang and Li, 2015; Rajagopalan et al. 2014). Anthropogenic heat, which was not used in this work, is also shown to have a substantial impact on the variation of day and nighttime temperatures of a large city (Rodríguez et al. 2020).

4.15 Conclusion

This chapter demonstrated microclimatic conditions in the DMA, based on in–situ measurements collected during the period of this study. Diurnal variability at the seasonal scale was the main way of analysing data to determine the temporal patterns of SUHI and CUHI. The study characterised the UHI but also looked at the ability of such features as rooftop gardens, open space plants, dominant rooftop vegetation and green/blue spaces to reduce ongoing heating effects. Major findings of the chapter are:

- The temperature was consistently higher across seasons in the urban area when compared with the rural site. At a seasonal scale, the average CUHI intensity was greater in winter (1.73 °C) followed by pre–monsoon (1.24 °C), post–monsoon (1.19 °C) and monsoon (0.53 °C) periods. Likewise, the intensity of SUHI was highest in winter (1.46 °C) followed by pre–monsoon (1.23 °C), and monsoon (0.70 °C) and lowest in the post–monsoon (0.09°C). At the monthly scale, February had the highest SUHI (2.04 °C) whereas January showed the greatest CUHI (1.96 °C).

- Results from the three traverse surveys indicated that the planned zones within the DMA experienced elevated air temperatures during the winter and pre–monsoon periods, while the unplanned site showed higher temperatures during the monsoon as compared to the other two sites (unplanned and mixed zones). In terms of surface temperature, the planned site recorded much higher temperatures during the monsoon and pre–monsoon than the other two sites, whereas the mixed land use zone had a higher SUHI during winter than the planned and unplanned sites.

- The thermo–physical behaviour of various urban features demonstrated that cooling rates can vary significantly depending on feature types. Glass coated buildings seemed to influence the daytime temperature of the immediate environment, while neon signs and billboards could significantly affect nighttime temperature.

- Rooftop garden showed huge potential in the ability to reduce urban heat during winter and monsoon seasons, however its effectiveness was seriously curtailed during the pre–monsoon due to the impacts of waste heat generated form air conditioners being used in the surrounding buildings.

- Among the open space plants examined, *Barringtonia* exhibited the greatest potential to mitigate urban heat generation during winter, while *Earleaf Acacia* could be useful in the pre–monsoon season. These are the two seasons when high SUHI and CUHI were recorded in the DMA.

- Experiments conducted with the commonly used rooftop plants indicated that *Combretum indicum* could be useful in reducing urban temperature and may also provide insulation to buildings.

- Green vertical walls have the potential to provide daylong benefits in regards heat mitigation, however, the role of parks and lakes in reducing temperature was largely inconclusive.

5 GREENSPACE SUITABILITY AND BUILDING RETROFITTING

5.1 Introduction

A number of mitigation measures have been proposed to reduce the increased warming of urban areas around the world. Among these measures, the use of green infrastructures has possibly the most potential for mitigation, though it should be noted that the effectiveness of using green infrastructure is dependent on local climatic conditions (Saaroni et al. 2018; Saneinejad et al. 2014; Bowler et al. 2010). This chapter provides some detail on greenspace distribution in the DMA area, followed by an evaluation of potential green roof retrofitting, and how "greening" of existing rooftops can assist in mitigating urban heating effects. In addition, suitable locations for greenspace development are explored.

5.2 Greenspace mapping

A database was constructed using parks, gardens, graveyard and playgrounds officially designated by local governments as greenspaces. During the initial data capture process, the entire DMA was divided into eight segments. A Google Earth image was used and heads–up digitising was performed on each segment. A completed, digitised Keyhole Markup (KML) file was then transferred to a mobile device (e.g. iPad) for field verification. Two key attributes (name/type and major surface cover) were recorded at each site. Once ground truthing for a segment was complete, corrections were made to the original database using desktop GIS software. A total of three months were required to complete the digitisation and field verifications of the eight segments.

5.3 Suitability of greenspace

The term greenspace generally refers to such things as parks and reserves; protected areas or areas of undeveloped, vegetated land located within the urban landscape, which have been set aside for recreational, ecological, environmental or aesthetic reasons. Due to the pace, extent and limited planning frameworks in which urban development has taken place across Dhaka city and surrounds, the current amount of greenspace is very limited. In the context of locating suitable areas for use in any urban heating mitigation strategies, this limited availability of suitable areas (especially around the main urbanised areas), is a major challenge.

Various datasets have been obtained for this study to assist in assessing the greenspace potential in the DMDP area. There have been issues with the ability to use some of the larger datasets efficiently and effectively in the GIS due to the intensive computing requirements involved. This refers particularly to the third–party RAJUK vector dataset. This very detailed dataset is understood to have been corrected; however, there have been issues in task completion when

attempting to use some of the more advanced GIS tools. These issues have not been resolved (despite the use of various dataset correction techniques) and will require input from the dataset providers. Due to these issues, the current work used land use/cover information from the 2017 raster classification dataset (30 m resolution), which has previously been reported (see Chapter 2). The development of a greenspace is essentially low impact and does not involve much construction or engineering work (apart from the possible provision of administration/maintenance buildings).

The potential for further development of greenspace is very limited within the highly urbanised DMA area, and defining any suitable areas is therefore very challenging. Unfortunately, the urbanised area is also where the impact of the UHI is greatest and the benefits of any greenspace would be maximised. The current work provides a higher–level assessment of other areas within the larger DMDP (Dhaka Metropolitan Development Plan), which may be suitable for the establishment of greenspace. It should be borne in mind however that the mitigation effects of a greenspace would be greatest nearer to urban areas.

The existing land use/cover categories have been developed based on an initial assessment of suitability. Three categories of land identified from the land use/cover assessment have been flagged as not suitable. Built–up areas, waterbodies (such as rivers), and cultivated land have all been removed from any further assessment. Those areas which will be looked at in more detail include vegetated areas, wetland/lowlands and bare landcover. Defined vegetation, which is mainly found in the north–east and extending along the eastern boundary of the DMDP, includes substantial areas of forest plantation. Wetland/lowland areas have the potential to be inundated during the monsoon season as flooding is a persistent problem in Bangladesh, and are generally not suited for normal development although they may have some potential as a greenspace. Areas of bare land are found at various locations within the DMDP with many being the result of ongoing clearing for subdivision, urban development and various construction–related activities.

5.4 Evaluation of green roof retrofitting

In this study, the building dataset for Dhaka compiled by RAJUK was utilised to gain an initial understanding of the potential suitability of structures in the DMA area for green retrofitting (http://www.rajukdhaka.gov.bd/rajuk/webHome). The basic structural requirements for the buildings were as follows:

- To be constructed of “pucca” i.e. concrete

- The number of floors to be limited to four and below. This “low” building definition

was based on the ability of a structure to support any retrofitting work, including ease of access

- To be located outside a buffer area from "tall" buildings (to avoid overshadowing effects). Two alternative buffer areas were used (50 and 100 m)

- Selection of areas (i.e. rooftops) recording a temperature exceeding a calculated average yearly solar insolation of 1,565,198.3 W/m^2

All buildings within the DMA boundary, which were made of pucca (concrete), and having a recorded number of floors equal to or below 4, were selected. Two processing options were used for these "low" building: i) those with <=3 floors; and ii) those with <=4 floors. All "tall" buildings (those over the selected floor height) were buffered at two defined distances (50 or 100 m) to mimic any possible overshadowing affects these buildings would have on the lower buildings, and as a result, on any rooftop garden. All "low" buildings were removed from within this buffer area. The remaining buildings were those, which were low and theoretically not impacted by any possible overshadowing affects.

A digital elevation model (DEM) with 20 m spatial resolution, also obtained from RAJUK, was used to determine the incoming solar insolation. The average solar area for the area was calculated using the GIS Area Solar Radiation tool (https://desktop.arcgis.com/en/arcmap/10.3/tools/spatial-analyst-toolbox/an-overview-of-the-solar-radiation-tools.htm). This tool calculates insolation based on methods from the hemispherical viewshed algorithm developed by Rich et al. (1994) and further developed by Fu and Rich (2000, 2002). The total amount of radiation calculated for a particular location or area is given as global radiation. A mean insolation value was calculated for the whole area. The solar radiation data calculated for the individual buildings was then joined to the associated building floor data file, and all buildings with a temperature exceeding the average solar insolation were selected (http://desktop.arcgis.com/en/arcmap/10.3/tools/spatial-analyst-toolbox/how-solar-radiation-is-calculated.htm).

5.5 Results

5.5.1 Distribution of greenspaces

A total of 321 greenspaces have been identified within the DMA boundary, of which 68% have been verified in the field. This includes all medium to large greenspaces. A summary of these areas is given in Table 5–1 and their spatial distribution is shown in Figure 5–1.

Table 5–1 Characteristics of greenspace types

Greenspace type	Surface cover	Number	Mean area (ha)	Percent (%)
Garden	Grass (with/without)	6	0.52	1.9
Graveyard	Full/partial grass	9	6.82	2.8
Park	Little to no grass	88	4.72	27.4
Playground	Grass, sand and no grass	218	1.10	67.9
Total		**321**		**100.0**

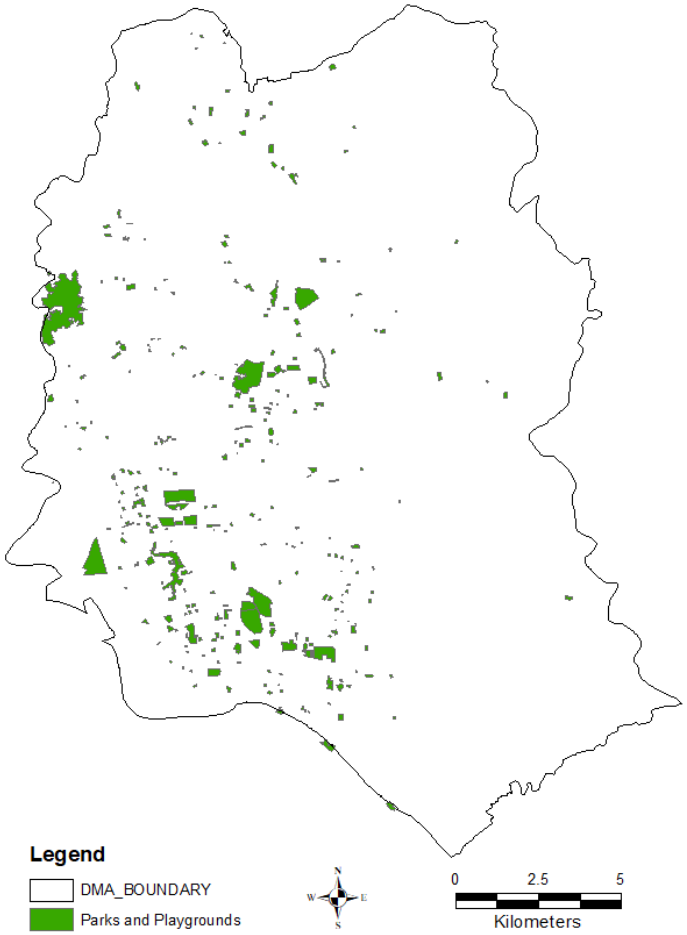

Figure 5–1 Distribution of greenspaces in DMA

The area of individual greenspace areas ranges from 0.3 to 146 ha in size, with an average of 2.25 ha. Based on surface cover, the identified greenspaces have the following properties, 16 (4.9%) are fully covered with grass, 1 (0.3%) has artificial grass, 1 (0.6%) has bush, 63 (19.6%) are partially covered with grass, 45 (14.0%) have sparse grass cover, 188 (58.6%) have no grass, 4 (1.2%) consist of sand and 3 (0.9%) were under renovation at the time of the ground truthing.

5.5.2 Suitable locations for greenspace

The total area of the individual classes of land use chosen to use in the process, as well as the percentage as compared to the total DMDP area of 1,464 km^2, is shown in Table 5–2. The locations of these areas are shown in Figure 5–2.

Table 5–2 Potential greenspace areas suitable for assessment

Land use/cover class	Area (km^2)	Percent (%)
Bare land	82.23	5.6
Wetland/lowland	18.26	1.2
Vegetation	90.45	6.1

Following the initial assessment, a number of variables were selected to further define suitable areas. In order to demonstrate the capability of the process, the following variables and values were considered:

- Underlying geology – this was assumed to have no or little impact on suitability so no geology data was utilised

- Slope – the study area is located predominantly in a low–lying deltaic environment, with sporadic, short slopes in the order of 24° maximum. Most of the area is essentially sub–horizontal in nature and so the influence of slopes on suitability was not given any weight

- Elevation – this is regarded as a major factor requiring inclusion in the suitability selection to effectively remove areas with possible flooding issues such as in the wetland/lowlands. The main waterbodies had already been removed from any calculations. Elevations > 5 m were thus selected

- Population density – this data was used to assess the potential customer base, i.e. those users willing to access and utilise the greenspace from the surrounding population catchment area. This was regarded as particularly important, if the greenspaces were to have any commercial potential. Population density of 2011 was subdivided using a natural breaks algorithm and a density (persons/km^2) of >23,668 (categorised as medium density) used as a threshold. No specific distance to population centre criteria were used so as to broaden the capture field

- Roads – the location of roads was to be used to define a maximum distance from a main road (national and regional highway, secondary/tertiary) for access, however there were issues with the vector file road and centreline attribute data, so this feature was not able

to be incorporated into the selection process. The location of a road within a potential greenspace area was not regarded as an issue at this level of assessment

ArcGIS (v. 10.6) Spatial Analyst tools were used in the raster processing – initially using the land use areas shown in Figure 5–2, then selecting by elevation, and finally by population. Statistics on the area were then generated. Table 5–3 provides information on the variables used and Figure 5–3 provides the finally defined locations.

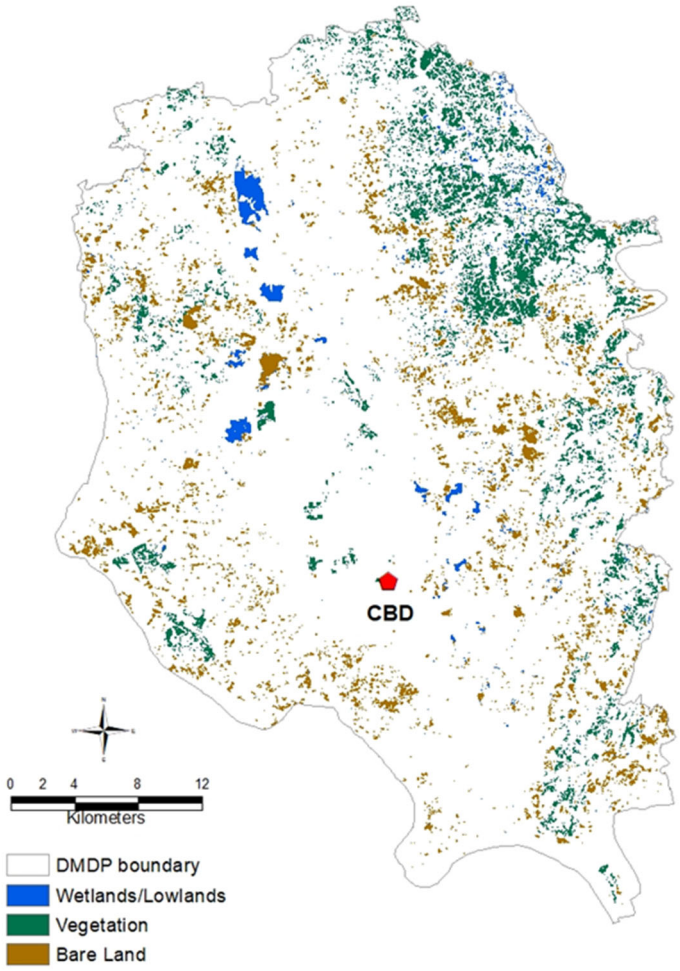

Figure 5–2 Location of potential greenspace areas within the DMDP

Using the above criteria, the selection process returned only nine discrete locations with areas greater than 10 ha. The maximum area recorded was 33 ha. The selected locations totalled 810 ha of recorded pixel values from a total area of 142,565 ha. This equates to approximately 0.6% of the available area. To assess the accuracy of the process, alignment with the original classified raster file and any possible issues with the processing, a base–map (ca. 2015) of the DMDP area was displayed in the GIS, and the generated areas overlain to provide a visual

check of the selected locations, and determine the relative accuracy of the final image as compared to the ground features.

Table 5–3 Selected variables used in the suitability process

Variable	Units	Range	Value used
Elevation	metres	0 – 23.2	>5 m
Population density	persons/km^2	<8,768 8,768 – 23,668 23,668 – 44,259 44,259 – 77,727 >77,727	>23,668

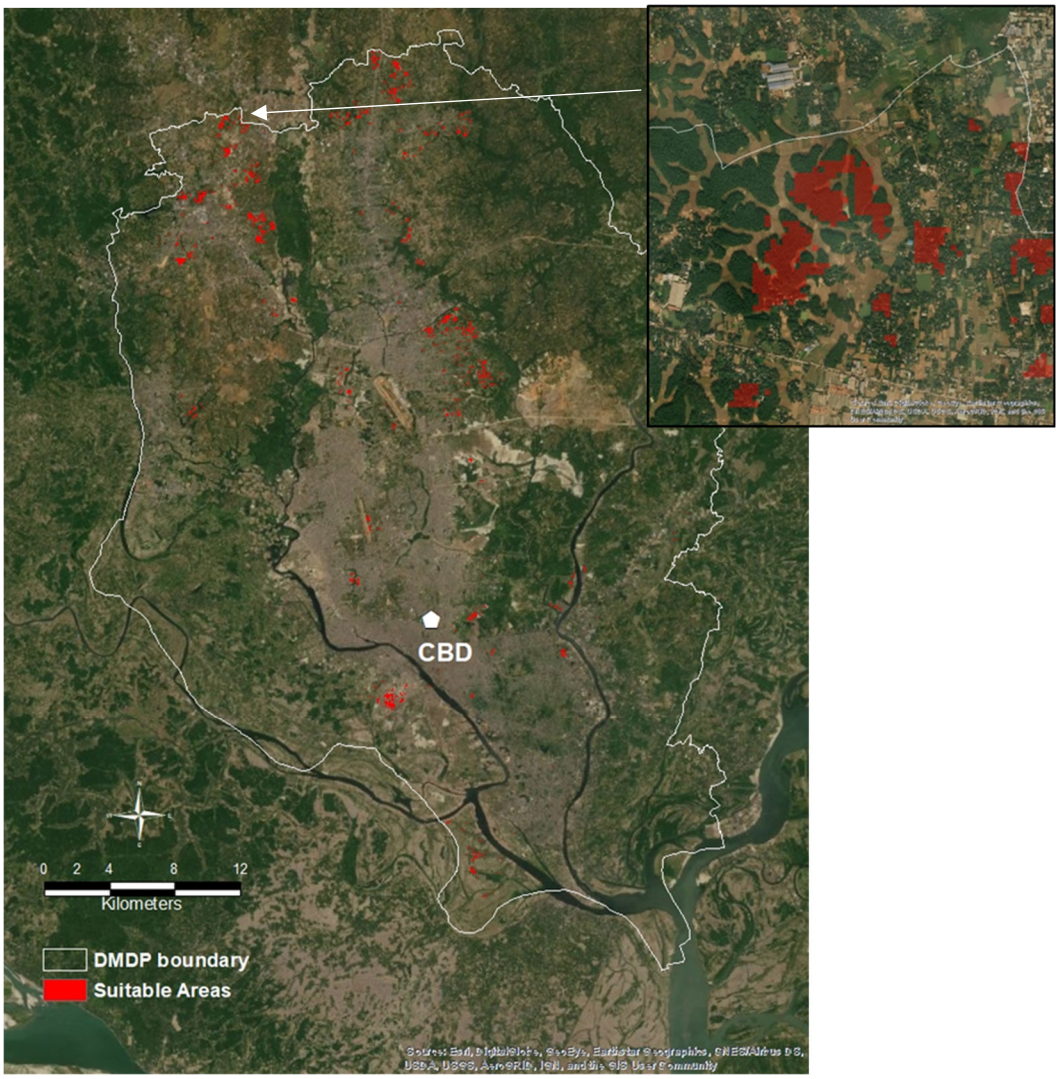

Figure 5–3 Location of final, potential greenspace areas within the DMDP (inset shows an example of area selected based on the criteria)

5.5.3 Building suitability for green roof retrofitting

The total number of buildings recorded within the DMA area in the original dataset was 681,216. Of these, the total number of structures constructed of concrete was 267,157. The average roof area of all buildings within the DMA area was 152.1 m^2. Figure 5–4 shows the location of suitable rooftops for potential greenspace retrofitting in locations outside each defined buffer area. Table 5–4 provides general details of the GIS processing results, indicating the two models used and some information on building numbers and roof area.

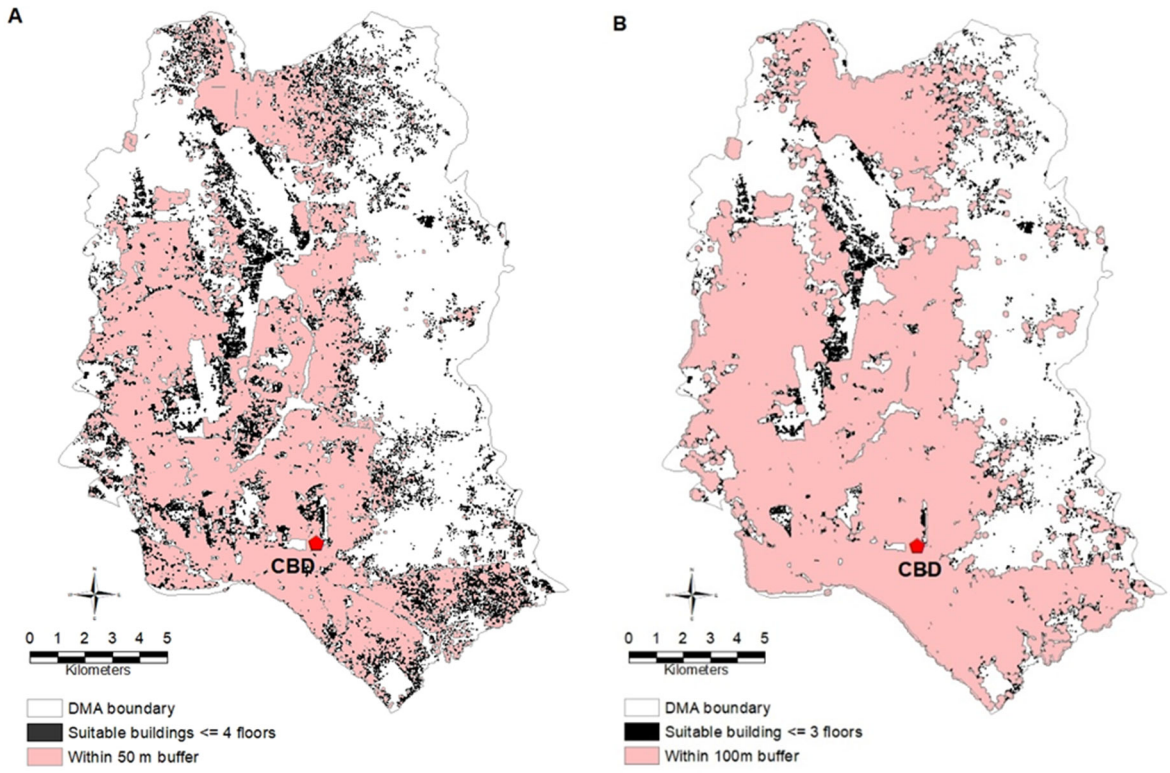

Figure 5–4 Location of rooftops (black areas) with potential for greenspace retrofitting outside areas of possible overshadowing: a) 50–m buffer around tall building; b) 100–m buffer around tall buildings

The two "low" building models obtained from the above process were examined in more detail to provide a breakdown of the percentage of buildings available according to floor number (Table 5–5). As expected, the majority of the buildings are one or two stories.

Table 5–4 Details of building/floor and buffer distances

Building (floors)	Buffer distance (m)	Pucca & floors		Outside buffer		Buildings > 1565198 (WH/m^2)		
Low		Count	%*	Count	%	Count	%	Roof**
<=3	100	148,621	21.8	14,524	2.1	8,855	1.3	232.4
<=4	50	182,744	26.8	42,856	6.2	28,255	4.1	157.1

*As a percentage of total DMA buildings; **mean roof area in m^2

Table 5–5 Details of "low" buildings outside the designated buffer distance (by floor)

Floor no. and building counts	Buffer distance (m)	Floors	Buildings (counts)	Buildings (%)
<=3	100	1	10,347	71.2
(14,524)		2	3,255	22.4
		3	922	6.3
<=4	50	1	22,002	51.3
(42,856)		2	12,901	30.1
		3	5419	12.6
		4	2,534	5.9

5.6 Discussion

The distribution of greenspaces in the DMA has been mapped (Figure 5–1) and it is clear that the per capita greenspace (the total greenspace number and area taking the total population of DMA into account) is far too low. There are only 321 greenspaces distributed over the DMA, giving a combined area of 723 hectares (7.23 km^2), and therefore, making up only 2.41% of the DMA area of 300 km^2. As Dhaka is continuing to expand into previously undeveloped, low–lying areas and this will continue into the foreseeable future, the construction of more greenspaces is considered to be a tool to use in mitigating any adverse effects. These can act as cool–islands during UHI occurrence (Doick et al. 2014; Chang and Li, 2014; Chang et al. 2007). They can also support the sense of physical and emotional well–being experienced by the population and assist in supporting the comfort levels expected by the citizens.

A high–level assessment was conducted to determine potential greenspace sites within the DMDP. The 2017 land use/cover data developed for this study was used, with potentially suitable bare land, wetland /lowland and vegetated areas making up approximately 13% of the total available lands. Further, proof–of–concept work on these using a number of selected variables (=>5 m elevation and > 23,668 persons/km^2 population density) defined an area of approximately 800 ha which was potentially viable. This comprised 0.6 % of the total DMDP area, and is very fragmented. Further work is required to ensure that the data output is fit–for–

use. This includes obtaining a corrected vector dataset from the relevant government agency in Bangladesh.

Any retrofitting (or adding) of green infrastructure into the existing fabric of cities has its challenges. In regards rooftop greening, the basic questions to look at are the potential of existing buildings to accommodate a retrofitted green roof and how many buildings are actually suitable for this addition. Baseline suitability criteria relate to the building construction materials (to support retrofitting work), the height of buildings (a maximum height being defined due to increasing logistical/access issues arising with increasing height as well as weight limitations) and the ability of the roof area to provide sufficient light for plant growth (minimal overshadowing affects by other buildings). Secondary criteria which impact on the basic building suitability include such things as amount and type of infrastructure on the roof, including HVAC (heating, ventilation and cooling) systems, structure position, location, orientation and pitch of roof as well as maintenance requirements (Wilkinson and Reed, 2009).

A general assessment of green roof retrofitting revealed that the assumptions made on the overshadowing effects of tall buildings adjacent to potential retrofitting sites (those with 4 or less floors) substantially impacts the number of buildings potentially available for retrofitting. Buildings recording a solar insolation component greater than the overall building average make up 1 and 4% of the total buildings in the DMA area. These buildings are considered potentially suitable for retrofitting. Research is required to further define the structural suitability of individual buildings that have been identified using the initial GIS analysis and assess the requirements for more detailed work on the overshadowing effects using more appropriate architectural procedures. The use of building information modelling software may allow more accurate determination of factors such as sun path, sun angle, shadowing and any other effects impacting on the ability to retrofit a building.

5.7 Conclusion

This chapter presented the distribution of greenspaces together with a general assessment of buildings suitable for green roof retrofitting. In addition, greenspace suitability analysis was carried out. The results revealed that only 321 variable–sized greenspaces exist (2.41% of the DMA), which is too low for the huge population–base. The analysis indicated that potential buildings make up 1 to 4% of the total buildings in DMA. Further, a study of suitable locations for greenspace developed identified an area of approximately 800 ha which was potentially available within the wider DMDP area, although the individual areas were small and widely dispersed, and included areas which were possibly of a commercial nature (plantations).

6 COST–BENEFIT ANALYSIS OF GREEN INFRASTRUCTURES (GI)

6.1 Introduction

A cost–benefit analysis (CBA) is a method used to compare the total costs of a programme/project with any benefits generated. This commonly uses monetary units and enables the calculation of the net cost or benefit associated with the programme. This chapter demonstrates a cost–benefit analysis of GI in the DMA which was undertaken as part of this work. A survey was conducted to determine the costs and benefits of private greenspaces. This included interviewing representatives of both private households and corporate buildings. Additionally, users of public green/blue spaces were interviewed to determine their perceptions regarding possible ideas on service improvements.

6.2 Selection of samples

Samples were selected from two sources. First, a list of households and corporate bodies who had actually implemented GI at their premises was collected from the Green Savers Association (https://www.thegreensavers.org). This association is a private organization providing various services, such as rooftop/indoor/vertical gardening and landscaping, to households and corporate offices in the DMA. The second source was the use of personal contacts obtained from one of the team members involved in this work. Consent was obtained for people to participate in the survey process. Four percent of people contacted were not willing to participate in the survey. In the event that a household/corporate head was absent, a second person with authority to speak about financial and other matters was interviewed. A total of 100 households/corporates (representing 94 residential and 6 corporate buildings) were finally interviewed (Figure 6–1).

A structured questionnaire was developed, and subsequently approved by the Curtin University Ethical Committee, for use in the survey. The questions canvassed such topics as demographic characteristics, perceptions about the role of greenspaces in reducing urban temperature, and any perceived benefits of adopting green infrastructures. In addition, individuals were asked about the costs of installed greenspace at their premises, and if they were willing to pay for green infrastructures. The respondents were also asked to assign a monetary value to greenspace components, which they regarded as beneficial. The survey was conducted from June to September 2019 and each interview took roughly 20–30 minutes.

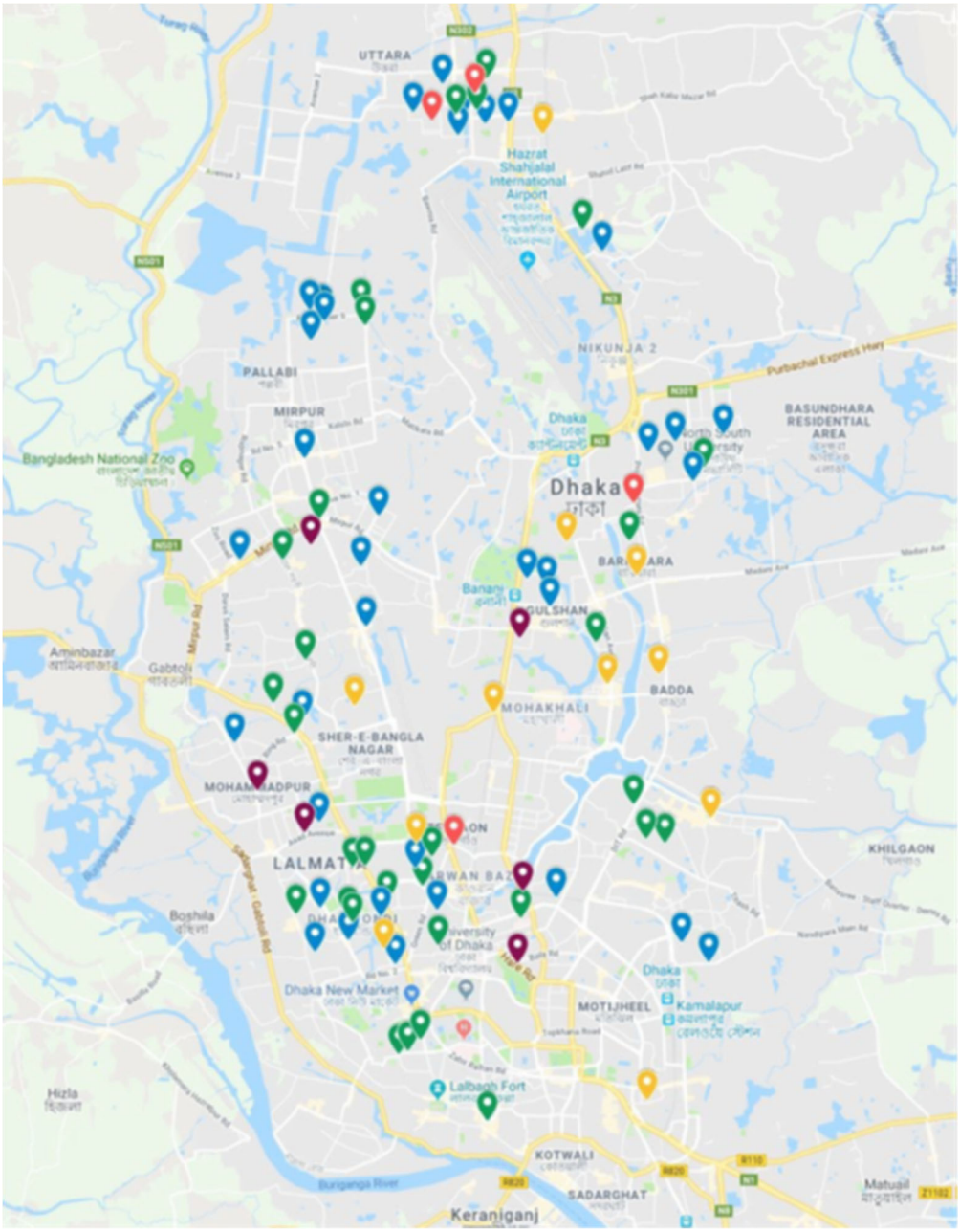

Figure 6–1 Location of buildings greenspace surveyed

In addition to the household/corporate survey, users of public green and blues spaces were also interviewed. Three major green–blue spaces (Ramna Park, Hatirjheel Lake and Dhanmondi Lake), all of which are owned and managed by the public sector, were selected. A total of 41 users were randomly sampled. To gain an understanding of the level of awareness and perception regarding the parks, and record possible ideas on service improvement, a questionnaire containing essentially the same elements as that developed for the building greenspace survey was used, with additional questions on possible ways in which the public sector could improve the quality of green and blue spaces. This survey was conducted during June–July, 2019. Each interview took 20–25 minutes.

Figure 6–2 Selected public green and blue spaces in DMA

6.3 Analytical techniques

The responses from both surveys were encoded in a statistical package and summarised. Even though a determination of monetary value for costs is easy in comparison to the stream of benefits for future periods, it was not possible to estimate the full stream of benefits due to unknown items and uncertainties. To overcome this difficulty, the interviewees were asked to provide the growth rate of benefits after the initial year. To understand the cost and benefits of greenspace at the buildings, Benefit–Cost Ratio (BCR) were used. The BCR for ten years were selected. A Net Present Value (NPV) was applied to estimate the present value of benefits of green infrastructures accrued for the period in the future and costed into equivalent current

value terms (Mahdiyar et al. 2016). The choice of an appropriate discount rate is important in deriving the present value of benefits and costs. Gollier and Weitzman (2010) used a constant three percent discount factor (3 percent for projects of 6–25 years) for all the future benefits, independent of the type of the benefit, and this factor was used in the current study. The NPV was calculated as follows for buildings, including with green infrastructures.

$$BCR_i = \frac{NPV\left(B_{i,t}\right)}{NPV\left(C_{i,t}\right)} \quad (1)$$

where, BCR is benefit–cost ratio, B and C represent benefit and cost, i implies types of GI, and t stands for time period of evaluation (i.e. 10 years). If BCR>1, then the project is economically viable. The NPV was calculated as:

$$NPV\left(B_{i,t}\right) = \sum_{t=1}^{10} \frac{, B_{i,t}}{(1+r)^t} \quad (2)$$

$$NPV\left(C_{i,t}\right) = \sum_{t=1}^{10} \frac{C_{i,t}}{(1+r)^t} \quad (3)$$

where, r indicates the discount rate. Two assumptions regarding the growth rate of monetary value of the benefits and costs were used. First, an increase of benefits, on average, by ten percent and costs by five percent per annum according to the respondents; and second, at an annual scale, both costs increase by five percent.

Currently, there is no user fee for accessing the three public green and blue spaces noted above. These spaces and related infrastructures cannot be developed and operated by private providers due to the size and high return from an alternative private use of the space. It is, therefore, difficult to ascertain the market equivalent values for such non–market goods and services. Given this uncertainty, the Contingent Valuation (CV) method was used to determine values. This method relies on the use of hypothetical market–like scenario, such as how much a user is willing to pay for ecosystem services. The value data generated from the structured questionnaire was then used to estimate the values for those services, provided by the green and blue spaces.

6.4 Results and discussion

6.4.1 Demographic characteristics of the respondents

Table 6–1 shows the demographic and occupational attributes of the respondents of the two independent surveys (e.g. buildings with GI and user of public green/blue spaces). The majority of the interviewees were within the 36–45 year age group. The respondents represented a range of occupational categories, including academics, housewives, professionals, NGO activists and students (Table 6–1).

Table 6–1 Demographic characteristics of the respondents (%)

Category	Sub–category	Household/ Corporate	Hatirjheel	Dhanmondi	Ramna
Age	16–25	3	12	9	0
	26–35	25	29	18	31
	36–45	42	35	45	54
	46–55	18	18	27	15
	56>	12	9	0	0
Gender	Male	47	53	55	54
	Female	53	47	45	46
Occupation	Business	23	18	18	31
	Academic	–	18	18	31
	ICT Service	12	12	–	–
	Student	3	18	9	–`
	Housewife	20	18	18	15
	NGO Worker	19	–	–	–
	Media Professional	9	–	–	–
	Technical (Physician and Engineer)	6	–	–	–
	Others	8	18	36	23

6.4.2 Educational attainment

An awareness about the effects of urban temperature on life and livelihoods depends, in a large part, on the level of education of the respondents. Three–quarters of the respondents who have adopted greenspace in their private properties were university graduates, while the rest had secondary and higher secondary education (Table 6–2). Likewise, among the users of the Hatirjheel and Dhanmondi Lakes, about four–fifths have tertiary degree, while almost all of the respondents of the Ramna Park were university graduates. This indicates that people with a higher level of education believe that the adoption and utilization of GI can be used to mitigate urban warming.

Table 6–2 Educational status of the respondents

Education level	Households/Corporate	Hatirjheel	Dhanmondi	Ramna
Primary	–	–	8	–
Secondary	6	12	15	9
Higher secondary	16	12	–	–
Graduate and above	78	76	77	91
Total	**100**	**100**	**100**	**100**

6.4.3 Buildings greenspace

The majority of the respondents opted for greening balcony, followed by rooftop, interior, and exterior wall and lawn (Table 6–3). The greenspace location and orientation does differs depending on whether this is located in a residential property or an office space of a building. The respondents also spend money on capital purchases and for recurrent purposes (such as planting and routine maintenance).

Table 6–3 Type of greenspace at buildings*

Building spaces	**%**
Rooftop	34
Wall (exterior)	4
Wall (interior)	10
Lawn	5
Balcony	47
Total	100

*Multiple responses are possible

The reasons given by the respondents for adopting green spaces in buildings are shown in Table 6–4. It has been determined that GI have many beneficial effects for users, including relaxation, reduction of stress, mental health restoration, as well as health or medical benefits. These factors are commonly captured under the term 'biophilia effect' (Wilson, 1984). Previous studies reported the effects of urban green and blue spaces on public health (Frumkin, 2005; Hartig et al. 2014; Wolf and Robbins, 2015). If green/blue spaces are private, these can then be used for a number of purposes including as a source of revenue through renting, and cultivating food and fruits for consumption, or for sale in the markets. In this study, it appears that most opted for greening for relaxation reason. Medical or health benefits, nutrition, and biophilia all have a role to play as catalysts in the greening of the surveyed buildings. All of the respondents reported that biophilia was one of the most reasons for all types of home gardening. Improved aesthetics (the improvement in the quality of the visual landscape) was another important reason of rooftop gardening, while psychological, health and nutritional benefits were also noted. Perceived health benefits were another reason for adopting both terrace and lawn gardening. Interestingly, temperature reduction was an important objective of terrace gardening noted by half the respondents. Awareness about the positive impacts of green space was one of the biggest drivers of this type of gardening according to the 80 percent of the respondents who have green terrace, and all the respondents who have a lawn. It was evident, however, that none of the respondents were convinced that rooftop gardening had the ability to reduce the indoor temperature and provide a better living environment.

Table 6–4 Reasons for preferring greenspace at buildings (%) *

Reasons	Rooftop	Balcony	Lawn	Interior wall	Exterior wall
Aesthetic	90	–	–	–	–
Beautification/biophilia	100	100	100	100	100
Relaxation	40	70	70	40	60
Medical/health benefit	40	55	55	35	30
Nutritional benefit	45	60	30	–	–
Temperature reduction	–	50	40	25	30
Awareness about green space	–	30	55	–	–
Improving air quality	–	–	30	–	–

*Multiple responses are possible

6.4.4 Costs and benefits of GI in buildings

The typical costs involved in greening a building are related to the initial construction, operation, maintenance, demolition, and disposal (Bianchini and Hewage, 2012a) as well as design and life cycle costs. There is a significant variation in price among the types of greenspace because of the type of materials used, building size and location (Bianchini and Hewage, 2012b), and labour and equipment costs, particularly in the initial stage. The cost of operation and maintenance (O&M) depends on the size of the green roof, the characteristics of the building, the complexity of the space where the green infrastructures are installed, the type of vegetation, as well as the market price or equivalent costs of O&M (Bianchini and Hewage, 2012a). Plants and garden materials also need to be disposed of, repaired, recycled and reused when impacted by floods or waterlogging, life cycle events and end of use. Other costs include water, electricity, use of technology, cleaning and other professional services such as pruning.

Respondents reported a diverse list of cost items (Table 6–5). The most important categories appear to relate to installation costs, the containers for the plants, growing medium, caregiver activities, seasonal changes and replacement of soil, seeds or trees. In addition, annual life cycle cost of plants (resulting from damage and loss) are other cost items to be accounted for in all types of gardens. Maintaining healthy lawns and landscape plants with the use of organic fertilizers and growing media were preferred by the respondents. Most of the respondents also opted for the use of professional services following initial installation.

Table 6–5 Annual average cost items for building greenspace in the initial year [US$]

Cost items	Rooftop	Balcony	Lawn	Interior wall	Exterior wall
Structural cost	–	–	160	–	–
Container	250	50	55	250	50
Plant	600	60	420	220	100
Damp proofing, if required depending on the design	–	–	–	–	–
Total installation cost, labor, transport	–	430	210	220	–
Fertilizer/pest control/nutrient management/IPM (natural)	20	50	55	50	40
Seed	20	–	–	–	–
Grooming media (soil, cow dung, coco dust, compost)	100	75	110	120	100
Accessories	10	30	–	–	40
Water	15	–	50	–	20
Timer/censor–based automatic irrigation system	–	–	200	–	–
Caregiver/plants doctor	225	225	215	225	225
Professional service	–	–	–	–	–
Maintenance	–	–	–	–	–
Seasonal change and replacement of soil, sapling or seeds	60	30	55	–	–
Annual life–cycle cost of plants (damage, loss)	50	20	55	50	50
Damage and loss of plants and accessories due to natural hazards	–	–	–	–	–
Cleaning	40	–	35	40	40

For rooftop gardens, the most common cost items include installation and maintenance, watering, caregiver and professional services. For lawn gardens, the main cost considerations are the structural costs, installation costs, labour, transport, and fertilizer/pest control/nutrient management. Healthy lawns and landscape plants were maintained with the use of organic fertilizers and grooming media.

The benefits of GI in residential and corporate buildings can include reductions in storm water runoff, improvements in air quality, mitigation of temperature and improvement of urban biodiversity (Driscoll et al., 2015; Connelly and Hodgson, 2008). Rooftop gardens and green roofs reduce energy consumption through shading, enhancement of evapotranspiration, insulation, increase in thermal mass, and reduction of heat loss through radiation especially in winter compared with conventional roofs (Berardi, 2016).

Due to the nature of a greenspace feature, most of the potential benefits of GI cannot be directly measured in monetary terms by the popular method of assigning a market value. Therefore, the

CV method was used to gain an understanding of the approximate monetary benefits. This was then used to calculate the BCR for the building greenspaces.

In regards the type of vegetation chosen for the greenspace, most opted for fruit plants, vegetables and spices and flower, green orchids, cactii, palms and other similar plants. The results suggest that the majority chose plants, which could be used as a source of organic foods, seasonal fruits, vegetables and flowers (Table 6–6). The annual benefit item of greenspace was the fruit/nutritional aspects. Vegetable/nutritional benefits, flowers and decreased recreation costs were also noted. Other benefits include health benefits/reduced adverse health events of family members (reduced medical costs), and savings in recreation costs. Higher productivity is another item, which appears to be common to all types of building gardens. The increased amount of money obtainable from renting buildings with a lawn garden is also an interesting benefit reported by property owners.

Table 6–6 Annual benefit items from buildings greenspace at the initial year [US$]

Benefit items	Rooftop	Balcony	Lawn	Interior wall	Exterior wall
Fruit/nutritional benefit	250	100	50	–	–
Vegetable/nutritional benefit	140	35	50	–	–
Flower	–	–	20	–	–
Reduction in electricity use	70			–	–
Less recreation cost (not going outside for recreation)	85	50	100	–	–
Health benefit (eye, heart, lung, etc.)/less disease of the family members/less medicine cost	155	200	355	–	–
Higher productivity (%)	20	25	25	–	–
Additional property value (rental)	–	–	2,000	–	–

In the case of lawn gardens, the perception of benefits was mostly related to the nutritional and health benefits derived from trees or plants. In the case of interior and exterior wall GI, however, less electricity use, health benefit and higher productivity were identified as important benefits. The monetary value, however, could not be defined.

The cost–benefit analysis undertaken on the three types of greenspaces found at the residential and corporate buildings, uses two different time horizons with alternative assumptions. With the first assumption, the NPV of annual benefits and costs were calculated for ten years. The results reveal that the cumulative NPV of benefits after ten years is higher than the NPV of costs for all the building greenspaces examined. However, because of the (self–reported)

additional benefit gained from the increased rental value of buildings with lawn gardens, both the annual and cumulative benefits are significantly higher than the costs. Based on the second assumption, the period of analysis was extended to 14 years. This is because the costs in the initial period are high due to the fixed installation costs, and means that it would take a longer period for the costs to become lower than the cumulative benefits, thereby making the micro projects financially viable.

Since the BCR for all surveyed greenspaces is greater than 1, these are all financially viable for the period of analyses (Table 6–7) and Figure 6–3.

Table 6–7 NPV for building GI for 10 years [US$]

	Year										Total
	1	2	3	4	5	6	7	8	9	10	
Benefit											
Rooftop	720	769	821	877	937	1,000	1,068	1,141	1,218	1,301	9,853
Balcony	410	438	468	499	533	570	608	650	694	741	5,610
Lawn	2,600	2,777	2,965	3,167	3,382	3,612	3,858	4,120	4,400	4,699	35,579
Cost											
Rooftop	1,390	540	551	561	572	583	595	606	618	630	6,648
Balcony	970	382	390	397	405	413	421	429	437	446	4,690
Lawn	1,620	775	790	805	821	837	853	870	886	904	9,160

6.4.5 Users of public green/blue spaces

Table 6–8 shows that the biggest social benefit of using public green and blue spaces is related to improved public health. This is due to the fact that regular users visit these places for physical activities such as walking and running. They also visit for psychological benefits. Higher productivity has been found to have a significant spill–over effect (Table 6–8). The monetized benefits are mostly comparable for each of these categories. This finding is quite interesting and a detailed study may be warranted to understand the developmental co–benefits of mitigation strategies of urban heat through green/blue spaces.

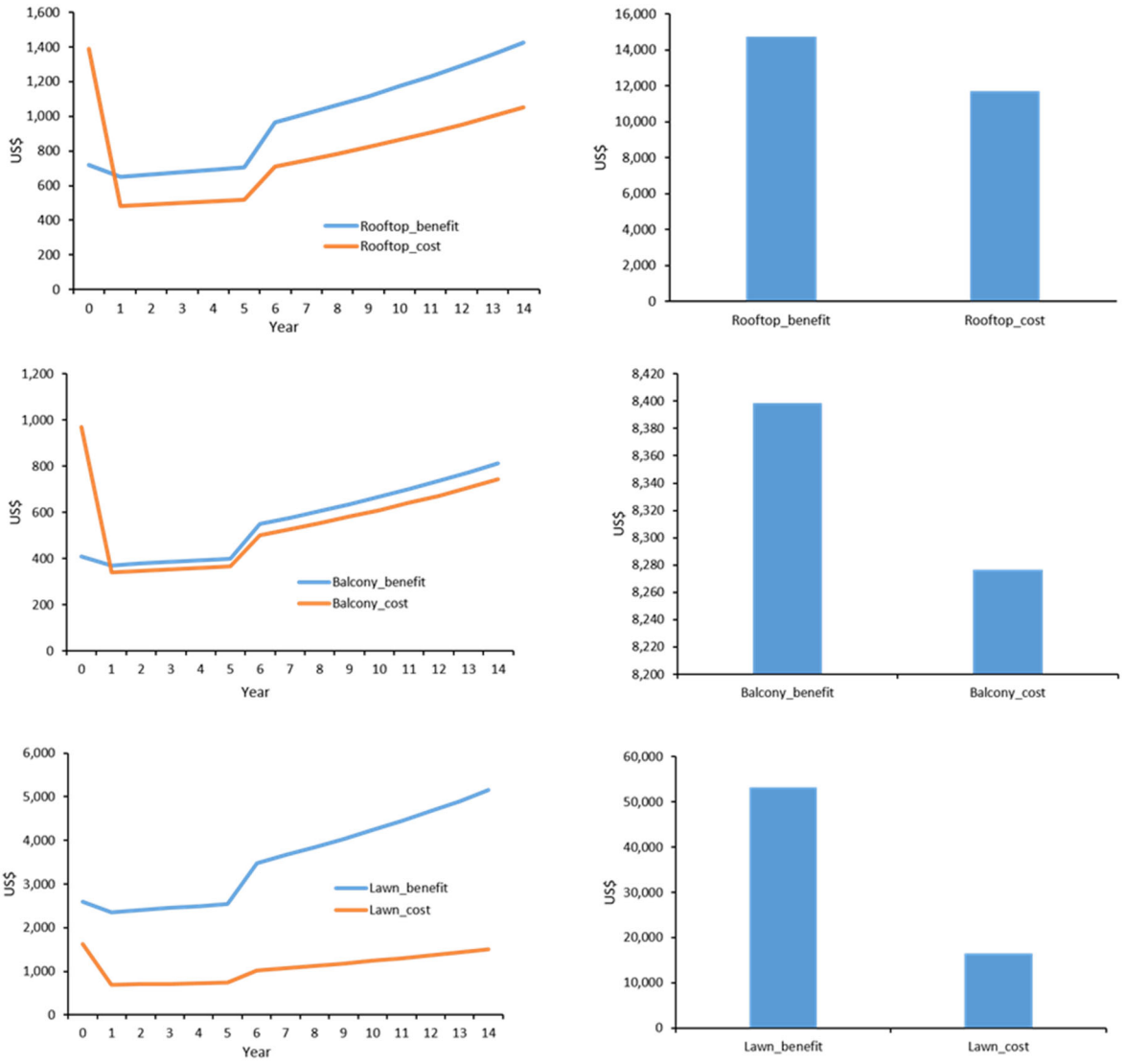

Figure 6–3 Net present value (NPV) for rooftop, balcony and lawn in US$ for 14 years (annual increase of benefits and costs by 5 percent was considered)

Table 6–8 Annual benefit items from public green/blue spaces [US$]

Benefit items	Hatirjheel	Dhanmondi	Ramna
Public health benefits	370	550	500
Less recreation cost	610	385	335
Higher productivity–based gain	325	425	230

Private operation and management would improve the quality of services, benefitting plantation and quality of waters in the public green/blue space, which would, in turn, contribute positively to reducing rising urban temperature. This is mainly due to the attraction of a higher number of visitors through improved services even with a user fee. Most of the respondents

(>80%), reported that they would continue using all the three publicly provided green–blue space, given that services would improve substantially (Table 6–9).

Table 6–9 Willingness to use public green/blue space, if services are privatized (annual average, US$)

Willingness to use, if privatized	Hatirjheel	Dhanmondi	Ramna
Yes	82	85	82
No	18	15	18

Finally, the survey intended to understand whether the respondents were willing to pay either a user fee (to improve services) or increased taxes (to maintain services). Although the willingness for respondents to pay both a user fee and taxes is low, the amount of users accepting a user fee was found to be nearly double when compared to the specific tax that could be imposed on the users (Table 6–10). It is thought that a user fee would be imposed by a private operator who could increase the amount of vegetation in the public greenspace, improve the quality of water in the blue space and provide better security arrangements for visitors. Taxation would only maintain the current status of the services. It, therefore, appears that private operation and maintenance of public green/blue space would be a more viable mitigation strategy to combat urban temperature rise.

Table 6–10 Willingness to pay for using public green/blue spaces [annual average, US$]

Types of policy instruments	Hatirjheel	Dhanmondi	Ramna
User–free after privatization of service	15	8	6
Tax for improving service	7	5	3

6.5 Conclusion

The goal of this chapter was to understand the cost–benefit of self–sustained GI in DMA based on information gained through a questionnaire survey. A total of 94 households and 6 corporate offices were interviewed. In addition, public users of green and blue spaces were interviewed to understand awareness and perception of these public spaces. Major findings of this chapter are as follows:

- Beautification or biophilia was the most important reason provided for having a GI at buildings. Other reasons were aesthetic, psychological, health and nutritional benefits. Reduction of indoor temperature and awareness about the positive side effects of home/office greenspace were also noted, pointing that the residents are possibly aware of rising temperature in their locales.

- Cost items related to the installation and maintenance of buildings GI included plants containers, installation cost, grooming media, caregiver requirements, seasonal changes, replacement of soil, seeds and saplings, and the annual life–cycle cost of plants (damage, loss). Benefit items included fruit/vegetable growing, flowers, higher productivity, and less recreation cost.

- The cumulative NPV of benefits and costs revealed that all building greening were financially viable for both similar and different growth rates of benefits and costs. However, to make them more viable (based on the same rate of growth of benefits and costs), the projects need to continue for 14 years, especially in the case of balcony gardens, due to the lower benefits accrued compared to other projects.

- The most important social benefit of using public green/blue spaces was related to improved public health, perceived higher productivity and positive psychological effects felt by regular users when using the areas for walking, running and recreation.

- Most of the respondents expressed a willingness to continue using the public green/blue space if private management and operation of the park resulted in substantially improved services. However, the average amount of tax or user (entry) fee they were willing to pay for improving or maintaining the services in these public was low.

7 POLICY IMPLICATIONS AND MITIGATION STRATEGIES

7.1 Introduction

A review of the existing literature reveals there have been a variety of strategies which have been implemented in cities (regardless of their size) to mitigate local warming or UHIs (Deilami et al. 2018; Gago et al. 2013). A major conclusion arising from these studies is that a 'one–size–fits–all' approach must be avoided as a number of factors influence the success of UHI mitigation, including local climatology, geography and site elevation (Aflaki et al. 2017). Any proposed mitigation strategies should take account of all factors, specifically the local geographical conditions and the urban context (Parsaee et al. 2019; He et al. 2015; Saneinejad et al. 2014; Houet and Pigeon, 2011).

Geospatial data obtained from a range of satellites (MODIS, Landsat and ASTER), were used to examine the spatio–temporal variability of heat islands, and to determine the main driving factors for the development of elevated temperatures. A nominal year of in–situ microclimatic observations was obtained through in–field site monitoring. Data was collected over the pre–monsoon, monsoon, post–monsoon and winter seasons and data related to the cooling potential of green and blue spaces was also collected. The mitigation ability of "green roofing" was also assessed. The overall results of the project indicated that the urban temperature in Dhaka is increasing, and that the heat island effect is becoming a matter of concern. It is expected that the current situation will worsen, exacerbated by an ever–increasing population and further urban expansion.

Following an extensive literature review, and analysis of the available geospatial and field data, the current work endeavours to formulate strategies, which address issues identified as specific to the Dhaka situation. Consideration and timely implementation of these strategies by the relevant government agencies may assist in mitigating the increased warming currently being experienced. Some possible directions are detailed below:

- Building numbers, high population density and waste heat from anthropogenic sources significantly affects the spatial and temporal microclimatic pattern of Dhaka. The overall population of a city has both direct (e.g. more metabolism) and indirect (e.g. vehicles) effects on heat generation (Rizwan et al. 2008). Increased impervious surface together with population density and rapid changes in land use/cover (essentially from vegetated to non–vegetated) are three factors driving the increase in the observed heat island. The current work identified a strong relationship between anthropogenic activities and increases in temperature, and all indications are that the Dhaka megacity will experience increasingly elevated temperatures in the coming years, mainly due to continuing rural to urban population migration. Though it may be difficult to undertake

urban regeneration activities in Dhaka, such measures may be a viable option as shown in China where urban regeneration is successfully implemented to mitigate the heat island effects (Li et al. 2012). Apart from urban regeneration, compact and smart growth types (Gusdorf and Hallegatte, 2007) could be adopted to buffer against increasing temperature.

- The form and morphology of the urban core of Dhaka keeps changing rapidly, with the addition of new buildings (particularly high–rise development) and replacement of natural surfaces with artificial ones (concrete, asphalt). As a result, the already densely–developed areas are becoming denser, and large, undeveloped open spaces, including greenspaces, are becoming few and far between. Because urban form and morphology have a tremendous influence on the local climate (Drach et al. 2018; Chatzidimitriou and Yannas, 2015; Ruiz et al. 2015; Kantzioura et al. 2012), the contribution of increased imperviousness and building density to microclimate variability is large (Coseo et al. 2014; Klok et al. 2012). To reduce this variability, the use of cool and permeable materials may be a cost–effective solution, as well as the use of plants to increase local evapotranspiration, one of the key parameters in reducing elevated environmental temperatures. The implementation of such measures can commence by isolating and documenting the densely–developed neighbourhoods exposed to the higher temperatures, and then examining the various planning variables (e.g. building volume density, height to width ratio) which have the potential to affect heat generation. Simulation and modelling can use various available data, including data generated in this study, to determine the relative performance of cool and permeable materials at the neighbourhood scale.

- Solid brick tends to store a greater amount of heat than concrete and hollow brick materials. One strategy could be the promotion of the use of hollow block bricks. These have less thermal admittance as compared to red/raw brick, with the former cooling more quickly than the latter type (Wong, 2007 cited in Kleerekoper et al. 2012). Though this work did not evaluate the thermal response of the individual brick materials commonly used in Dhaka, the thermal response of building walls (analysed via handheld thermal images) constructed with different materials (e.g. concrete, plaster, red brick) during the three seasons (pre–monsoon, monsoon and winter), indicated that walls made with red/raw brick cool at a slower rate than plastered/painted or concrete building walls.

- Urban canyons constitute a major part of the urban fabric in many cities. Deep urban canyons with a north–south orientation appear to trap less heat than streets with an east–west orientation (Ruiz et al. 2015; Kleerekoper et al. 2012). The results of an analysis of traverses undertaken in three locations in Dhaka (planned, unplanned and mixed land

use zones) generally aligns with this observation. Implementation of a north–south development orientation and determination of suitable canyon dimensions should be a priority for any new construction and when new roads are planned. Microclimate data developed in this study could be utilised to determine the heat generation mechanisms of various canyon features (such as deep and narrow streets) in more detail, using simulation techniques. The results could then be incorporated into strategies, targeting heat mitigation in urban canyons exposed to high solar radiation.

- Increasing solar reflectance due to cool roof and pavement materials has been identified as an important mitigation measure in various cities of the world (Akbari and Kolokotsa, 2016; Santamouris, 2014; Synnefa et al. 2008). Densely–developed urban areas where green coverage is seriously lacking or non–existent can be targeted for cool material adoption. Where feasible, urban canyons, rooftops, sidewalks and parking lots could be replaced with materials that enhance solar reflectance and albedo, factors which have been shown to reduce ambient temperature. As solar radiation and seasonality determine the cooling effect of increased albedo of different land covers such as pavement (Li and Kendall, 2013), area–specific strategies will be required. Since it is also possible for cool materials to lose reflectance over time due to aging and weathering (Sleiman et al. 2011), location–specific materials will need to be sourced to maximise the benefits of cool materials and the enhancement of any albedo effects (Georgescu et al. 2014). Although the use of rooftop materials to enhance albedo could result in local cooling, on a global scale such a strategy may actually enhance warming (Jacobson and Ten, 2012). An evaluation of three important mitigation measures (e.g. evaporative cooling, increasing surface albedo and enhancing shade) demonstrates that shading reduces surface temperatures to a greater degree than the other two measures. Overall, the effectiveness of mitigation measures largely depends on the specific climatic conditions, and an optimal strategy may differ between different areas (Saneinejad et al. 2014).

- High wind speeds affect the magnitude of the heat island due to a general reduction in urban atmospheric stability, a factor particularly noticeable during the night (Balling and Cerveny, 1987). Chaotic urban growth, characterised by uneven building heights and density, is prevalent in Dhaka. This may possibly be the reason for the poor airflow, and hence inadequate heat dispersal. In general, poor ventilation intensifies the heat island effect (Rajagopalan et al. 2014). One way of achieving good ventilation is to adjust the canopy layout, thereby increasing the potential mixing of air (Kleerekoper et al. 2012). To achieve this, however, building heights would need to be controlled. In a numerical simulation study, Xiaomin et al. (2006) demonstrated that both urban canyons and building heights (commonly expressed in a height to width (aspect) ratio)), significantly influence the ventilation capacity of an urban area. The study indicates

that the best ventilation outcome could be achieved using an aspect ratio of 0.5. The development of a ventilation map (Wong et al. 2010; Alcoforado et al. 2009) of the city is essential in order to delineate locations/neighbourhoods experiencing poor ventilation and high thermal stress across the different seasons. These mapped neighbourhoods can then be targeted for ventilation improvements and the associated enhanced mixing of the air. The step–up configuration of buildings also appears to distribute wind evenly and allows wind currents to reach the leeward (sheltered) side of buildings (Rajagopalan et al. 2014). Building designs incorporating wind flow influencing structures may be effective cooling strategies in urban areas, but may also be challenging (Kleerekoper et al. 2012). Further research is needed in this domain to provide more information on the effectiveness of using this method.

- Buildings constructed with a large glass component feature strongly in current developments in Dhaka. Neon sign billboards, plastic advertising boards and materials made of iron have also become widespread in shopping malls, at major intersections and at many popular locations. Despite glass–coated buildings, both warm and cool quickly, they are also instrumental in elevating daytime temperature in the immediate building/micro environment, a factor which may influence the diurnal cycle of temperature. The use of plastic billboards, neon signs and similar types of materials should be strongly discouraged as these materials contribute to elevated nighttime temperatures, as evidenced by the results of the handheld thermographic assessment.

- Urban green infrastructures (UGI) types include urban parks, trees, rooftop and green wall coverage of buildings (Saaroni et al. 2018). Although the role of vegetation in reducing urban heat is unquestionable (see Gunawardena et al. 2017; Bowler et al. 2010; Rizwan et al. 2008), background climate and population density heavily influence heat island variability in any given city. As a result, the effectiveness of urban vegetation in heat mitigation is uncertain, particularly in tropical cities (Manoli et al. 2019). It was noted that cities in South Asia might require a range of innovative design solutions, as vegetation alone is not able to reduce the core urban temperature. Within the DMA, greenspace covers only 2.41% of the total area, a figure too low to have any real effect on the increasing temperature. It is proposed that new development areas must have adequate greenspace provision and that evergreen trees be planted to obtain year–round benefits. Trees reduce street temperature and provide more thermal comfort to local inhabitants and park users. More trees should be added to road dividers/islands and sidewalks, which could enhance both shading and evaporative cooling (Saneinejad et al. 2014). Random increases in green cover, however, would have little impact on temperature reduction; rather the strategic placement of vegetation in heat–exposed areas should be the aim (Zölch et al. 2016).

- Vegetation type and water requirements, the spatial arrangement of trees, varying canopy density and the geometry of greenspace all influence the cooling mechanism of the UGI (Chun and Guldmann, 2018; Zhang et al. 2017; Li et al. 2016). Ideally plant species that survive in low water conditions, and which have high potential for reducing urban heat, should be utilised as much as possible. The current work identified *Barringtonia*, *Beharda* and *Teak* plants as being effective in the winter months, with *Earleaf acacia* plant performing best during the pre–monsoon. *Loha kat* species also shows some promise in reducing local environmental heating. These vegetation species could be planted along urban canyons, parks and in other locations, however further information on the soil water requirements of these plants is required.

- The urban core of Dhaka has already been extensively developed, so further development of UGI features such as parks or urban forest is not realistically possible. An alternative, used in other countries, is the promotion of green retrofitting of older, existing buildings. In the current study, buildings in a number of areas have been provisionally demarcated for possible retrofitting using a limited number of criteria. Further scrutiny is required, however, as load–bearing capacity, roof slope and roof infrastructures, building height, position and orientation, as well as insolation, are all additional features that affect the suitability of an individual building for green retrofitting (Wilkinson and Reed, 2009). The benefits of widespread green retrofitting include a reduction in excess heat generation via increasing evapotranspiration of vegetation, energy savings due to increased insulation and possible reductions in CO_2 generation (Santamouris, 2014).

- Rooftop gardening should be promoted. An examination of the impact of rooftops with/without a garden showed rooftop gardens offer great potential for reducing the heat of the immediate environment, particularly during the winter season when temperatures show the greatest diurnal variation. Data obtained during the monsoon season also showed temperature reduction effects, however responses during the pre–monsoon were impacted by the waste heat produced from the air conditioners operating on nearby buildings. Even though the results of the current work are based on only one rooftop garden with sparse vegetation, the results appear promising. The relevant authorities could possibly include a requirement for rooftop gardens to be incorporated into the planning codes. Among the rooftop plants tested, *Combretum indicum* showed the greatest potential for reducing heat in all three seasons (winter, pre–monsoon and monsoon), followed by *Bougainvillea* species. Public and private building owners should be encouraged to consider these species for their rooftop gardens. It should be noted, however, that the cooling potential of a green roof depends on the density of vegetation, the distance, and a low building height (<10 m) (Santamouris, 2014).

- A vertical greening system is also a very effective mitigation measure during the winter and pre–monsoon seasons, with the system showing great potential for reducing daytime temperature. The heat flux and cooling demand of the indoor areas could be substantially reduced using this feature, and this type of UGI should be encouraged. Climbing plants can be attached to exposed walls along the streets (Perini et al. 2011), and/or the walls of private buildings that receiving year–round solar radiation.

- A review of previous research has shown mixed results in regards the cooling potential of blue space. This may be due to various factors, including location, seasonality, water feature type (static vs flowing), spatial arrangements and heat exchange capacity (Gunawardena et al. 2017). Whilst waterbodies act positively to reduce heat in a variety of environments (Voelker et al. 2013), negative relationships have also been reported (Steeneveld et al. 2014). Observational data, measured using logging instruments, revealed that both distance and directions are important parameters in determining the cooling potential of a blue space (e.g. lake) in DMA. Its theoretical role in reducing temperature, however, can potentially be nullified by surrounding urban forms and anthropogenic activities. Although both flowing and static blue spaces do reduce environmental heat, they operate using different mechanisms. This study indicates that flowing water (such as a river) has a higher cooling potential than ponds (static). River networks around Dhaka could be potentially be used to reduce UHI effects. Fountains also appear to be effective in reducing temperature (Nishimura et al. 1998), so UHI hotspots could be identified for fountain development in areas such as important intersections, front yard of shopping malls, urban squares and residential/educational locations.

- Current urban design and development is based on the premise of a stationary climate. Because stationarity is deemed dead (Milly et al. 2008), the traditional approach is no longer applicable when designing climate–sensitive cities. In order to holistically and strategically address the effects of a changing climate, various climatic parameters are now crucial for inclusion in the urban planning process (Ren et al. 2011). Unfortunately, the newly proposed draft structure plan that will guide the future growth of Dhaka from 2016 to 2035 does not include any climatic parameters (http://www.rajukdhaka.gov.bd). Dhaka, therefore, requires the implementation of some innovative approaches, including the construction of climatopes (Scherer et al. 1999), local climate zones (Stewart and Oke, 2012), urban climate maps (UCMap) and urban climate planning recommendation map (UC–ReMap) (He et al. 2015; Ren et al. 2011). Even though climatopes traditionally factor land use and climate data into the local planning process (Mora, 2010; Evans and Schiller, 1990; Bründl, 1988), the use of multiple techniques such as building design (Erell et al. 2003), wind corridors (Wong et al. 2010), and ventilation maps (Alcoforado et al. 2009) in preparing urban UCMaps

(He et al. 2015) could prove to be further innovative strategies in curbing heat island impacts (Ren et al. 2011). Microclimatic data, land use, topography, urban form, energy load and balance data, ventilation maps and demographic information can all be integrated into a GIS to build a UCMap (Parsaee et al. 2019). This particular type of map delivers local climatic data to architects, planners and decision–makers, allowing the design of cities to be incorporated into a holistic planning framework. Further research is needed to determine ways to easily and successfully assimilate heat island mitigation strategies into UCMaps for planning and design use.

- Dhaka receives a substantial amount of rainfall during the monsoon season so the harvesting of rainwater in public spaces could be useful. Vegetation can be planted around the blue space (Kleerekoper et al. 2012), providing shading of the water surface so that the maximum cooling benefit can be obtained. A potential issue, however, is again the availability of adequate land since urban expansion is increasingly consuming both open space and cultivated land within the city (Corner et al. 2014). It is also possible that rooftops can be used to store rainwater, however the suitability of rooftops for water storage warrants further examination.

- Multiple organisations (54 different organisations from 7 ministries) are involved in the management of the Dhaka megacity. A serious lack of coordination is one of the biggest challenges to the implementation of the policies and planning regulations. For example, the Capital Development Authority (RAJUK), on average, receives up to 90,000 plans for approval every year. Normally only 3,750 plans are officially approved, leaving the rest to be built without approval (RAJUK, 2017). RAJUK does not have the capacity (in terms of workforce or resources) to influence other agencies in regards the implementation of policies. Violation of planning regulations are therefore common events, leading to haphazard urban growth. To better respond to the changing environment, new planning codes must be prepared under which spatial planning of the megacity can be undertaken, with the planning, design and construction phases based on UCMap/UCReMaps. The relevant agencies must be encouraged to come up with realistic, short and long–term action plans so that urban development policies (UDP) and action plans (AP) can be seen to be intrinsically linked with local planning practices, and focused on the common goal of urban heat mitigation (Parsaee et al. 2019; Ren et al. 2011).

Table 7–1 provides a summary of the mitigation measures described above. This also indicates the different scales at which these measures will operate. Note that area–specific measures may differ between the implementation scales. Appendix XI describes lesson learnt through this work and recommendations for further improvement, and Appendix XII provides a summary of the risks identified for this project.

Table 7–1 Summary of proposed mitigation measures

Measures	**Strategies**	**Spatial scale**
Green and blue space	Rooftop gardens/green retrofitting	Micro–scale
	Parks and green corridors	Meso and micro–scale
	Blue space (lake, fountains)	Meso and micro–scale
	Rooftop water retention	Micro–scale
	Vertical greening system	Micro–scale
	Planting evergreen trees along both sides/islands of streets	Micro–scale
	Open space with greenery areas	Meso and micro–scale
	Greening building façade/exterior walls	Micro–scale
	Strategic plantation	Micro and meso–scale
Built–up form, morphology and urban design	Building heights	Meso and micro–scale
	Airflow and ventilation	Meso and micro–scale
	Building density	Meso and micro–scale
	Thermo–shield building materials	Micro–scale
	Aspect ratio (building to road width) and orientation	Meso and micro –scale
	Floor area ratio (FAR)/building geometry	Meso and micro–scale
	Neon sign billboard and plastic advertising materials	Micro–scale
	Adjusting canopy layout	Meso and micro–scale
	Hollow block brick	Micro–scale
	Heat load reduction	Micro–scale
	Shading	Meso and micro–scale
	Building with glass coat	Micro–scale
	Cooling of pavement and roofs	Meso and micro–scale
	Urban regeneration	Micro–scale
UC–Map	Local climatic classifications	Meso and micro–scale
UCReMap	Planning regulations	Meso–scale

(Modified after Ren et al. 2011)

7.2 Policy implications

7.2.1 Outcome of existing plans and policies

A review of the existing, available plans and polices dealing with climate and urbanisation has been conducted. These documents include the Bangladesh Climate Change Strategy and Action Plan 2009 (MoEF, 2009), Bangladesh Climate Public Expenditure and Institutional Review (GED, 2013), Bangladesh Climate Fiscal Framework (Finance Division, 2014), Seventh Five Year Plan (GED, 2016), Bangladesh Delta Plan 2100 (BDP2100) (GED, 2018) and draft Dhaka Structure Plan (2016–2035) (http://www.rajukdhaka.gov.bd). Except for the BDP2100, none of the documents consider the urban heat island issue, although a variety of environmental problems are mentioned; environmental pollution, waterlogging and a lack of vegetation and biodiversity in major urban areas (including in Dhaka). The draft Dhaka Structure Plan (2016–2035) provides design guidelines for buildings, sidewalks, commercial places, and the principles to be considered in urban design. The design guidelines do not incorporate any UC–Map principles to alleviate urban warming effects. These documents also do not stipulate any requirements for the development of action plans to use in combating heat island impacts on any of the major urban agglomerations. Very recently, however, BDP2100 recognized urban temperature increase as an issue, and suggested a number of policy measures to assist in tackling this (GED, 2018). These measures include:

- The plan recognises that urban green/blue space plays an important role in mitigating local warming and maintaining the thermal comfort of cities. In line with the recent literature and scientific evidence, the policies argue that large urban parks that include waterbodies are useful in mitigating heat island effects, as well as facilitating recreation, providing space for water storage, contributing to the general quality of urban life, and maintaining ecological values. The policy document specifies that the strategic development of functional green/blue spaces that include retention areas and canals should be accompanied by an effective and properly enforced spatial planning system.

- The plan aims to promote urban green and blue spaces. It also flags the preparation of a regional spatial plan that would incorporate green and blue ecological and recreational spaces and networks. In addition, it intends to formulate an urban strategy for green blue and recreational networks of different scales, such as urban parkways, city parks, neighbourhood parks and green routes.

- The plan intends to encourage investment in green space areas through planting trees and in the creation of blue spaces within cities. It also suggests adopting land use zoning schemes aimed at retaining existing green and blue spaces. The following suggestions are notable: street profiles should include green strips and trees, and green strips should

be maintained between the street and building envelope on private plots in neighbourhoods (where applicable). Incorporating vegetation/plants in the interior and green exterior spaces of buildings for new building designs have also been suggested.

7.2.2 Key informant interview (KII)

A KII was conducted from September to November 2019. Nine key personnel were selected based on their involvement in organisations with an interest in the environment and climate change. Officials from the Ministry of Planning, Ministry of Finance, and Ministry of Environment, Forest and Climate Change, urban planners from Dhaka North and South City Corporations, RAJUK, vice–president of Real Estate and Housing Association of Bangladesh (REHAB) and a member of National Housing Authority (NHA) were interviewed. Each interview took 20–30 minutes to complete. Interestingly, most of the interviewees were not aware of the heat island effect in the Dhaka megacity. Even though the BDP2100 mentions various mitigation strategies, personnel could not specifically define the desired role of the government and other agencies in planned efforts to tackle the urban heat issue. This appears mainly due to the fact that although resource allocations in line with the directives of the Plan document have been undertaken, the relevant ministries have not been allocated specific responsibilities at this stage. Consultation with the key personnel resulted in the following policies being noted:

- Under Dhaka South City Corporation (DSCC), micro–green projects such as rooftop gardening, greening balcony or the compound of privately–owned buildings, are rewarded with a 10 percent tax rebate as a part of a green city prioritisation incentive. This policy is aimed at encouraging residents to develop green buildings. There is, however, a need to revise the rebate policy on holding tax. Specifically, the rebate should be a minimum for any micro–greening (garden) in the building, and should be in the order of 30 per cent of the holding tax, depending on the extent of gardening on the rooftop, balcony, lawn, and interior/exterior of the building. Currently, there is no fiscal benefit for rented houses to utilise greening. Income tax rebates should be introduced for renters, to encourage greening of building facades, rooftops, walls, balconies, lawns and interior.

- In rented locations, private firms and business owners are not eligible to get any tax benefit even though many of these entities use plants inside their premises and balcony for beautification. To encourage such initiatives, private offices and business places should also be able to access tax benefits.

- Appropriate building designs should be encouraged through special fiscal incentives. The buildings should be designed in such a way that they provide sufficient space in

both interior and exterior areas (as well as in the ground space) to allow for suitable greening activities. A corporate tax waiver and cash incentives should be provided to architectural firms that concentrate primarily on designing green buildings. Construction companies and private builders should also be able to claim corporate tax rebates if they construct green building and spaces. For new apartments, creating greenspaces in balcony areas could be encouraged with a higher tax rebate in the first year of vegetation installation. Tax rebates should also depend on the ratio of greenspace to total space within the apartment.

- Nursery businesses should be promoted as a prime green space enabler and included in strategies to create more greenspace. A nursery contributes significantly to the ability of people to easily install plants in homes, private spheres, buildings, offices and businesses. However, they currently do not receive any extra benefits for running their business, other than the reduced interest rate on credit from banks which the overall agriculture sector enjoys. An interview with a nursery owner (https://www.thegreensavers.org/) revealed that there is minimal dependence on bank credits in this sector. They generally operate independently of mainstream banking due to the complicated procedure of mortgages and the formalities inherent in the banking system. Given these circumstances, soft loan facilities should be provided, with the support of Bangladesh Bank, to expand existing businesses and encourage the development of new nurseries across the megacity.

- The government should pursue a greening strategy through the Real Estate and Housing Association of Bangladesh (REHAB), the apex organization of construction firms and builders within the country. Currently it has 1007 members, most of whom are located in Dhaka. Even though there are many non–member builders, REHAB is a key player, able to set the standard of building code, design and construction through which the individual building and housing areas (cluster of buildings and amenities in a specified area developed by a company or authority) can provide designs which allow enough room for installing plants including on rooftops, balconies, and common spaces utilizing sunlight. In addition, it can also play a significant role in installing private blue spaces, such as water roofs, swimming pools, fountains, and lakes in residential locations.

- Rajdhani Unnayan Kartripakkha (RAJUK) has the authority to approve building designs, and conducts inspections after construction to ensure the approved design is properly adhered to. It can issue guidelines for all building designs so that a bare minimum space can be dedicated for the use of green and blue spaces.

- The National Housing Authority, an organization under the auspices of the Government of Bangladesh (GoB), has been implementing housing projects in Dhaka. Most of the building designs are traditional in nature, however, and there is no requirement to include UGI when designing amenities and common space. This policy should be amended to include maximum micro green/blue space within these housing areas.

- A Green Building Fair should be organized jointly by the National Housing Authority and REHAB. Best buildings and best designs should be awarded with cash incentives. Similar awards should be initiated for housing areas to inform the industry, as well as the general public, about urban warming and to promote and reward the development of innovative mitigation measures.

- Dhaka North and South City Corporations should both have an appropriately–sized workforce able to check whether green/blue spaces are being installed and maintained in all private spaces in their jurisdiction areas. They should also undertake awareness activities for owners and renters within the private sphere, providing information about micro green/blue projects and announcing special incentive packages and rewards for those proactively implementing corporation strategies.

- Recently, a few three–wheeler auto–rickshaw vehicles operating in Dhaka have appeared featuring a small garden on the vehicle roof, and the vehicle body partly covered with grasses (Appendix XIII). This creates thermal comfort for the passengers, especially during summer, and an awareness among street users about creating greenspaces through innovative means. Initiatives of this sort need to be promoted through fiscal incentives (such as a tax waiver), soft loans to people buying rental vehicles that install micro greenspaces, and cash incentives.

- Due to a lack of knowledge on the subject matter and unclear policy directions, government agencies are yet to fully design an action plan for mitigating heat island effects in line with the SDGs. Ministries and agencies should be assigned specific responsibilities in line with the directive of BDP2100, so that these can be incorporated into the respective business plans.

- Currently few fountains are available on street islands and at roundabouts. Since these fountains reduce heat on the streets, more street fountains should be installed by the Department of Roads and Highways. Currently fountains are operated and managed by private enterprises and banks. The cost of operation and maintenance mean that they do not operate during the daytime when the benefits are greatest and thermal comfort is required. A public–private partnership fund should be incorporated into budget planning for the installation, operation and maintenance of these fountains so that they

remain active during the daytime and can provide a greater contribution to temperature reduction.

- A “Blue and Green Network” should be established. This can be a holistic approach to countering the UHI effect by combining discrete public and private green and blue spaces. Large canals, lakes and parks should be integrated and rejuvenated. New multipurpose parks with lakes/water bodies should be established. The Detailed Area Plan (DAP) of Dhaka must incorporate plantation development and new waterbodies, as well as restoration of old canals (keeping in mind urban morphological issues). Public resources and donor funds (e.g. projects from the World Bank and other multilateral agencies) should be dedicated to this. Such big investments, however, must be managed appropriately.

- Innovative ideas and private initiatives on green technologies and support services should be encouraged and promoted. Fiscal incentives are regarded as one of the best ways to do this. For example, Green Savers Association (https://www.thegreensavers.org/) is a private social movement, advocating rooftop gardening. It acts as a caregiver to trees/plants through services, which are termed “doctors of trees”. Some schools in Dhaka have started rooftop gardening with the support of Green Savers and are implementing some of the cost–saving ideas available. The concept of “Oxygen Banking”, “Green Club”, “Environtainment” (environment and entertainment together) have been initiated by the Green Savers at schools, and use a “tree ambulance” for providing treatment for wounded trees with support from Dhaka North City Corporation (DNCC). These types of approaches and ideas should be promoted by the government through the use of tax and cash incentives. This again will assist in the promotion of micro technologies and projects for greening private places and buildings.

7.3 Conclusion

This chapter presented a range of mitigation measures based on the scientific data generated through this study, as well as a comprehensive literature review. In addition, public policies were reviewed and a KII was conducted. The results demonstrate that a ‘one–size–fits-all’ approach must be avoided when developing strategies to reduce the increasing heat being felt by Dhaka megacity as there are multiple factors accountable for the growth of UHI in large cities. A range of public policies are suggested to ensure the development of sustainable cities, policies without which it will be difficult to achieve the SDGs defined for having healthier and more comfortable cities.

REFERENCES

Aflaki, A., Mirnezhad, M., Ghaffarianhoseini, A., Ghaffarianhoseini, A., Omrany, H., Wang, Z. H., & Akbari, H. (2017). Urban heat island mitigation strategies: A state-of-the-art review on Kuala Lumpur, Singapore and Hong Kong. *Cities*, 62, 131-145.

Ahmed, B., Kamruzzaman, M., Zhu, X., Rahman, M., & Choi, K. (2013). Simulating land cover changes and their impacts on land surface temperature in Dhaka, Bangladesh. *Remote Sensing*, 5, 5969-5998.

Akbari, H., & Kolokotsa, D. (2016). Three decades of urban heat islands and mitigation technologies research. *Energy and Buildings*, 133, 834-842.

Akbari, H., Cartalis, C., Kolokotsa, D., Muscio, A., Pisello, A. L., Rossi, F., Santamouris, M., Synnefa, A., Wong, N.H., & Zinzi, M. (2016). Local climate change and urban heat island mitigation techniques–the state of the art. *Journal of Civil Engineering and Management*, 22, 1-16.

Akbari, H., Pomerantz, M., & Taha, H. (2001). Cool surfaces and shade trees to reduce energy use and improve air quality in urban areas. *Solar Energy*, 70, 295-310.

Alcoforado, M. J., Andrade, H., Lopes, A., & Vasconcelos, J. (2009). Application of climatic guidelines to urban planning: the example of Lisbon (Portugal). *Landscape and Urban Planning*, 90, 56-65.

Alexander, C. (2020). Normalised difference spectral indices and urban land cover as indicators of land surface temperature (LST). *International Journal of Applied Earth Observation and Geoinformation*, 86, 102013.

Anguelovski, I., Chu, E., & Carmin, J. (2014). Variations in approaches to urban climate adaptation: Experiences and experimentation from the global South. *Global Environmental Change*, 27, 156-167.

Arnfield, A. J. (2003). Two decades of urban climate research: a review of turbulence, exchanges of energy and water, and the urban heat island. *International Journal of Climatology*, 23(1), 1-26.

Arsiso, B. K., Tsidu, G. M., Stoffberg, G. H., & Tadesse, T. (2018). Influence of urbanization-driven land use/cover change on climate: The case of Addis Ababa, Ethiopia. *Physics and Chemistry of the Earth, Parts A/B/C*, 105, 212-223.

Artis, D. A., & Carnahan, W. H. (1982). Survey of emissivity variability in thermography of urban areas. *Remote Sensing of Environment*, *12*, 313-329.

Avdan, U., & Jovanovska, G. (2016). Algorithm for automated mapping of land surface temperature using LANDSAT 8 satellite data. *Journal of Sensors*, 2016, 1480307

Baklanov, A., Grimmond, C. S. B., Carlson, D., Terblanche, D., Tang, X., Bouchet, V., Lee, B., Langendijk, G., Kolli, R.K., & Hovsepyan, A. (2018). From urban meteorology, climate and environment research to integrated city services. *Urban Climate*, 23, 330-341.

Baldinelli, G., Bonafoni, S., & Rotili, A. (2017). Albedo retrieval from multispectral Landsat 8 observation in urban environment: Algorithm validation by in situ measurements. *IEEE Journal of Selected Topics in Applied Earth Observations and Remote Sensing*, 10, 4504-4511.

Balling Jr, R. C., & Cerveny, R. S. (1987). Long-term associations between wind speeds and the urban heat island of Phoenix, Arizona. *Journal of Climate and Applied Meteorology*, 26, 712-716.

Bangladesh Bureau of Statistics (BBS). (2012). *Bangladesh Population Census 2011*. Ministry of Planning, Dhaka.

Barsi, J. A., Schott, J. R., Palluconi, F. D., & Hook, S. J. (2005). Validation of a web-based atmospheric correction tool for single thermal band instruments. In *Earth Observing Systems X* (Vol. 5882, p. 58820E). International Society for Optics and Photonics.

Basara, J. B., Hall Jr, P. K., Schroeder, A. J., Illston, B. G., & Nemunaitis, K. L. (2008). Diurnal cycle of the Oklahoma City urban heat island. *Journal of Geophysical Research: Atmospheres*, 113(D20).

Berardi, U. (2016). The outdoor microclimate benefits and energy saving resulting from green roofs retrofits. *Energy and Buildings*, 121, 217-229.

Bianchini, F., & Hewage, K. (2012a). How "green" are the green roofs? Lifecycle analysis of green roof materials. *Building and Environment*, 48, 57-65.

Bianchini, F., & Hewage, K. (2012b). Probabilistic social cost-benefit analysis for green roofs: a lifecycle approach. *Building and Environment*, 58, 152-162.

Bosilovich, M. G. (2006). A comparison of MODIS land surface temperature with in situ observations. *Geophysical Research Letters*, 33, L20112.

Bottyán, Z., Kircsi, A., Szegedi, S., & Unger, J. (2005). The relationship between built-up areas and the spatial development of the mean maximum urban heat island in Debrecen, Hungary. *International Journal of Climatology*, 25, 405-418.

Bowler, D. E., Buyung-Ali, L., Knight, T. M., & Pullin, A. S. (2010). Urban greening to cool towns and cities: A systematic review of the empirical evidence. *Landscape and Urban Planning*, 97, 147-155.

Bründl, W. (1988). Climate function maps and urban planning. *Energy and Buildings*, 11, 123-127.

Buyadi, S. N. A., Mohd, W. M. N. W., & Misni, A. (2013). Green spaces growth impact on the urban microclimate. *Procedia-Social and Behavioral Sciences*, 105, 547-557.

Ca, V. T., Asaeda, T., & Abu, E. M. (1998). Reductions in air conditioning energy caused by a nearby park. *Energy and Buildings*, 29, 83-92.

Cameron, R. W., Taylor, J. E., & Emmett, M. R. (2014). What's 'cool'in the world of green façades? How plant choice influences the cooling properties of green walls. *Building and Environment*, 73, 198-207.

Cao, C., Lee, X., Liu, S., Schultz, N., Xiao, W., Zhang, M., & Zhao, L. (2016). Urban heat islands in China enhanced by haze pollution. *Nature Communications*, 7, 1-7.

Carter, T., & Keeler, A. (2008). Life-cycle cost–benefit analysis of extensive vegetated roof systems. *Journal of Environmental Management*, 87, 350-363.

Chakraborty, T., & Lee, X. (2019). A simplified urban-extent algorithm to characterize surface urban heat islands on a global scale and examine vegetation control on their spatiotemporal variability. *International Journal of Applied Earth Observation and Geoinformation*, 74, 269-280.

Chakraborty, T., Sarangi, C., & Tripathi, S. N. (2017). Understanding diurnality and inter-seasonality of a sub-tropical urban heat island. *Boundary-Layer Meteorology*, 163, 287-309.

Chander, G., & Markham, B. (2003). Revised Landsat-5 TM radiometric calibration procedures and postcalibration dynamic ranges. *IEEE Transactions on Geoscience and Remote Sensing*, 41, 2674-2677.

Chander, G., Markham, B. L., & Helder, D. L. (2009). Summary of current radiometric calibration coefficients for Landsat MSS, TM, ETM+, and EO-1 ALI sensors. *Remote Sensing of Environment*, 113, 893-903.

Chandler, T. J. (1967). Night-time temperatures in relation to Leicester's urban form. *Meteorological. Magazine*, 96, 244-250.

Chang, C. R., & Li, M. H. (2014). Effects of urban parks on the local urban thermal environment. *Urban Forestry & Urban Greening*, 13, 672-681.

Chang, C. R., Li, M. H., & Chang, S. D. (2007). A preliminary study on the local cool-island intensity of Taipei city parks. *Landscape and Urban Planning*, 80, 386-395.

Chapman, S., Watson, J. E., Salazar, A., Thatcher, M., & McAlpine, C. A. (2017). The impact of urbanization and climate change on urban temperatures: a systematic review. *Landscape Ecology*, 32, 1921-1935.

Chatzidimitriou, A., & Yannas, S. (2015). Microclimate development in open urban spaces: The influence of form and materials. *Energy and Buildings*, 108, 156-174.

Chavez Jr, P. S. (1988). An improved dark-object subtraction technique for atmospheric scattering correction of multispectral data. *Remote Sensing of Environment*, 24, 459-479.

Chen, A., Yao, X. A., Sun, R., & Chen, L. (2014). Effect of urban green patterns on surface urban cool islands and its seasonal variations. *Urban Forestry & Urban Greening*, 13, 646-654.

Chen, G., Li, X., Liu, X., Chen, Y., Liang, X., Leng, J., Xu, J., Liao, W., Qiu, Y., Wu, Q., & Huang, K. (2020). Global projections of future urban land expansion under shared socioeconomic pathways. *Nature Communications*, 11, 1-12.

Christidis, N., Mitchell, D., & Stott, P.A. (2019). Anthropogenic climate change and heat effects on health. *International Journal of Climatology*, 39, 4751-4768.

Chudnovsky, A., Ben-Dor, E., & Saaroni, H. (2004). Diurnal thermal behavior of selected urban objects using remote sensing measurements. *Energy and Buildings*, 36, 1063-1074.

Chun, B., & Guldmann, J. M. (2018). Impact of greening on the urban heat island: seasonal variations and mitigation strategies. *Computers, Environment and Urban Systems*, 71, 165-176.

Clay, R., Guan, H., Wild, N., Bennett, J., & Ewenz, C. (2016). Urban Heat Island traverses in the City of Adelaide, South Australia. *Urban Climate*, 17, 89-101.

Clement, F., Orange, D., Williams, M., Mulley, C., & Epprecht, M. (2009). Drivers of afforestation in Northern Vietnam: assessing local variations using geographically weighted regression. *Applied Geography,* 29*,* 561-576.

Clinton, N., & Gong, P. (2013). MODIS detected surface urban heat islands and sinks: Global locations and controls. *Remote Sensing of Environment*, 134, 294-304.

Cole, M. A., & Neumayer, E. (2004). Examining the impact of demographic factors on air pollution. *Population and Environment*, 26, 5-21.

Connelly, M., & Hodgson, M. (2008). Thermal and acoustical performance of green roofs: sound transmission loss of green roofs. In *Greening Rooftops for Sustainable Communities Conference, Awards and Trade Show-Baltimore. Vancouver*.

Connolly, C., Keil, R., & Ali, H. (2020). Extended urbanisation and the spatialities of infectious disease: Demographic change, infrastructure and governance. *Urban Studies*, doi: 10.1177/0042098020907277

Corner, R. J., Dewan, A. M., & Chakma, S. (2014). Monitoring and prediction of land-use and land-cover (LULC) change. In Dhaka Megacity (pp. 75-97). Springer Netherlands.

Coseo, P., & Larsen, L. (2014). How factors of land use/land cover, building configuration, and adjacent heat sources and sinks explain Urban Heat Islands in Chicago. *Landscape and Urban Planning*, 125, 117-129.

Coutts, A. M., Harris, R. J., Phan, T., Livesley, S. J., Williams, N. S., & Tapper, N. J. (2016). Thermal infrared remote sensing of urban heat: Hotspots, vegetation, and an assessment of techniques for use in urban planning. *Remote Sensing of Environment*, 186, 637-651.

Dai, Z., Guldmann, J. M., & Hu, Y. (2018). Spatial regression models of park and land-use impacts on the urban heat island in central Beijing. *Science of the Total Environment*, 626, 1136-1147.

de Faria Peres, L., de Lucena, A. J., Rotunno Filho, O. C., & de Almeida França, J. R. (2018). The urban heat island in Rio de Janeiro, Brazil, in the last 30 years using remote sensing data. *International Journal of Applied Earth Observation and Geoinformation*, 64, 104-116.

Deilami, K., Kamruzzaman, M., & Liu, Y. (2018). Urban heat island effect: A systematic review of spatio-temporal factors, data, methods, and mitigation measures. *International Journal of Applied Earth Observation and Geoinformation*, 67, 30-42.

Deng, C., & Wu, C., (2012). BCI: A biophysical composition index for remote sensing of urban environments. *Remote Sensing of Environment 127*, 247–259

Dewan, A, M., & Yamaguchi, Y. (2009). Land Use and Land Cover Change in Greater Dhaka, Bangladesh: Using Remote Sensing to Promote Sustainable Urbanization, *Applied Geography,* 29, 390-401.

Dewan, A. M., & Corner, R. J. (2014a). Impact of land use and land cover changes on urban land surface temperature. In Dhaka Megacity (pp. 219-238). Springer Netherlands.

Dewan, A. M., & Corner, R. J. (2014c). Spatiotemporal analysis of urban growth, sprawl and structure. In *Dhaka megacity* (pp. 99-121). Springer, Dordrecht.

Dewan, A., & Corner, R. (Eds.). (2014b). Dhaka megacity: Geospatial perspectives on urbanisation, environment and health. Springer Science & Business Media.

Doick, K. J., Peace, A., & Hutchings, T. R. (2014). The role of one large greenspace in mitigating London's nocturnal urban heat island. *Science of the Total Environment*, 493, 662-671.

Drach, P., Krüger, E. L., & Emmanuel, R. (2018). Effects of atmospheric stability and urban morphology on daytime intra-urban temperature variability for Glasgow, UK. *Science of the Total Environment*, 627, 782-791.

Driscoll, C. T., Eger, C. G., Chandler, D. G., Davidson, C. I., Roodsari, B. K., Flynn, C. D., Lambert, K.F., Bettez, N.D., & Groffman, P. M. (2015). Green Infrastructure: Lessons from Science and Practice, A publication of the Science Policy Exchange [available at https://science-policy-exchange.org/resources/reports/green-infrastructure-lessons-science-and-practice]

Dwivedi, A., & Khire, M. V. (2018). Application of split-window algorithm to study Urban Heat Island effect in Mumbai through land surface temperature approach. *Sustainable Cities and Society*, 41, 865-877.

Dwivedi, A., & Mohan, B. K. (2018). Impact of green roof on microclimate to reduce Urban Heat Island. *Remote Sensing Applications: Society and Environment,* 10, 56-69.

Eliasson, I. (2000). The use of climate knowledge in urban planning. *Landscape and Urban Planning*, 48, 31-44.

Emmanuel, R., Rosenlund, H., & Johansson, E. (2007). Urban shading—a design option for the tropics? A study in Colombo, Sri Lanka. *International Journal of Climatology*, 27, 1995-2004.

Erell, E., Portnov, B. A., & Etzion, Y. (2003). Mapping the potential for climate-conscious design of buildings. *Building and Environment*, 38, 271-281.

ESRI (2011). http://resources.esri.com/help/9.3/arcgisdesktop/com/gp_toolref/spatial_statistics_toolbox/regression_analysis_basics.htm (accessed at 10 March 2019)

ESRI (2012). http://resources.arcgis.com/en/help/main/10.1/index.html#//005p00000018000000 (accessed at 28 February 2019)

Estoque, R. C., & Murayama, Y. (2015). Classification and change detection of built-up lands from Landsat-7 ETM+ and Landsat-8 OLI/TIRS imageries: A comparative assessment of various spectral indices. *Ecological Indicators*, 56, 205-217.

Estoque, R. C., Murayama, Y., & Myint, S. W. (2017). Effects of landscape composition and pattern on land surface temperature: An urban heat island study in the megacities of Southeast Asia. *Science of the Total Environment*, 577, 349-359.

Evans, J. M., & de Schiller, S. (1990). Climate and urban planning: The example of the planning code for Vicente Lopez, Buenos Aires. *Energy and Buildings*, 15, 35-41.

Ferreira, L. S., & Duarte, D. H. S. (2019). Exploring the relationship between urban form, land surface temperature and vegetation indices in a subtropical megacity. *Urban Climate*, 27, 105-123.

Feyisa, G. L., Dons, K., & Meilby, H. (2014). Efficiency of parks in mitigating urban heat island effect: An example from Addis Ababa. *Landscape and Urban Planning*, 123, 87-95.

Finance Division (2014). *Bangladesh Climate Fiscal Framework*, Dhaka: Ministry of Finance, Government of the People's Republic of Bangladesh, Dhaka.

Fotheringham, A. S., Brunsdon, C., & Charlton, M. (2003). Geographically weighted regression: the analysis of spatially varying relationships. John Wiley & Sons.

Fotheringham, A. S., Charlton, M. E., & Brunsdon, C. (2001). Spatial variations in school performance: a local analysis using geographically weighted regression. *Geographical and Environmental Modelling,* 5*,* 43-66.

Frumkin, H. (2005). Guest editorial: health, equity, and the built environment. *Environmental Health Perspectives* 113, A290–A291.

Fu, P., & Rich, P. M. (2000). The solar analyst 1.0 manual. *Helios Environmental Modeling Institute (HEMI), USA*.

Fu, P., & Rich, P. M. (2002). A geometric solar radiation model with applications in agriculture and forestry. *Computers and Electronics in Agriculture*, 37, 25-35.

Gago, E. J., Roldan, J., Pacheco-Torres, R., & Ordóñez, J. (2013). The city and urban heat islands: A review of strategies to mitigate adverse effects. *Renewable and Sustainable Energy Reviews*, 25, 749-758.

Gallo, K. P., Adegoke, J. O., Owen, T. W., & Elvidge, C. D. (2002). Satellite-based detection of global urban heat-island temperature influence. *Journal of Geophysical Research: Atmospheres*, 107, ACL-16.

General Economics Division (GED). (2013). *Bangladesh Climate Public Expenditure and Institutional Review*, Bangladesh Planning Commission, Government of the People's Republic of Bangladesh, Dhaka.

General Economics Division (GED). (2016). *7th Five Year Plan: Accelerating Growth, Empowering Citizens*, Bangladesh Planning Commission, Government of the People's Republic of Bangladesh, Dhaka.

General Economics Division (GED). (2018). *Bangladesh Delta Plan 2100, Volume 1: Strategy*, Dhaka: Bangladesh Planning Commission, Government of the People's Republic of Bangladesh, Dhaka.

Georgescu, M., Morefield, P. E., Bierwagen, B. G., & Weaver, C. P. (2014). Urban adaptation can roll back warming of emerging megapolitan regions. *Proceedings of the National Academy of Sciences*, 111, 2909-2914.

Getter, K. L., & Rowe, D. B. (2006). The role of extensive green roofs in sustainable development. *HortScience*, 41, 1276-1285.

Gillespie, A., Rokugawa, S., Matsunaga, T., Cothern, J. S., Hook, S., & Kahle, A. B. (1998). A temperature and emissivity separation algorithm for Advanced Spaceborne Thermal Emission and Reflection Radiometer (ASTER) images. *IEEE Transactions on Geoscience and Remote Sensing*, 36, 1113-1126.

Gillies, R. R., Kustas, W. P., & Humes, K. S. (1997). A verification of the 'triangle' method for obtaining surface soil water content and energy fluxes from remote measurements of the Normalized Difference Vegetation Index (NDVI) and surface. *International Journal of Remote Sensing*, 18, 3145-3166.

Giridharan, R., & Emmanuel, R. (2018). The impact of urban compactness, comfort strategies and energy consumption on tropical urban heat island intensity: a review. *Sustainable Cities and Society*, 40, 677-687.

Golden, J. S. (2004). The built environment induced urban heat island effect in rapidly urbanizing arid regions–a sustainable urban engineering complexity. *Environmental Sciences*, 1, 321-349.

Gollier, C., & Weitzman, M. L. (2010). How should the distant future be discounted when discount rates are uncertain? *Economics Letters*, 107, 350-353

GoogleEarth. Available online: https://www.google.com/earth

Grimmond, C. S. B., Roth, M., Oke, T. R., Au, Y. C., Best, M., Betts, R., Carmichael, G., Cleugh, H., Dabberdt, W., Emmanuel, R., Freitas, E., Fortuniak, K., Hanna, S., Klein, P., Kalkstein, L.S., Liu, C.H., Nickson, A., Pearlmutter, D., Sailor, D., & Voogt, J. (2010). Climate and more sustainable cities: climate information for improved planning and management of cities (producers/capabilities perspective). *Procedia Environmental Sciences*, 1, 247-274.

Guhathakurta, S., & Gober, P. (2007). The impact of the Phoenix urban heat island on residential water use. *Journal of the American Planning Association*, 73, 317-329.

Gunawardena, K. R., Wells, M. J., & Kershaw, T. (2017). Utilising green and bluespace to mitigate urban heat island intensity. *Science of the Total Environment*, 584, 1040-1055.

Guo, G., Wu, Z., Xiao, R., Chen, Y., Liu, X., & Zhang, X. (2015). Impacts of urban biophysical compsotion on land surface temperature in urban heat island clusters. *Landscape and Urban Planning* 135, 1-10.

Guo, G., Zhou, X., Wu, Z., Xiao, R., & Chen, Y. (2016). Characterizing the impact of urban morphology heterogeneity on land surface temperature in Guangzhou, China. *Environmental Modelling & Software*, 84, 427-439.

Gusdorf, F., & Hallegatte, S. (2007). Compact or spread-out cities: Urban planning, taxation, and the vulnerability to transportation shocks. *Energy Policy*, 35, 4826-4838.

Halisçelik, E., & Soytas, M. A. (2019). Sustainable development from millennium 2015 to Sustainable Development Goals 2030. *Sustainable Development*, 27, 545-572.

Hamoodi, M. N., Corner, R., & Dewan, A. (2019). Thermophysical behaviour of LULC surfaces and their effect on the urban thermal environment. *Journal of Spatial Science*, 64, 111-130.

Hapfelmeier, A., & Ulm, K. (2014). Variable selection by Random Forests using data with missing values. *Computational Statistics & Data Analysis*, 80, 129-139.

Hart, M. A., & Sailor, D. J. (2009). Quantifying the influence of land-use and surface characteristics on spatial variability in the urban heat island. *Theoretical and Applied Climatology*, 95, 397-406.

Hartig, T., Mitchell, R., De Vries, S., & Frumkin, H. (2014). Nature and health. *Annual Review of Public Health*, 35, 207-228.

Hartz, D. A., Prashad, L., Hedquist, B. C., Golden, J., & Brazel, A. J. (2006). Linking satellite images and hand-held infrared thermography to observed neighborhood climate conditions. *Remote Sensing of Environment*, 104, 190-200.

Hathway, E. A., & Sharples, S. (2012). The interaction of rivers and urban form in mitigating the Urban Heat Island effect: A UK case study. *Building and Environment*, 58, 14-22.

He, B. J. (2018). Potentials of meteorological characteristics and synoptic conditions to mitigate urban heat island effects. *Urban Climate*, 24, 26-33.

He, X., Shen, S., Miao, S., Dou, J., & Zhang, Y. (2015). Quantitative detection of urban climate resources and the establishment of an urban climate map (UCMap) system in Beijing. *Building and Environment*, 92, 668-678.

Hien, W. N., Yok, T. P., & Yu, C. (2007). Study of thermal performance of extensive rooftop greenery systems in the tropical climate. *Building and Environment*, *42*(1), 25-54.

Hopkins, F. M., Ehleringer, J. R., Bush, S. E., Duren, R. M., Miller, C. E., Lai, C. T., Hsu, Y-K., Carranza, V., & Randerson, J. T. (2016). Mitigation of methane emissions in cities: How new measurements and partnerships can contribute to emissions reduction strategies. *Earth's Future*, 4, 408-425.

Houet, T., & Pigeon, G. (2011). Mapping urban climate zones and quantifying climate behaviors–an application on Toulouse urban area (France). *Environmental Pollution*, 159, 2180-2192.

Howard, L. (1833). *The climate of London deduced from meteorological observations*. Vol 1, Harvey and Darton, London.

Hsieh, C. M., & Huang, H. C. (2016). Mitigating urban heat islands: A method to identify potential wind corridor for cooling and ventilation. *Computers, Environment and Urban Systems*, 57, 130-143.

Hu, L., & Brunsell, N. A. (2013). The impact of temporal aggregation of land surface temperature data for surface urban heat island (SUHI) monitoring. *Remote Sensing of Environment*, 134, 162-174.

Huang, Q., Huang, J., Yang, X., Fang, C., & Liang, Y. (2019). Quantifying the seasonal contribution of coupling urban land use types on Urban Heat Island using Land Contribution Index: A case study in Wuhan, China. *Sustainable Cities and Society*, 44, 666-675.

Huete, A. R. (1988). A soil-adjusted vegetation index (SAVI*). Remote Sensing of Environment,* 25, 295-309.

Imamura, I. R. (1970). Role of soil moisture in the determination of urban heat island intensity in different climate regimes. *WIT Transactions on Ecology and the Environment*, 1, 395-402.

Imhoff, M., Zhang, P., Wolfe, R, E., & Bounoua, L. (2010). Remote sensing of the urban heat island effect across biomes in the continental USA. *Remote Sensing of Environment* 114, 504–513.

Itzhak-Ben-Shalom, H., Alpert, P., Potchter, O., & Samuel, R. (2017). MODIS Summer SUHI Cross-sections Anomalies over the Megacities of the Monsoon Asia Region and Global Trends. *The Open Atmospheric Science Journal,* 11, 121-136

Jacobson, M. Z., & Ten, J. E.H. (2012). Effects of urban surfaces and white roofs on global and regional climate. *Journal of Climate*, 25, 1028-1044.

Jia, W., & Zhao, S. (2020). Trends and drivers of land surface temperature along the urban-rural gradients in the largest urban agglomeration of China. *Science of The Total Environment*, 711, 134579.

Jim, C. Y. (2015). Assessing climate–adaptation effect of extensive tropical green roofs in cities. *Landscape and Urban Planning*, 138, 54-70.

Jiménez-Muñoz, J. C., & Sobrino, J. A. (2003). A generalized single-channel method for retrieving land surface temperature from remote sensing data. *Journal of Geophysical Research: Atmospheres*, 108, 4688.

Jin, M., Dickinson, R. E., & Zhang, D. A. (2005). The footprint of urban areas on global climate as characterized by MODIS. *Journal of Climate*, 18, 1551-1565.

Jin, S. & Sader, S. A. (2005). Comparison of time series tasselled cap wetness and the normalized difference moisture index in detecting forest disturbances. *Remote Sensing of Environment*, 94, 364-372.

Jusuf, S. K., Wong, N. H., Hagen, E., Anggoro, R., & Hong, Y. (2007). The influence of land use on the urban heat island in Singapore. *Habitat International*, 31, 232-242.

Kakon, A. N., Mishima, N., & Kojima, S. (2009). Simulation of the urban thermal comfort in a high density tropical city: Analysis of the proposed urban construction rules for Dhaka, Bangladesh. *Building Simulation*, 2, 291 - 305.

Kalnay, E., & Cai, M. (2003). Impact of urbanization and land-use change on climate. *Nature*, 423, 528.

Kantzioura, A., Kosmopoulos, P., & Zoras, S. (2012). Urban surface temperature and microclimate measurements in Thessaloniki. *Energy and Buildings*, 44, 63-72.

Karnieli, A., Agam, N., Pinker, R. T., Anderson, M., Imhoff, M. L., Gutman, G. G., Panov, N., & Goldberg, A. (2010). Use of NDVI and land surface temperature for drought assessment: merits and limitations. *Journal of Climate*, 23, 618-633.

Katpatal, Y. B., Kute, A., & Satapathy, D. R. (2008). Surface-and air-temperature studies in relation to land use/land cover of Nagpur urban area using Landsat 5 TM data. *Journal of urban planning and Development*, 134, 110-118.

Kawamura, M., Jayamanna, S. and Tsujiko, Y. (1996). Relation between social and environmental conditions in Colombo, Sri Lanka and the urban index estimated by satellite remote sensing data, *International Archives of Photogrammetry and Remote Sensing*, XXXI, 321-326.

Ke, X., van Vliet, J., Zhou, T., Verburg, P. H., Zheng, W., & Liu, X. (2018). Direct and indirect loss of natural habitat due to built-up area expansion: A model-based analysis for the city of Wuhan, China. *Land Use Policy*, 74, 231-239.

Kerr, Y. H., Lagouarde, J. P., Nerry, F., & Ottlé, C. (2004). Land surface temperature retrieval techniques and applications: Case of the AVHRR. In *Thermal Remote Sensing in Land Surface Processing* (pp. 55-131). CRC Press.

Kim, Y. H., & Baik, J. J. (2005). Spatial and temporal structure of the urban heat island in Seoul. *Journal of Applied Meteorology*, 44, 591-605.

Kleerekoper, L., Van Esch, M., & Salcedo, T. B. (2012). How to make a city climate-proof, addressing the urban heat island effect. *Resources, Conservation and Recycling*, 64, 30-38.

Klok, L., Zwart, S., Verhagen, H., & Mauri, E. (2012). The surface heat island of Rotterdam and its relationship with urban surface characteristics. *Resources, Conservation and Recycling*, 64, 23-29.

Konarska, J., Holmer, B., Lindberg, F., & Thorsson, S. (2016). Influence of vegetation and building geometry on the spatial variations of air temperature and cooling rates in a high-latitude city. *International Journal of Climatology*, 36, 2379-2395.

Kotharkar, R., & Bagade, A. (2018). Evaluating urban heat island in the critical local climate zones of an Indian city. *Landscape and Urban Planning*, 169, 92-104.

Kotharkar, R., & Surawar, M. (2015). Land use, land cover, and population density impact on the formation of canopy urban heat islands through traverse survey in the Nagpur urban area, India. *Journal of Urban Planning and Development*, 142, 04015003.

Kotharkar, R., Ramesh, A., & Bagade, A. (2018). Urban heat island studies in South Asia: a critical review. *Urban Climate*, 24, 1011-1026.

LaDeau, S. L., Allan, B. F., Leisnham, P. T., & Levy, M. Z. (2015). The ecological foundations of transmission potential and vector-borne disease in urban landscapes. *Functional Ecology*, 29, 889-901.

Lai, J., Zhan, W., Huang, F., Quan, J., Hu, L., Gao, L., & Ju, W. (2018a). Does quality control matter? Surface urban heat island intensity variations estimated by satellite-derived land surface temperature products. *ISPRS Journal of Photogrammetry and Remote Sensing*, 139, 212-227.

Lai, J., Zhan, W., Huang, F., Voogt, J., Bechtel, B., Allen, M., Peng, S., Hong, F., Liu, Y., & Du, P. (2018b). Identification of typical diurnal patterns for clear-sky climatology of surface urban heat islands. *Remote Sensing of Environment*, 217, 203-220.

Lau, K. K. L., Ren, C., Ho, J., & Ng, E. (2016). Numerical modelling of mean radiant temperature in high-density sub-tropical urban environment. *Energy and Buildings*, 114, 80-86.

Lazzarini, M., Marpu, P. R., & Ghedira, H. (2013). Temperature-land cover interactions: The inversion of urban heat island phenomenon in desert city areas. *Remote Sensing of Environment*, 130, 136-152.

Levermore, G., Parkinson, J., Lee, K., Laycock, P., & Lindley, S. (2018). The increasing trend of the urban heat island intensity. *Urban Climate*, 24, 360-368.

Li, D., Liao, W., Rigden, A. J., Liu, X., Wang, D., Malyshev, S., & Shevliakova, E. (2019). Urban heat island: Aerodynamics or imperviousness?. *Science Advances*, 5, eaau4299.

Li, H., Harvey, J., & Kendall, A. (2013). Field measurement of albedo for different land cover materials and effects on thermal performance. *Building and Environment*, 59, 536-546.

Li, H., Zhou, Y., Wang, X., Zhou, X., Zhang, H., & Sodoudi, S. (2018). Quantifying urban heat island intensity and its physical mechanism using WRF/UCM. *Science of the Total Environment*, 650, 3110-3119.

Li, J., Song, C., Cao, L., Zhu, F., Meng, X., & Wu, J. (2011). Impacts of landscape structure on surface urban heat islands: A case study of Shanghai, China. *Remote Sensing of Environment*, 115, 3249-3263.

Li, N., & Li, X. (2020). The Impact of Building Thermal Anisotropy on Surface Urban Heat Island Intensity Estimation: An Observational Case Study in Beijing. *IEEE Geoscience and Remote Sensing Letters*, doi: 10.1109/LGRS.2019.2962383

Li, X., Li, W., Middel, A., Harlan, S. L., Brazel, A. J., & Turner, B. L. (2016). Remote sensing of the surface urban heat island and land architecture in Phoenix, Arizona: Combined effects of land composition and configuration and cadastral–demographic–economic factors. *Remote Sensing of Environment*, 174, 233-243.

Li, Y. Y., Zhang, H., & Kainz, W. (2012). Monitoring patterns of urban heat islands of the fast-growing Shanghai metropolis, China: Using time-series of Landsat TM/ETM+ data. *International Journal of Applied Earth Observation and Geoinformation*, 19, 127-138

Liang, S. (2001). Narrowband to broadband conversions of land surface albedo I: Algorithms. *Remote Sensing of Environment*, 76, 213-238.

Liao, W., Liu, X., Li, D., Luo, M., Wang, D., Wang, S., Baldwin, J., Lin, L., Li, X., Feng, K., Hubacek, K., & Yang, K. (2018). Stronger contributions of urbanization to heat wave trends in wet climates. *Geophysical Research Letters*, 45, 11-310.

Lin, B. S., & Lin, C. T. (2016). Preliminary study of the influence of the spatial arrangement of urban parks on local temperature reduction. *Urban Forestry and Urban Greening*, 20, 348-357.

Lin, P., Lau, S. S. Y., Qin, H., & Gou, Z. (2017). Effects of urban planning indicators on urban heat island: a case study of pocket parks in high-rise high-density environment. *Landscape and Urban Planning*, 168, 48-60.

Liu, H. Q. & Huete, A. R. (1995). A feedback-based modification of the NDVI to minimize canopy background and atmospheric noise. *IEEE Transactions on Geoscience and Remote Sensing*, 33, 457-465.

Liu, S., Zang, Z., Wang, W., & Wu, Y. (2019). Spatial-temporal evolution of urban heat Island in Xi'an from 2006 to 2016. *Physics and Chemistry of the Earth, Parts A/B/C*, 110, 185-194.

Lo, C. P., & Quattrochi, D. A. (2003). Land-use and land-cover change, urban heat island phenomenon, and health implications. *Photogrammetric Engineering & Remote Sensing*, 69, 1053-1063.

Luber, G., & McGeehin, M. (2008). Climate change and extreme heat events. *American Journal of Preventive Medicine*, 35, 429-435.

Ma, Y., Kuang, Y. & Huang, N. (2010). Coupling urbanization analyses for studying urban thermal environment and its interplay with biophysical parameters based on TM/ETM+ imagery. *International Journal Applied Earth Observation and Geoinformation*, 12, 110-118.

Macarof, P., & Statescu, F. (2017). Comparasion of ndbi and ndvi as indicators of surface urban heat island effect in landsat 8 imagery: A case study of iasi. *Present Environment and Sustainable Development*, 11, 141-150.

Mahdiyar, A., Tabatabaee, S., Sadeghifam, A. N., Mohandes, S. R., Abdullah, A., & Meynagh, M. M. (2016). Probabilistic private cost-benefit analysis for green roof installation: A Monte Carlo simulation approach. *Urban Forestry & Urban Greening*, 20, 317-327.

Maheshwari, B., Pinto, U., Akbar, S., & Fahey, P. (2020). Is urbanisation also the culprit of climate change?–Evidence from Australian cities. *Urban Climate*, 31, 100581.

Manoli, G., Fatichi, S., Schläpfer, M., Yu, K., Crowther, T. W., Meili, N., Burlando, P., Katul, G.G., & Bou-Zeid, E. (2019). Magnitude of urban heat islands largely explained by climate and population. *Nature*, 573, 55-60.

Martilli, A., Krayenhoff, E. S., & Nazarian, N. (2020). Is the Urban Heat Island intensity relevant for heat mitigation studies?. *Urban Climate*, 31, 100541.

McFeeters, S. K. (1996). The use of the Normalized Difference Water Index (NDWI) in the delineation of open water features. *International Journal of Remote Sensing,* 17, 1425-1432.

McMillin, L. M. (1975). Estimation of sea surface temperatures from two infrared window measurements with different absorption. *Journal of Geophysical Research*, 80, 5113-5117.

Metz, M., Rocchini, D., & Neteler, M., (2014). Surface Temperatures at the Continental Scale. Tracking Changes with Remote Sensing at Unprecedented Detail. *Remote Sensing, 6,* 3822-3840.

Milly, P. C., Betancourt, J., Falkenmark, M., Hirsch, R. M., Kundzewicz, Z. W., Lettenmaier, D. P., & Stouffer, R. J. (2008). Stationarity is dead: Whither water management? *Science*, 319, 573-574.

Ministry of Environment and Forest (MoEF) (2009). *Bangladesh Climate Change Strategy and Action Plan 2009*, Government of the People's Republic of Bangladesh, Dhaka.

Mohan, M., Kikegawa, Y., Gurjar, B. R., Bhati, S., & Kolli, N. R. (2013). Assessment of urban heat island effect for different land use–land cover from micrometeorological measurements and remote sensing data for megacity Delhi. *Theoretical and Applied Climatology*, 112, 647-658.

Montanaro, M., Gerace, A., Lunsford, A., & Reuter, D. (2014). Stray light artefacts in imagery from the Landsat 8 Thermal Infrared Sensor. *Remote Sensing*, 6, 10435-10456.

Mora, C. (2010). A synthetic map of the climatopes of the Serra da Estrela (Portugal). *Journal of Maps*, 6, 591-608.

Moretti, E. (2014). *Cities and growth*. International Growth Center, The UK.

Moyer, A. N., & Hawkins, T. W. (2017). River effects on the heat island of a small urban area. *Urban Climate*, 21, 262-277.

Muniz-Gäal, L. P., Pezzuto, C. C., de Carvalho, M. F. H., & Mota, L. T. M. (2020). Urban geometry and the microclimate of street canyons in tropical climate. *Building and Environment*, 169, 106547.

Mushore, T. D., Odindi, J., Dube, T., & Mutanga, O. (2017). Prediction of future urban surface temperatures using medium resolution satellite data in Harare metropolitan city, Zimbabwe. *Building and Environment*, 122, 397-410.

Nastran, M., Kobal, M., & Eler, K. (2019). Urban heat islands in relation to Greenland use in European cities. *Urban Forestry & Urban Greening,* 37, 33–41.

Ndossi, M. I., & Avdan, U. (2016). Application of open source coding technologies in the production of land surface temperature (LST) maps from Landsat: a PyQGIS plugin. *Remote sensing*, 8, 413.

Netusil, N. R., Levin, Z., Shandas, V., & Hart, T. (2014). Valuing green infrastructure in Portland, Oregon. *Landscape and Urban Planning*, 124, 14-21.

Nichol, J. E. (1996). Analysis of the urban thermal environment with LANDSAT data. *Environment and Planning B: Planning and Design*, 23, 733-747.

Nichol, J. E., & Wong, M. S. (2008). Spatial variability of air temperature and appropriate resolution for satellite-derived air temperature estimation. *International Journal of Remote Sensing*, 29, 7213-7223.

Nichol, J. E., Fung, W. Y., Lam, K. S., & Wong, M. S. (2009). Urban heat island diagnosis using ASTER satellite images and 'in situ' air temperature. *Atmospheric Research*, 94, 276-284.

Nishimura, N., Nomura, T., Iyota, H., & Kimoto, S. (1998). Novel water facilities for creation of comfortable urban micrometeorology. *Solar Energy*, 64, 197-207.

Oke, T. R. (1988). The urban energy balance. *Progress in Physical Geography*, 12, 471-508.

Oke, T. R. (1995). The heat island of the urban boundary layer: characteristics, causes and effects. In Wind climate in cities (pp. 81-107). Springer, Dordrecht.

Oke, T. R. (2004). Urban observations. World Meteorological Organization, IOM Report No 81, WMO/TD no 1250.

Oke, T. R., (1982). The energetic basis of the urban heat island. *Quarterly Journal of the Royal Meteorological Society*, 108, 1-24.

Onishi, A., Cao, X., Ito, T., Shi, F., & Imura, H. (2010). Evaluating the potential for urban heat-island mitigation by greening parking lots. *Urban forestry & Urban greening,* 9, 323-332.

Pachauri, R. K. , Allen, M. R. , Barros, V. R. , Broome, J. , Cramer, W. , Christ, R. , Church, J. A. , Clarke, L. , Dahe, Q. , Dasgupta, P. , Dubash, N. K. , Edenhofer, O. , Elgizouli, I. , Field, C. B. , Forster, P. , Friedlingstein, P. , Fuglestvedt, J. , Gomez-Echeverri, L. , Hallegatte, S. , Hegerl, G. , Howden, M. , Jiang, K. , Jimenez Cisneroz, B. , Kattsov, V. , Lee, H. , Mach, K. J. , Marotzke, J. , Mastrandrea, M. D. , Meyer, L. , Minx, J. , Mulugetta, Y. , O'Brien, K. , Oppenheimer, M. , Pereira, J. J. , Pichs-Madruga, R. , Plattner, G. K. , Pörtner, H. O. , Power, S. B. , Preston, B. , Ravindranath, N. H. , Reisinger, A. , Riahi, K. , Rusticucci, M. , Scholes, R. , Seyboth, K. , Sokona, Y. , Stavins, R. , Stocker, T. F. , Tschakert, P. , van Vuuren, D. and van Ypserle, J. P. (2014): Climate Change 2014: Synthesis Report. Contribution of Working Groups I, II and III to the Fifth Assessment Report of the Intergovernmental Panel on Climate Change / R. Pachauri and L. Meyer (editors), IPCC, 151 p., Geneva, Switzerland.

Pandey, A. K., Singh, S., Berwal, S., Kumar, D., Pandey, P., Prakash, A. Lodhi, N., Maithani, S., Jain, V.K., & Kumar, K. (2014). Spatio–temporal variations of urban heat island over Delhi. *Urban Climate*, 10, 119-133.

Park, S., Tuller, S. E., & Jo, M. (2014). Application of Universal Thermal Climate Index (UTCI) for microclimatic analysis in urban thermal environments. *Landscape and Urban Planning,* 125, 146-155.

Parsaee, M., Joybari, M. M., Mirzaei, P. A., & Haghighat, F. (2019). Urban heat island, urban climate maps and urban development policies and action plans. *Environmental Technology and Innovation*, 14, 100341.

Peng, J., Jia, J., Liu, Y., Li, H., & Wu, J. (2018). Seasonal contrast of the dominant factors for spatial distribution of land surface temperature in urban areas. *Remote Sensing of Environment*, 215, 255-267.

Peng, J., Ma, J., Liu, Q., Liu, Y., Li, Y., & Yue, Y. (2018). Spatial-temporal change of land surface temperature across 285 cities in China: An urban-rural contrast perspective. *Science of the Total Environment*, 635, 487-497.

Peng, S., Feng, Z., Liao, H., Huang, B., Peng, S., & Zhou, T. (2019). spatial-temporal pattern of, and driving forces for, urban heat island in China. *Ecological Indicators*, 96, 127-132.

Peng, S., Piao, S., Ciais, P., Friedlingstein, P., Ottle, C., Bréon, F. M., Nan, H., Zhou, L., & Myneni, R. B. (2011). Surface urban heat island across 419 global big cities. *Environmental Science and Technology*, 46, 696-703.

Peng, S., Piao, S., Ciais, P., Myneni, R. B., Chen, A., Chevallier, F., & Vicca, S. (2013). Asymmetric effects of daytime and night-time warming on Northern Hemisphere vegetation. *Nature,* 501, 88-92.

Perini, K., & Rosasco, P. (2013). Cost–benefit analysis for green façades and living wall systems. *Building and Environment*, 70, 110-121.

Perini, K., Ottelé, M., Fraaij, A. L. A., Haas, E. M., & Raiteri, R. (2011). Vertical greening systems and the effect on airflow and temperature on the building envelope. *Building and Environment*, 46, 2287-2294.

Peterson, T. C. (2003). Assessment of urban versus rural in situ surface temperatures in the contiguous United States: No difference found. *Journal of Climate*, 16, 2941-2959.

Petralli, M., Massetti, L., Brandani, G., & Orlandini, S. (2014). Urban planning indicators: useful tools to measure the effect of urbanization and vegetation on summer air temperatures. *International Journal of Climatology*, 34, 1236-1244.

Phelan, P. E., Kaloush, K., Miner, M., Golden, J., Phelan, B., Silva III, H., & Taylor, R. A. (2015). Urban heat island: mechanisms, implications, and possible remedies. *Annual Review of Environment and Resources*, 40, 285-307.

Pyrgou, A., Hadjinicolaou, P., & Santamouris, M. (2020). Urban-rural moisture contrast: Regulator of the urban heat island and heatwaves' synergy over a Mediterranean city. *Environmental Research*, 182, 109102.

Qi, J., Chehbouni, A., Huete, A. R., Kerr, Y. H., & Sorooshian, S. (1994). A modified soil adjusted vegetation index. *Remote Sensing of Environment*, 48, 119-126.

Qin, Z., Karnieli, A., & Berliner, P. (2001). A mono-window algorithm for retrieving land surface temperature from Landsat TM data and its application to the Israel-Egypt border region. *International Journal of Remote Sensing*, 22, 3719-3746.

Rajagopalan, P., Lim, K. C., & Jamei, E. (2014). Urban heat island and wind flow characteristics of a tropical city. *Solar Energy*, 107, 159-170.

Rajasekar, U., & Weng, Q. (2009). Urban heat island monitoring and analysis using anon-parametric model: A case study of Indianapolis. *ISPRS Journal of Photogrammetry and Remote Sensing,* 64*,* 86–96.

RAJUK, (2017). *Detailed Area Plan (DAP) Survey Report*, Rajdhani Unnayan Katropakka, Dhaka.

Rana, M. M. P. (2011). Urbanization and sustainability: challenges and strategies for sustainable urban development in Bangladesh. *Environment, Development and Sustainability*, 13, 237-256.

Ren, C., Ng, E. Y. Y., & Katzschner, L. (2011). Urban climatic map studies: a review. *International Journal of Climatology*, 31, 2213-2233.

Rich, P., Dubayah, R. C., Hetrick, W., & Saving, S. (1994). Using viewshed models to calculate intercepted solar radiation: applications in ecology. American Society for Photogrammetry and Remote Sensing Technical Papers. In *American Society of Photogrammetry and Remote Sensing* (pp. 524-529).

Rizwan, A. M., Dennis, L. Y., & Chunho, L. I. U. (2008). A review on the generation, determination and mitigation of Urban Heat Island. *Journal of Environmental Sciences*, 20, 120-128.

Rodríguez, L. R., Ramos, J. S., de la Flor, F. J. S., & Domínguez, S. Á. (2020). Analyzing the Urban Heat Island: comprehensive methodology for data gathering and optimal design of mobile transects. *Sustainable Cities and Society*, 55, 102027.

Roth, M. (2007). Review of urban climate research in (sub) tropical regions. *International Journal of Climatology*, 27, 1859-1873.

Rouhollahi, M., & Masouleh, Z. P. (2016). Housing and microclimate: improving liveability in Adelaide. In Zuo, J. & Soebarto, D.V., (2016) (eds.), Fifty years later: revisiting the role of architectural science in design and practice, The Architectural Science Association and The University of Adelaide, pp. 149-158.

Rouse, J.W.J., Haas, R.H., Schell, J.A. and Deering, D.W., 1974. Monitoring vegetation systems in the Great Plains with ERTS, In Freden S.C., Mercanti, E.P. and Becker, M.A. (eds.), Third Earth Resources Technology Satellite-1 Symposium, Volume 1, NASA, pp. 309-351.

Ruiz, M. A., Sosa, M. B., Cantaloube, E. N. C., & Cantón, M. A. (2015). Suitable configurations for forested urban canyons to mitigate the UHI in the city of Mendoza, Argentina. *Urban Climate*, 14, 197-212.

Saaroni, H., Amorim, J. H., Hiemstra, J. A., & Pearlmutter, D. (2018). Urban Green Infrastructure as a tool for urban heat mitigation: Survey of research methodologies and findings across different climatic regions. *Urban Climate*, 24, 94-110.

Salata, F., Golasi, I., Petitti, D., de Lieto Vollaro, E., Coppi, M., & de Lieto Vollaro, A. (2017). Relating microclimate, human thermal comfort and health during heat waves: An analysis of heat island mitigation strategies through a case study in an urban outdoor environment. *Sustainable Cities and Society*, 30, 79-96.

Saneinejad, S., Moonen, P., & Carmeliet, J. (2014). Comparative assessment of various heat island mitigation measures. *Building and Environment*, 73, 162-170.

Santamouris, M. (2014). Cooling the cities–a review of reflective and green roof mitigation technologies to fight heat island and improve comfort in urban environments. *Solar Energy*, 103, 682-703.

Santamouris, M., Cartalis, C., Synnefa, A., & Kolokotsa, D. (2015). On the impact of urban heat island and global warming on the power demand and electricity consumption of buildings—A review. *Energy and Buildings*, 98, 119-124.

Santamouris, M., Paraponiaris, K., & Mihalakakou, G. (2007). Estimating the ecological footprint of the heat island effect over Athens, Greece. *Climatic Change*, 80, 265-276.

Scherer, D., Fehrenbach, U., Beha, H. D., & Parlow, E. (1999). Improved concepts and methods in analysis and evaluation of the urban climate for optimizing urban planning processes. *Atmospheric Environment*, 33, 4185-4193.

Scherer, D., Fehrenbach, U., Lakes, T., Lauf, S., Meier, F., & Schuster, C. (2014). Quantification of heat-stress related mortality hazard, vulnerability and risk in Berlin, Germany. *DIE ERDE–Journal of the Geographical Society of Berlin*, 144, 238-259.

Schwarz, N., Lautenbach, S., & Seppelt, R. (2011). Exploring indicators for quantifying surface urban heat islands of European cities with MODIS land surface temperatures. *Remote Sensing of Environment*, 115, 3175-3186.

Schwarz, N., Schlink, U., Franck, U., & Großmann, K. (2012). Relationship of land surface and air temperatures and its implications for quantifying urban heat island indicators—An application for the city of Leipzig (Germany). *Ecological Indicators*, 18, 693-704.

Scott, A. A., Waugh, D. W., & Zaitchik, B. F. (2018). Reduced Urban Heat Island intensity under warmer conditions. *Environmental Research Letters*, 13, 064003.

Scott, A. A., Zaitchik, B., Waugh, D. W., & O'Meara, K. (2017). Intra-urban temperature variability in Baltimore. *Journal of Applied Meteorology and Climatology*, 56, 159-171.

SENES Consultants Limited. (2007). Dhaka metropolitan development plan strategic environmental assessment, The World Bank, Washington DC.

Seto, K. C., Fragkias, M., Güneralp, B., & Reilly, M. K. (2011). A meta-analysis of global urban land expansion. *PLoS One*, 6, e23777.

Seto, K. C., Sánchez-Rodríguez, R., & Fragkias, M. (2010). The new geography of contemporary urbanization and the environment. *Annual Review of Environment and Resources*, 35, 167-194.

Shahidan, M. F., Jones, P. J., Gwilliam, J., & Salleh, E. (2012). An evaluation of outdoor and building environment cooling achieved through combination modification of trees with ground materials. *Building and Environment*, 58, 245-257.

Sharmin, T., Steemers, K., & Matzarakis, A. (2015). Analysis of microclimatic diversity and outdoor thermal comfort perceptions in the tropical megacity Dhaka, Bangladesh. *Building and Environment*, 94, 734-750.

Sharmin, T., Steemers, K., & Matzarakis, A. (2017). Microclimatic modelling in assessing the impact of urban geometry on urban thermal environment. *Sustainable Cities and Society*, 34, 293-308.

Shashua-Bar, L., & Hoffman, M. E. (2003). Geometry and orientation aspects in passive cooling of canyon streets with trees. *Energy and Buildings*, 35, 61-68.

Shastri, H., Barik, B., Ghosh, S., Venkataraman, C., & Sadavarte, P. (2017). Flip flop of day-night and summer-winter surface urban heat island intensity in India. *Scientific Reports*, 7, 1-8.

Shen, H., Huang, L., Zhang, L., Wu, P., & Zeng, C. (2016). Long-term and fine-scale satellite monitoring of the urban heat island effect by the fusion of multi-temporal and multi-sensor remote sensed data: A 26-year case study of the city of Wuhan in China. *Remote Sensing of Environment*, 172, 109-125.

Sheng, L., Tang, X., You, H., Gu, Q., & Hu, H. (2017). Comparison of the urban heat island intensity quantified by using air temperature and Landsat land surface temperature in Hangzhou, China. *Ecological Indicators*, 72, 738-746.

Shiflett, S. A., Liang, L. L., Crum, S. M., Feyisa, G. L., Wang, J., & Jenerette, G. D. (2017). Variation in the urban vegetation, surface temperature, air temperature nexus. *Science of the Total Environment*, 579, 495-505.

Silva, J. S., da Silva, R. M., & Santos, C. A. G. (2018). Spatiotemporal impact of land use/land cover changes on urban heat islands: A case study of Paço do Lumiar, Brazil. *Building and Environment*, 136, 279-292.

Sleiman, M., Ban-Weiss, G., Gilbert, H. E., François, D., Berdahl, P., Kirchstetter, T. W. & Levinson, R. (2011). Soiling of building envelope surfaces and its effect on solar reflectance—Part I: Analysis of roofing product databases. *Solar Energy Materials and Solar Cells*, 95, 3385-3399.

Soares, A. L., Rego, F. C., McPherson, E. G., Simpson, J. R., Peper, P. J., & Xiao, Q. (2011). Benefits and costs of street trees in Lisbon, Portugal. *Urban Forestry and Urban Greening*, 10, 69-78.

Sobrino, J. A., Jiménez-Muñoz, J. C., Sòria, G., Romaguera, M., Guanter, L., Moreno, J., Plaza, A. & Martínez, P. (2008). Land surface emissivity retrieval from different VNIR and TIR sensors. *IEEE Transactions on Geoscience and Remote Sensing*, 46, 316-327.

Sobrino, J. A., Oltra-Carrió, R., Sòria, G., Jiménez-Muñoz, J. C., Franch, B., Hidalgo, V., Matter, C., Julien, Y., Cuenca, J., Romaguera, M., Gómez, J.A., Miguel, E.D., Bianchi, R. & Paganini, M. (2013). Evaluation of the surface urban heat island effect in the city of Madrid by thermal remote sensing. *International Journal of Remote Sensing*, 34, 3177-3192.

Socioeconomic Data and Applications Center (SEDAC), 2019. https://sedac.ciesin.columbia.edu/ (accessed 22 January 2019)

Son, N. T., & Thanh, B. X. (2018). Decadal assessment of urban sprawl and its effects on local temperature using Landsat data in Cantho city, Vietnam. *Sustainable Cities and Society*, 36, 81-91.

Song, C., Woodcock, C. E., Seto, K. C., Lenney, M. P., & Macomber, S,A. (2001). Classification and change detection using Landsat TM data: when and how to correct atmospheric effects? *Remote Sensing of Environment,* 75, 230-244

Song, Y., & Wu, C. (2016). Examining the impact of urban biophysical composition and neighboring environment on surface urban heat island effect. *Advances in Space Research*, 57, 96-109.

Sòria, G., & Sobrino, J. A. (2007). ENVISAT/AATSR derived land surface temperature over a heterogeneous region. *Remote Sensing of Environment*, 111, 409-422.

Steeneveld, G. J., Koopmans, S., Heusinkveld, B. G., & Theeuwes, N. E. (2014). Refreshing the role of open water surfaces on mitigating the maximum urban heat island effect. *Landscape and Urban Planning*, 121, 92-96.

Stewart, I. D. (2011). A systematic review and scientific critique of methodology in modern urban heat island literature. *International Journal of Climatology*, 31, 200-217.

Stewart, I. D., & Oke, T. R. (2012). Local climate zones for urban temperature studies. *Bulletin of the American Meteorological Society*, 93, 1879-1900.

Stone, B. (2007). Urban and rural temperature trends in proximity to large US cities: 1951–2000. *International Journal of Climatology*, 27, 1801-1807.

Sudhira, H, S., Ramachandra T, V., & Jagadish, K, S. (2004). Urban sprawl: metrics, dynamics and modelling using GIS. *International Journal of Applied Earth Observation and Geoinformation,* 5, 29-39.

Sulla-Menashe, D., & Friedl, M, A. (2018). User Guide to Collection 6 MODIS Land Cover (MCD12Q1 and MCD12C1) Product, available at https://lpdaac.usgs.gov/documents/101/MCD12_User_Guide_V6.pdf

Sun, R., & Chen, L. (2012). How can urban water bodies be designed for climate adaptation? *Landscape and Urban Planning*, 105, 27-33.

Sun, R., Li, Y., Yang, X., & Chen, L., (2019). Understanding the variability of urban heat islands from local background climate and urbanization, *Journal of Cleaner Production,* 208, 743-752.

Susca, T., Gaffin, S. R., & Dell'Osso, G. R. (2011). Positive effects of vegetation: Urban heat island and green roofs. *Environmental Pollution*, 159, 2119-2126.

Synnefa, A., Dandou, A., Santamouris, M., Tombrou, M., & Soulakellis, N. (2008). On the use of cool materials as a heat island mitigation strategy. *Journal of Applied Meteorology and Climatology*, 47, 2846-2856.

Synnefa, A., Santamouris, M., & Livada, I. (2006). A study of the thermal performance of reflective coatings for the urban environment. *Solar Energy*, 80, 968-981.

Tan, C. L., Wong, N. H., & Jusuf, S. K. (2013). Outdoor mean radiant temperature estimation in the tropical urban environment. *Building and Environment*, 64, 118-129.

Tan, C. L., Wong, N. H., & Jusuf, S. K. (2014). Effects of vertical greenery on mean radiant temperature in the tropical urban environment. *Landscape and Urban Planning*, 127, 52-64.

Tan, J., Zheng, Y., Tang, X., Guo, C., Li, L., Song, G., Zhen, X., Yuan, D., Kalkstein, A.J., Li, F., & Chen, H. (2010). The urban heat island and its impact on heat waves and human health in Shanghai. *International Journal of Biometeorology*, 54, 75-84

Tan, Z., Lau, K. K. L., & Ng, E. (2016). Urban tree design approaches for mitigating daytime urban heat island effects in a high-density urban environment. *Energy and Buildings*, 114, 265-274.

Tang, H. and Li, Z-L., 2014. Land surface temperature retrieval from thermal infrared data: theory and applications, Springer-Verlag, pp. 93-143.

Tomlinson, C. J., Chapman, L., Thornes, J. E., & Baker, C. J. (2012). Derivation of Birmingham's summer surface urban heat island from MODIS satellite images. *International Journal of Climatology*, 32, 214-224.

Trlica, A., Hutyra, L. R., Schaaf, C. L., Erb, A., & Wang, J. A. (2017). Albedo, land cover, and daytime surface temperature variation across an urbanized landscape. *Earth's Future*, 5, 1084-1101.

Trotter, L., Dewan, A., & Robinson, T. (2017). Effects of rapid urbanisation on the urban thermal environment between 1990 and 2011 in Dhaka Megacity, Bangladesh. *AIMS Environmental Science*, 4, 145-167.

Tyrväinen, L., & Väänänen, H. (1998). The economic value of urban forest amenities: an application of the contingent valuation method. *Landscape and Urban Planning*, 43, 105-118.

Tzoulas, K., Korpela, K., Venn, S., Yli-Pelkonen, V., Kaźmierczak, A., Niemela, J., & James, P. (2007). Promoting ecosystem and human health in urban areas using Green Infrastructure: A literature review. *Landscape and Urban Planning*, 81, 167-178.

United Nations, 2018. World Population Prospects: the 2018 Revision, Key Findings, UN, Department of Economic and Social Affairs, Population Division.

United States Geological Survey (USGS), 2018a. Landsat 8 surface reflectance code, USGS, South Dakota.

United States Geological Survey (USGS), 2018b. Landsat 4-7 surface reflectance (LEDAPS) product guide, USGS, South Dakota.

Ürge-Vorsatz, D., Rosenzweig, C., Dawson, R. J., Rodriguez, R. S., Bai, X., Barau, A. S., Seto, K.C.,. & Dhakal, S. (2018). Locking in positive climate responses in cities. *Nature Climate Change*, 8, 174.

Voelker, S., Baumeister, H., Classen, T., Hornberg, C., & Kistemann, T. (2013). Evidence for the temperature-mitigating capacity of urban blue space—A health geographic perspective. *Erdkunde*, 67, 355-371.

Voogt, J. A. (2008). Assessment of an urban sensor view model for thermal anisotropy. *Remote Sensing of Environment*, 112, 482-495.

Wan, Z. (2014). New refinements and validation of the collection-6 MODIS land-surface temperature/emissivity product. *Remote Sensing of Environment*, 140, 36-45.

Wan, Z., & Dozier, J. (1996). A generalized split-window algorithm for retrieving land-surface temperature from space. *IEEE Transactions on Geoscience and Remote Sensing*, 34, 892-905.

Wang, K., Jiang, S., Wang, J., Zhou, C., Wang, X., & Lee, X. (2017). Comparing the diurnal and seasonal variabilities of atmospheric and surface urban heat islands based on the Beijing urban meteorological network. *Journal of Geophysical Research: Atmospheres*, 122, 2131-2154.

Weng, Q. (2001). A remote sensing GIS evaluation of urban expansion and its impact on surface temperature in the Zhujiang Delta, China. *International Journal of Remote Sensing*, 22, 1999-2014.

Weng, Q. (2009). Thermal infrared remote sensing for urban climate and environmental studies: Methods, applications, and trends. ISPRS *Journal of Photogrammetry and Remote Sensing*, 64, 335-344.

Weng, Q., Lu, D. & Schubring, J. (2004). Estimation of land surface temperature–vegetation abundance relationship for urban heat island studies. *Remote Sensing of Environment*, 89, 467-483.

Wilkinson, S. J., & Reed, R. (2009). Green roof retrofit potential in the central business district. *Property Management*, 27, 284-301.

Wilson, E. O. (1984). *Biophilia*, MA: Harvard University Press.

Wolf, K. L., & Robbins, A. S. (2015). Metro nature, environmental health, and economic value. *Environmental Health Perspectives*, 123, 390-398.

Wong, J. K. W., & Lau, L. S. K. (2013). From the 'urban heat island'to the 'green island'? A preliminary investigation into the potential of retrofitting green roofs in Mongkok district of Hong Kong. *Habitat International*, 39, 25-35.

Wong, M. S., Nichol, J. E., To, P. H., & Wang, J. (2010). A simple method for designation of urban ventilation corridors and its application to urban heat island analysis. *Building and Environment*, 45, 1880-1889.

Wong, N. H., Chen, Y., Ong, C. L., & Sia, A. (2003). Investigation of thermal benefits of rooftop garden in the tropical environment. *Building and Environment*, 38, 261-270.

Wong, N. H., Tan, A. Y. K., Chen, Y., Sekar, K., Tan, P. Y., Chan, D., Chiang, K., & Wong, N. C. (2010). Thermal evaluation of vertical greenery systems for building walls. *Building and Environment*, 45, 663-672.

Wu, A., Xiong, X., Doelling, D. R., Morstad, D., Angal, A., & Bhatt, R. (2013). Characterization of Terra and Aqua MODIS VIS, NIR, and SWIR spectral bands' calibration stability. *IEEE Transactions on Geoscience and Remote Sensing*, 51, 4330-4338.

Wu, C., & Murray, A. T. (2003). Estimating impervious surface distribution by spectral mixture analysis. *Remote Sensing of Environment*, 84, 493-505.

Wulder, M. A., Loveland, T. R., Roy, D. P., Crawford, C. J., Masek, J. G., Woodcock, C. E., Allen, R.G., Anderson, M.C., Belward, A.S., Cohen, W.B., Dwyer, J., Erb, A., Gao, F., Griffiths, P.,

Helder, D., Hermosilla, T., Hipple, J.D., Hostert, P., & Zhu, Z., (2019). Current status of Landsat program, science, and applications. *Remote Sensing of Environment*, 225, 127-147.

Xiaomin, X., Zhen, H., & Jiasong, W. (2006). The impact of urban street layout on local atmospheric environment. *Building and Environment*, 41, 1352-1363.

Xu, H. (2006). Modification of normalised difference water index (NDWI) to enhance open water features in remotely sensed imagery. *International Journal of Remote Sensing*, 27, 3025-3033.

Xu, Z., Zhang, Z., & Li, C. (2019). Exploring urban green spaces in China: Spatial patterns, driving factors and policy implications. *Land Use Policy*, 89, 104249.

Yang, J., Su, J., Xia, J. C., Jin, C., Li, X., & Ge, Q. (2018). The impact of spatial form of urban architecture on the urban thermal environment: A case study of the Zhongshan district, Dalian, China. *IEEE Journal of Selected Topics in Applied Earth Observations and Remote Sensing*, 11, 2709-2716.

Yang, J., Wang, Z. H., & Kaloush, K. E. (2015). Environmental impacts of reflective materials: Is high albedo a 'silver bullet' for mitigating urban heat island?. *Renewable and Sustainable Energy Reviews*, 47, 830-843.

Yang, X., & Li, Y. (2015). The impact of building density and building height heterogeneity on average urban albedo and street surface temperature. *Building and environment*, 90, 146-156.

Yang, X., Peng, L. L., Jiang, Z., Chen, Y., Yao, L., He, Y., & Xu, T. (2020). Impact of urban heat island on energy demand in buildings: Local climate zones in Nanjing. *Applied Energy*, 260, 114279.

Yang, Y., Zheng, Z., Yim, S. Y., Roth, M., Ren, G., Gao, Z., Wang, T., Li, Q., Shi, C., Ning, G., & Li, Y. (2019). PM2. 5 Pollution Modulates Wintertime Urban Heat Island Intensity in the Beijing-Tianjin-Hebei Megalopolis, China. *Geophysical Research Letters*, 47, e2019GL084288.

Yao, R., Wang, L., Huang, X., Chen, J., Li, J., & Niu, Z. (2018a). Less sensitive of urban surface to climate variability than rural in Northern China. *Science of the Total Environment*, 628, 650-660.

Yao, R., Wang, L., Huang, X., Niu, Z., Liu, F., & Wang, Q. (2018b). Temporal trends of surface urban heat islands and associated determinants in major Chinese cities. *Science of the Total Environment*, 609, 742-754.

Yoo, S. (2018). Investigating important urban characteristics in the formation of urban heat islands: a machine learning approach. *Journal of Big Data*, 5, doi: 10.1186/s40537-018-0113-z

Yu, X., Guo, X., & Wu, Z. (2014). Land surface temperature retrieval from Landsat 8 TIRS—Comparison between radiative transfer equation-based method, split window algorithm and single channel method. *Remote Sensing*, 6, 9829-9852.

Zha, Y., Gao, J., & Ni, S. (2003). Use of normalized difference built-up index in automatically mapping urban areas from TM imagery. *International Journal of Remote Sensing*, 24, 583-594.

Zhang, H., Qi, Z. F., Ye, X. Y., Cai, Y. B., Ma, W. C., & Chen, M. N. (2013). Analysis of land use/land cover change, population shift, and their effects on spatiotemporal patterns of urban heat islands in metropolitan Shanghai, China. *Applied Geography,* 44*,* 121-133.

Zhang, Y., & Sun, L. (2019). Spatial-temporal impacts of urban land use land cover on land surface temperature: Case studies of two Canadian urban areas. *International Journal of Applied Earth Observation and Geoinformation*, 75, 171-181.

Zhang, Y., Murray, A. T., & Turner Ii, B. L. (2017). Optimizing green space locations to reduce daytime and nighttime urban heat island effects in Phoenix, Arizona. *Landscape and Urban Planning*, 165, 162-171.

Zhao, C., Fu, G., Liu, X., & Fu, F. (2011). Urban planning indicators, morphology and climate indicators: A case study for a north-south transect of Beijing, China. *Building and Environment*, 46, 1174-1183.

Zhao, L., Lee, X., Smith, R. B., & Oleson, K. (2014). Strong contributions of local background climate to urban heat islands. *Nature*, 511, 216-219.

Zhao, S., Zhou, D., & Liu, S. (2016). Data concurrency is required for estimating urban heat island intensity. *Environmental Pollution*, 208, 118-124.

Zheng, B. J., Myint, S. W. & Fan, C. (2014). Spatial configuration of anthropogenic land cover impacts on urban warming. *Landscape and Urban Planning*, 130, 104-111.

Zhou, D., Bonafoni, S., Zhang, L., & Wang, R. (2018). Remote sensing of the urban heat island effect in a highly populated urban agglomeration area in East China. *Science of the Total Environment*, 628, 415-429.

Zhou, D., Zhao, S., Liu, S., Zhang, L., & Zhu, C. (2014). Surface urban heat island in China's 32 major cities: Spatial patterns and drivers. *Remote Sensing of Environment,* 152, 51-61.

Zölch, T., Maderspacher, J., Wamsler, C., & Pauleit, S. (2016). Using green infrastructure for urban climate-proofing: An evaluation of heat mitigation measures at the micro-scale. *Urban Forestry and Urban Greening*, 20, 305-316.

Zullo, F., Fazio, G., Romano, B., Marucci, A., & Fiorini, L. (2019). Effects of urban growth spatial pattern (UGSP) on the land surface temperature (LST): A study in the Po Valley (Italy). *Science of The Total Environment*, 650, 1740-1751.

Appendix I Inception Workshop

Inception Seminar

"Mitigation strategies for the Urban Microclimate of Dhaka Megacity to reduce adverse Climatic Change impacts"

Brief Report

Inception workshop of the research titled "Mitigation Strategies for the Urban Microclimate of Dhaka Megacity to Reduce Adverse Climate Change Impacts" was held on 28 November 2018 at the BIISS auditorium. The research is being jointly undertaken by Bangladesh Institute of International and Strategic Studies (BIISS), Curtin University, Australia and Department of Meteorology, University of Dhaka; under the funding of World Bank's "Innovation Funding and Global Partnership for Sustainable Development Data" initiative. **Professor Dr. Shamsul Alam**, Member (Senior Secretary), General Economics Division, Planning Commission, Government of the People's Republic of Bangladesh, graced the occasion as the Chief Guest. **Professor Dr Towhida Rashid**, Chairman, Department of Meteorology, University of Dhaka, chaired the workshop.

Major General A K M Abdur Rahman, ndc, psc, Director General, BIISS, delivered the Welcome Address at the workshop. In his speech, he highlighted that Dhaka megacity was witnessing a phenomenon known as Urban Heat Island (UHI) effect which is a unique feature of climate change and the city dwellers are suffering greatly from it. He also described his own personal experience to illustrate how quickly the city of Dhaka was expanding, and emphasised on the demerits like land filling, waterlogging and removal of vegetation.

Main Presentation:

The workshop began with a presentation titled "Mitigation Strategies for the Urban Microclimate of Dhaka Megacity to Reduce Adverse Climate Change Impacts", which was presented by **Dr Ashraf Dewan**, School of Earth and Planetary Sciences, Curtin University, Australia and **Dr Mahfuz Kabir**, Research Director, BIISS. Dr. Dewan focused his part of the presentation on the study design and scientific components while Dr. Kabir concentrated on the cost-benefit analysis part of the study.

The presenters gave a brief description of the funding for the study. They said that the World Bank's Development Data group, together with the Global Partnership for Sustainable Development Data, had called for ideas to improve the production, management, and use of data in the two thematic areas of "Leave No One Behind" and 'the environment'. The funding was awarded to the research team in response to the international call in 2017. The project is among

the 12 awardees from over 230 submitted projects. Following sections show some of the issues highlighted in the presentation:

In 2016, 54.5% of the world's population will live in urban areas though urban areas cover only 4.5 % of the Earth's surface. The number of megacities around the world is increasing and in 2050, Dhaka is set to become the 4th largest megacity in terms of population.

The phenomenon called Urban Heat Island effect is having global and local implications. The observed Global Urban Heat Island Intensity is 1.1 to 6.5 degree Celsius and International Panel on Climate Change (IPCC) reports share data that are also supportive of this trend. Globally, there is a consistent increase in the Surface Urban Heat Island (SUHI). In this context, Asian cities will face a huge number of adversities. If the dry bulb temperature exceeds 35 degree Celsius, it is considered unlivable for humans.

Changes in land-use, population density, street geometry, Sky View Factor etc. are some of the major factors that causes Urban Heat Island (UHI). Changes in wind systems in the city is also highly responsible. There are three types of UHI: a) Boundary Layer UHI, b) Canopy Layer UHI and c) Sub-surface and Skin Layer UHI. There are also two principal mechanisms behind UHI: i) advection of rural wind to urban areas and ii) availability of green and blue spaces.

In 2015, 1500 people were killed in Pakistan because of heat wave and Urban Heat Island effect could further intensify this kind of impact. The outbreak of vector borne disease, Dengue, was regenerated after 2000. Indications of other vector borne diseases that are prevalent in Dhaka city includes Chikungunya and also Cholera. These too are possibly related with the increase of urban temperature. This research is important because it will focus on the Urban Heat Island effect and its mitigation measures.

In the Dhaka city, minimum temperature is also rising. Some past studies conducted on the UHI in Dhaka including Sharmin et al. 2015, Ahmed et al. 2013 and Trotter et al. 2017 showed that the intensity of the UHI effect was increasing in Dhaka with intensities ranging from 1-2 degree Celsius. Past studies conducted also showed significant loss in vegetations and increase in built up areas. However, significant research gap exists in this area of research, such as:

- Majority works are based on single season which is not sufficient to deal with this issue
- Combined approach of remotely sensed data and in-situ measurements is missing
- Seasonality of UHI is overlooked
- Role of green and blue space is generally contradictory
- Only a few studies highlighting the cost-benefit aspects of green infrastructures.

Given this backdrop, the research will look into the following issues:

- Relation between demographic shifts, land use transformation and spatio-temporal pattern of UHI effect
- Impacts of various factors concerning urban morphology and built infrastructure on the urban micro-climate of Dhaka city
- Cost-Benefit analysis of green infrastructures
- Assessment and evaluation of government policies

The research activities under this project have been divided into 7 different segments:

Research Activity 1: Meso-scale study. Here the Surface Urban Heat Island effect will be assessed. Impacts of daytime and night-time temperature changes during the winter season will be most significant in the future.

Research Activity 2: Microscale study. Canopy layer Urban Heat Island Effect. There are variations between diurnal temperature changes between the CBD and the Rural areas.

Research Activity 3: Identifying the best plant species for the effectiveness of green infrastructure in an effort of mitigation of urban warmth

Research Activity 4: Construction of green space database and statistical analysis of temperature and planning indicators

Research Activity 5: Suitability analysis of green spaces. A '3D GIS' technique will be used for analysing the best rooftop garden retrofitting. It will also include 'site suitability analysis' for underdeveloped areas

Research Activity 6: Cost-Benefit Analysis (CBA): there is a lack of standard CBA methods which can be applied to measure the economic costs and benefits of the green projects. Under this project, economic, social and aesthetic benefits and costs of green spaces will be evaluated using pilot survey and in-depth case studies focusing on green spaces and blue spaces. The respondents will be building owners and management authorities. Pilot Survey questionnaire has already been prepared

The economic viability of the green -blue spaces will be calculated by Net Present Value (NPV) and Internal Return Rate (IRR). Overall costs including the planting, removal, maintenance and other associated costs will be considered. Aesthetic benefits like the love to plants, energy savings, direct benefits from the products such as fruits and vegetables, government benefit like tax will be considered as well.

Research Activity 7: Development of mitigation measures based on UHI and microclimatic parameters. Existing public policies shall be reviewed and the best policies will be suggested. The research will also arrange meeting with the stakeholders and experts

The research is unique from the others because a holistic approach has been considered in it by the combination of remote sensing with in-situ measurements. Upon compilation this research shall provide a comprehensive database for micro-climate studies and this shall be made freely available to the public. It also incorporates green space planning. Finally, it combines scientific data and management aspects.

Panel Session:

Following the presentation, the assigned panelists gave their valuable opinion on the study: The key points highlighted by the panelists are presented below:

Dr. Abdus Salam, Department of Chemistry, University of Dhaka

- Heat islands and air pollution aspects should be emphasised.
- The impact of black carbon on the solar heat absorption.
- There is a lack of quality data in this area of research.
- Remote sensing-based data could be misleading and therefore the approach of combining remote sensing and in-situ data is appreciable.

Dr. AK Ekramul Haque, Department of Economics, East West University

- Generating micro level data is very important, the study's initiative to make the database is appreciated.
- The number of mitigating strategies considered in the research should be reduced for a more focused study
- The mitigation options could take into the consideration the design strategies and the management strategies. If this framework for mitigation is adapted, this will give better outputs.
- Another way of consideration for mitigation options could be the public interventions and private interventions.
- Proper planning even in terms of road geometry can play a vital role.
- The existing mitigation strategies needs to be identified first.
- Instead of cost-benefit analysis the study can look into the cost effectiveness of different strategies. The scientific temperature data that will be generated in this research could be used to assess the per degree cost reduction due to several mitigation measures.
- Aspects of urban planning such as relations between floor-area ratio and exposure to sun-light could also be considered.

Dr. Kazi Maruful Islam, Department of Development Studies, University of Dhaka

- Instead of focus on mitigation issues, the focus could be on "resilience". In that way, both mitigation and adaptation aspects could be integrated into the study.
- Looking into the "enforcement" of the existing policies is important. There are a large number of policies but not enough implementation of them.
- Cost benefit analysis should include the cost of the lack of implementations. Here, instances of better implementation could be assessed along with instances of poor implementation.

Mr. Iqbal Habib, Bangladesh Poribesh Andolob (BAPA)

- In 2010, it was observed that Dhaka has increased 19 times in terms of area and 25 times in terms of population
- The terms "Blue Space" and "Green Space" should be replaced with "Blue and Green Networks". This is because the larger *khals* (water canals) and parks are more important. Dhaka was one a city of *Khals*. Running water has major impacts in the reduction of temperature of the city.
- Restoration of *Khals* and creation of new parks should be emphasized.
- The plantation of trees should be incorporated in the DAP, government must enforce and make rules that a certain area of plot has to have a fixed number of trees.
- The urban morphology needs to be taken into consideration and urban renewal and revitalization process should be initiated. 72% of the buildings in Dhaka City are still only 3-4 storied high. Therefore, considering cluster of plots instead of individual plots for an urban renewal plan will be useful. This will ensure that there are some spaces for the green and blue.
- Public-Private partnerships need to be emphasised in terms of implementations.

Mr. Ahsan Rony, Green Savers Association

- The Green Savers Association is a social movement for rooftop gardening.
- Provides services such as 'doctors for trees.
- With their help, some schools have already started to rooftop gardening.
- The concept of "Oxygen Banking" and "Green Club" has been initiated by Green Savers.
- "Environtainment" Initiatives are being taken to involve the children.
- One major concern for rooftop gardening is that there are not sufficient number of skilled gardeners.

Open Discussion:

Following the discussion by the panelists, the forum was opened for the participants to share their thoughts on the issue. A number of the participants expressed their ideas, gave suggestions for the improvement of study and made some policy recommendation as well.

Dr Helal Ahmed, Professor, North South University, strongly appreciated the method of cost-benefit analysis. He said that this method measures the cost and the benefit from what have been invested. He focused on the importance of opportunity cost. He said that the people will have to bear the burden of an unplanned Dhaka city.

Dr. Md. Abdus Salam, Principal Scientific Officer, Bangladesh Space Research and Remote Sensing Organization (SPARRSO), pointed out three things. He firstly highlighted the limitation that the remote sensing measurement system. He said that if the research collects data from global dataset, it will produce less reliable information. He suggested collecting from the local perspective. Secondly, he advised not to use commercial data because these are not developed by highly skilled professionals and have many shortcomings. He suggested hiring someone to write new computer programme that will be tailored for the need of the study. Thirdly, he requested to co-relate the research project with the goal of Sustainable Development Goal and the "7th Five Year Plan" of Bangladesh Government.

Dr. Abdul Mannan, Meteorologist, Department of Meteorology, Government of Bangladesh, mentioned that Meteorology Department has highly sorted data on temperature collected from 6 weather stations and it can provide on demand. He said that microclimate is now being prioritised by the government. He said Meteorology Department is working with many national and international stakeholders like World Bank and NASA. And they are establishing 25 new microclimate stations that will be fully operational from July next year. He advised the researchers to reduce the threshold of RCB from 8.5 to 4.5 degree Celsius and the temperature from 35 to 30 degree Celsius for better results in the study.

Dr. A. Atique Rahman, Executive Director, Bangladesh Centre for Advanced Studies (BCAS), said that whether one does research on micro or macro level, the focus should be on all the policies and programs to ensure water, energy and foods are all taken into consideration. He argued that micro level analysis will generate knowledge but it will not solve the problems. He also advised using satellite image for micro level analysis. He said that he feels that Bangladesh doesn't need Dhaka city anymore, the whole of Bangladesh will be a city.

Sujit Kumar Debsarma said that the researchers should use local data because it will increase the acceptability of the research. He suggested a number of technical measures including the inclusion of upper air data with surface observation in order to get better results in the study.

Dr. Aminul Islam, Senior Advisor, Centre for Natural Resources Studies (CNRS), highlighted three issues for substantive policy on heat, energy, building code. These three are- land use and planning, circular economy and green corridor.

Eng. Mir Mosharrof Hossen Chowdhury, Managing Director, Praakrita Nirman Ltd., asked to include the professionals so that they can participate in the process of implementation of government policy.

At the end of the open discussion, the honorable chief guest of the workshop, **Professor Dr. Shamsul Alam**, delivered his speech. He started his speech thanking the organisers of the programme, the researchers of the study and the World Bank for funding the study. He said that the changes to the microclimate and the land is very important. The temperature varies from place to place even within the city. He highlighted some data on his speech that showed how the climate of Dhaka city has changed over time and has had an influence on the ecological setting, agro-production, industrial production, human behavior and disease. He emphasised that all climate related problems are interrelated and that is why there is a need for comprehensive and long-term plans. He said that the 'Delta Plan-2100' of Bangladesh government is a 100-year plan and an initiative to look ahead into the future. He also said that the government had adopted the plan based on the data available at that time and the delta plan can be revised within five- or ten-years' period to update itself. He mentioned that both adaptation and mitigation measures needs be considered in combating climate change. Finally, He said that the government is going to start working on formulating the "8th Five Year Plan" soon, and hoped that the results of the study will be presented in time so that they can be reflected in that document.

Appendix II Details of Landsat data used in this study

Year	Total samples	Months (number of samples)	Sensor
2000	3	Jan (1), Feb (1), Oct (1)	TM, ETM+
2001	2	Jan (2)	TM, ETM+
2002	6	Feb (2), Mar (1), Oct (1), Nov (1), Dec (1)	ETM+
2003	4	Jan (1), Mar (2), Dec (1)	TM, ETM+
2004	6	Feb (1), Mar (1), Nov (2), Dec (2)	TM
2005	1	Nov (1)	TM
2006	7	Feb (1), Mar (1), Apr (1), Nov (2), Dec (2)	TM
2007	4	Jan (1), Feb (1), Mar (2)	TM
2008	6	Mar (1), Apr (2), Nov (2), Dec (1)	TM
2009	6	Jan (1), Feb (1), Apr (1), Oct (1), Nov (2)	TM
2010	5	Jan (1), Feb (1), Nov (2), Dec (1)	TM
2011	6	Jan (2), Feb (2), Mar (1), Apr (1)	TM
2012	NA	NA	NA
2013	2	Nov (1), Dec (1)	L08
2014	4	Jan (1), Feb (1), Mar (1), Nov (1)	L08
2015	5	Jan (1), Mar (1), Oct (1), Nov (1), Dec (1)	L08
2016	4	Jan (1), Feb (1), Nov (2)	L08
2017	3	Mar (1), Nov (1), Dec (1)	L08
2018	6	Feb (1), Mar (1), May (1), Oct (1), Nov (1), Dec (1)	L08

Number in bracket shows available data in the respective month

Appendix III Spatial distribution of daytime LST, 2000–2018

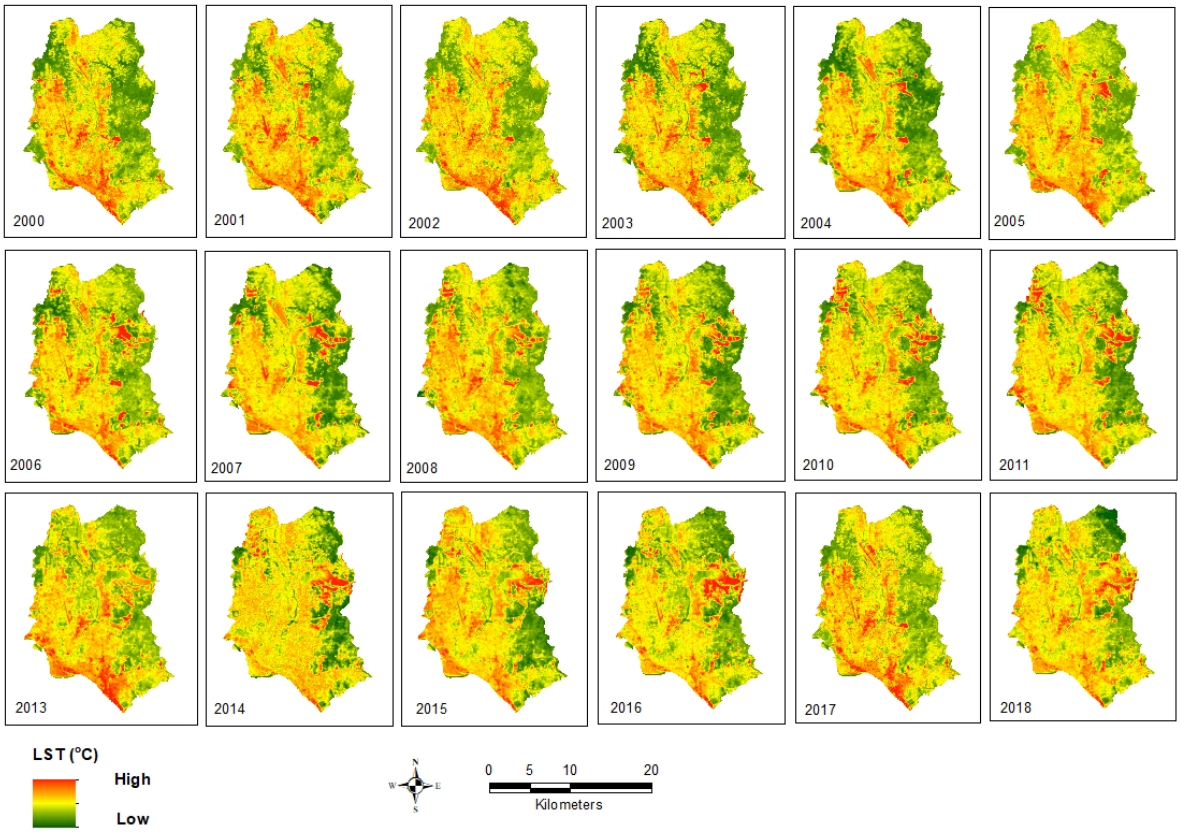

Appendix IV Spatial distribution of nighttime LST, 2005–2018

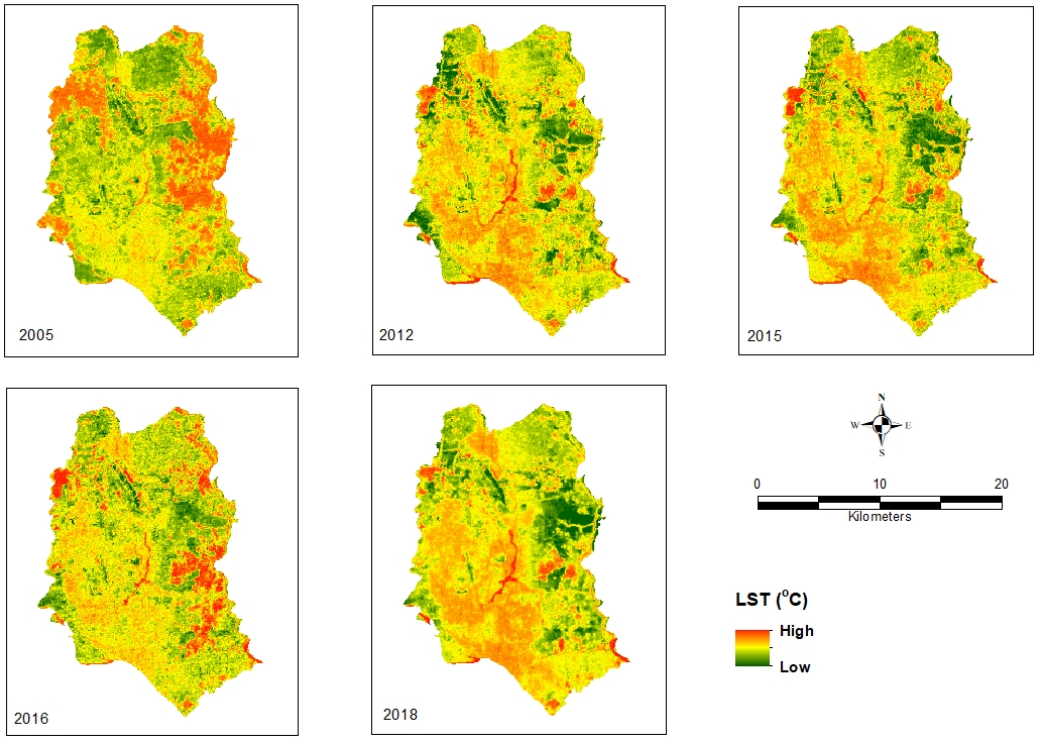

Appendix V Representative thermal images of different sites along three traverse routes

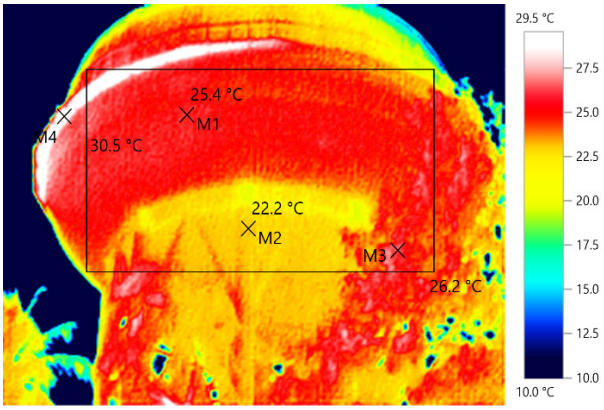

Planned zone (SPOT 3) – thermal

Visible

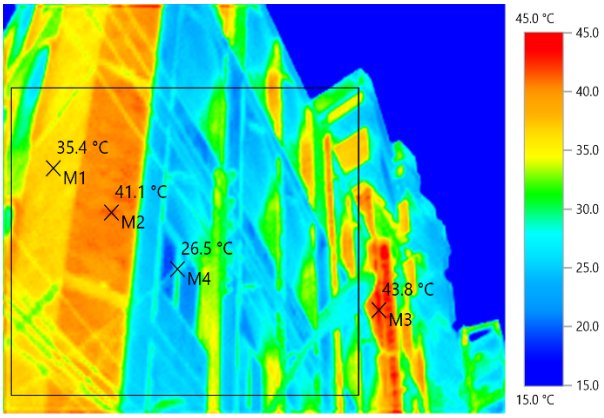

Unplanned zone (SPOT 2) – thermal

Visible

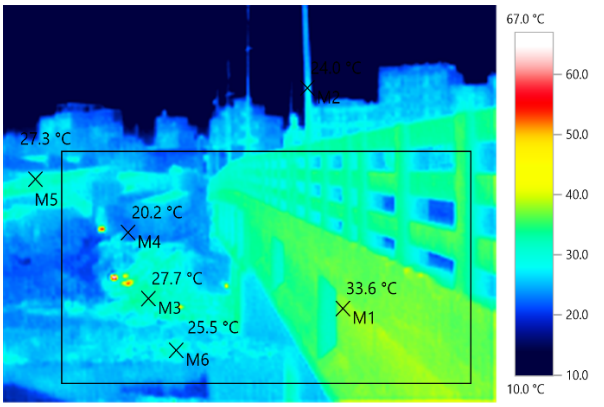

Mixed zone (SPOT 1) – thermal

Visible

Appendix VI Dominant rooftop plants considered in this work: (a) Bougainvillea; (b) Guava; (c) Maltes; (d) Combretum indicum; and (e) Lemon

Appendix VII Average wind speed and solar radiation during the winter, monsoon and pre–monsoon seasons at the Suhrawardi Uddyan

	Pre–monsoon		Monsoon		Winter	
Time	Wind speed (m/s)	Solar radiation (W/m^2)	Wind speed (m/s)	Solar radiation (W/m^2)	Wind speed (m/s)	Solar radiation (W/m^2)
9:00	1.40	114.29	2.43	68.51	1.03	93.04
10:00	1.87	222.73	3.22	71.01	1.36	218.43
11:00	1.96	224.21	3.88	74.04	1.49	248.99
12:00	2.10	311.96	3.36	124.84	1.59	380.23
13:00	2.01	276.49	4.11	170.08	1.49	353.59
14:00	2.01	214.61	3.13	157.74	1.49	310.23
15:00	1.73	125.09	2.57	99.54	1.40	208.29
16:00	1.78	82.11	1.63	42.66	1.31	91.09
17:00	1.59	31.88	1.21	7.81	0.70	27.65
18:00	0.98	3.42	1.07	0.68	0.33	1.23

Appendix VIII Experimental setup of a green hanging wall

Appendix IX Descriptive characteristics of 15 data loggers around Suhrawardi Uddyan

Station ID	Name	Latitude	Longitude	Distance to Park (m)	Direction
WB-1	Fuller road	23.731	90.391	812.3	West
WB-2	Kuwait moitry hall*	23.732	90.380	1823.5	West
WB-15	Ramna park**	23.735	90.401	389.9	North
WB-18	DU central library	23.733	90.394	341.4	West
WB-19	Tanaka tower	23.733	90.406	858.1	East
WB-20	Bakshi bazar	23.721	90.395	1383.1	South
WB-21	IEB*	23.733	90.400	258.7	East
WB-22	Iskaton	23.750	90.400	1807.9	North
WB-23	Mohosin hall	23.734	90.389	911.8	West
WB-24	Bijoy nagar	23.733	90.410	862.4	East
WB-25	Sufia kamal hall	23.726	90.405	1110.0	South
WB-26	BIISS	23.744	90.400	1410.1	North
WB-27	Moulvibazar	23.715	90.399	2085.9	South
WB-28	AGB colony	23.735	90.420	2280.9	East
WB-29	DU science library	23.728	90.399	609.6	South

*Missing since installation on December 15, 2018

** Missing since February 6, 2019 but replaced later

Appendix X Descriptive characteristics of 15 data loggers around Dhanmondi lake

Station ID	Name	Latitude	Longitude	Distance to Lake (m)	Direction
WB-3	Kantar Ltd.	23.747	90.379	200.9	East
WB-4	Biswas coaching	23.746	90.375	286.4	West
WB-5	Gyantapas bidya	23.745	90.376	259.3	South
WB-6	Keraye plaza	23.743	90.371	759.5	South
WB-7	Modhubazar	23.745	90.368	923.1	West
WB-8	Dhanmondi 28	23.753	90.372	918.0	East
WB-9	Leather institute	23.733	90.368	1672.4	South
WB-10	Lake Circus	23.748	90.381	444.3	North
WB-11	Somorita hospital	23.753	90.384	1050.5	North
WB-12	Anwar khan med	23.745	90.382	555.0	East
WB-13	Dhanmondi 4	23.742	90.381	619.4	East
WB-14	Firmgate	23.756	90.393	1950.8	North
WB-16	Shankar	23.750	90.368	1081.1	West
WB-17	Lalmatia	23.755	90.366	1531.7	West
WB-30	Jigatola	23.740	90.371	916.5	South

Appendix XI Lessons learned and recommendations for improvement

A number of lessons have been learnt while conducting this work and these are detailed below. The incorporation of these lessons into future work would be very beneficial.

- Due to budgetary constraints, it was not possible to undertake traverse surveys during the post–monsoon season. Although three seasons were assessed, the inclusion of the post–monsoonal period could have benefit to the project outcomes. It is anticipated that the findings regarding the local climatic conditions observed during the three seasons may still provide valuable information when developing urban heating mitigation measures.

- Any future work of this nature should consider factors such as labour availability, as the field data collection was very expensive and difficult. The project team also had to hire a green hanging wall and rooftops, both with and without gardens, to examine the ability of these features to reduce urban environmental temperatures. Future work should factor in these requirements.

- All microclimate data collected via traversing should be collected concurrently in order to provide better information regarding CUHI and SUHI phenomena. Due to budgetary constraints, devices that were deployed in the field were not able to record simultaneous measurements. Future work should also have a back–up device as the non–availability (due to theft or withdrawn by concerned authority due to security reason) of a few low–cost sensors interrupted the measurement of green/blue space thermal response.

- The collection and analysis of additional parameters such as soil moisture could have been highly beneficial as it is an important parameter in influencing UHI development. Although albedo was collected along the three traverse routes, the measurement of the albedo (both shortwave and longwave) of various urban land use categories on a continuous basis could prove useful. Measuring the thermal response of various land use classes over time could also add additional value.

- During the study, it was noted that the wind direction recorded in the rural and urban areas seemed to diametrically opposite (different by approximately 180 degrees), from March to November. While the wind direction of the urban areas aligned well with an available, independent data source, the validity of the rural area wind direction could not be confirmed due to a lack of any independent measurements. As wind direction seriously influences UHI growth, further research could examine this issue by installing a greater number of automated weather stations both at urban and rural sites.

- A large number of samples are required to properly characterise the microclimatic variation of SUHI. In its current overpass configuration, Landsat provides data in the morning hours (10.30 am local time). Likewise, ASTER provided few samples to characterise nighttime SUHI. Time of acquisition and number of samples are very important in mapping LST and providing accurate SUHI data in the DMA.

- The study could not use such factors as the waste heat generated from transport, residential and commercials sectors to provide a more detailed assessment of the urban microclimate due to the scarcity of this type of data. Inclusion of these types of variables into any future work could provide valuable information regarding the observed spatiotemporal variability of urban heat. Also, traffic counts data along major roads could be useful in understanding the nature of UHI hotspots.

- Inclusion of local resident groups into future work would add value. To obtain their support, some incentives in the form of reimbursement could be provided. This could ensure the safety and security of the recording devices.

- The status of data should be also assessed in advance and factored into any timelines. Third–party data was used in the greenspace suitability and green roof potential assessments, but inherent issues with the data prevented the use of more advanced GIS analysis techniques to provide more detailed information on these particular features.

- Processing the voluminous amounts of data generated, and delivering the results in a timely manner, was difficult. It is suggested that the milestone requirements be limited to two–three for any future projects.

- We could not utilise three–dimenional data over any urban boundary layers due to the absence of such data. Further study is needed in order to use three–dimensional urban morphology, vegetation structure and boundary layer data to determine spatiotemporal variability and any causative factors. This has the potential to advance our knowledge regarding the details of urban and/or local warming.

Appendix XII Summary of study risks

Risks addressed	Risk mitigation
Functionality of low cost devices	Some devices malfunctioned and/or were stolen during field data collection. Stolen devices were replaced at our own cost. Adverse environmental conditions were also responsible for causing malfunctioning issues
Installation of weather stations and data loggers	Initially the installation of devices in the field was an issue which was addressed with the assistance of local residents. To try and ensure the weather stations were not stolen or damaged, a monthly lump sum was paid to locals during the project duration
Field data collectors	It was difficult to get skilled personnel to collect data from the field due to the nature of the work. Additional personnel were therefore employed during the data collection periods
Hiring of rooftop garden and vertical green wall	The rooftop garden and vertical green wall used in the study were leased during the seasons in order to obtain the required data. This cost was paid from the project budget
Satellite data processing	Due to the voluminous amount of data obtained from the remote sensing, additional time was required for the processing and validation work

Appendix XIII CNG–run auto–rickshaw with rooftop green grass and vegetation

(https://m.bdnews24.com/amp/en/detail/photodetail/1590205; https://www.alamy.com/dhaka-bangladesh-may-12-2018-a-green-environmental-friendly-bangladeshi-cng-three-wheeler-transport-with-mini-garden-on-its-rooftop-in-dhaka-ba-image187841497.html?)